Industrial Applications of Photonuclear Resonance Excitation

by

David Lee Chichester

B.S., Engineering Physics, University of Illinois, 1993
M.S., Nuclear Engineering, University of Illinois, 1995

SUBMITTED TO THE DEPARTMENT OF NUCLEAR ENGINEERING IN PARTIAL
FULFILLMENT OF THE REQUIREMENTS FOR THE DEGREE OF

DOCTOR OF SCIENCE IN NUCLEAR ENGINEERING
AT THE
MASSACHUSETTS INSTITUTE OF TECHNOLOGY

June 2000
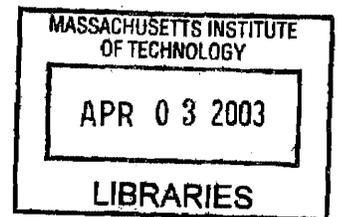
Signature of Author: _____
Nuclear Engineering Department
May 18, 2000

Certified by: _____
Lawrence M. Lidsky
Professor of Nuclear Engineering
Thesis Supervisor

Certified by: _____
Richard C. Lanza
Senior Research Scientist, Nuclear Engineering Department
Thesis Reader

Accepted by: _____
Sow-Hsin Chen
Professor of Nuclear Engineering
Chairman, Department Committee on Graduate Students
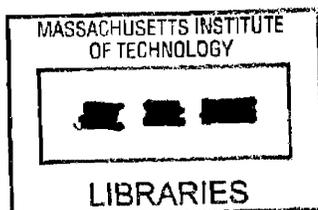
Industrial Applications of Photonuclear Resonance Excitation

by

David Lee Chichester

Submitted to the Department of Nuclear Engineering
on May 15, 2000 in Partial Fulfillment of the Requirements for the Degree of
Doctor of Science in Nuclear Engineering

ABSTRACT

Photonuclear resonance excitation refers to a variety of photonuclear interaction processes that lead to the excitation of a nucleus from some initial state to a higher energy nuclear state. Typical excited nuclear state lifetimes are short, ranging from nanoseconds to femtoseconds or less; however, some isotopes have unusually long-lived excited nuclear energy states, or isomers. This dissertation examines the feasibility of using bremsstrahlung irradiation sources to produce isomers for industrial applications. In contrast with charged particle based isomer production, the use of high energy photons allows for the irradiation and production of isomers in bulk materials. The commercial availability of reliable, high power industrial electron accelerators means that isomer activities sufficient for industrial applications may be achieved using bremsstrahlung, in contrast with neutron based approaches where suitable neutron sources of sufficient intensity for these applications are lacking.

In order to design a system for creating nuclear isomers using photons, the resonant photon absorption isomeric excitation cross section must be known. Unlike neutron absorption and scattering cross sections, comparatively little information exists for photon isomeric excitation. To address this, a theoretical model based upon statistical probability distributions of nuclear energy levels has been developed for calculating photon excitation cross sections at energies below neutron and proton binding energies; the ideal region of operation for most applications in order to minimize long term activation of materials. Isomeric excitation cross sections calculated using this technique have been compared with experimentally measured values and are found to agree to within a factor of two or better. Using this, a general transition equation suitable for both nuclear resonance fluorescence and isomer excitation has been developed for calculating nuclear level distribution probabilities for materials undergoing photon irradiation.

Experiments have been carried out using an industrial 6 MeV electron accelerator to identify obstacles related to nuclear resonance fluorescence measurements as well as measurements of the decay of short-lived isomers using scintillators in the vicinity of high intensity bremsstrahlung sources. Use of a fast switching gating circuit in combination with a pulsed accelerator was found to be a satisfactory solution for dealing with problems related to the performance of a detectors photomultiplier tube as a result of exposure to scattered radiation during the beam pulse.

Calculations have been carried out to assess the performance characteristics which could be expected from industrial photonuclear resonance excitation systems, based upon a 10 MeV electron accelerator. For simple isomer production, specific activities on the order of 1 mCi/g/mA can be expected for irradiation periods sufficiently long for equilibrium to be reached. For the analysis of arsenic concentrations in environmental samples, sensitivities of 1 ± 0.1 ppm could be achieved using accelerator currents of $50 - 100$ μA with irradiations times of a few minutes or less. A system designed to analyze ore traveling along a conveyor belt could be used to sort gold ore based upon a lower grade cutoff of 5 ppm using an accelerator of 10 mA with a processing volume exceeding 100 tons of ore per hour.

Committee:
L. M. Lidsky, Professor, Nuclear Engineering Department, MIT (Thesis Advisor)
R. C. Lanza, Senior Research Scientist, Nuclear Engineering Department, MIT (Thesis Reader)
P. Burstein, President, Skiametrics, Inc.
J. P. Freidberg, Professor, Nuclear Engineering Department, MIT
J. Schweitzer, Professor, Physics Department, University of Connecticut

ACKNOWLEDGMENTS

Of all the marvelous experiences and opportunities I have had at MIT since my arrival, I am most thankful for having had the good fortune of meeting my advisor Professor Larry Lidsky at the beginning. I have never met anyone with both the breadth and depth of knowledge Larry has in so many widely varying fields of interest. I am most inspired, however, by his ability to maintain such a healthy balance between family, work and life. Working on this thesis Larry's guidance was eagerly sought, freely given and always helpful. I feel fortunate to be able to refer to him as advisor, mentor and friend. Thank you.

I came to MIT because of Richard Lanza; thanks to his generosity and interest in this work, I stayed at MIT. During our short meeting together during my visit to the institute as a prospective graduate student in the spring of 1995 Dick's excitement for science and engineering were clearly evident. After working in his lab for the past two years, I now know that that first impression revealed only a glimpse of his unique drive and ingenuity for work in this field. It has been my good fortune to have had the opportunity to work with him on this dissertation and I can only hope that I will share his same enthusiasm for learning throughout my career.

I would like to thank Dr. Paul Burstein, Professor Jeff Freidberg and Professor Jeff Schweitzer, members of my committee. The time they took to read through this dissertation and their insightful comments and suggestions are greatly appreciated.

I would like to thank all of my friends from Illinois, Ashdown and MIT, without whom I have no doubt I would never have done this.

I would like to thank Brandon Blackburn and Jo O'Meara.

I would like to thank Heather MacLean.

Thanks, mom and dad.

TABLE OF CONTENTS

LIST OF TABLES

LIST OF FIGURES

14

Chapter 1

INTRODUCTION

Photonuclear resonance excitation (PRE) refers to a variety of photonuclear interaction processes involving photons and nuclei that lead to the excitation of an atomic nucleus from some initial state to some higher energy nuclear state. Different PRE reaction pathways include direct photon absorption, photon scattering with the nucleus and photon scattering with atomic electrons. Depending upon the type of interaction, the incident photon energy and the nuclear structure of the nucleus involved in the reaction, PRE might lead to prompt nucleon emission (ejection of one or more neutrons and/or protons or photofission). If nucleon emission does not occur, the only de-excitation pathways for an excited nucleus are natural decay (e.g., α, electron capture, β^+ or β^-) or de-excitation via internal conversion or photon emission. Although excited nuclear states of radioactive isotopes typically have much larger particle emission probabilities than those of their groundstate, the decay probabilities for competing electromagnetic de-excitation pathways are generally several orders of magnitude larger than these.

Typical excited nuclear state half-lives are very small, in the range from 10^{-9} to 10^{-15} seconds. Since these nuclear lifetimes are so short, it is difficult to develop experimental techniques to measure the characteristic photons associated with their decay, especially when considering the intense background radiation signals which most often accompany the PRE process. It is equally difficult to conceive of *practical* industrial applications based in some way on the use of characteristic decay photons accompanying the prompt decay

of excited nuclear eigenstates, although several designs have been discussed in the literature.[1-8] However, in some nuclei there also exist long lived excited nuclear eigenstates with half-lives of 10^{-3} seconds or greater. Contrasted with short-lived, promptly decaying excited energy states, the development of commercially attractive industrial applications based on the use of these 'long-lived' excited states ('isomers') is straightforward and can result in realistic designs expected to appeal to potential users based upon both performance and economic criteria.

This dissertation is a study of how the photonuclear resonance excitation process could be used to produce isomers for industrial purposes, with particular emphasis on the generation of high activity isomeric sources, the design of systems for determining isomeric isotope concentrations in materials in trace quantities and the design of machines capable of quickly assaying large volumes of materials to identify the presence of isomeric isotopes above some minimum threshold. In particular, factors related to the production of isomeric isotopes using bremsstrahlung photon sources is explored together with practical issues addressing the uses of PRE generated isomers. A multidisciplinary undertaking, this work incorporates aspects of nuclear physics, radiation physics, nuclear engineering, statistics, electronics, nuclear instrumentation, environmental engineering and mining engineering.

1.1 MOTIVATION

The original motivation for this work was narrowly focused on assessing the feasibility of incorporating an accelerator based photon source into an online measurement system for determining the grade of gold ore passing along a conveyor belt for use in the gold mining industry.[9, 10, 11, 12] Based upon an economic analysis of the potential economic benefits of gold ore sorting, the development of a commercially attractive system was seen as a project worth further consideration.[13, 14] Similar on-line sorting systems have been suggested or developed for assaying materials in other media such as the detection of sulfur in coal or the identification of plutonium in contaminated soil and have been recognized as important technological tools for these applications.[15]

As a benchmark consider a mine with an ore processing rate of ~100 tons per hour and a volume averaged gold concentration of 2 milligrams of gold per kilogram of ore. This would result in a gold production rate of 2 kilograms per day (64.4 troy ounces per day). At a price of $400 per oz the value of the gold extracted from the mine would be $25,720 per day, reaching a yearly value of $9.4 M.[a] For a mine with a log-normal gold distribution, which is typical of South African gold mines, approximately 90% of the gold is actually found in less than 10% of the ore actually extracted from the mine. Thus, if such a mine employed a sorting technique it might be possible to reduce the post excavation ore processing volume by 90% and yet still recover 90% of the excavated gold. Depending upon the cost structures present at a mine, namely the fraction of costs which are fixed and those which vary according with volume of ore processed, ore sorting might result in considerable improvements in a mine's net income despite a decrease in the mine's gross revenues resulting from a decrease in the mass of gold actually recovered from the ore.

Currently, most mines send all of their mined ore through the gold extraction process, only occasionally separating the ore in a very coarse way into high grade and low grade ore streams. The ore extraction process involves large volumes of physical processing including crushing, sifting, pulverizing and solid and liquid transport (>100 tons per day) as well as chemical processing including dissolution with strong acids and gold leaching using hazardous materials including massive quantities of cyanide. Assaying of gold ore is most commonly performed using the flame assay technique, other proposed techniques include using synchrotron radiation (SR), differential-pulse polarography (DPP) and x-ray fluoresence(XRF).[16,17,18] All of these techniques involve taking grab samples of material from the ore, crushing it to reduce its size and soemtimes chemical processing. For the flame assay method analyses are preformed by measurement of the emission spectrum from the sample upon heating or vaporization, for the DPP method electrode current measurements are taken while for the SR and XRF methods low energy x-rays are measured. Due to the intensive sample preparation needed for this type of analysis and the need for careful laboratory based measurements, it is impossible to carry out analyses in anything approaching a continuous fashion using the current technology. In addition, the heterogeneous nature of the distribution of gold within ore, combined

---

[a] Based upon a 365 day per year operating schedule.

20

with the necessarily limiting nature of statistical analyses based on grab sample measurements, often limits the ability to use extrapolated results of grab sample measurements to draw conclusions regarding the ore as a whole.[19] Although other techniques have been proposed for assaying gold ore for sorting purposes, none have been accepted by industry due to technical difficulties (too slow – low throughput, poor sensitivity, too expensive) as well as cultural issues (change is bad).[20-24] Concerning the use of neutrons to excite nuclear eigenstates for example, This work was originally intended to determine if a PRE based system could be designed to meet the technical requirements for use in a commercial mining venture.

Investigating the issue in more detail, additional benefits beyond the direct economic implications of ore sorting can also be identified. Most notable are reductions in the volume of dangerous chemicals from levels which are currently used and reductions in the volumes of mining tailing generated as a result of the gold extraction process.[25,26] Accidents related to the breaching of dams containing gold mine tailings are not uncommon throughout the world and often result in the release of enormous quantities of processed ore contaminated with acids, various heavy metals and cyanide.[27, 28, 29] Although costs associated with the waste products of gold mining may be somewhat difficult to quantify, especially environmental and societal risks associated with the consequences of accidents, it is clear that a 90% reduction in the total volume of wastes generated in this industry would provide far reaching benefits beyond those mostly easily found on the company ledger. In addition to using PRE based techniques for assaying ore for sorting, on line gold analyses capabilities might also be found to be a useful analytical tool in other aspects of the gold mining and processing industry as well.

As work for this dissertation progressed towards addressing the application of PRE for gold analyses, other potential applications became apparent as understanding of the principles involved in the process grew. In particular, the use of photonuclear resonance excitation to create high activity samples of isomeric isotopes presented itself. To address this possibility, an investigation of the maximum induced isomeric activity yields which might be expected using targets and instruments specifically designed for that purpose was carried out. Although a specific case study focusing on a particular application using a high activity isomeric source is not discussed, the general relationship between accelerator current, sample size and irradiation geometry is presented to allow the reader to extrapolate the information presented to specific cases.

The possibility that PRE based *analytical* techniques might have useful advantages over existing techniques was identified as another area worth investigation.[30,31,32] The original application identified as a candidate for isomeric based analyses was the analysis of soil contaminated with arsenic from the Industri-Plex superfund hazardous waste site in Woburn, Massachusetts. For analyzing environmental samples, PRE could be a fast, uncomplicated analytical tool, requiring little sample preparation, with the potential for quick analytic turn around times. Additionally, it was felt that, in an analogous manner, similar measurement protocols could be developed for analyzing other materials to determine their arsenic contents well as other important elements including Ba, Cd, Pb, Hg, Se and Ag. For example, a PRE based detector could be used to interrogate artillery shells to determine if they contain the chemical weapons agent Lewisite (L), a blister agent developed during World War One.[33,34]

Finally, in addition to examining the production and application of isomers using photonuclear resonance excitation, work was also carried out to study the nuclear resonance fluorescence (NRF) process and any potential NRF applications. In NRF, photons associated with the decay of very short-lived (nanosecond to femtosecond) high energy eigenstates are measured rather than the characteristic photons associated with the decay of longer lived isomeric states. Unfortunately, significant hurdles exist between conceptual ideas of how NRF might be used for practical purposes[7,8] and actually conducting NRF investigations[35,36]. Chief among these problems when attempting to quantify the amount of trace quantities in a sample is the poor signal to noise ratio resulting from scattered radiation when a bremsstrahlung source is used. Additional difficulties are encountered due to the need for high intensity radiation fields to carry out measurements in a reasonable amount of time. Although a considerable amount of time and effort was expended, limitations in the operating characteristics of the equipment available for this work precluded the conceptualization and development of any practical NRF based industrial applications.

1.2 RESEARCH GOALS

In the broadest sense, the goal of this work is to examine the feasibility of using photonuclear resonance excitation in applications of interest for industrial purposes. Specifically, the aim was to consider the development of a non-destructive, isotope specific industrial scale analytical technique for characterizing the elemental make-up of materials using photon-excited *isomeric* nuclei. The feasibility of such a system has not been examined previously beyond the cursory level of reporting 'it could be done'. The potential benefit of the systems described in this dissertation are significant, including not only direct financial returns as in the case of gold assaying but also far reaching ecological and environmental benefits resulting from the ability to fundamentally change the nature of current industrial processes to reduce energy consumption, material processing and waste generation and pollution. In order to reach this end, however, information is required dealing with photon-nucleus interactions and isomer excitation. Additionally, understanding of the issues relating photon production, isomer creation and radiation detection instrumentation is needed for the design process.

Research goals included:
- the development of an analytical model for calculating isomeric excitation cross sections at energies below nucleon separation energies
- the development of a general mathematical formalism for modeling the buildup and decay of isomeric eigenstates in nuclei, including all possible excitation pathways, and then simplification of this model for use when analyzing industrial applications
- a thorough review of naturally occurring isomeric isotopes and readily available radioactive isomeric isotopes, resulting in a tabulation of nuclear structure and decay information relevant to the development of PRE applications
- demonstration of PRE
- identification of problems related to the implementation of PRE, based upon a historical literature on the subject and experimental investigations, and the identification, development and demonstration of practical solutions to these problems
- the development and demonstration of a practical, cost effective technique for analyzing short-lived isomers
- the development of a methodology for designing and assessing the performance of PRE based systems
- the design of a system for assaying bulk materials on a conveyor belt to determine the presence of one or more isomers and examining the relationships between different operational parameters such as irradiation source geometry and detector efficiency to asses its feasibility
- the design of a system for analyzing environmental samples to identify the presence of elements that are classified as hazardous materials and examining the relationships between different operational parameters to assess its feasibility.

1.3 OUTLINE

In Chapter 2 a detailed review of the physical processes through which photons interact with nuclei is presented. Particular emphasis is placed on evaluating the probability of those photonuclear interactions that leave the nucleus in an isomeric state. The most important photon interaction mechanism involving bremsstrahlung that results in isomer formation is the absorption of high energy photons leading to high energy excited states which eventually decay to the isomeric state. Since isomeric excitation cross sections involving photons in the 2 to 10 MeV range have only been reported for a few of the many isomeric isotopes, a theoretical model for predicting these probabilities based upon compound nucleus theory and the use of statistical models of nuclear structure is presented as well. Using this information relating the physics of photonuclear resonance excitation and isomer creation, a general mathematical framework is developed for analyzing the buildup of isomeric nuclei in a material irradiated with an arbitrary photon spectrum. This general equation is then simplified for the case where the irradiation field is that from the bremsstrahlung of an electron accelerator operating at energies below proton and neutron binding energies (so that competition from prompt nucleon emission channels may be neglected).

Building upon knowledge of the physics of the isomeric excitation process presented in Chapter 2, Chapter 3 presents a thorough analysis of three important issues that must be addressed when contemplating the feasibility and design of a PRE system for some arbitrary purpose. In the first section of Chapter 3 *the isomer* is considered by presenting the nuclear data needed for examining the usefulness of isomeric excitation for fifty-three isotopes having excited energy states with half-lives of 1 millisecond or greater. Additionally, a review of previous research dealing with the excitation of isomers from literature is presented. Following this, consideration is given to *the radiation source* by comparing and contrasting the advantages and disadvantages of using different photon sources for industrial purposes. In this section, the possible radiation sources considered include isotopic sources, reactor-based sources and accelerator based sources. Further distinction is made by subcategorizing these sources into those which are continuous in time and those that are discontinuous, or pulsed. Although electron accelerator based radiation sources are the most desirable for isomeric excitation, there are some situations for which other sources might be equally useful or even advantageous. Finally, *the radiation detector* to be used for applications requiring measurement of the isomeric decay is discussed. Of all currently available radiation detection and measurement instruments, inorganic scintillator based photon detectors are the most suitable for the broadest array of industrial PRE applications. A review is presented of the myriad of different types of inorganic scintillators with emphasis placed on those properties which are important when the crystals are exposed to high photon dose rates.

Chapter 4 focuses on analyzing practical design aspects which must be considered in assessing the performance of a PRE based instrument for an industrial purpose. For applications intended to produce high activity isomeric materials, Monte Carlo calculations were performed to understand the trade-offs between the energy of the electron beam, the thickness of the electron beam stop used to create the bremsstrahlung, the location and size of the target material and the optimal irradiating scheme. This analysis is performed so that a designer can adequately balance factors such as the photon spectrum and intensity in the target, minimizing convertor plate-target distance while still providing enough room for cooling and potentially electron beam sweeping and maximizing both the material output rate and material activity within constraints based upon the photon intensity and isomer half-life. Finally, the results of experimental studies examining the creation of isomers having half-lives from 16.8 milliseconds to 48.5 minutes are presented. In addition, the information gathered from these experiments elucidates practical problems likely to be encountered in the extrapolation of laboratory based PRE techniques for use in industry and described solutions to these problems.

In Chapter 5 the modeling tools and information presented in the previous three chapters are put to use in two separate case studies where proposed PRE systems designs are presented. In the first case study, a material analysis instrument is proposed for use as an analytical instrument for quantifying the concentration of arsenic present in 25 cm^3 soil samples. The relationship between accelerator current and counting time in terms of analytical precision and sensitivity is presented at a benchmark analytical sensitivity of 1 ppm As. The analysis is presented in such a way that the results may also be used to understand the importance of sample size and detector efficiency in assessing the performance of the proposed system. Further, performance characteristics of a system for analyzing a real sample of arsenic-polluted soil (arsenic concentration ~3000 ppm) from a Massachusetts superfund site are discussed.

In the second case study, a high throughput material assay instrument designed to analyze unprocessed ore to determine the presence of gold above a threshold concentration is described. In this instance, the design constraints include both material throughput, set at 100 tons per hour for a baseline analysis, and the size of the ore, limited to crushed ore capable of passing through a 2 by 4 inch channel. Demonstrating the use of a dual irradiation beam geometry to achieve a more uniform irradiation intensity throughout the ore, results are presented in terms of the minimum gold concentration that can be determined at different accelerator currents as a function of the speed of the material passing along a conveyor belt. Finally, information related to the nature of the distribution of gold in a typical South African ore is used to define the system requirements needed for determining gold over the 5 to 10 ppm range with false positive and false negative error rates both being less than 5%.

1.4 REFERENCES

[1] I. F. Isaev and L. P. Kudrin, "Diagnosis of Dense Plasma by Means of Resonance Scattering of Gamma Rays," High Temperature **6**, 737-740 (1968).

[2] B. D. Sowerby, "A New Method of Element Analysis Using Nuclear Resonance Scattering of Gamma Rays," Nucl. Instr. Meth. **94**, 45-51 (1971).

[3] Sowerby, Ellis and Greenwood-Smith, "Bulk Analysis for Copper and Nickel In Ores Using Gamma-Ray Resonance Scattering," Report IAEA-SM-216/4, Nuclear Techniques and Mineral Resources Proceedings, 499-521 (1977).

[4] Wielopolski, Vartsky and Cohn, "Possible Application of Nuclear Resonance Fluorescence to Study Surface Effects," J. Appl. Phys. **54**, 5449-5450 (1983).

[5] J. C. Palathingal, "Nuclear Resonance-Fluorescence Analyser of Ores and Surfaces," Capture Gamma-Ray Spectroscopy and Related Topics – 984, AIP Conference Proceedings No. 125, 847-850 (1984).

[6] D. J. S. Findlay, "Applications of Photonuclear Reactions," Nucl. Instr. Meth. Phys. Res. **B50**, 314-320 (1990).

[7] W. Bertozzi, "Explosives Detection Using Resonance Fluorescence of Bremsstrahlung Radiation," United States Patent No. 5,115,459, May 19, 1992.

[8] W. Bertozzi, "Detection of Explosives and Other Materials Using Resonance Fluorescence, Resonance Absorption, and Other Electromagnetic Processes With Bremsstrahlung Radiation," United States Patent No. 5,420,905, May 30, 1995.

[9] Marsden, Mansanti and Sass, "Innovative Methods For Precious Metals Recovery in North America," Mining Engineering, 1144-1151 September (1993).

[10] G. M. Bernard, "Andacollo Gold Production – Ahead of Schedule and Under Budget," Mining Engineering, 42-47 August (1996).

[11] W. R. Yernberg, "Santa Fe Pacific Gold Targets Million Ounces/Year Production," Mining Engineering, 39-43 September (1996).

[12] R. L. Lawson, "The United States," Mining, Annual Review, 70-75 (1996).

[13] J. I. W. Watterson, "A Theoretical Study of the Sorting of Witwatersrand Gold Ore," Report No. SRCNS 86/03, Schonland Research Centre for Nuclear Science, University of the Witwatersrand, South Africa 1986.

[14] Korotaeva, prokopchukand Emets, "Is It Possible to Optimize the Blending of Gold-Bearing Ore Samples," trans. from Zhurnal Analiticheskoi Khimii **40**, 1230-1236 (1985).

[15] E. T. Bramlit, "Plutonium Mining for Cleanup," Health Physics **55**, 451-53 (1988).

[16] J. R. Chen et. al., "Determination of the Occurrence of Gold in an Unoxidized Carlin-Type Ore Sample Using Synchrotron Radiation," Nucl. Instr. Meth. Phys. Res. **B22**, 394-400 (1987).

[17] J. Shukla and K. S. Pitre, "Eectrochemical Analysis of Gold in Ore," Analyst **121**, 79-81 (1996).

[18] B. de Celis, "X-Ray Fluorescence Analysis of Gold Ore," Applied Spectroscopy **50**, 572-575 (1996).

[19] B. David and C. Widham, "Statistical Control for the Production of Assay Laboratory Standards," Mining Engineering, 73-76 March (1996).

[20] Y. N. Bourmistenko, "Gamma-Activation Installation for Fast Determination of Gold and Its Accompanying Elements in Ore Samples," Isotopenpraxis 17, 241-243 (1980).

[21] B. N. Rybkin et. al., "Analysis of Geological Samples or Gold and Silver by the Method of Spectral Ratios," trans. from Atomnaya Energiya **66**, 42-44 (1989).

[22] I. A. Miransky et. al., "Multielemental Automated INAA System for Gold Ore Samples," J. Radioanal. Nucl. Chem, Articles **168**, 329-336 (1993).

[23] T. K. Magagula, "The Production of Nuclear Isomers by the (n,n') Reaction and Its Application to Selective Activation Analysis," M.S. Dissertation, University of the Witwatersrand, Johannesburg, South Africa (1998).

[24] Tonchev, Harmon and Brey, "Analysis of Ore Samples Employing Photon Activation of the Metastable States of Gold and Silver," Nucl. Instr. Meth. Phys. Res. A **422**, 926-928 (1999).

[25] D. Clifford, "Stacking Systems In Heap Leaching," Mining Magazine, 90-95 Mining Magazine (199).

[26] T. Mudder et. al., "Lab Evaluation of an Alternative Heap-Leach Pad Closure Method," Mining Engineering, 1007-1014 November (1995).

[27] "Handling Tailings, South African Experience, At Home and Abroad, and Work in Tajikistan," Mining Magazine, 90-95 February (1997).

[28] S.G. Vick, "Tailings Dam Failure at Omai in Guyana," Mining Engineering, 34-37 November (1996).

[29] R. G. Robins, "The Stability of Arsenic In Gold Mine Processing Wastes," *Precious Metals: Mining, Extraction and Processing*, Kudryk, Corrigan and Liang, eds., The Metallurgical Society of AIME, 241-249 (1984).

[30] P. Breban et. al., "Etude Des Possibilites D'Utilisation Analytique Des Isomeres Nucleaires Produits Par Reactions (γ,γ') Entre 6 et 8 MeV," Nucl. Instr. Meth. **158**, 205-215 (1979).

[31] R. Brey et. al., "The Possibility of Photon Activation Analysis of Radionuclides at Environmental-Levels," 6th International Conference on Nuclear Engineering, ICONE-6456 (1998).

[32] Tonchev, Harmon and King, "Application of Low Energy Photon Spectroscopy in Isomer Production of Hf, W, Ir, Pt, Au and Hg Using (γ,γ') Reactions," Nucl. Instr. Meth. Phys. Res A **422**, 510-512 (1999).

[33] Petrov, Trubachyev and Khan, "Processing of Solutions, Formed at Destruction Lewisite, With production of Arsenic Sulphide," 6th CBW Protection Symposium, Stockholm, Sweden, May (1998).

[34] Vettese, Asselineau and Dhermain, "Neutron Activation Analysis Techniques To Identify Arsenic In Chemical Weapons," 5th International Symposium On Protection Against Chemical and Biological Warfare Agents, Stockholm, Sweden, June (1995).

[35] Robinson, Swann and Rasmussen, "Gamma-Ray Widths of the 3.00-MeV Level of Al^{27} and the 3.13-MeV Level of P^{31}," Phys. Rev. 174, 1320-1323 (1968).

[36] F. R. Metzger, "Width of the 2.186-MeV 1- Level in Nd^{144}," Phys. Rev. 187, 1700-1704 (1969).

Chapter 2

PHOTONUCLEAR RESONANCE EXCITATION PHYSICS

In order to analyze potential industrial applications of nuclear isomer production using photonuclear resonance excitation (PRE), an understanding of the physics involved in the process is needed. Besides providing the tools necessary for determining the feasibility of exploiting this phenomenon, knowledge of the principles underlying the resonance excitation process is valuable in making decisions regarding selection of the different components to be used in an industrially attractive system. In this sense, attractive means a system capable of performing not only the particular function but in doing so practically, in a safe, economical and reliable fashion. This information is important for selecting the source and characteristics of the excitation radiation to use, identification and selection of the isomeric isotopes to be excited and the selection and layout of radiation measurement instrumentation. These areas can be addressed only with a thorough understanding of the physics of the photonuclear resonance excitation process. In particular, calculation of the induced isomeric activity for specific PRE applications must be carried out in order to optimize the system to meet desired performance goals.

In the broadest sense, photonuclear reactions may be thought of as including any and all interactions involving a photon and a nucleus either directly or indirectly. For the purposes of this project, however, attention is primarily focused on only those photonuclear reaction processes expected to be significant for industrial PRE applications. Investigation of the various photonuclear interaction processes indicates that resonant photon absorption of photons by nuclei leading to nuclear excitation has a larger interaction probability than other nuclear excitation pathways including non-resonant photon absorption and nuclear photon scattering. In light of this, the discussion below is heavily focused on the description and development of the physics of resonant photon absorption while more qualitative descriptions are given for other processes. Additionally, since the main emphasis of this research is the study of industrial applications of this phenomenon, in particular the photonuclear excitation of isomers rather than nuclear transformation reactions such as (γ,n), the majority of this work is focused on situations where the incident photons are less than or only slightly greater than neutron binding energies.

Following a brief introduction to photonuclear interactions, the different photonuclear excitation mechanisms broadly categorized into resonant and non-resonant reactions are explored in detail in §2.1. This section provides a qualitative understanding of the phenomenon and presents the mathematical tools necessary for carrying out induced isomer activity calculations relevant to industrial applications of photonuclear resonance excitation. In §2.2 different photonuclear and nuclear transformation processes are integrated into a system of equations for calculation of the population of a nuclear level of an arbitrary isotope in a sample undergoing photon irradiation. Following this, §2.3 discusses the use of this model to determine the activity of an isomer at some time during or after photon irradiation.

2.1 PHOTONUCLEAR INTERACTIONS PRIMER

In general terms, the physics involved in the production and use of nuclear isomers by PRE for any application can be broken into three parts: a) absorption of a photon by a nucleus resulting in excitation of the nucleus to either some discrete higher energy state or formation of a compound nuclear state, b) if the excited state is higher in energy than the isomer, de-excitation of this higher energy or compound nuclear state, through one or more reaction channels, to the isomeric state and c) de-excitation of the isomeric state of the nucleus. These different stages are addressed in this section starting with a brief introduction in §2.1.1 to some of the terms and analytical tools which are used in discussing nuclear excitation and decay. Following this §2.1.2 discusses photon excitation of the nucleus with attention being given first to a description of elastic absorption of photons by nuclei and then shifting to a discussion of elastic and inelastic photon scattering mechanisms which may also influence the photonuclear excitation. After this, the prompt decay of excited (or compound) nuclei and subsequent delayed decay of longer lived isomeric nuclei is explored. For the case of the higher energy excitations associated with compound nuclei, it is often useful to refer to statistical representations of the distribution of energy levels in the nucleus and use these together with similar models of the distribution of angular momentum at higher energy levels to calculate nuclear decay. At the lower excitation energies typical of isomeric nuclei, the discrete nature of the nuclear level structure together with reasonably well known tabulated values permits a more exact treatment of the de-excitation process. Together these sections on the photon excitation and decay of nuclear levels allows for the development of the analytical model describing the buildup and decay of particular isomeric levels in §2.2.

2.1.1 Background

One of the key elements of photonuclear resonance excitation is the radiation source. As will be discussed in the next chapter, for most applications practical design constraints such as power, current, induced activity, size and cost will lead the designer of a PRE system to choose a bremsstrahlung radiation source with a maximum endpoint energy of from 7 to 10 MeV. Limiting the radiation flux to this energy range simplifies the application in most situations by eliminating the need to include nucleon emission channels

in the calculations. This is because either the incident photon energies are too low for nucleon liberation or, when the photon energy is sufficiently high, because the actual photon flux at these energies according to the classical bremsstrahlung spectrum is so small that it may be neglected.

On the whole, the photon interaction mechanisms that will be of most interest for PRE applications will be resonant absorption of incident photons by the nucleus leading to excitation of discrete nuclear states at lower energies and excitation of compound nuclear states at higher energies.[a] The mathematics for describing these excitations is presented in detail in §2.1.2.1.1.1 and §2.1.2.1.1.2. Resonant photon absorption is not, however, the only photonuclear reaction which can occur in this energy range. In another resonant process superficially similar to the stimulated emission process observed in atomic electron transitions, an incident photon of the correct energy can stimulate the decay of an excited nuclear eigenstate resulting in the emission of a photon. Additional, non-resonant photon absorption interactions leading to nuclear excitation are also possible and are briefly discussed as well. However, due to the exceptionally small interaction probabilities for these second-order interactions, their influence in a commercial PRE applications will likely be negligible and therefore they are not included in the final modeling of the process.

Besides the various photon absorption interactions there are a number of photon-nucleus scattering interactions possible at these energies too. For completion, these are described in the subsection on scattering below where the basic mechanisms for the different processes are put forth. As with the non-resonant photon absorption processes, the full physical and mathematical description for the scattering pathways are not presented since their ultimate contribution to any commercial PRE applications would be negligible in comparison with resonant interactions.

Throughout this chapter reference will be made to one of the two schematic nuclear level diagrams of Figure 2-1, the specific diagram being distinguishable by the notation used. The diagram labeled a) presents the case where an incident photon of energy $E = E_f - E_i$ is absorbed by a nucleus initially in $| i \rangle$, the ground state, exciting the nucleus to a final state $|f\rangle$. In this diagram, $|f\rangle$ may either be a discrete level, having an exact energy, spin and parity, or it may represent a non-discrete state (compound state) of energy E where the spin is characterized using a probability distribution function rather than being exactly defined. This picture of the photonuclear excitation process is used in §2.1.2.1.1.1 and §2.1.2.1.1.2 which describe resonant photon excitation of discrete and compound nuclear levels. In the figure a more general picture is developed in diagram b) for use in the transition model of §2.2, where the initial state $| h \rangle$ need not necessarily be the ground state of the nucleus and transitions are allowed both to and from $| i \rangle$, involving states of higher and lower energies. In addition, diagram b) also alludes to the possibility that additional transition mechanisms to and from nuclei of different isotopes might also be possible; these are discussed in the final sections of the transition model.

---

[a] At higher excitation energies the discrete level structure of most nuclei (increasing with atomic mass) begins to blur as the average spacing between energy levels decreases. Eventually, at high enough energies, it becomes impossible to distinguish individual levels at a specific energy in most nuclei in terms of a specific spin and parity. To describe the excitation of nuclei at these energies use is often made of statistical models predicting the probability that an excited nuclear level at some energy exists having a particular spin and parity. Essentially, these models treat such excited nuclear levels as a collection of levels of different spin and parity at each energy, the sum of the probabilities of all such levels at each energy adding to unity. These models are said to describe a collective, or compound, nucleus.
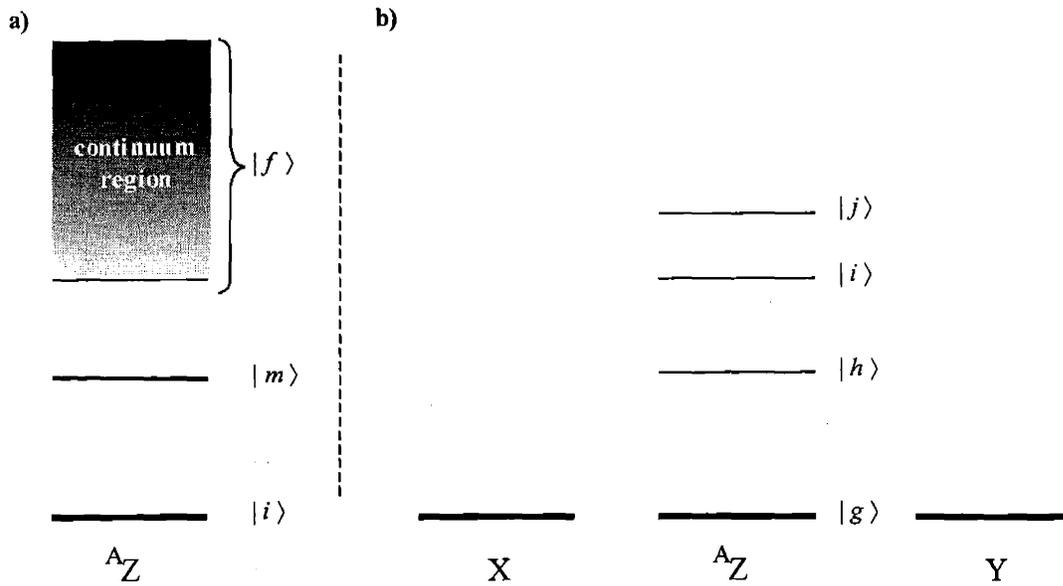
Figure 2-1 Nuclear level diagrams for *a)* specific interactions involving excitation from an initial state |*i*⟩ to some final state |*f*⟩ eventually with the potential of decaying to a metastable state |*m*⟩ and *b)* general transition reactions which may involve the ground state |*g*⟩ and arbitrary higher energy states |*h, i* and *j* ⟩.

For the industrial PRE applications explored in this dissertation, the ultimate objective of the photonuclear excitation process is the creation of isomers, regardless of whether the isomeric state is formed directly from photon absorption, from the decay of discrete higher energy nuclear states or the decay of even higher energy compound nuclear states. The transition times for the decay of higher energy states decaying to the isomer are by definition many orders of magnitude greater than typical isomer lifetimes; this allows one to neglect the path taken to form the isomer when evaluating its decay. There are two competing mechanisms involved in the decay of isomers, namely, decay through the emission of gamma-rays and decay via internal conversion. While decay through either gamma-ray transition or internal conversion can be measured, in photonuclear resonance excitation applications interest is focused primarily on the measurement of gamma-rays involved in the isomeric decay process. This is because of the superior penetrating ability of gamma-rays in comparison with electrons and low-energy x-rays, allowing measurements to be performed on bulk samples rather than limiting investigations to surface measurements and also allowing greater flexibility in the selection of the measurement instrumentation.

While an isomeric state |*m*⟩ will decay with some total decay probability $\lambda_T = \Gamma_m/\hbar$, it is often convenient to split the decay probability into a term representing the decay probability via gamma-ray emission, λ_γ, and a term representing the decay probability via internal conversion, λ_e,

$$\lambda_T = \lambda_\gamma + \lambda_e.$$

2-1

This relation is often simplified by introducing the internal conversion coefficient of the nuclear level, α_m, which is the ratio of the internal conversion decay probability to the gamma-ray decay probability,

$$\alpha_m = \frac{\lambda_e}{\lambda_\gamma}$$

2-2

which allows the total decay probability to be rewritten in the form

$$\lambda_T = \lambda_\gamma (1 + \alpha_m).$$

For many of the isomeric nuclei which are of interest for industrial photonuclear resonance excitation applications the internal conversion coefficient is small. In the construction of the eigenstate transition model below the de-excitation pathway, gamma emission vs. internal conversion, is irrelevant since only the total nuclear level decay probabilities are involved. When the isomeric gamma-ray activity (i.e., rate of photon emission) of an irradiated sample is determined from the actual number of isomeric nuclei existing in the sample, the internal conversion coefficient must be accounted for.

2.1.2   Photon Induced Nuclear Excitation

A great deal of theoretical and experimental work has been carried out over the past sixty years to understand the physical mechanisms through which electromagnetic radiation interacts with the atomic nucleus. In particular, a large body of work exists examining the excitation and de-excitation of nuclei via photon emission and absorption. Included in this area are theoretical studies aimed at explaining: the interaction of electromagnetic radiation with the nucleus, the structure of nuclei, the absorption of photons in giant dipole resonances, and the nature of long lived isomeric nuclei. A staggering effort has also focused on experimental endeavors aimed at: measuring the gamma decay of nuclei, verifying different models of the nucleus, determining the level structure of nuclei, and quantifying the nature of the interaction of electromagnetic radiation with nuclei. The theoretical foundations for understanding the scattering, absorption and emission of photons by nuclei were first laid out by Dirac in 1930, then elaborated upon by Bethe and Placzek in 1937.[1,2,3] Additional theoretical and experimental work has since been carried out, especially following the development of Mossbauer spectroscopy.[4-18]

In order for the nucleus to be excited from some arbitrary initial energy eigenlevel $|h\rangle$ to some arbitrary final energy eigenlevel $|i\rangle$, such that $E_i > E_h$, energy must be introduced into the nuclear system. For the case of photon-nucleus interactions, the incident photon must have an energy of at least $E_{ih} = E_i - E_h + \varepsilon$ (ε being a kinematic correction always > 0 depending upon the interaction). The principle mechanism through which photons excite nuclei is two-body photon absorption, wherein an incident photon having an energy equal to the difference in energy between some excited level in a nucleus and the current state (plus a small amount needed to correct for recoil) is completely absorbed by the nucleus. These reactions are often referred to as absorption interactions because following the reaction no outgoing photons are produced.

In addition to absorption, the possibility also exists that an incident photon could participate in a three way interaction involving the nucleus as well as some intermediate structure such as individual atomic electrons, the atomic electron Coulombic field or the nuclear Coulombic field. In these reactions, the sum of the energy of the incident photon radiation must be shared with this intermediate structure due to conservation requirements. In many cases, these three-body processes are referred to as scattering interactions because a second photon is observed leaving the reaction.

2.1.2.1   Absorption

As mentioned above, the principal photon interaction mechanism responsible for nuclear excitation is direct photon absorption, which is a resonant process. In addition to direct absorption, however, it is also theoretically possible for photons to excite nuclei via more complicated processes. In comparison with direct absorption, the interaction probabilities for three-body interactions are typically many times smaller;

however, in some cases nuclear excitation through these other, non-resonant processes could be of interest if care is given in choosing an appropriate irradiation source. The direct excitation of the nucleus via resonant processes is presented in §2.1.2.1.1, including excitation of both discrete levels as well as excitation of compound nuclear levels. Following this, consideration is given to non-resonant excitation mechanisms in §2.1.2.1.2.

2.1.2.1.1 Resonance Interactions

When a nucleus is irradiated by photons having an energy corresponding to the difference in energy between the nucleus' current energy eigenstate and some other eigenstate of the nucleus (either higher or lower in energy) the possibility exists that the nucleus will be induced to make a transition to that other eigenstate. In upward transitions, where the photon energy is absorbed by the nucleus, the resulting system is said to be an excited state. In general, at lower incident photon energies (~2 to 4 MeV), nuclear excitation results from the transitioning of the nucleus to discrete higher energy eigenstates. At higher incident photon energies nuclear excitation results in the formation of higher energy, collective states of the nucleus and creation of a compound nucleus. If the nucleus subject to irradiation happens to be in an excited state it is also possible that, provided photons of the correct energy are present, the nucleus will be induced to make a downward transition to a lower energy excited state or the ground state. This phenomenon, which is similar in principle to the stimulated emission process employed in lasers, takes place with an interaction probability similar to the complimentary excitation process and could be of importance in the analysis of situations where a significant fraction of the nuclei are present in the excited state. The following three sections discuss in some detail the mathematical tools used for analyzing the resonant excitation and de-excitation of nuclei involving discrete and compound states.

2.1.2.1.1.1 Discrete Level Photon Absorption

In discrete level photon absorption the nucleus makes a transition from some initial eigenstate $|i\rangle$ of spin J_i and energy E_i to a final eigenstate $|f\rangle$ having spin J_f and energy E_f. This is a resonant process and thus the incident photon must have an energy[a] near $E_{f-i} = E_f - E_i$ in order for the reaction to proceed with an appreciable interaction probability. Based upon a theoretical derivation, the cross section $\sigma_{i \to f}(E)$ for the resonant absorption of a photon of energy E by a nucleus leading to the excitation of a discrete nuclear state is given by[1,2,10]

$$\sigma_{i \to f}^{abs}(E) = \frac{\pi \lambda^2}{2} \frac{(2J_f + 1)}{(2J_i + 1)} \frac{\Gamma_{fi}(\Gamma_f + \Gamma_i)}{(E - E_{f-i})^2 + \frac{1}{4}(\Gamma_f + \Gamma_i)^2}, \qquad 2\text{-}4$$

where λ is the wavelength of the absorbed photon divided by 2π and E_{f-i} is the difference in energy between $|f\rangle$ and $|i\rangle$. The term Γ_{fi} is the partial width for decay from the eigenstate $|f\rangle$ to the eigenstate $|i\rangle$, Γ_f is the total width of the eigenstate $|f\rangle$ and Γ_i is the total width of the eigenstate $|i\rangle$ (which is zero if $|i\rangle$ represents the groundstate). Using this equation it is possible to calculate the probability that an absorbed incident photon resonantly excites a nucleus to any excited nuclear state. If the excited state $|f\rangle$ is the isomer than the equation gives the isomeric excitation cross section. If $|f\rangle$ represents some state higher in

---

[a] For resonant absorption the energy available for transfer from the incident photon to the nucleus must exactly match the difference in energy between the initial and final states in the nuclear transition. Due to external factors such as recoil and thermal broadening, however, the actual energy of an incident photon needed for resonant absorption might be slightly different from the transition energy.

energy than the isomer the isomeric excitation cross section is calculated by multiplying the cross section for direct excitation to $|f\rangle$ by the absolute branching ratio[a] from $|f\rangle$ to the isomer.

As the mechanism underlying the field of Mossbauer spectroscopy, the physics of the direct resonance photon absorption process has been extensively studied. In that context an important complication in the resonant absorption process arises due to thermal vibrations in the target nuclei as well as the isotopic radiation sources used for irradiation, where thermal motion of the nuclei results in an effective broadening of the resonant absorption cross section by many orders of magnitude. In addition to this thermal, or Doppler, broadening of the absorption cross section, recoil effects in the emission of the decay photon and similar recoil effects in the absorbing nucleus require that for an incident photon to be absorbed it must have an energy slightly greater than the actual energy difference between the initial and final nuclear states of the transition. By accounting for these slight energy differences and the Doppler effect, it is possible to decipher various properties of the matrix containing the nuclei.

For an industrial application where the intermediate goal is excitation of nuclei to isomeric states many of the interesting factors mentioned above which make Mossbauer spectroscopy such a useful tool become a hindrance when discrete, isotopic radiation sources are used. In later chapters it will become clear that most industrial application systems will be designed to maximized the induced isomeric activity in the target or sample being irradiated. When isotopic radiation sources are used to create isomers, direct resonant photon absorption is essentially the only excitation mechanism having a sufficiently large enough interaction probability (cross section and photon intensity) to be considered relevant. While nuclei may occasionally be excited to a short lived higher energy state and then decay to the isomer, depending upon the availability of appropriate sources, the excitation of isomers with such sources is predominately based upon directly creating the isomer itself through resonant photon absorption. In order to increase the isomer production rate in light of thermal and recoil effects a number of tricks can be employed including: the cooling of emitter and/or target to reduce thermal broadening, the use of novel crystal matrices to alter recoil effects, the heating of the emitter to thermally boost the emitted photon energy or the use of a mechanical system (e.g., high speed rotor or piezoelectric vibrator) to increase the emitted photon energy.[19,20,21]

Using a continuous photon source, such as the x-ray output from electron accelerator bremsstrahlung, the direct resonance photon absorption pathway for isomer creation becomes much more practical. With such a radiation source the thermal broadening and recoil problems associated with discrete radiation sources essentially disappear. In addition, due to the continuous distribution in the energy of such sources many higher energy levels can be excited, thereby increasing the potential for creation of the isomeric state resulting from the decay of higher energy levels. It is worth noting here that, for essentially the same reason isomeric states are long lived compared to other nuclear states (large differences in angular momentum between isomeric states and ground states for most nuclei), the decay of most nuclear states within about 1 to 2 MeV in energy of isomeric states do not typically have significant branching ratios to isomeric states. This is primarily because large differences in angular momentum require higher order electromagnetic transitions and have correspondingly smaller probabilities of occurring.

---

[a] The absolute branching ratio is simply the sum of the products of the normalized transition probabilities for each decay pathway of a nucleus in some eigenstate $|f\rangle$ which yield the isomer $|m\rangle$. For example, if a nucleus has the decay scheme below the branching ratio of the eigenstate $|f\rangle$ to the isomeric state $|m\rangle$ is 50% but the absolute branching ratio for the decay of $|f\rangle$ to the isomer, including the intermediary eigenstgate $|j\rangle$, is 62.5%.
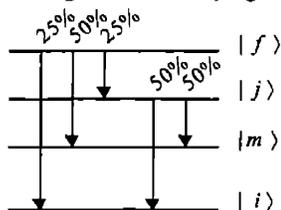
As will be seen in the following section, excluding isomeric levels which have unusually large angular momentum for their energy, the probability distribution for the spin of nuclear levels at lower energies is rather narrow. Since these levels have spins closer in magnitude to the groundstate and other short lived states, the probability that the decay of these states skips over an isomer in the ultimate return to the groundstate is usually large. At higher energies though, as the spin probability distribution broadens and more of the higher energy states have spins closer in magnitude to that of the isomer, branching ratios to isomeric states grow larger. In addition to the broadening of the spin probability distribution at higher energies, the spacing between nuclear levels becomes smaller; eventually the spacing between levels becomes so narrow that a more complicated approach must be taken in calculating the isomeric excitation cross section.

2.1.2.1.1.2   Compound Nucleus Photon Absorption

When photon radiation sources of higher energy are used to excite isomeric nuclei, energies exceeding those of discrete energy eigenstates in the nucleus, the possibility exists that these photons may be resonantly absorbed by the nucleus as well. In this case, we consider the combined system of the photon and nucleus as a compound nuclear system in accordance with Bohr's assumption for compound nuclei. That is, we assume that this process can be separated into two distinct components: (a) creation of the compound nucleus and (b) the decay of the compound nucleus. In doing this one essentially considers compound nucleus photon absorption as absorption by an infinite distribution of nuclear levels continuous in energy and quantized in spin. At these energies, instead of referring to exact nuclear structure features of the nuclear level such as energy, momentum or parity, we instead refer to a statistical model, or level probability density, of the angular momentum of the excited nuclear states, $\rho\,(J)$. There are a number of papers in the literature exploring the application of this model in different processes; several of these address the study of isomeric yield ratios through various excitation pathways including photonuclear reactions such as (γ,n) and $(\gamma,2n)$.[22-32] In the paragraphs that follow, a new theoretical approach is developed for calculating photonuclear resonance excitation cross sections, at energies below neutron binding energies, for the production of isomers.

The calculations are carried out by breaking the problem up into a number of smaller pieces as follows:

a) *photon absorption by the nucleus* To begin the calculations, the photon absorption cross section for an incident photon of energy E is calculated for excitation of the nucleus of interest from an initial energy and angular momentum state $|E_i, J_i\rangle$ ($E_i = 0$ for the ground state) to a final, excited state $|E_f, J_f\rangle$. For incident photon energies less than 1to 2 MeV, knowledge of nuclear structure is sufficient for most nuclei to allow exact calculations. At higher energies, as the energy spacing between discrete nuclear levels for nuclei of higher masses decreases, it becomes necessary to rely upon a statistical model to predict the probability of finding nuclear states of distinct angular momentum at a particular energy. Using such a model, the absolute resonant photon absorption cross section is calculated. In addition to the angular momentum dependence in the absorption stage, the absorption cross section is also dependent upon the final state branching ratio to the initial state. It is known that the decay transition rates are sensitive to the multipole order, l, of the transition; for this work only electric dipole excitations, having the strongest interaction probabilities, will be considered such that $J_f = J_i - 1, J_i, J_i + 1$.

b) *gamma-ray cascade decay of the compound nucleus* After the photon absorption cross section has been calculated, the next step is to calculate the decay of the excited state. Due to the statistical nature of the model and the restriction of transitions to dipole excitations, for each incident photon energy there will be a distribution of 3 excited states (2 if the initial eigenstate is 0 or ½) depending upon the angular momentum of the initial nuclear state. The approach taken in this paper is to calculate the average number of transitions, or photon multiplicity, taking place in the decay of a particular excited energy state and then to calculate the spin dependent probability density of the nucleus after decay through the calculated number of gamma-ray transitions. As in part a) all transitions in the cascade decay are limited to dipole transitions.

c) *final evaluation of eigenstates and partitioning between ground and isomeric states* Once the final spin dependent probability distribution has been tracked through the gamma ray cascade decay of the excited nucleus, the final step is to partition the resulting distribution between the ground state $|0, J_i\rangle$ and isomeric state $|E_m, J_m\rangle$ where, in general J_i is less than J_m. The approach taken in this paper is to assign all probability densities $J \geq J_m$ to the isomer, some fraction D of the $J = J_m - 1$ probability density to the isomer and the remaining probability density to the ground state, where D is determined by inspection of the known nuclear transition probabilities for the target nucleus at lower energies.

Although numerous sources have addressed different aspects of the problem addressed here, the extensive body of experimental work dealing with the issue significantly overshadows the few theoretical attempts to analyze the problem. This methodology is similar to that originally proposed by Huizenga and Vandenbosch[22,28] for the analysis of isomeric cross section ratios. Since then, significant advances have been made to this approach including the introduction theoretical derivations of various nuclear structure parameters, which the original formalism was forced to address through parametric analysis, and comparison with experimental data. The most comprehensive application of the VH[a] formalism has been in the development of the GNASH-FKK computer code for the calculation of cross sections and emission spectra.[33]

We start with the cross section $\sigma_{i \to f}(E)$ for the absorption of a photon of energy E by a nucleus originally in the state $|i\rangle$, exciting the nucleus to the state $|f\rangle$, which is given in §2.1.2.1.1.1. When the incident photon energy exactly matches that of some nuclear eigenstate of energy U (taking into account a small correction factor δ described below), and assuming the absorbing nucleus is initially in the ground state, the photon absorption cross section becomes

$$\sigma_{0 \to f}^{abs}(E) = \frac{\pi \lambda^2}{2} \frac{(2J_f + 1)}{(2J_0 + 1)} 4 \frac{\Gamma_{f0}}{\Gamma_f}. \qquad \text{2-5}$$

Due to the complex nature of most nuclei, unfortunately, it is impractical to analytically determine the partial widths or decay branching ratios of particular nuclear levels for nuclei larger than the deuteron. However, in some cases rather simple models may be used for the reckoning of isomeric transition probabilities between nuclear levels, the most useful of which being that proposed by Weisskopf for transitions in nuclei between energy eigenstates having large net differences in angular momentum.[10] Typically these simplistic models are found to agree with observations to within an order of magnitude at best. A more sophisticated modeling approach, which combines some experimentally observed characteristics of the nuclear giant dipole resonance to form a gamma-ray strength function, is used here. Noting that the ratio of radiation widths above is simply the branching ratio of the eigenstate $|f\rangle$ to the ground state, also known as the transmission coefficient $T^{X l}(U)$, this equation may be rewritten as

$$\sigma_{0 \to f}^{abs}(E) = \frac{\pi \lambda^2}{2} \frac{(2J_f + 1)}{(2J_0 + 1)} 4 T^{Xl}(U), \qquad \text{2-6}$$

where $T^{X l}(U)$ may be evaluated in terms of the energy-dependent gamma-ray strength function, $f_{Xl}(E)$, according to

$$T^{Xl}(E) = 2\pi f_{Xl}(E) E^{2l+1}, \qquad \text{2-7}$$

where $X l$ indicates the multipolarity of the gamma-ray transition.

---

[a] Although the original paper describing this technique was published by Huizenga and Vandenbosch it is more commonly referred to in the literature the using the term VH.

A number of different relations for $f_{X_1}(E)$ have been published in the literature. For this work a relationship for the gamma-ray strength function, including a Lorentzian resonance component related to the nuclear giant dipole resonance, along with a low-energy correction factor, of the following form is used.[34]

$$f_{E1}(E) = K_{E1} \left[\frac{E\,\Gamma(E)}{(E^2 - E'^2)^2 + E^2\,\Gamma(E)^2} + \frac{0.7\,\Gamma\,4\pi^2\,T(E)^2}{E^5} \right] \sigma_0\,\Gamma \qquad \text{2-8}$$

In this equation K_{E1} is a normalization constant (K_{E1} = 8.68 x 10^{-8} mb^{-1} MeV^{-2}), $\Gamma(E)$ is given by

$$\Gamma(E) = \Gamma \frac{E^2 + 4\pi^2\,T^2}{E^2}, \qquad \text{2-9}$$

T is the nuclear temperature given by

$$T(E) = \sqrt{\frac{B_n - E}{a}}, \qquad \text{2-10}$$

σ_0, Γ and E' are parameters describing the nuclear giant dipole resonance and a represents the nuclear level density parameter (described below). For dipole transitions from one state to another, a change in parity of the transition indicates an $E1$ transition while no change indicates an $M1$ transition. Since $f_{E1}(E)$ is larger than $f_{M1}(E)$, taking all transitions to be $E1$ transitions will overestimate the actual strength function, and thus the eventual isomeric excitation cross section, assuming an even distribution exists in the parity of the compound nucleus excited states.[22]

Following the VH scheme, the statistical model[3,35] used in this paper to predict the density of nuclear states as a function of angular momentum J is given by

$$\rho(J) = \rho(0)(2J+1)\exp\left[\frac{-(2J+1/2)^2}{\sigma^2} \right], \qquad \text{2-11}$$

where $\rho(0)$ is the probability density of levels with spin 0 and σ, the spin cut-off factor, serves to limit the distribution of spins at higher values of angular momentum. A large number of papers exploring the use of Eq. (2-11) have analyzed the sensitivity of $\rho(J)$ upon the spin cut-off factor.[12,23-35] Originally, σ was assumed to be a constant independent of the energy of excitation U of the compound nucleus but is now usually related to the nuclear temperature T and the moment of inertia θ of the nucleus according to

$$\sigma^2 = \frac{T\theta}{2} = C_{SC}\,\sqrt{aU}\,A^{\frac{2}{3}}, \qquad \text{2-12}$$

where C_{SC} is a constant determined empirically through comparison with experiments, a is the density of energy eigenstates in the nucleus at the excitation energy U and A is the mass number of the nucleus.[36,37]

The nuclear excitation energy U has been introduced to distinguish this value from the energy of the incident photon E inducing the excitation, which are related according to[38]

$$U = E - \delta, \qquad \text{2-13}$$

where δ is a small correction of the form

$$\delta = \frac{a}{A^{\frac{2}{3}}}$$

2-14

which accounts for the pairing energy between nucleons. A number of papers have been published exploring different approaches for modeling the nuclear level probability density $\rho(U)$ and the nuclear level density a.[30,39,40,41,42,43] The level density has been shown to have an energy dependence[44]; however, the sensitivity of $\rho(J)$ to this dependence for the calculations in this work is small. In this paper the level density is taken as[45]

$$a = a_0 \, A^{\frac{2}{3}} \left(\bar{j}_Z + \bar{j}_N + 1 \right),$$

2-15

where the constant $a_0 = (0.095 \pm 0.007)\,\mathrm{MeV}^{-1}$ has been determined experimentally and the quantities $\bar{j}_Z$ and $\bar{j}_N$ are the mean spin values of protons and neutrons averaged over shells near the Fermi level of the nucleus, respectively.

Combining the resonant photon absorption cross section with the above statistical model, the first step in the calculations as outlined above may be carried out. Following calculation of the initial population density after photon absorption, the next step is to evaluate the nuclear spin probability distribution of the nucleus through the subsequent gamma-ray cascade decay. In order to do this an estimate must be made of the number of gamma-rays involved in the cascade, the gamma-ray multiplicity. In many papers the gamma-ray multiplicity is assumed to be independent of the excitation energy. However, at higher excitation energies it seems reasonable to expect more photons to participate in the decay cascade; for this paper the average number of photons involved in the gamma-ray cascade is taken to be of the form[46,47]

$$N_\gamma(E) = \frac{(a\,E_f)^{\frac{1}{2}}}{L+1}$$

2-16

where L is the multipolarity of the electromagnetic transition ($L = 1$ for dipole transitions). As illustrated below, predictions of non-integral numbers of photons in the nuclear gamma-ray cascade of nuclei are interpreted as weighted combinations of the integral numbers just greater than and less than the predicted multiplicity. This is done by calculating the multiplicity probabilities according to

$$P_<(E) = N_> - N_\gamma(E) \quad \text{and} \quad P_>(E) = N_\gamma - N_<(E)$$

2-17

such that $P_<(E) + P_>(E) = 1$, where $P_<(E)$ represents the probability that the multiplicity of the decay is $N_<$ and $P_>(E)$ represents the probability that the multiplicity of the decay is $N_>$, where $N_<$ and $N_>$ are the integral numbers just less than and just greater than the theoretical multiplicity, $N_\gamma(E)$, respectively.

In order to illustrate the application of the equations introduced here, the following will demonstrate the use of the resonant photon absorption cross section and statistical model equations to determine the isomeric excitation cross section for 4 MeV photons exciting the 16.06 second isomer of [89]Y. A list of the nuclear constants used in these calculations is provided in Table 2-1. The first step in the calculations is to determine the level density according to Eq. (2-15). Using the mean proton and neutron spin values of Abdelmalek and Stavinsky yields $a = 8.834$ MeV^{-1}. With the level density, the next step is to determine the effective excitation energy of the nucleus corresponding to absorption of a 4 MeV photon using Eqs.(2-13) and (2-14), which results in $U = 3.557$ MeV. One final preliminary calculation to carry out is the determination of the spin cut-off factor, which, using Eq. (2-12), is found to be 3.15 where a constant factor of $C_{SC} = 0.0888$ was used.

TABLE 2-1. Parameters of the ^{89}Y ground state and isomeric nuclear levels and the giant dipole resonance (GDR) used to calculate the ^{89}Y(γ, γ')^{89m}Y cross-section.

Nuclear Parameters:			Values:	Reference Source:
	Z		39	
	N		50	
	A		89	
Neutron Binding Energy,	B_N	[MeV]	11.478	48
Proton Binding Energy,	B_P	[MeV]	7.073	48
Ground State Energy,	E_0	[MeV]	0	48
Ground State Spin,	J_0	[$\hbar$]	1/2	48
Isomeric State Energy,	E_m	[MeV]	0.90896	48
Isomeric State Spin,	J_m	[$\hbar$]	9/2	48
	$\bar{j}_z$		1.165	45
	$\bar{j}_N$		2.5	45
GDR Parameters:				
Energy,	E'	[MeV]	16.79	49
Temperature,	T	[MeV]	0.605	49
Width,	Γ	[MeV]	3.96	49
	σ_0	[MeV]	205	49

With the level density parameter a, excitation energy U and the spin cut-off factor σ, both the spin probability density for ^{89}Y corresponding to excitation from a 4 MeV photon and the resonant photon absorption cross section at 4 MeV may be calculated for various excited state spins, J. These two results are presented in Figure 2-2 for excited state spins $1/2 \leq J \leq 31/2$. Excluding transitions of quadrupole or higher multipolarity, resonant photon excitation of the $J = 1/2$ ground state of ^{89}Y leads only to the $J = 1/2$ and 3/2 states in the excited nucleus. Multiplying the spin probability distribution at 4 MeV and resonant photon absorption cross section at these two spins and summing the results yields the absolute resonant photon absorption cross section for ^{89}Y for 4 MeV photons, $\sigma_{0 \to f}^{abs}(E = 4\,\text{MeV}) = 0.440\,\text{mb}$.
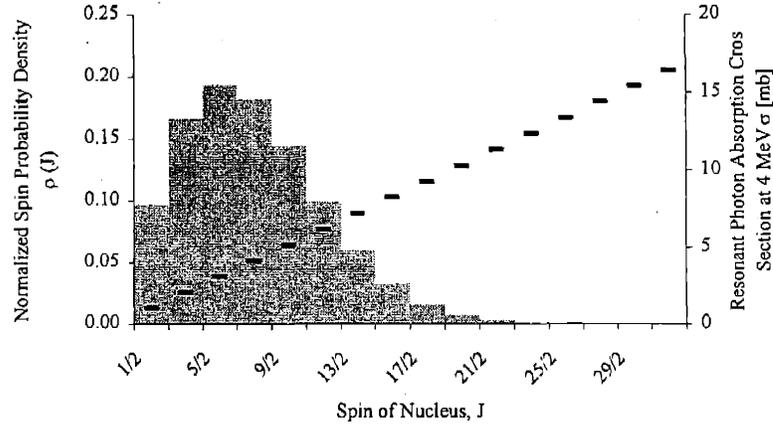
Figure 2-2 Normalized probability spin distribution (gray histogram) for the ^{89}Y nucleus excited by resonant absorption of a 4 MeV photon and theoretical 4 MeV resonant photon absorption cross sections (bars) for different excited state spins.

Individually, the product of the resonant photon absorption cross sections for the two spins 1/2 and 3/2 and the transition probability to reach these spin states are 0.099 mb and 0.341 mb, respectively. With these two values, the second step in the calculations can take place, namely, decay of the excited nuclear states through a multiple photon gamma-ray cascade. Using Eq. (2-16), the photon multiplicity is found to be N_γ (4 MeV) = 2.97 which, applying Eqs. (2-17), indicates a 97% probability that the cascade will contain 3 photons and a 3% probability that the cascade will consist of two photons. For both possible excited state spins J, the spin probability densities of the three possible dipole transition states (J - 1, J and J + 1) following the decay of one and two photons have been calculated and are presented in Table 2-2.

Table 2-2. Change in the spin probability distribution of ^{89}Y originally excited by resonant absorption of a 4 MeV photon, starting with spin J =1/2 and J = 3/2, after one, two and three electromagnetic dipole transition decays.

Number of transitions in the gamma-ray cascade	Normalized Spin Probability Distribution				
	$J = \dfrac{1}{2}$	$J = \dfrac{3}{2}$	$J = \dfrac{5}{2}$	$J = \dfrac{7}{2}$	$J = \dfrac{9}{2}$
0	1				
1	0.37	0.63			
2	0.25	0.43	0.31		
3	0.15	0.38	0.34	0.13	
0		1			
1	0.22	0.37	0.42		
2	0.12	0.37	0.34	0.17	
3	0.10	0.29	0.36	0.20	0.05

At this point it is possible to calculate the resonant photon absorption cross section at 4 MeV for ^{89}Y as a function of the probability that the nucleus will be left in a spin J following a gamma-ray cascade decay of

the initially excited ^{89}Y nucleus. To do this, we first multiply the normalized spin probability distributions of Table 2-2 by the appropriate weighting probabilities (3% and 97%) for the occurrence of two or three photons in the cascade and then multiply by the appropriate resonant photon absorption cross sections corresponding to the starting spin state. After this, the resultant cross sections from the two possible starting spins are summed together for each final spin state, which yields the cross section for excitation of a nucleus of ^{89}Y to a spin J by absorption of a 4 MeV photon after the cascade decay of the excited nucleus, which is presented in the following table.

Table 2-3. Cross section in millibarns for the resonant excitation of 4 MeV photons of ^{89}Y leading to the indicated spin states following the dipole decay of the initially excited nucleus through a gamma-ray cascade.

$J = \dfrac{1}{2}$	$J = \dfrac{3}{2}$	$J = \dfrac{5}{2}$	$J = \dfrac{7}{2}$	$J = \dfrac{9}{2}$
0.049	0.137	0.156	0.080	0.016

The photonuclear resonant excitation cross section for the reaction ^{89}Y(γ,N$_\gamma\gamma$)^{89m}Y can now be calculated by evaluating the final decay of the post-cascade nucleus, which we take to have the spin probability distribution of Table 2-3. Examining the nuclear structure of ^{89}Y (see Table 2-4) one observes that: a) the decay of nuclear levels with $J < 5/2$ does not generally lead to the isomeric state while the decay of nuclear levels with $J > 5/2$ generally does lead to the formation of the isomeric state and b) the decay of nuclear levels with the same parity as the isomeric state generally leads to formation of the isomer while opposite parity nuclear levels generally do not lead to isomer formation. Considering this, we parse the distribution of Table 2-3 by assuming that the fraction of the isomeric cross section leading to spins 1/2 and 3/2 decay without formation of the isomeric state, that all spins of 7/2 or greater do lead to formation of the isomeric state and that a quarter of the time the decay of the 5/2 spin state leads to formation of the isomeric state while the rest of the time the decay of this state skips over the isomeric state. (Based on assuming that the 5/2 state has an equal chance of having either + or - parity and that only 50% of those cascade decays which result in 5/2+ yield the isomer.) Therefore, the cross section for excitation of ^{89}Y by a 4 MeV photon is calculated to be 0.135 mb.

Table 2-4 Low energy nuclear level parameters of ^{89}Y and the fraction
of decay transitions for each level which eventually lead to formation
of the yttrium isomeric state (bold).[48]

Nuclear Energy Level [MeV]	Nuclear Level: Angular Momentum and Parity				Eventual Branching Ratio to ^{89m}Y
0	1/2$^-$				——
0.90896			9/2$^+$		——
1.50726	3/2$^-$				0
1.74457		5/2$^-$			0
2.22239		5/2$^+$			0.69
2.52987			7/2$^+$		1.00
2.56624				11/2$^+$	1.00
2.62204			9/2$^+$		1.00
2.8718			7/2$^+$		1.00
2.8812	3/2$^-$				0
2.8947				13/2$^+$	1.00
3.0676	3/2$^-$				0

Following the procedure outlined above, it is straightforward to evaluate the isomeric photonuclear resonant excitation cross section for energies less than the neutron binding energy. However, the usefulness of this approach is limited to energies above a few MeV, being applicable only in the nuclear continuum regime. At lower energies, where nuclear structure knowledge is more complete, the isomeric excitation cross section can be evaluated exactly in most cases. The complete results of the analysis of the energy dependent photonuclear resonant excitation cross sections for the formation of ^{89m}Y, ^{103m}Rh and ^{197m}Au are presented next.

Although an appreciable amount of work has been done to study the creation of isomers through photonuclear processes, comparatively few experimental results have been reported presenting energy dependent resonant photon absorption cross sections leading to isomer creation. That which does exist is published only in graphical form, generally without any indication of errors related to either the measurement or interpretation of the experimental data. The results of the analytical procedure described above are compared to data for the isotopes ^{89}Y, ^{103}Rh and ^{197}Au in the following sections. Of these three nuclei, the model closely agrees with experimental data for yttrium for all energies up to the neutron binding energy while the model is less accurate for rhodium and gold as the photon energy approaches the neutron binding energy.

2.1.2.1.1.2.1   Yttrium-89

Following the assumptions outlined in the sample calculations above, the energy dependent photonuclear isomeric excitation cross section for ^{89}Y has been calculated and is presented together with an interpretation of published experimental results[50] for the process in
Figure 2-3. The reported experimental results were determined by carrying out irradiations and excitation measurements with increasing bremsstrahlung beam energies and then applying the usual photon difference method to determine the energy dependent cross section. Silva and Goldemberg performed measurements down to 4 MeV and extrapolated their results to lower energies. Examining the original experimental results presented in the paper, the excitation measurements appear to have uncertainties of ~50%; the reported cross section however provides no estimate of uncertainty. In the figure below, the data was read from the reference by hand and is presented as individual points while in the reference the data is presented as a curve.
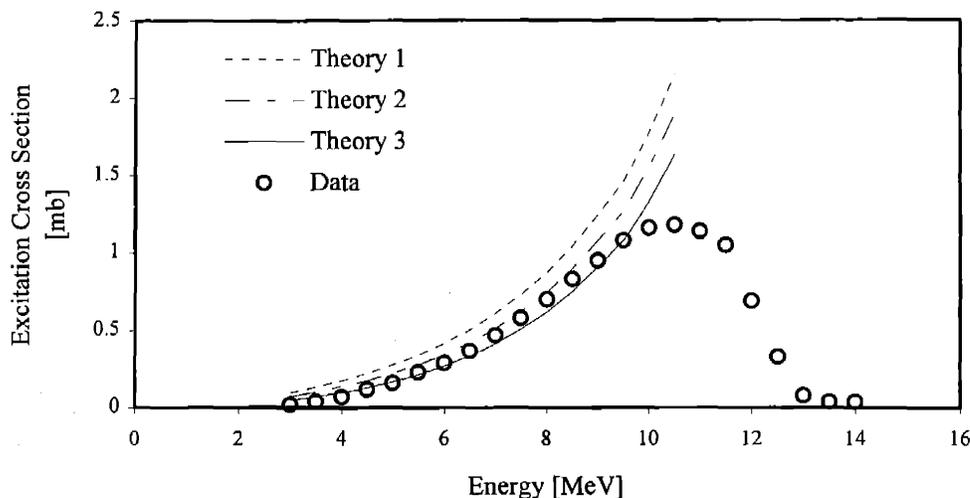
Figure 2-3 The theoretical (line) and measured (circles) photonuclear resonant
absorption cross section for production of the isomeric state of ⁸⁹Y. The
Theory 1 line assumes a 50% contribution from 5/2 spins states. The
Theory 2 line assumes a 25% contribution from 5/2 spin states. The
Theory 3 line assumes no contribution from the 5/2 spin state. All three
theory lines assume complete feeding from spin states greater than 7/2.

For yttrium, the statistical model approach appears to be effective at predicting the isomeric excitation
cross section for all energies up to the neutron binding energy. Looking over the low energy structure of
the nucleus in Table 2-4, trends in the branching ratios of different levels to the isomer can be inferred in
terms of both spin and parity. This allows one to assign the different spin densities following the decay
cascade to the isomeric state with a high level of confidence.

2.1.2.1.1.2.2   Rhodium-103

For calculation of the photonuclear excitation cross section of ^{103m}Rh, interpretation of the tabulated nuclear
structure data is less transparent. Referring to Table 2-5, the decay of higher energy states in ^{103}Rh to the
isomeric level is not quite as unequivocal as for yttrium. While for this nucleus both the 3/2 and 5/2 states
appear to feed into the 7/2 isomeric state completely, dependent upon a match in parity with the isomer, the
decay of many of the higher energy states including even the 7/2⁺ 0.60745 MeV level cannot be so easily
generalized. Calculations have been carried out for 3/2 spin state branching ratios of 0% together with 5/2
spin state feedings of 50%, 25% and 0% while levels of spin 7/2 and greater have been assigned complete
branching to the isomeric state.

Table 2-5 Low energy nuclear level parameters of ^{103}Rh and the fraction of decay transitions for each level which eventually lead to formation of the rhodium isomeric state (bold).[48]

Nuclear Energy Level [MeV]	Nuclear Level: Angular Momentum and Parity							Eventual Branching Ratio to ^{103m}Rh
0	$1/2^-$							—
0.039756				$\mathbf{7/2^+}$				—
0.09304					$9/2^+$			1.000
0.294284		$3/2^-$						0
0.357408			$5/2^-$					0
0.536838			$5/2^+$					0.996
0.60745				$7/2^+$				0.248
0.650085			$5/2^+$					0.873
0.651798		$3/2^+$						0.998
0.65772					$11/2^+$			0
0.7805					$9/2^+$			0.479
0.80307	$1/2^-$	$3/2^-$						
0.82146						$13/2^+$		
0.84758			$7/2^-$					
0.88047			$5/2^-$					
0.9201					$9/2^-$			
1.27704		$3/2^-$						
1.3495						$13/2^+$		
1.52465							$15/2^+$	
1.63764						$13/2^-$		
1.71741							$17/2^+$	
2.2212							$15/2^-$	
2.34535							$17/2^-$	
2.4186							$17/2^-$	0

Carrying out the model calculations for rhodium in the manner outlined above, the theoretical excitation cross section has been determined for incident photon energies from 4 to 10 MeV and may be compared with experimentally determined values,[51-54] both of which are plotted in Figure 2-4. For the experiments used to collect these data a bremsstrahlung beam was again used as the irradiation source. In this case experiments were carried out in ~1 MeV increments starting with a beam having a maximum energy of 5.9 MeV; uncertainties in the original measurements appear to have ranged from ~50 to 25% as the energy was increased but no estimate of uncertainty is provided in the deduced (γ,γ') cross section. In Figure 2-4, the experimental data is presented as discrete points while in the reference the data is given as a curve.
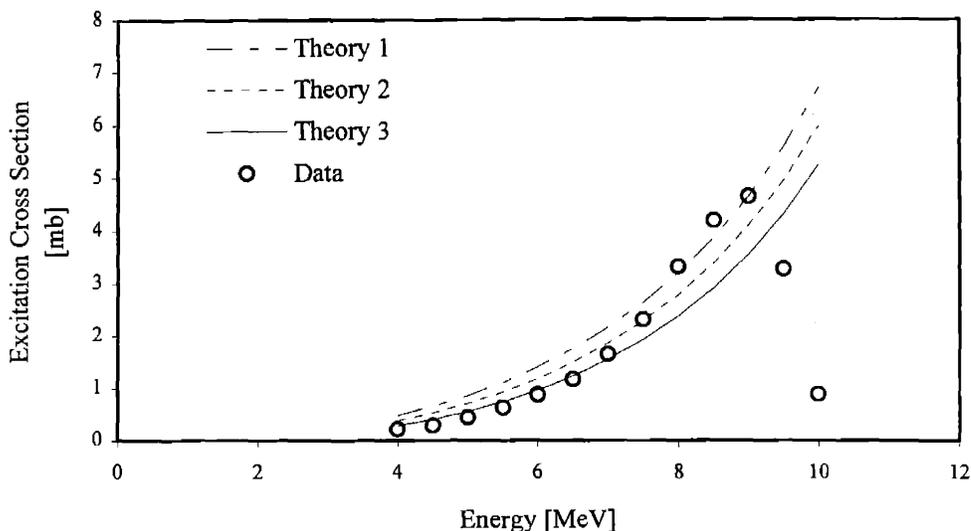
Figure 2-4 The theoretical (lines) and measured (circles) photonuclear resonant absorption cross section for production of the isomeric state of ^{103}Rh. The Theory 1 line assumes a 50% contribution from the 5/2 spin state. The Theory 2 line assumes a 25% contribution the 5/2 spin state. The Theory 3 line assumes no contribution from the 5/2 spin state. All three theory lines assume complete feeding from spin states greater than 5/2.

For the rhodium the statistical model calculations do not appear to match the reference experimental results quite as well as for yttrium. Overall, the general trend is followed but from ~7 to 9 MeV the calculations seem to under predict the strength of the isomeric excitation cross section. As can be seen in the figure, for the energy region of interest in this paper the overall magnitude of the isomeric excitation cross section is increased in a nearly uniform fashion as the feeding ratio of the lower spin state to the isomer is increased. Inaccuracies in the behavior of the predicted cross section at higher energies do not, however, appear to be strongly correlated with this.

2.1.2.1.1.2.3   Gold-197

As with rhodium, extrapolation of the low energy nuclear structure of gold for the determination of the spin state branching ratios is recondite. Examining Table 2-6 we see that none of the nuclear levels of gold for which the spin is known have decays leading to the 0.40915 keV isomeric state. However, based upon experiments it is clear that at least some higher energy nuclear levels for this nucleus do decay to the isomer. Without empirical examples of higher energy ^{197}Au isomeric branching ratios to use as a guide, a reasonable first hypothesis for this case, based upon yttrium and rhodium, is to assume complete feeding of the isomeric level from post cascade spins equal to or greater than the isomer's spin J_m (11/2), 25% feeding from the J_m-1 spin state, and no feeding from states less than J_m-1.

Table 2-6 Low energy nuclear level parameters of [197]Au and the fraction of decay transitions for each level which eventually lead to formation of the gold isomeric state (bold).[48]

Nuclear Energy Level [MeV]	Nuclear Level: Angular Momentum and Parity					Eventual Branching Ratio to [197m]Au
0		$3/2^+$				——
0.077351	$1/2^+$					——
0.268786		$3/2^+$				——
0.27899			$5/2^+$			——
0.40915					$11/2^-$	——
0.5025			$5/2^+$			0
0.5475				$7/2^+$		0
0.7367				$7/2^+$		0
0.8555					$9/2^+$	0
0.88811	$1/2^+$					0
0.9360			$5/2^+$			0
1.0451			$5/2^+$			0
1.1505		$3/2^+$	$5/2^+$			0
1.2173		$3/2^+$				0
1.231					$11/2^+$	0
1.2420	$1/2^+$					0

Applying the statistical model calculations to gold, which has a neutron binding energy B_n = 8.071 MeV, the photonuclear isomeric excitation cross section has been calculated for incident photon energies from 3 to 8 MeV. The calculated values for a 25% isomer branching ratio of the J_m-1 spin state have been plotted in Figure 2-5 together with experimentally reported values[55,56] for this cross section. The experiments utilized bremsstrahlung beam irradiations with end point energies increasing in 0.5 MeV increments starting at the low end with an energy of 4 MeV. As with the other experimental results presented in this paper, the authors did not present estimates of the uncertainties in their final results but, based upon statistical considerations alone, their initial activity yield data indicates errors of approximately 75% to 10% in the 4 to 8 MeV range. The reference values were taken from the paper in the same fashion as for yttrium and rhodium.

^{197m}Au

^{197m}Au
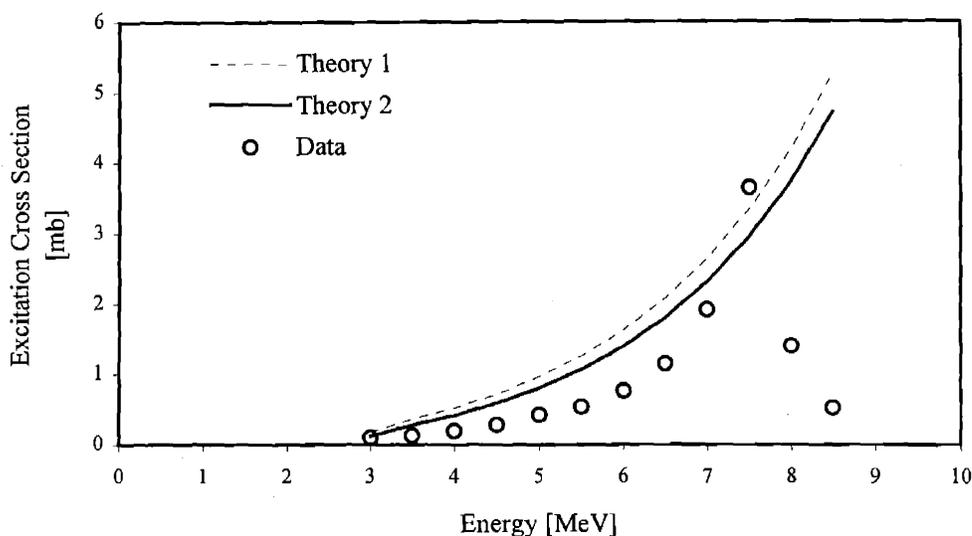
Figure 2-5 The theoretical (line) and measured (circles) photonuclear resonant
absorption cross section for production of the isomeric state of ^{197}Au. The
Theory 1 line assumes a 25% contribution from the 9/2 spin state. The
Theory 2 line assumes no contribution from 9/2 spin state. Both theory
lines assume complete feeding from spin states greater than 9/2.

Comparing the statistical value calculations with the reported values, the results for ^{197}Au seem to follow the same general trends as do the rhodium calculations. Overall, the excitation cross section's calculated dependence upon the excitation energy is smaller than the reported values suggest it should be. As can be seen both the 25 % and 0% cases for contribution from the J_m-1 spin state seem to over predict the cross section at lower energies and then begin to approach the reported values at energies near B_n.

2.1.2.1.1.2.4 Discussion

The statistical model formalism presented here for the calculation of the photonuclear resonance excitation cross sections of nuclear isomeric states is generally in good agreement with experiments for the three nuclei studied. The model closely predicts the excitation cross section over the entire range of applicability for yttrium but predicts larger values for rhodium and gold at lower energies. One reason for the agreement in the yttrium case may rest on the fact that several of the statistical model parameters are derived from general observations of trends in nuclear structure (not at a particular excitation energy) and that yttrium, which has a 'magic number; of 50 neutrons, is expected to have a more constant nuclear structure over the energy range of the calculations.

One factor possibly contributing to the models discrepancies may be the limitation of all excitation and cascade decay transitions to dipole transitions. As the excitation energy increases, transition probabilities of quadrupole order become larger and the apparent under prediction of the statistical model at higher energies for rhodium and gold may be due in part to the failure to account for these quadrupole order electromagnetic transitions. Additionally, the assumption of an equal distribution in the parity of excited nuclear states in the continuum regime may also not be completely valid at the excitation energies studied. Review of yttrium's low energy structure indicates a strong asymmetry in parity as a function of spin (higher order spins, which the model feeds to the isomer, match the parity for isomeric yttrium though)

46

while gold's nuclear structure indicates a nearly complete asymmetry in parity over all spins (the isomer being the only reported spin of negative parity).

For the calculations presented in this paper the average nuclear energy level density parameter a was taken to be independent of the excitation energy of the nucleus. As mentioned earlier, this is a simplification of the actual behavior of a which does have an energy dependence; however, the calculated excitation cross section has only a weak dependence upon a through parameters such as the nuclear temperature, spin cut-off factor and gamma-ray multiplicity and thus is only slightly dependent upon energy through a. Another possible source for the discrepancies in the calculated excitation cross sections might be found in the value of the multiplicity used for the gamma-ray cascade. A higher order dependence upon the excitation energy in this relationship would yield a predicted excitation cross section which increases more sharply at higher incident photon energies. One promising improvement to increase the overall accuracy of the calculated cross sections would be to extrapolate this method from the discrete model of calculating the post cascade spin distribution which is presented above to a continuum approach similar to existing numerical approaches.[33] In addition, inclusion of particle evaporation channels such as (γ,n) and (γ,p) reactions would allow the applicable energy range for this calculation to be increased significantly beyond the neutron separation energy.

2.1.2.1.1.3   Stimulated Photon Emission [57-63]

A final resonant interaction to be considered is the induced de-excitation of an excited nucleus caused by the coupling of a photon having the same energy as the de-excitation transition with the excited nucleus. This process is essentially the nuclear analogue of the familiar atomic stimulated emission phenomenon which takes place in a laser. The cross section for the stimulated emission of a photon from a nucleus is the same as that for the resonant absorption of a photon for the inverse process but the functional dependence upon the spins of the final and initial states remains the same,

$$\sigma_{i \to f}^{stim}(E) = \frac{\pi \lambda^2}{2} \frac{(2J_f + 1)}{(2J_i + 1)} \frac{\Gamma_{fi}(\Gamma_f + \Gamma_i)}{(E - E_{f-i})^2 + \frac{1}{4}(\Gamma_f + \Gamma_i)^2} .$$

2-18

In most cases, the spin of an isomeric state is larger than that of the isotope's ground state. Because of this, the stimulated emission cross section will usually be somewhat smaller than the direct resonant photon absorption cross section. As will be illustrated in §2.3.2, indirect resonant excitation of the isomeric state through formation of compound nuclear states will typically be the dominant mechanism of isomer creation for applications using bremsstrahlung irradiation sources.

2.1.2.1.2   Non-Resonance Interactions

The vast majority of theoretical and experimental research exploring the excitation of nuclei using photons has focused on resonant processes but there has been some work, however, aimed at exploring the possibility of nuclear excitation via non-resonant processes. In particular, well known photon interaction mechanisms such as the photoelectric effect, Compton scattering and pair production have been studied to analyze their potential to excite nuclei through indirect, non-resonant processes. There has been some controversy in the literature regarding the interpretation of experimental results claiming significant non-resonant nuclear excitation probabilities. Researchers on both sides of this debate seem to agree though that such reactions could take place, the disagreement being over the probabilities of such reactions in comparison with resonant excitation.

2.1.2.1.2.1   Inelastic Photoelectric Effect (IPE) Excitation[64]

In the inelastic photoelectric effect (IPE), the nucleus is hypothesized to become excited during interactions between photons, bound orbital electrons (which are ejected) and the nucleus in a fashion similar to the traditional photoelectric effect. According to theoretical derivations presented by Pisk et. al. for interactions in which the energy available for nuclear excitation, q (the incident photon energy less the energy of the ejected electron) is not close to the energy of the excited nuclear level, ω, the interaction cross section varies as Z^3. When $q = \omega$, the cross section displays a Z^2 dependence. In addition, for the same nucleus and incident photon energy, the cross-section for excitation of higher and higher nuclear levels is predicted to fall off quite rapidly.

In nearly all physical set-ups imaginable for the study or application of photonuclear resonance excitation, large numbers of non-resonant photons will also be present. Depending upon their energy distribution and the nuclear level probability density in the target, these background photons could play some roll (however small) in exciting nuclei. Pisk et. al. predict that, for the case of ^{60}Co photons acting to excite the 1078 keV level of ^{115}In, the excitation cross section would be from ~5 x 10^{-37} cm^2 to 5 x 10^{-36} cm^2.

Experimental work comparing the resonant and non-resonant contributions to the excitation of nuclei has been conducted by a small number of researchers.[65-68] Reported experimental observations have been contradictory. Krčmar et. al. claim that non-resonant processes play a strong role in the excitation process, several orders of magnitude greater than that predicted by their theoretical calculations.[69] In a 'comment' to that paper, von Neumann-Cosel et. al. suggest that the seemingly unexplainably large excitation rates might in fact due to the presence of resonant energy photons in their experimental setup due to scattering of cobalt photons.[70] Ljubičić et. al.'s reply to this suggestion is that, based upon their calculations, the resonant photons present due to scattering are insufficient in number to account for the observed nuclear excitation.[71] From these papers, the exact degree to which the non-resonant IPE phenomenon can act to excite nuclei is unclear. However, in comparison with direct excitation via resonant absorption the IPE interaction cross section is most likely several orders of magnitude smaller. Therefore, in most cases where incident photon beams having a continuous and decreasing photon spectrum are used, the non-resonant IPE process may play a small role but is not likely to be the primary excitation mechanism.

2.1.2.1.2.2   Nuclear Compton Effect (NCE) Excitation[72]

A second mechanism through which the nucleus might be excited is the nuclear Compton effect (NCE). In NCE excitation an incident photon interacts with a loosely bound atomic electron, in an analogous fashion to that found in traditional Compton scattering. At high incident photon energies ($E_\gamma >> (\alpha Z)^2 mc^2$), where the energy of the photon is greater than electron binding energies, NCE excitation results primarily from the inelastic scattering of a loosely bound atomic electron. In this case, a bound atomic electron is removed from the atom, followed then by the creation of an electron as a free electron. At lower incident photon energies ($E_\gamma \approx (\alpha Z)^2 mc^2$), where the energy of the photon is on the order of the electron binding energy, NCE excitation results from the creation of a bound excited electron, or a 'barely' free electron, and subsequent elimination of a lower energy bound electron. When incident photons are of intermediate energy, NCE excitation takes place in part through each of these mechanism.

The NCE is essentially the inverse process of the nuclear decay process known as the internal Compton effect, in which the energy released during the transition of a nucleus from one energy eigenlevel to a lower level is accompanied by either excitation or ejection of an atomic electron and the emission of a photon.[73] In potential PRE applications, the high energy case described above for Nuclear Compton effect excitation may take place in addition to resonant excitation. As an example, Batkin calculated the NCE excitation cross section for quadrupole excitation of a generic heavy nucleus (A $\approx$ 200) to be on the order of 10^{-34} cm^2. This value is rather small in comparison with the indirect resonant absorption excitation cross sections discussed above and it does not appear that NCE excitation will be significant in bremsstrahlung based PRE applications.

At lower excitation energies it does not appear that NCE excitation will be of particular use for the production of nuclear isomers either. Although very intense, low energy x-ray sources are available, low energy NCE excitation probabilities are found to drop off quickly as the multipolarity of the excitation transition increases, the cross section being roughly proportional to $(R/a)^{2L}$, where R is 13.6 eV, a the radius of the electron shell and L is the multipolarity order. Since one of the reasons that isomers have long half-lives is because of differences in angular momentum between ground and excited states, longer lived isomers are always found to be coupled to their ground states through higher order multipole transitions. Because of this, NCE excitation cross sections for the production of isomers with half lives greater than milliseconds are unacceptably low. For the same reason, photon irradiation is equally unlikely to produce isomers in a cascade fashion by first using the NCE to excite a short-lived energy level and then exploiting some existing branching ratio feeding to a useful isomer. Due to angular momentum considerations the transition probabilities of low energy nuclear levels produced through the NCE to isomeric states would typically be small. A brief comparison of some low energy NCE excitation cross sections for isotopes of varying multipole transitions is presented in Table 2-7.

Table 2-7 Selected theoretical NCE excitation cross sections in the low energy regime.[72]

Isotope	NCE Excited Energy Level (keV)	Excited Level Half Life (ns)	Type of Transition	NCE Cross Section σ_{NCE} (μb)
^{119}Sn	23.9	18.0	M1	4
^{125}Te	36.5	1.48	M1	0.14
^{129}I	27.8	16.8	M1	5
^{161}Dy	43.8	0.83	M1	110
^{169}Tm	8.42	4.08	M1	196
			E2	0.0004
^{181}Ta	6.24	6.05	E1	0.0004
^{189}Os	69.5	1.62	M1	26
^{193}Ir	73.0	6.09	M1	9
^{197}Au	77.4	1.91	M1	10
^{201}Hg	1.57		M1	17
^{205}Pb	2.33		E2	0.03
^{235}U	13.0	0.50	M2	0.000004

Although neither high energy nor low energy NCE mechanisms are likely to be significant in industrial PRE applications aimed at producing nuclear isomers, the existence of very high intensity, low energy photon sources may still lead to the development of some innovative radiation based technologies. As Batkin has pointed out, for example, relative nuclear excitation probabilities per incident gamma ray for low lying nuclear energy states via NCE are on the order of $10^{-8} - 10^{-9}$.[72] Investigating this phenomenon in the context of currently available high intensity synchrotron radiation (SR) sources, Batkin and Berkman have calculated that with an SR flux of $\sim 10^{23}$ photons per second, irradiation of a thick target of ^{210}Hg would produce on the order of 10^{16} excited nuclei per second.[74] In a similar paper, theoretical calculations investigating the excitation of the ultra low energy nuclear state of ^{229m}Th ($E \approx 3.5$ eV) have indicated that a suitably chosen laser or lamp could be used to generate an induced thorium activity, in a 1 μg sample, of as much as 10^{12} Bq.[75]

2.1.2.1.2.3 Inelastic Pair Production (IPP) Excitation

Continuing their previous investigations of non-resonant photonuclear excitation mechanisms, Horvat, Pisk and Logan have also performed an analytical study of the excitation of a nucleus resulting from the creation of an electron – positron pair in the vicinity of the nuclear Coulomb field by an incident photon.[76] According to their calculations, the cross section for nuclear excitation resulting from the transfer of energy to the nucleus during pair production follows the general Z and energy dependence observed in the cross section for simple pair production. The magnitude of the pair production nuclear excitation cross section only appears to have significance at energies greater than a few MeV. At these energies, the energy dependence of the pair production excitation and regular pair production cross sections are similar but as the energy of the incident photon increases the magnitude of the regular pair production cross section grows less quickly than that of the pair production excitation cross section (assuming the same excited nuclear energy level for comparison).

At an incident photon energy of ~ 4 MeV, the total integrated cross sections for regular pair production with a Z = 50 element is reported as ~ 10^{-23} cm^2 MeV^{-1} while that for the excitation of a 1 MeV nuclear level in a Z = 50 element is reported to be on the order of ~ 10^{-27} cm^2 MeV^{-1} ($\sigma_{PP}/\sigma_{PPNE} \approx 10^4$). For incident photons having an energy of ~50 MeV, the two cross sections have magnitudes of 7×10^{-22} cm^2 MeV^{-1} and 2×10^{-24} cm^2 MeV^{-1}, respectively ($\sigma_{PP}/\sigma_{PPNE} \approx 350$). As an additional investigation of the likelihood of PPE taking place, the analysis of the phenomenon has also been applied towards predicting the probability of exciting a resonance in ^{238}U using 15 MeV photons. A giant dipole resonance having a width of 2.9 MeV and centered at 10.96 MeV was used as the excited uranium energy level. For this case, the authors obtained a PPE cross section of 2×10^{-30} cm^2, while the corresponding cross section for direct absorption of a photon into this level is reported as 3×10^{-25} cm^2.

By examining these calculated PPE interaction cross sections one can again conclude that, for cases where moderate endpoint energy bremsstrahlung is used the photon irradiation source (such that the photon energy spectrum is not constant but rather continuously decreasing in energy), the PPE interaction mechanism is not probably a significant pathway for the excitation of nuclei, especially in light of expected direct photon absorption excitation.

2.1.2.2 Scattering

In one sense it is difficult to make a clear distinction between the absorption and scattering processes because in many cases absorption of a photon by a nucleus leading to a very short lived eigenstate is then immediately followed by the decay of that state and the emission of a second photon. One way of distinguishing between absorption and scattering, and that which is used here, is to define absorption as the interaction of a photon with a nucleus leading to the excitation of the nucleus to some higher energy eigenstate with the caveat that, if that higher energy state then immediately de-excites to the starting eigenlevel with the emission of a single photon, it is instead referred to as elastic scattering. According to this definition, nuclear photon scattering cannot lead to the creation of isomeric nuclei. In the common notation, photonuclear reactions are often written using the shorthand notation X(γ,γ')Y. Unfortunately, this simplistic notation provides no indication of the actual photon interaction involved.

Nuclear photon scattering interactions are sometimes characterized as being either elastic or inelastic events. For this discussion, elastic interactions may be considered as the set of interactions where the sum of the kinetic energies of the initial reaction participants is equal to the sum of the kinetic energies of the final reaction participants; all other photonuclear reactions being termed inelastic. Using this definition it is clear that photonuclear interactions resulting in the excitation of the nucleus are inelastic interactions. Of course, not all inelastic interactions necessarily result in the excitation of the nucleus.

Another set of classifications used to distinguish scattering interactions involving photons and nuclei is to describe them as either coherent or incoherent. In coherent photonuclear scattering, the nucleus is left in

the exact state following the interaction as it was prior to the interaction. Conversely, applying the term incoherent to the scattering of a photon from a nucleus indicates that some change has occurred in the state of the nucleus following the interaction. According to these definitions, coherent scattering is by definition an elastic event; incoherent scattering however may be either elastic or inelastic in nature.

2.1.2.2.1   Nuclear Thompson (NT) Scattering[77,78]

This scattering mechanism is characterized by the synchronous oscillation of both the nuclear charge and the center of mass of a target nucleus at the same frequency as that of an incident photon. In general terms, the NT differential scattering cross section for a nucleus of atomic number A having a rigid body of charge $-Ze$ and having a mass AM is given by

$$\sigma_{NT}(\theta) = \sigma_{NT}(E,\theta) = \left(\frac{Z^2 e^2}{4\pi\varepsilon_0 A M c^2} \right)^2 \frac{(1 + \cos^2(\theta))}{2} \,, \qquad \text{2-19}$$

where e represents the charge of the electron, M the mass of a nucleon and c is the speed of light. Integrating over θ, the total NT scattering cross section may be written as

$$\sigma_{NT} = \sigma_{NT}(E) = \frac{8\pi}{3} \left(\frac{Z^2 e^2}{4\pi\varepsilon_0 A M c^2} \right)^2 . \qquad \text{2-20}$$

It is worthwhile to note that this cross section is independent of the energy of the incident photon, proportional to Z^4 (as seen below) and, additionally, this expression for the NT scattering cross section is formulated in a completely analogous fashion to the derivation of the atomic Thomson scattering cross section.
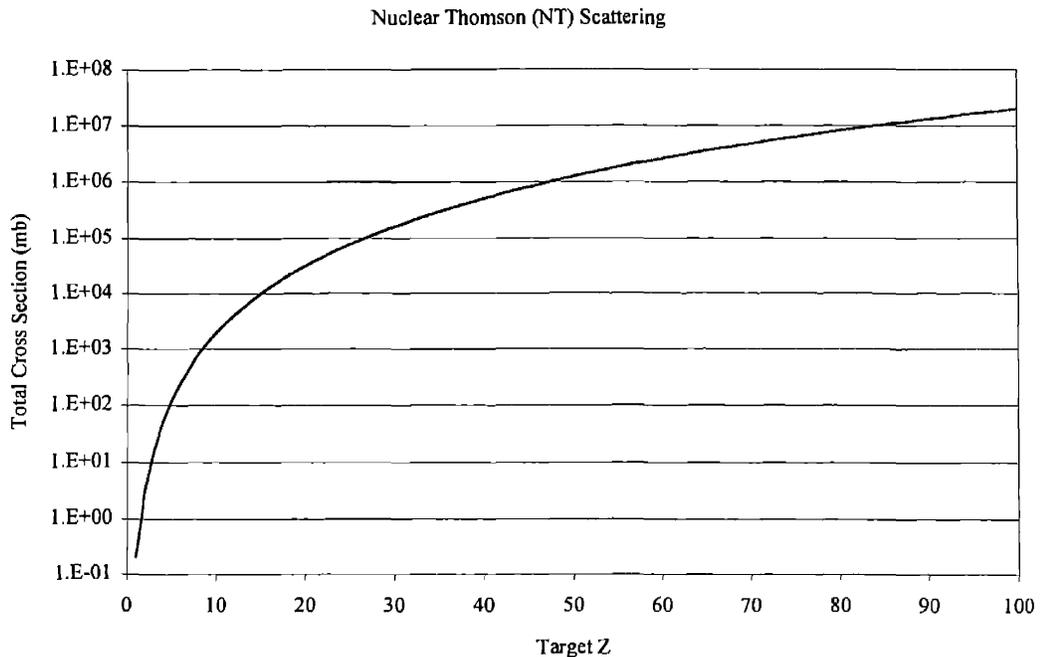
Figure 2-6 Nuclear Thomson scattering cross section for Z = 1 to 100 (high energy limit).

2.1.2.2.2   Nuclear Resonance

The broad category of nuclear resonance (NR) scattering refers to direct interactions between incident photons and the nucleus where photons incident upon a nucleus are observed leaving the nucleus at some angle without a change in energy. In this section attention is focused on photonuclear interactions which do not result in the excitation of nuclear isomers, namely elastic resonant scattering; since these reactions deal with the temporary excitation of nuclei but not in the formation of isomers; their brief descriptions are included here for completeness. Traditionally, reactions of this sort have been categorized into one of three general types: fluorescence (F) scattering, giant dipole resonance (GDR) scattering and elastic incoherent nuclear Raman (NRa) scattering. A large body of work has been devoted to the application of nuclear resonance scattering to probe the structure of nuclei. Unfortunately, as discussed in greater detail below, there are a number of technical challenges which would need to be addressed in order to incorporate these interactions into useful industrial tools.

The basic concept behind these three interactions is essentially the same and they all are closely related to the idea of resonance excitation discussed in §2.1.2.1.1, the difference being in that for elastic scattering the excited nucleus immediately decays back to the original energy state of the nucleus prior to the interaction. Because of this, resonance excitation and resonance scattering probabilities are related to the decay branching of the resonant state (either discrete or compound) to the original state and to other states.

2.1.2.2.2.1   Fluorescence (F) Scattering

Nuclear resonance fluorescence (F) scattering occurs when a photon of energy E_S and width Γ_S interacts with a nucleus having a discrete energy level E_r (taking into account recoil) and width Γ_r such that there is sufficient overlap between the two energy values that absorption of the photon by the nucleus, following a Breit-Wigner resonance, may take place.
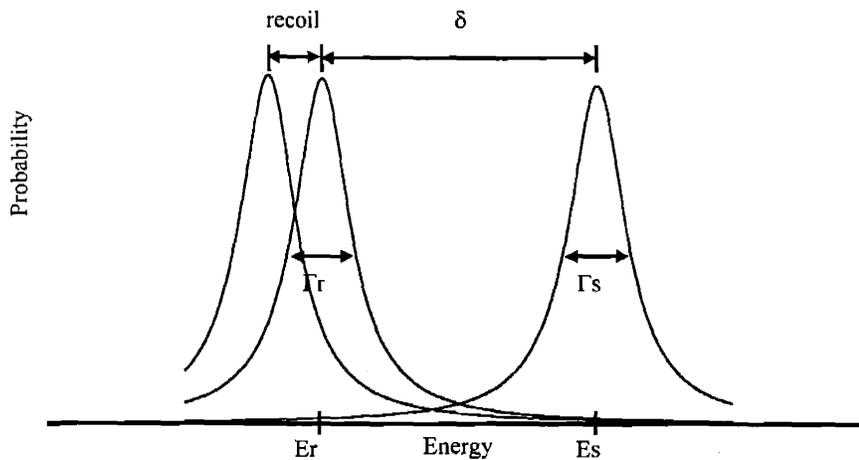
Figure 2-7   Representation of photon and nuclear level energy overlap in NRF.

This is of course the same process as the discrete level photon absorption discussed in §2.1.2.1.1.1. However, when the excited nuclear level, having a very short half-life, immediately decays via emission of a photon of the same energy as the absorbed photon, the process is given the special name of resonance fluorescence. To an observer, the process appears to be one of elastic scattering with the redirection of the photon from its original path without a change in energy. As discussed above the cross section for this resonant reaction is large. However, a number of practical considerations limit the applicability of F scattering for industrial purposes. Chief among these is the inability to achieve a satisfactory signal to noise ratio in practical measurement times and with reasonable measurement equipment due to the large background radiation field produced from other scattering reactions (e.g., Compton scattering). This is especially true for applications aimed at measuring trace quantities of isotopes in bulk materials, when large fluorescence signals from the matrix containing the isomer and fluorescence signals form surrounding structures overwhelm the small fluorescence signal of the isotope of interest. One method for reducing the background signal due to atomic scattering is to place the detector in front of the target (on the side where the irradiation beam is incident on the target) so that only low energy Compton scattered radiation (<26 keV) enters the detector.

In spite of the challenges that would be involved in the development of NRF based industrial probe techniques the issue is still worth consideration. Since NRF does not rely upon the ultimate excitation of isomeric states but upon the excitation of any nuclear state, the process could in principle be applied to the measurement of nearly all isotopes. In addition, by measuring the prompt decay of these excited states rather than the measurement of decaying isomeric states which have much longer half-lives in comparison, analysis times could potentially be short, capable of high throughput rates, non-destructive and truly multi-elemental.

2.1.2.2.2.2   Giant Dipole Resonance (GDR) Scattering[78]

Giant Dipole Resonance (GDR) scattering is characterized as the coherent elastic scattering of photons by the nucleus in reactions involving the GDR of nuclei and, in terms of the end result, can be thought of as F scattering, only taking place at higher energies. That is to say that in both cases photons of the same energy are absorbed and then emitted from a nucleus in a short period of time such that to an observer it looks like the photon was scattered from the nucleus, the actual interaction being irrelevant. In GDR scattering, which is defined here as an elastic interaction, the nucleus is left in the same energy eigenstate after the reaction as that prior to the reaction. Rather than exciting individual nuclear levels, as in F scattering though, GDR scattering involves the collective excitation of the entire nucleus. Typically, giant dipole resonance energies range from 10 to 20 MeV for most nuclei with resonances having widths of from 1 to 5 MeV.

Rather than the elastic interaction mentioned above, however, GDR photon absorption is more often associated with nucleon emission, primarily neutrons, as well as multinucleon emission reactions such as (γ,2n) and (γ,np). In instances where nucleon emission does not occur there are two alternatives, either decay by emission of a photon of the same energy as the absorbed photon (elastic scattering) or the nucleus may decay to some intermediate energy state which could in principle be an isomeric state (inelastic scattering). In general, when excited at such energies nucleon emission is the dominant reaction pathway. Although isomer formation can occur through GDR excitation (with cross sections on the order of 5 to 10 mb), the probability is small in comparison with cross sections for particle emission (typically >100 mb at the GDR energy).

Since one concern regarding the industrial implementation of PRE is the minimization (or complete avoidance) of any long term induced radioactivity in either the target materials being irradiated or the instrumentation and shielding, resonance excitation at GDR energies is probably not an option except possibly in some radioisotope production applications. As with F scattering, achieving an adequate signal

to noise ratio using giant dipole resonance scattering as a probing technique is unlikely as a viable industrial technique.

2.1.2.2.2.3   Nuclear Raman (NRa) Scattering[78]

As a counterpart to GDR scattering, nuclear Raman scattering deals with the incoherent elastic scattering of photons interacting with the giant dipole resonance. In this case, the term incoherent is used because, although the nucleus returns to its original energy state following the scattering event (i.e. elastic), coupling between the excited nucleus, the GDR and the rotational motion of the nucleus can result in a change of the orientation of the nucleus in space with it still having the same angular momentum which it had prior to the reaction. By changing the spatial spin orientation of the nucleus in this way, NRa scattering is of relevance only for photons interacting with deformed nuclei. Other than the ability to alter the physical orientation of the nucleus though, NRa scattering is very similar to GDR scattering and the discussion above regarding the disadvantages of exploiting GDR scattering for industrial purposes applies equally well to NRa scattering. In fact, since both of these processes can occur NRa scattering is actually more difficult to isolate and investigate, requiring the added complexity of measuring changes in polarization between the incident and scattered photons.

2.1.2.2.3   Delbrück (D), Rayleigh (R) and Nuclear (or Internal) Compton (NC) Scattering[78-82]

These three photon scattering mechanisms, Delbrück (D), Rayleigh (R) and Nuclear (or Internal) Compton (NC) Scattering, account for the remaining photon scattering mechanisms encountered in the study of photon interactions with nuclei at energies less than about 10 MeV. Delbrück scattering involves the elastic interaction of photons with the Coulomb field of the nucleus, Rayleigh scattering the elastic interaction of photons with bound atomic electrons and nuclear Compton scattering the coherent elastic scattering of photons with the nucleus. Delbrück and nuclear Compton scattering are mentioned here because their interaction probabilities depend upon the nuclear parameters of the atom they are scattered from and thus could in principle be used for investigating various materials. Rayleigh scattering is mentioned because, although not directly involved with the nucleus, it has been shown to have an interference effect with D scattering. While none of these three scattering mechanisms leads to the excitation of the nucleus, their existence can lead to increases in background activities during some types of measurements (in particular, photon spectrum measurements conducted while the irradiating photon source is 'on').

2.1.3   Nuclear De-Excitation and Photon Emission

Generally speaking, when a broad energy spectrum of photons is used as the irradiation source for photonuclear resonance excitation purposes many nuclear levels have the potential of being excited. At lower excitation energies these may be discrete energy eigenstates such as the isomer but at higher excitation energies the initial excitation of the nucleus is more likely to result in the creation of a compound nuclear state. Because of this, nuclear isomers may be created during photon irradiation as a result of the decay of these higher energy states which are created during irradiation. In fact, except for isotopic irradiation sources which exactly match the energy levels of a targets nuclei, the predominant method of isomer creation is through this two stage, trickle-down process.

If the isomeric level is produced directly then the equations of §2.1.2.1.1.1 may be used to determine the isomeric level production rate. When discrete energy eigenstates having a higher energy than the isomeric level are produced, these same equations may still be used to determine the isomer production rate by

taking into account the ultimate branching ratio of these discrete states to the isomeric state. At even higher energies, the equations of §2.1.2.1.1.2 must be used to determine the isomeric production rate.

In addition to these resonant excitation pathways; however, in some extreme cases there may also be additional transformation mechanisms significantly affecting the production and decay of the isomeric state. For example, in stellar environments stimulated photon emission could act to accelerate the depletion of the isomeric state directly while it could also act to increase its production rate through the depletion of higher energy states.[58,62] When higher energy photon sources are used, photonuclear reactions resulting in neutron or proton emission for example could act to deplete the total number of nuclei available for isomeric excitation. In addition, natural radioactive decay could influence the isomeric production and decay rate.

Accounting for these different photonuclear and natural radioactive transition processes, it is possible to analytically model the buildup and decay of nuclear isomeric states. Described in detail in the following section, this general transition model may be used to determine the instantaneous isomeric decay rate and activity for a sample. By accounting for the branching ratio of the isomeric state to individual lower energy levels and taking into account the possibility that competition may exist between photon emission and internal conversion in the decay of the isomeric state, it is also possible to calculate the intensity and flux of photons of a particular energy associated with the decay of the isomer.

2.2 TRANSITION MODEL

For the situation where the energy levels of a nucleus are sufficiently separated from one another (level spacing >> level width), the energy levels can be thought of as a discrete set of energy eigenstates. In this domain, perturbation theory may be used to determine the probability that a photon of energy E will interact with a nucleus; the result of these calculations is the resonant photon absorption cross section.

In the most general sense, prior to the photonuclear reaction the nucleus will be in a state $|m\rangle$ corresponding to an energy E_m and, following the reaction, the nucleus will be in some state $|n\rangle$ corresponding to an energy E_n. If E_n is greater than E_m, the reaction is that of photon excitation; if E_n is less than E_m, the reaction is that of photon de-excitation. If E_n equals E_m, the possibilities are that either no reaction has taken place or that elastic scattering has taken place. Depending upon the energy of the incident photon and the structure of the scattering nucleus, the nature of the scattering will be either dispersive or resonant in nature. In either case, though, the energy level of the nucleus after the reaction is the same as at the beginning.

In addition to these interaction phenomena, there are other mechanisms which may potentially alter nuclear level populations in a sample. Nuclei in excited states (both short and long lived) will eventually decay to lower lying states. In some cases these transitions are direct from the excited state to the groundstate but in the majority of cases the nucleus transitions via one or more intermediate, lower energy states prior to reaching the groundstate. For nuclei which are naturally unstable, it is possible that these nuclei may undergo nuclear decay transforming to different isotopes, this decay taking place in either excited or groundstate nuclei. One can also imagine a situation in which a second nuclear species, which has some probability of decaying into the species of interest, is present in a sample. In this case, the nuclear level population of the nucleus of interest will depend upon the decay of this parent species which, in general, may yield the daughter nucleus in some excited energy state which is not necessarily the groundstate.

A schematic representation of the way the processes described here may act to populate a given nuclear level $|i\rangle$ is given in Figure 2-8, the transitions are labeled as follows:

- *A1* represents population of $|i\rangle$ via resonant photon absorption
- *A2* represents de-population of $|i\rangle$ via resonant photon absorption
- *B1* represents population of $|i\rangle$ via stimulated photon emission

- $B2$ represents de-population of $|i\rangle$ via stimulated photon emission
- $C1$ represents population of $|i\rangle$ via photonuclear reaction
- $C2$ represents de-population of $|i\rangle$ via photonuclear reaction
- $D1$ represents population of $|i\rangle$ via natural decay
- $D2$ represents de-population of $|i\rangle$ via natural decay
- $E1$ represents population of $|i\rangle$ due to nuclear decay
- $E2$ represents de-population of $|i\rangle$ due to nuclear decay.
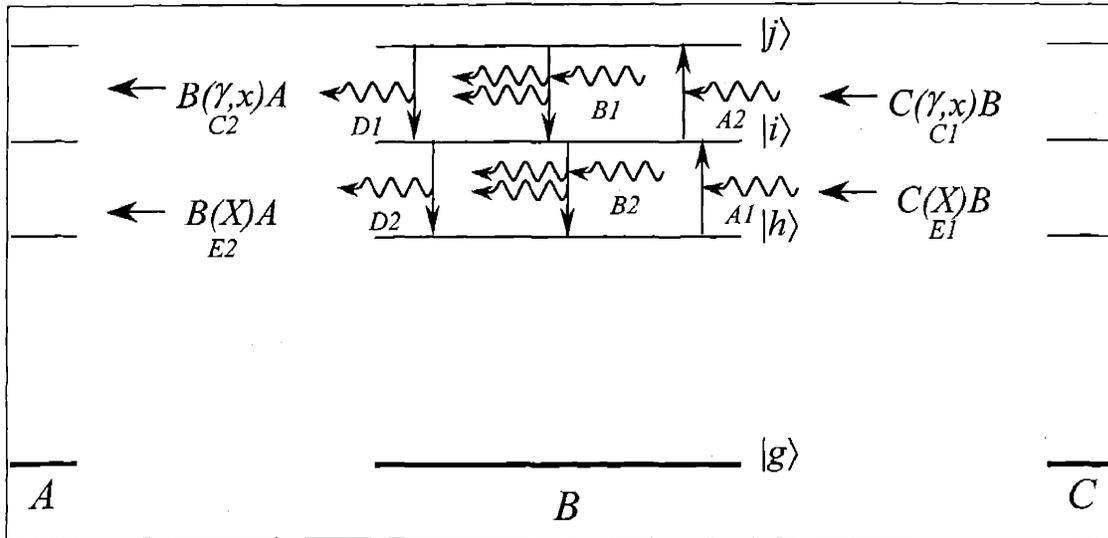
Figure 2-8 Photonuclear processes influencing nuclear level densities.

2.2.1 Transition Mechanisms

By accounting for all of the different mechanisms which can lead to changes in the nuclear level probability density of a sample undergoing photon irradiation, by a source having some arbitrary spectrum distribution $\varphi(E)$, and allowing for the possibility that additional atoms of the species of interest might be introduced due to photonuclear transformations in atoms of different isotopes in the sample, one can create a complete analytical model for predicting the nuclear level probability distribution of the sample isotope. In the sections below, the individual components of such an analytical tool are introduced for some of the factors likely to influence the nuclear level probability distribution of some isotope in industrial photonuclear resonance excitation applications. Since the probability of nuclear excitation through resonant processes is much larger than excitation probabilities resulting from non-resonant interactions or photon scattering interactions under most circumstances these second-order excitation processes are not included.

2.2.1.1 Resonant Photon Absorption

For a sample, the time dependence of the population of the ith level due to resonant photon absorption is given by

$$\frac{dN_i(t)}{dt} = \sum_{h=0}^{i-1} \left(\int_0^{E_{max}} \sigma_{h \to i}^{abs}(E)\varphi(E)dE + \int_{E_{cont}}^{E_{max}} \sigma_{h \to i}^{abs*}(E)\varphi(E)dE \right) N_h(t)$$

$$- \sum_{j=i+1}^{k} \int_0^{E_{max}} \sigma_{i \to j}^{abs}(E)\varphi(E)dE \, N_i(t) + \sum_{j=i+1}^{k} \int_0^{E_{max}} \sigma_{j \to i}^{abs*}(E)\varphi(E)dE \, N_j(t)$$

.   **2-21**

In the above equation, the first summation accounts for the feeding of the ith population level by direct resonant photon absorption in lower energy eigenstates $|h\rangle$ as well as indirect feeding via compound nuclear states in the energy continuum region. The second term accounts for the depletion of the ith population level by photon absorption to higher energy eigenstates $|j\rangle$. The third term accounts for indirect isomeric excitation resulting from resonant photon absorption in already existing higher energy eigenstates through formation of a compound nucleus. The summation is through the eigenstate $|k\rangle$, the highest energy level achievable with the photon flux $\varphi(E)$, including both discrete and compound states. In this equation, $\sigma_{h \to i}^{abs}(E)$ represents the cross section for absorption of a photon of energy $E_{i-h} = E_i - E_h$ by a nucleus originally in the eigenstate $|h\rangle$ which leaves the nucleus in the eigenstate $|i\rangle$, $\sigma_{h \to i}^{abs*}(E)$ and $\sigma_{j \to i}^{abs*}(E)$ represent the cross section for absorption of higher energy photons by levels lower and higher in energy than the isomer, respectively, leading to the formation of a compound nucleus which subsequently decays to the isomer and $\sigma_{i \to j}^{abs}(E\,)$ represents the cross-section for absorption of a photon of energy

$E_{j-i} = E_j - E_i$ by a nucleus originally in the eigenstate $|i\rangle$ which leaves the nucleus in the eigenstate $|j\rangle$. The population of the energy eigenstates $|h\rangle$ in the sample is represented by $N_h(t)$ while that for the eigenstate $|i\rangle$ is $N_i(t)$.

Fortunately, if in Eq. (2-21) the photon spectrum $\varphi(E)$ may be assumed to be smooth and continuous over the effective energy range of the discrete absorption cross-section (typically ~1-2 eV), this function may be pulled out of the integral which allows the cross-section to be integrated directly. In this case, the shape of the cross-section is no longer important and Eq. (2-4) may be used directly without correction for Doppler broadening,

$$\int_0^{E_{max}} \sigma_{h \to i}^{abs}(E)\varphi(E)dE = \varphi(E_i) \int_0^{E_{max}} \sigma_{h \to i}^{abs}(E)dE = \varphi(E_i)\pi^2 \lambdabar^2 \frac{2I_i+1}{2I_h+1}\Gamma_{ih}. \qquad \textbf{2-22}$$

2.2.1.2   Stimulated Isomeric Decay

For a nucleus in an excited energy state, interaction with a photon can also result in the stimulated de-excitation of the nucleus and the concurrent emission of a photon. The probability, $\sigma_{j \to i}^{stim}(E)$, for such a reaction to occur, and the nucleus making a transition from an original state $|j\rangle$ to a lower energy eigenstate $|i\rangle$, the two states being separated by an energy E_{j-i}, is the same as that for the inverse process of photon absorption and may be taken directly from the previous two equations . Noting that, for an eigenstate $|i\rangle$ this phenomena can serve to both populate and depopulate the ith energy level, the time dependence of the energy eigenstate $|i\rangle$ in an ensemble of nuclei N_i due to photon induced stimulated emission is given by

$$\frac{dN_i(t)}{dt} = \sum_{j=i+1}^{k} \int_0^{E_{max}} \sigma_{j \to i}^{stim}(E)\varphi(E)dE \, N_j(t) - \sum_{h=0}^{i-1} \int_0^{E_{max}} \sigma_{i \to h}^{stim}(E)\varphi(E)dE \, N_i(t). \qquad \textbf{2-23}$$

2.2.1.3 Photonuclear Reactions

If a photon interacting with a nucleus has more energy than the binding energy of the nucleons comprising that nucleus, photonuclear reactions are possible (this might also include photon induced fission). For sample nuclei in the eigenstate $|i\rangle$, photonuclear reactions will result in the reduction of the $|i\rangle^{\text{th}}$ eigenstate population. However, there is the possibility that photonuclear reactions in nuclei of different isotopes M_j, in the eigenstates $|j\rangle$, will undergo photonuclear reactions leading to the formation of sample nuclei N_i. Addressing this pathway for altering nuclear level populations, the following equation contains components for both the growth and depletion of the $|i\rangle^{\text{th}}$ level due to photonuclear reactions,

$$\frac{dN_i(t)}{dt} = \sum^{M}\sum_{j=0}^{k} \int_0^{E_{\max}} \sigma^{M_j \to N_i}(E)\varphi(E)dE\, M_j(t) - \sum^{M}\sum_{j=0}^{k} \int_0^{E_{\max}} \sigma^{N_i \to M_j}(E)\varphi(E)dE\, N_i(t).$$

2-24

In this equation, $\sigma^{M_j \to N_i}(E)$ represents the photonuclear cross-section for the reaction transforming nuclei of species M_j in the eigenstate $|j\rangle$ to nuclei of species N_i in the eigenstate $|i\rangle^{\text{th}}$. Similarly, $\sigma^{N_i \to M_j}(E)$ represents the photonuclear cross-section for the reaction transforming nuclei of species N_i in the eigenstate $|i\rangle^{\text{th}}$ to nuclei of species M_j in the eigenstate $|j\rangle$. Both terms are summed over the possible energy eigenstates $|j\rangle$ of the non-sample species M, up to the maximum eigenstate $|k\rangle$ and are summed to include all of the potential photonuclear reactants and end products.

2.2.1.4 Natural Isomeric Decay

Sample nuclei in excited eigenstates which do not interact with the radiation field may still emit characteristic gamma rays and decay to lower energy states. For nuclei in the eigenstate $|i\rangle$ undergoing natural isomeric decay, this transformation mechanism reduces the eigenstate population at a rate proportional to the width of the $|i\rangle^{\text{th}}$ eigenstate divided by Planck's constant, $\Gamma_i/\hbar$. However, if sample nuclei exist in eigenstates of higher energy, these nuclei may also decay via isomeric transition. Some of these higher energy eigenstates, $|j\rangle$, may decay to the sample eigenstate $|i\rangle$, the rate being determined by the partial width $\Gamma_{ji}/\hbar$ for transition from $|j\rangle$ to $|i\rangle$. The following equation indicates the dependence of the $|i\rangle$ eigenstate population on natural isomeric decay in sample nuclei,

$$\frac{dN_i(t)}{dt} = \sum_{j=i+1}^{k} \frac{\Gamma_{ji}}{\hbar} N_j(t) - \frac{\Gamma_i}{\hbar} N_i(t).$$

2-25

2.2.1.5 Nuclear Decay

In addition to nuclear transitions among the energy eigenstates of the sample nuclei, the population of nuclei in the $|i\rangle^{\text{th}}$ eigenstate may also be influenced by other decay mechanisms. If the nuclei of the sample population, N, are naturally radioactive, then sample nuclei (in either the groundstate or some excited state $|i\rangle$) will transform to nuclei of some other species, M. Examining the nature of various decay mechanisms (α, $\beta-$, $\beta+$, EC,), one sees that the decay probability for these transformations, λ_i, is inherently dependent upon the energy of the nucleus, $|i\rangle$. Unfortunately, nuclear data regarding the decay constants of nuclei in

excited states is rare. Just as sample nuclei in the $|i\rangle^{th}$ eigenstate can be lost due to decay of N_i nuclei, though, the population of nuclei in the $|i\rangle^{th}$ eigenstate could also be increased by the nuclear decay of other isotopes M_j in arbitrary eigenstates $|j\rangle$, which yields nuclei N_i in the sample population level $|i\rangle$. The equation describing changes in the $|i\rangle^{th}$ population level due to the nuclear decay mechanism described here is

$$\frac{dN_i(t)}{dt} = \sum_{j=0}^{M}\sum^{k} \lambda^{M_j \rightarrow N_i} M_j(t) - \lambda_i N_i(t),$$ 2-26

where $\lambda_j^{M \rightarrow N}$ is the decay constant for nuclei of species M_j in the energy eigenstate $|j\rangle$ transforming to nuclei of species N_i in the energy eigenstate $|i\rangle$ and λ_i is the decay constant for nuclear transformation of sample nuclei N_i.

2.2.2 The General Transition Equation

Summarizing the previous sections, there are five general mechanisms which might alter the nuclear level densities of a sample undergoing photon irradiation – photon absorption, stimulated emission, photonuclear transformations, natural isomeric decay, and natural nuclear decay. Adding together the equations describing these effects independently as given above yields a general equation describing the time dependence of the population of the ith energy eigenstate of an ensemble of similar nuclei N undergoing photon irradiation,

$$\frac{dN_i(t)}{dt} = -\left[\begin{array}{c} \displaystyle\sum_{h=0}^{i-1} \int_0^{E\max} \sigma_{i \rightarrow h}^{stim}(E)\varphi(E)dE + \sum_{j=i+1}^{k} \int_0^{E\max} \sigma_{i \rightarrow j}^{abs}(E)\varphi(E)dE \\ + \displaystyle\sum_{j=0}^{M}\sum^{k} \int_0^{E\max} \sigma^{N_i \rightarrow M_j}(E)\varphi(E)dE + \frac{\Gamma_i}{\hbar} + \lambda_i \end{array} \right] N_i(t)$$

$$+ \sum_{j=i+1}^{k} \left(\int_0^{E\max} \sigma_{j \rightarrow i}^{stim}(E)\varphi(E)dE + \int_{Econt}^{E\max} \sigma_{j \rightarrow i}^{abs*}(E)\varphi(E)dE + \frac{\Gamma_{ji}}{\hbar} \right) N_j(t) .$$ 2-27

$$+ \sum_{h=0}^{i-1} \left(\int_0^{E\max} \sigma_{h \rightarrow i}^{abs}(E)\varphi(E)dE + \int_{Econt}^{E\max} \sigma_{h \rightarrow i}^{abs*}(E)\varphi(E)dE \right) N_h(t)$$

$$+ \sum_{j=0}^{M}\sum^{k} \left(\int_0^{E\max} \sigma^{M_j \rightarrow N_i}(E)\varphi(E)dE + \lambda^{M_j \rightarrow N_i} \right) M_j(t)$$

Using this equation it is possible, in principle, to determine the buildup and decay of particular nuclear energy levels in a sample irradiated by photons. However, due to a lack of adequate information regarding the values of most of the parameters in the above equation for most nuclei, calculations of isomeric buildup unrestricted by incident photon energy limits or time constraints can not be done for most isotopes. Fortunately, due to the time scales involved and the sizes of cross-sections and transition rates, the full

array of mechanisms affecting level populations will only be important for a few cases. Calculations examining steady state level populations in the high flux backgrounds found in stellar environments will be sensitive to many of the components of this equation, for example, but calculations for the production of isomers from stable nuclei using bremsstrahlung photon sources will not.

2.3   CALCULATION OF ISOMERIC ACTIVITY

Potential industrial applications involving the photonuclear resonance excitation of isomers can be categorized into two general areas: a) applications aimed at quantifying how much of a particular isotope is present in something and b) applications aimed at producing isomeric nuclei for some purpose such as tracer studies or medical diagnostics. In the design stages of the development of either of these applications it is necessary to be able to calculate the activity of the isomeric isotope(s) being produced in order to optimize the set up of the particular process and to determine the operational parameters of the equipment needed. For applications designed to analyze materials to discern the amount of some isotope they contain, general information such as a ball park estimate of the expected isomeric concentration, the material matrix, the presence of potential interferences in the matrix and desired measurement times are required. This information is used in an iterative process involving the calculation of the induced isomeric activity to determine the radiation source strength and detector efficiency needed for the application. When production of isomeric isotopes is the intent of the PRE process, isomeric activity calculations must be carried out to determine the radiation source strength needed to achieve specified output goals such as absolute or specific activity of the isomer, constrained by other factors such as irradiation time or cost.

Using the general transition equation of §2.2.2 to compute the rate at which the isomeric nuclei population $N_i(t)$ of some isotope in a sample is changing at some time t, one can determine the activity, $A_i(t)$, of the isomer in a sample using

$$A_i(t) = -\frac{dN_i(t)}{dt} \ . \tag{2-28}$$

If the total number of isomeric nuclei at some time t is calculated, the isomer activity may be found using

$$A_i(t) = \lambda N_i(t) \ , \tag{2-29}$$

where λ is the decay constant of the isomer.

For the majority of applications, the interest in producing isomers is related to measuring or somehow else using photons associated with the decay of the isomer. Because of this, care must be taken in using the isomer activity as calculated above. In some cases, the decay of the isomer may yield photons having a specific energy of interest for some application only a fraction of the time due to the branching ratio of the decay. In addition, since the internal conversion process sometimes occurs instead of gamma ray emission for some nuclei, activity calculations for isomeric nuclei having significant internal conversion coefficients must be corrected for this phenomenon to find the actual isomeric photon intensity for use in later analysis.

2.3.1   Simplifications

The general transition equation includes many interaction pathways which can affect the population level density of the isomeric state of an isotope. In applying this equation for the calculation of isomeric activities for PRE applications, however, there are practical considerations that allow many of the terms in the equation to be eliminated. To begin with, in most cases the irradiation source that will be used will be a bremsstrahlung x-ray source with an end point energy of somewhere between 5 and 10 MeV. This is primarily because of the continuous distribution of x-rays in the bremsstrahlung spectrum, which helps to

fully maximize isomeric activation taking place through the compound nucleus channel in comparison with isotopic sources, and because as the energy of the photons begins to be increased much beyond 10 MeV significant secondary issues regarding neutron production, long term instrumentation and sample activation and health physics shielding start to become important. Restricting the irradiation spectrum endpoint energy in this way allows the photonuclear terms involving particle emission to be omitted from the equation. Additionally, since few applications will involve the excitation of isomeric states in either naturally radioactive nuclei or of nuclei in samples mixed together with other isotopes which naturally decay to the isomer, the terms for these two natural radioactive decay transition mechanisms may also be omitted. With these simplifications, the general transition equation may be rewritten as

$$
\frac{dN_i(t)}{dt} = -\left(\sum_{h=0}^{i-1} \int_0^{E\max} \sigma_{i \to h}^{stim}(E)\varphi(E)dE + \sum_{j=i+1}^{k} \int_0^{E\max} \sigma_{i \to j}^{abs}(E)\varphi(E)dE + \frac{\Gamma_i}{\hbar} \right) N_i(t)
$$

$$
+ \sum_{j=i+1}^{k} \left(\int_0^{E\max} \sigma_{j \to i}^{stim}(E)\varphi(E)dE + \int_{Econt}^{E\max} \sigma_{h \to i}^{abs*}(E)\varphi(E)dE + \frac{\Gamma_{ji}}{\hbar} \right) N_j(t) \qquad . \qquad 2\text{-}30
$$

$$
+ \sum_{h=0}^{i-1} \left(\int_0^{E\max} \sigma_{h \to i}^{abs}(E)\varphi(E)dE + \int_{Econt}^{E\max} \sigma_{h \to i}^{abs*}(E)\varphi(E)dE \right) N_h(t)
$$

The simplifications above involved assumptions concerning the irradiation spectrum maximum energy and the natural decay of the isomeric isotope and other constituents in its matrix. Continuing with the assumption that a bremsstrahlung source will be used for irradiation, additional simplifications may be made relating to the intensity of such sources. Comparing the magnitudes of the first two terms in the first bracket with that of the third term for a bremsstrahlung source, the three of which account for the different transition pathways that deplete the isomeric state population, the natural decay of the isomeric state is found to be dominant[a], allowing the first two terms to be neglected. Similar reasoning allows the first two terms of the second bracket to be eliminated as well, the equation is then simplified as

$$
\frac{dN_i(t)}{dt} = -\frac{\Gamma_i}{\hbar} N_i(t) + \sum_{j=i+1}^{k} \frac{\Gamma_{ji}}{\hbar} N_j(t) + \sum_{h=0}^{i-1} \left(\int_0^{E\max} \sigma_{h \to i}^{abs}(E)\varphi(E)dE + \int_{Econt}^{E\max} \sigma_{h \to i}^{abs*}(E)\varphi(E)dE \right) N_h(t).
$$

2-31

Recognizing that for most applications at the start of irradiation the only eigenlevel populated is the groundstate, $N_0(t)$, it is unlikely that the isomeric level will experience significant feeding resulting from the absorption of photons by excited levels. Because of this, we may simplify the terms of the third bracket by limiting the summation to only include $h = 0$, the groundstate. Taking this observation into account, the transition equation may be written as

---

[a] For a 250 μA electron accelerator, the photon flux at the 409.15 keV level of the ^{197m}Au isomer is 8.56×10^{11} [photons•cm^{-2}•sec^{-1}] per 0.5 MeV (see Figure 2-9). The integrated cross section for stimulated emission of a photon from this level to the ground state is 4.52×10^{-7} barn•MeV. Taken together, these result in an induced isomeric level decay rate, resulting from stimulated emission, of 7.73×10^{-19} sec^{-1}. In comparison, the decay rate of the ^{197m}Au isomer resulting from natural decay of the isomeric level to the ground state ($T_{1/2} = 7.73$ sec) is 8.97×10^{-2} sec^{-1}.

$$\frac{dN_i(t)}{dt} = -\frac{\Gamma_i}{\hbar} N_i(t) + \sum_{j=i+1}^{k} \frac{\Gamma_{ji}}{\hbar} N_j(t) + \left(\int_0^{E_{max}} \sigma_{0\to i}^{abs}(E)\varphi(E)dE + \int_{E_{cont}}^{E_{max}} \sigma_{0\to i}^{abs*}(E)\varphi(E)dE \right) N_0(t).$$

<div align="right">2-32</div>

2.3.2 Example Calculation

Since calculation of the induced activity in a sample will play an integral part in the actualization of PRE based applications, this section presents an example of the calculation for a generic example – irradiation of gold. For this example, the irradiation source is taken to be bremsstrahlung radiation generated using a 250 µA, 6 MeV electron accelerator with a thick tungsten beam stop. An illustration of the x-ray spectrum such a radiation source might generate on the beam axis, 20 cm from the convertor plate has been calculated using MCNP and is presented in Figure 2-9. The sample taken for this example is a 1 µm thick, circular gold foil with a 1 cm radius, having a surface density of 1932 µg/cm^2, for a total mass of 6.0696 mg. The duration of the irradiation for this example is 4 seconds.

Generic Bremsstrahlung Spectrum - 6 MeV electrons
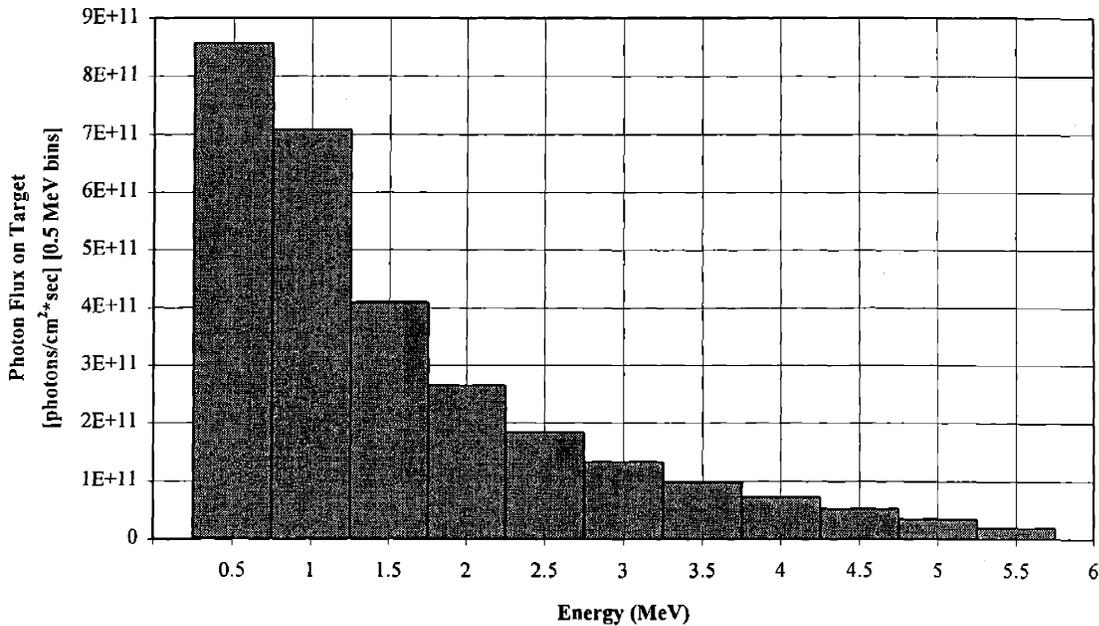
Figure 2-9 A generic 6 MeV bremsstrahlung spectrum created using MCNP.

Examining the decay scheme of the discrete, lower energy eigenstates of [197]Au (Table 2-6) we notice that none of the excited levels has a decay leading to the isomeric level, which allows us to eliminate the second term of Eq. (2-32). The first part of the third term, representing the direct excitation of a nucleus in the ground state to the isomeric state by resonant photon absorption may be evaluated as

$$\int_0^{E_{max}} \sigma_{0\to i}^{abs}(E)\varphi(E)dE = \varphi(E_i) \int_0^{E_{max}} \sigma_{0\to i}^{abs}(E)dE = \pi^2 \lambdabar^2 \left(\frac{2J_i +1}{2J_0 +1} \right) \Gamma_{i0}\, \varphi(E_i), \qquad 2\text{-}33$$

where the width of gold's 7.73 sec isomeric level Γ_i is 5.902 x 10^{-11} MeV, the branching ratio b_{i0} of the isomeric state to the ground state is 0.0329 and the partial width of the isomeric level to the ground sate

$\Gamma_{i0} = b_{i0} \, \Gamma_i$ is 1.95 x 10^{-12} MeV. Evaluating this expression, the direct photon absorption excitation rate is found to be 1.15 x 10^{-19} excitations per second per ground state nucleus. The second part of the third term, representing the indirect excitation of a nucleus from the ground state to the isomeric state through the formation of an intermediate compound nucleus state, may be evaluated as well. Using the reported isomeric excitation cross section of Bogdankevich, Lazareva and Moiseev[51] and the irradiation spectrum of Figure 2-9, the indirect isomeric excitation rate is found to be 8.04 x 10^{-14} excitations per second per ground state nucleus. Comparing the magnitudes of these two isomer production rates two findings may be made: a) direct photon excitation of the isomeric state is negligible in comparison with excitation through higher energy compound nuclear states and b) examining the isomeric production rate in light of the total number of gold nuclei in the target, 1.85 x 10^{19} nuclei, and the isomer's half-life, the total number of ground state nuclei in the target may be assumed to be essentially a constant value. With these observations, the general transition equation may be easily solved for $N_i(t)$,

$$N_i(t) = \frac{\int_{Econt}^{Emax} \sigma_{0 \to i}^{abs*}(E)\varphi(E)dE}{\dfrac{\Gamma_i}{\hbar}} \, N_0 \left(1 - \exp^{-\frac{\Gamma_i}{\hbar} t} \right).$$ 2-34

In the following figure the isomeric gold activity induced in the gold foil of the sample problem is plotted as a function of time after the start of irradiation. Up until the end of the irradiation, at 4 seconds, the induced activity steadily increases, asymptotically trending towards a steady state value. Knowledge of the induced isomeric activity will be needed in PRE applications involving both measurement of the amount of the isomeric isotope in a sample as well as applications aimed at the production of isomers for secondary purposes and this number is included as well. Also in the figure is the cumulative total number of isomeric nuclei to have decayed since the beginning of the irradiation and the cumulative number of isomeric nuclei which will decay after the irradiation has ended. Computation of the total number of nuclei that have decayed in some period of time will be useful for designing the radiation detection and measurement systems utilized in applications measuring the presence and amount of isomeric isotopes in samples as well. The results of calculations similar to these will be used in subsequent chapters as the starting point for choosing the technical specifications of irradiation and radiation detection components which will be used in general PRE applications.
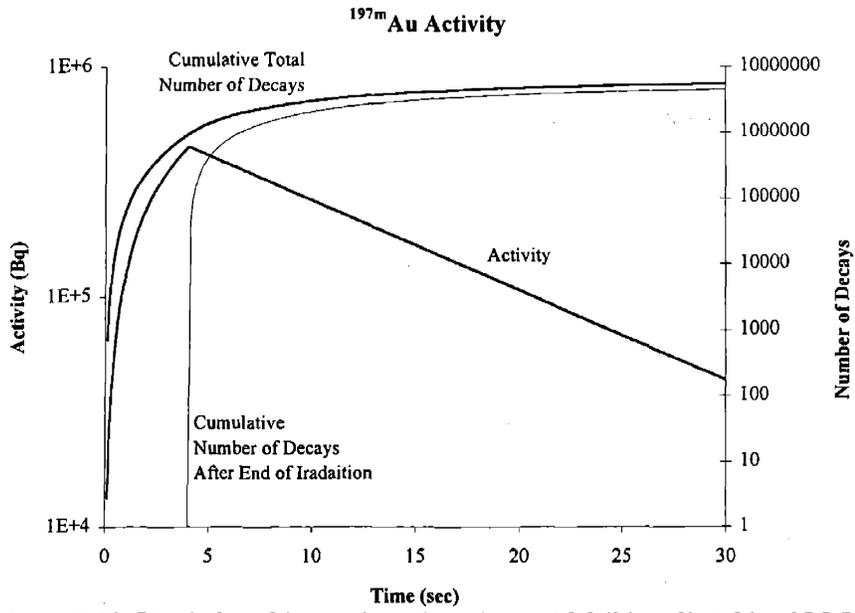
Figure 2-10 The induced isomeric activity in a gold foil irradiated by 6 MeV bremsstrahlung. Also included in this figure is the cumulative total number of isomeric decays and the cumulative number of isomeric decays after the end of irradiation.

2.4 REFERENCES

[1] P. A. M. Dirac, The Principles of Quantum Mechanics, Fourth Edition, Oxford University Press, Oxford, 1958.

[2] H. A. Bethe and G. Placzek, "Resonance Effects in Nuclear Processes," Phys. Rev. **51**, 150 (1937).

[3] H. A. Bethe, "Nuclear Physics B. Nuclear Dynamics, Theoretical," Rev. Mod. Phys., **9**, 220 (1937).

[4] G. B. Collins et. al., "Nuclear Excitation of Indium by X-Rays," Phys. Rev. **55**, 507 (1939).

[5] G. B. Collins and B. Waldman, "Energy Distribution of Continuous X-Rays from Nuclear Excitation," Phys. Rev. **59**, 109 (1941).

[6] E. Guth, "Radiative Transition Probabilities in Heavy Nuclei, Excitation of Nuclei by X-Rays," Phys. Rev. **59**, 325-331 (1941).

[7] B. Waldman and M. L. Wiedenbeck, "The Nuclear Excitation of Indium by X-Rays and Electrons," Phys. Rev. **63**, 60 (1943).

[8] M. L. Wiedenbeck, "The Nuclear Excitation of Silver and Cadmium," Phys. Rev. **67**, 92-97 (1945).

[9] M. L. Wiedenbeck, "The Nuclear Excitation of Rhodium," Phys. Rev. **67**, 267-268 (1945).

[10] J. M. Blatt and V. F. Weisskopf, Theoretical Nuclear Physics, John Wiley & Sons, Inc., New York, 1952.

[11] F. R. Metzger, "Resonance Fluorescence in Nuclei," Progress In nuclear Physics, O. R. Frisch, ed., Vol. 7, Pergamon Press (1959).

[12] P. Axel, "Electric Dipole Ground-State Transition Width Strength Function and 7-MeV Photon Interactions," Phys. Rev. **126**, 671 (1962).

[13] Boivin, Cauchois and Heno, "Photoactivation Nucleaire Du ^{77}Se, ^{107,109}Ar, ^{111}Cd, ^{115}In et ^{199}Hg," Nucl. Phys. **A137**, 520-530 (1969).

[14] C. B. Collins et. al., "Activation of ^{115}In^m by Single Pulses of Intense Bremsstrahlung," Phys. Rev. C **38**, 1852-1856 (1988).

[15] J. A. Anderson et. al., "Nuclear Photoactivation Cross Sections for Short-Lived Isomeric States Excited with a 6 MeV Linac," Nucl. Instr. Meth. Phys. Res. **B40/41**, 452-454 (1989).

[16] J. J. Carroll et. al., "Excitation of ^{123}Te^m and ^{125}Te^m Through (γ,γ') Reactions," Phys. Rev. C **43**, 897-900 (1991).

[17] V. V. Lomonosov and S. B. Sazonov, "Temporal Theory of Resonant Gamma-Ray Scattering from a Nuclear Isomer: Calculation of Scattering Interaction Time," JETP, **80**, 45-49 (1995).

[18] V. I. Vysotskii, "Controlled Spontaneous Nuclear γ Decay: Theory of Controlled Excited and Radioactive Nuclei γ Decay," Phys. Rev. C **58**, 337-350 (1998).

[19] Sowerby, Ellis and Greenwood-Smith, "Bulk Analysis for Copper and Nickel in Ores Using Gamma-Ray Resonance Scattering," Report IAEA-SM-216/4, Nuclear Techniques and Mineral Resources Proceedings, 499-521 (1977).

[20] G. Kehlenbeck et. al., "The Slowing-Down of Low Energy Recoil Atoms in Solids and Liquids Investigated by Nuclear Resonance Fluorescence," Z. Phys. B **66**, 147-151 (1987).

[21] W. Muckenheim et. al., "Nuclear Resonance Fluorescence in 238U and a New Approach to Doppler-Shift-Attenuation Using High Speed Rotation," Z. Phys. A **300**, 43-46 (1981).

[22] P. Axel and J. D. Fox, "Implications of the Photonuclear Effect in Zr^{90}," Phys. Rev. **102**, 400-414 (1956).

[23] T. Ericson and V. Strutinski, "On Angular Distributions in Compound Nucleus Processes," Nucl. Phys. **8**, 284-293 (1958).

[24] T. Ericson and V. Strutinsky, "On Angular Distributions in Compound Nucleus Processes," Nucl. Phys. **9**, 689-690 (1958/59).

[25] T. Ericson, "A Statistical Analysis of Excited Nuclear States," Nucl. Phys. **11**, 481-491 (1959).

[26] K. J. Le Couteur and D. W. Lang, "Neutron Evaporation and Level Densities in Excited Nuclei," Nucl. Phys. **13**, 32-52 (1959).

[27] J. R. Huizenga and R. Vandenbosch, "Interpretation of Isomeric Cross-Section Ratios for (n,γ) and (γ,n) Reactions," Phys. Rev. **120**, 1305-1312 (1960).

[28] R. Vandenbosch and J. R. Huizenga, "Isomeric Cross-Section Ratios for Reactions Producing the Isomeric Pair Hg^{197,197m}," Phys. Rev. **120**, 1313-1318 (1960)

[29] J. L. Need, "Analysis of the Energy Dependence of the Isomer Ratio in the $Sn^{120}(p,\alpha)In^{117,117m}$ Reaction," Phys. Rev. **129**, 1302-1307 (1963).

[30] Vandenbosch, Haskin and Norman, " Isomer Ratios for $Y^{87,87m}$ and the Spin Dependence of the Nuclear Level Density," Phys. Rev. **137**, B 1134-1144 (1965).

[31] N. D. Dudey and T. T. Sugihara, "Statistical-Model Analysis of Isomeric Ratios in (α,xn) Compound Nuclear Reactions," Phys. Rev. **139**, B 896 (1965).

[32] W. B. Walters and J. P. Hummel, "Studies of Isomeric Yield Rations in the Production of Sc44, Mn52, and Y87 by Photonuclear Reactions," Phys. Rev. **150**, 867-876 (1966).

[33] PSR-125/GNASH-FKK Code Package, Radiation Shielding Information Center, Oak Ridge National Laboratoy, USA.

[34] J. Kopecky and M. Uhl, "Test of Gamma-Ray Strength Functions In Nuclear Reaction Model Calculations," Phys. Rev. C **41**, 1941-1955 (1990).

[35] C. Bloch, "Theory of Nuclear Level Density," Phys. Rev. **93**, 1094-1106 (1954).

[36] W. D. Myers and W. J. Swiatecki, "Anomalies in Nuclear Masses," Arkiv For Fysik 36, 343-352 (1966).

[37] Wapstra, Audi and Hoekstra, "Atomic Masses From (Mainly) Experimental Data," Atomic Data and Nuclear Data Tables **39**, 281-287 (1988).

[38] P. E. Nemirovsky and Yu. V. Adamchuk, "Neutron and Proton Pair Interaction Energy," Nuclear Phys. **39**, 551-562 (1962).

[39] J. M. B. Lang and K. J. Le Couteur, "Statistics of Nuclear Levels," Proc. Phys. Soc. A **67**, 585-600 (1954).

[40] T. D. Newton, "Shell Effects on the Spacing of Nuclear Levels," Can. J. Phys. **34**, 804-829 (1956).

[41] A. G. W. Cameron, "Nuclear Level Spacings," Can. J. Phys. **36**, 1040-1057 (1958).

[42] D. W. Lang, "Nucleon Correlations and Nuclear Level Densities," Nucl. Phys. **42**, 353-366 (1963).

[43] U. Facchini and E. Saetta-Menichella, "level Density Parameter values From Neutron and Proton Resonances," Energia Nucleare **15**, 54-62 (1968).

[44] A. V. Ignatyuk, G. N. Smirenkin and A. S. Tishin, "Phenomenological Description of the Energy Dependence of the Level Density Parameter," Sov. J. Nucl. Phys. **21**, 255-257 (1975).

[45] N. N. Abdelmalek and V. S. Stavinsky, "Semi-Expirical Formula for Nuclear Level Density and Fission Asymmetry," Nuclear Phys. **58**, 601-610 (1964).

[46] N. D. Dudey and T. T. Sugihara, "Statistical-Model Analysis of Isomeric Ratios in (α,xn) Compound Nuclear Reactions," Phys. Rev. **139**, B 896-904 (1965).

[47] W. P. Ponitz, "A Gamma-Ray Cascade Model for the Calculation of Average γ-Ray Multiplicities and Isomeric Cross Section Ratios," Zeit. Physik **197**, 262-275 (1966).

[48] R. B. Firestone, "Table of Isotopes CD-ROM," S. Y. Frank Chu, CD-ROM editor, Eighth Edition. v1.0, (1996).

[49] S. S. Dietrich and B. L. Berman, "Atlas of Photoneutron Cross Sections Obtained With Monoenergetic Photons," Atomic Data and Nucear Data Tables **38**, 199-338 (1988).

[50] E. Silva and J. Goldemberg, "Inelastic Scattering of Photons in Y^{89},"Phys. Rev. **110**, 1102-1103 (1958).

[51] M. L. Wiedenbeck, "The Nuclear Excitation of Krypton and Rhodium," Phys. Rev. **68**, 237-239 (1945).

[52] Bogdankevich, Lazareva and Moiseev, "Inelastic Scattering of Photons on Rh^{103} Nuclei," Sov. Phys. JETP **12**, 853-856 (1961).

[53] P. Kruger et. al., "Excitation of Isomeric States In Rh^{103} and In^{115} by Electrons," Nucl. Phys. **62**, 584-592 (1965).

[54] J. Safar et. al., "$^{103}Rh^{m}$ Production By Inelastic Gamma Scattering in the Giant Dipole Resonance Region," Phys. Rev. C **44**, 1086-1090 (1991).

[55] L. Meyer-Schützmeister and V. L.Telegdi, "Inelastic Scattering of Photons from Au^{197}," Phys. Rev. **100**, 961 (1955).

[56] L. Meyer-Schützmeister and V. L.Telegdi, "Inelastic Nuclear Scattering of Photons by Au^{197}," Phys. Rev. **104**, 185-190 (1956).

[57] E. V. Tkalya, "γ Decay of Isomeric Nuclei in an Intense External Field: The Role of Giant Dipole Resonances," Sov. J. Nucl. Phys. **49**, 992-994 (1989).

[58] J. J. Carroll et. al., "Accelerated Decay of ^{180}Ta^m and ^{176}Lu In Stellar Interiors Through (γ,γ') Reactions," The Astrophysical Journal **344**, 454-459 (1989).

[59] C. B. Collins et al., "The Gamma-Ray Laser – Status and Issues in 1988," Laser and Particle Beams 7, 357-367 (1989).

[60] C. B. Collins et. al., "Resonant Excitation of the Reaction ^{180}Ta$^m(\gamma,\gamma')^{180}$Ta," Phys. Rev. C **42**, R1813-R1816 (1990).

[61] C. B. Collins et. al., "Status and Issues in the Development of a γ-Ray Laser. II. Giant Resonances for the Pumping of Nuclei," Laser and Particle Beams **11**, 43-54 (1993).

[62] S. Olariu and A. Olariu, "Induced Emission of γ Radiation From Isomeric Nuclei," Phys. Rev. C **58**, 333-336 (1998).

[63] S. Olariu and A. Olariu, "Power Densities for Two-Step γ-Ray Transitions From Isomeric States," Phys. Rev. C **58**, 2560-2562 (1998).

[64] K. Pisk et. al., "Nuclear Excitation by the Inelastic Photoelectric Effect," Phys. Rev. C **25**, 2226-2230 (1982).

[65] A. Ljubičić et. al., "Photoactivation Investigations With ^{115}In," Phys. Rev. C **23**, 2238-2244 (1981).

[66] M. Krěmar et. al., "Photoactivation of ^{111}Cd," Phys. Rev. C **25**, 2097-2099 (1982).

[67] M. Krěmar et. al., "Photoactivation of Isomeric Levels in ^{113}In and ^{87}Sr," Phys. Rev. C **33**, 293-295 (1986).

[68] J. A. Anderson, "Activation of ^{111}Cd^m By Single Pulses of Intense Bremsstrahlung," Phys. Rev. C **38**, 2838-2842 (1988).

[69] M. Krěmar et. al., "Resonant and Nonresonant Contributions to the Photoactivation of ^{111}Cd," Phys. Rev. C **41**, 771-774 (1990).

[70] P. Von Neumann-Cosel et. al., "Comment on 'Resonant and Nonresonant Contributions to the Photoactivation of ^{111}Cd,'" Phys. Rev. C **44**, 554-558 (1991).

[71] M. Krěmar et. al., "Reply to "Comment on 'Resonant and Nonresonant Contributions to the Photoactivation of ^{111}Cd,'"" Phys. Rev. C **47**, 906-909 (1993).

[72] I. S. Batkin, "Compton Excitation of Nuclear Levels," Sov. J. Nucl. Phys. **29**, 464-469 (1979).

[73] L. Spruch and G. Goertzel, "Magnetic Internal Compton Coefficients in the Born Approximation," Phys. Rev. **94**, 1671-1678 (1954).

[74] S. Batkin and M. I. Berkman, "Excitation of Low-Lying Nuclear States by Synchrotron Radiation," Yadernaya Fiz. 32, 972-977 (1980).

[75] E. V. Tkalya et. al., "Processes of the Nuclear Isomer ^{229m}Th $(3/2^+, 3.5 \pm 1.0$ eV) Resonant Excitation by Optical Photons," Physica Scripta **53**, 296-299 (1996).

[76] R. Horvat et. al., "Nuclear Excitation During Pair Production," Phys. Rev. C **29**, 1614-1616 (1984).

[77] E. G. Fuller and E. Hayward, "Nuclear Elastic Scattering of Photons," Phys. Rev. **101**, 692-700, (1956).

[78] R. Moreh, "Studies of Fundamental Photon Scattering Processes Using n-Capture Gamma-Rays," Nucl. Inst. Meth. **166**, 91-103 (1979).

[79] P. Papatzacos and K. Mork, "Delbrück Scattering Calculations," Phys. Rev. D **12**, 206-218 (1975).

[80] M. Schumacher and P. Rullhusen, "Delbrück and Rayleigh Scattering Below 5 MeV," Nucl. Inst. Meth. **166**, 85-90 (1979).

[81] Schumacher, Rullhusen and Baumann, "Nuclear Compton Scattering at Intermediate Energies," Il Nuovo Cimento **100**, 339-356 (1988).

[82] Kahane, Moreh, and Shahal, "Interferences Between Rayleigh, Delbrück and Nuclear Resonance Scattering Processes," Phys. Rev. C **28**, 1519-1526 (1983).

Chapter 3

INDUSTRIAL IMPLEMENTATION OF PRE

There are three physical components comprising an industrial photonuclear resonance excitation system: the target of the irradiation (more specifically, the isomeric isotope in the target), the source of the radiation and, for material analysis applications, radiation measurement instrumentation to measure the decay of isomeric nuclei. The relationship between these physical components in the planning and design of an industrial system is shown in Figure 3-1. The initial step in the design of such a system is the identification of some problem which might be addressed using photonuclear resonance excitation (PRE) and realization that an isomeric isotope exists for that application; this is done by examining the availability of isomeric isotopes and their properties in the context of the problem. Assuming that a suitable isotope exists for an application, the next step in the design process is to decide upon the operating characteristics of the irradiation source that will be needed. These specifications are made by examining not only the actual physics of the excitation process for the particular isomer but are also decided upon by taking into account the desired performance requirements of the final system (e.g., material throughput, induced activity, ancillary material activation limits, cost, etc.) Additionally, for material assay applications the technical specifications of the irradiation source will be determined in conjunction with choosing the radiation measurement instrumentation where additional performance requirements such as analysis speed, detection limits, measurement accuracy, durability and instrumentation cost also come into play.
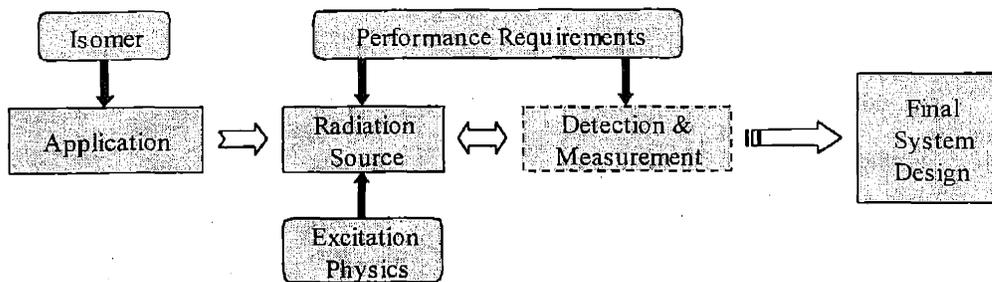
Figure 3-1 Design process for developing an industrial PRE system.

This chapter examines the three components mentioned above. In §3.1 a survey of the naturally occurring isotopes with isomeric states is presented together with a review of the characteristics of isomeric nuclei that are relevant to the industrial use of PRE. Additionally, a summary of some of the published literature focusing on the excitation of isomers for various applications is presented. Following this, §3.2 explores issues related to radiation sources used for isomeric excitation. The section begins with an overview of different sources which might be considered for use in irradiations, comparing their advantages and disadvantages relative to the physics presented in the previous chapter as well as their abilities to meet likely system performance requirements. After deducing that the most favorable choice of irradiation source for most applications is the x-ray spectrum produced in high energy electron bremsstrahlung, a more detailed discussion examines the relationship between parameters commonly used to characterize bremsstrahlung fields. Section §3.3 explores issues related to the detection and measurement of radiation to identify those detector materials and components most suitable for use in industrial PRE applications taking into account factors such as the detector efficiency, the performance of the detectors under prolonged exposure to intense photon radiation, timing and cost.

Before examining in detail those issues dealing with the engineering design of an industrial PRE system one should, of course, first evaluate the desirability of such a system in comparison with potential alternatives. In materials assay applications, the advantages of a PRE system in comparison with existing technologies are its specificity, accuracy and that it is non-destructive and has the potential ability to operate in real time to analyze bulk materials. Disadvantages include its specificity, space requirements to house the radiation and detection systems and its cost. Considering these different factors it would be unlikely that a PRE system would be deemed cost effective for an application where, for example, material composition of the bulk material is a slowly changing and relatively constant function of time such that grab sampling and remote laboratory analysis provide an effective solution. Similarly, if it is desired to produce a particular isomeric isotope or a radioisotope demonstrating particular decay characteristics, PRE may be less favorable in comparison with other radioisotope production pathways. An analysis of the attractiveness of a PRE based solution to a particular problem must include an assessment of other potential solutions to the problem as well.

3.1 ISOMERS

Depending upon various nuclear properties, the lifetimes of excited nuclear eigenstates spans 33 orders of magnitude, ranging from less than a femtosecond for many excited levels ($<10^{-15}$ sec) to longer than the age of the universe as for ^{180m}Ta, which has a half-life of 1.2×10^{15} years ($>10^{18}$ sec). There is no accepted definition for classifying an excited state as an isomer, some researchers place the lower limit on the half-life of an isomer at 1 microsecond while others set the lower limit at 1 millsecond and some even as long as

1 second. All isotopes can be excited to higher energy eigenstates through photonuclear resonance excitation and, in principle, all nuclei can be used for industrial PRE. However, not all isotopes can be *easily* examined using photonuclear resonance excitation analysis. For isotopes with only short lived energy eigenstates data must be collected concurrently with excitation. Because of this complicated shielding arrangements must be used to protect the measuring equipment from both the irradiating photons as well as scattered photons. Examples of the elaborate physical set-up which must be employed to reduce these scattered background signals for the analysis of simple, homogeneous samples are evident in the published literature describing nuclear resonance fluorescence (NRF) experiments for physics experiments as well as a few industrial related applications.[1 - 18] NRF would be the ideal technique for examining materials to determine their elemental composition since it is applicable to every isotope (except hydrogen) and because of the high PRE excitation cross sections for short lived high energy eigenstsates. Unfortunately, full realization of this type of technology for industrial applications is limited because of the need for high current accelerators (>> mA) and detector systems having large detection efficiencies at affordable prices. Further, complications arise from the presence of interference lines and overall background in the measured gamma ray spectrum when measuring trace quantities o materials, which originate from the decay of eigenstates of other nuclei in the irradiation target as well as surrounding materials and scattered radiation from the target and surrounding materials.

In choosing to measure the decay of longer lived eigenstates, however, many of the difficulties mentioned above vanish. For the analysis of isomers, measurements may be taken in between the pulses of a cyclic radiation source or after the irradiation entirely. By doing this, the radiation measurement and data acquisition system does not need to be collecting data during the excitation phase of the procedure and thus problems associated with the reduction in the signal to noise ratio related to the presence of scattered irradiation photons and interfering decay lines are eliminated. In addition, if the detector system is resilient enough to endure exposure to the irradiation field, much of the elaborate shielding required in the prompt excitation experiments may be eliminated as well. For this approach, the only extraneous source of degradation of the signal to noise ratio other than natural background radiation is the presence of additional isomeric nuclei. Unlike short-lived excited eigenstates, however, the half-lives of isomeric nuclei a) tend to be long compared to the amount of time required to actually acquire and process data and b) span a larger range in magnitude. These two factors allow for the reduction of interferences from the decay of isomers of adventitious isotopes, which have half-lives that are different from that of the desired isomer by a factor of ~2 or more, by discriminating between changes in the intensity of the signal over time.

Depending upon the characteristics of the irradiation and detection system, the lower limit on half-life for isomers which could be analyzed is probably on the order of 10 μs. Due to sample self shielding, which depends upon the size and composition of the sample matrix, the lower energy of the emitted photon radiation from the decay of the isomer is probably ~100 keV, although for small samples this minimum might be lower. For reference, a list of isotopes which have excited energy states with half-lives greater than 1 μs is given in Table 3-1.

For PRE applications aimed at producing the isomer for some secondary use such as a tracer or as for some medical application, additional conditions determining the suitability of a particular isomer include the half-life (which must be long enough to transport the isomer to where it will be used) and the total and specific activities which may be achieved. For these applications the shorter lived isomers will in general prove less useful except for situations where the isomer may be excited in-situ in the place where it will be used. As an example, tracer studies of short-lived isomers could be conducted in a pipeline system by directly irradiating normally (or externally introduced) isomeric material in the pipeline during normal operation and then conducting measurements at some downstream location. For applications requiring very small, intense isomeric sources or sources with high specific activities, additional factors such as the natural abundance of the isotope and the intensity of the decay photon of interest become important.

Table 3-1 A partial[a] list of naturally occurring isotopes having isomers.[19]

Isotope	Natural Abundance[b] (%)	Isomer Half-Life	Transition Type to Ground	Photons Observed in Isomeric Decay (keV, (Intensity in %))
^{67}Zn	4.1	9.16 μs	E2	93.3 (100)
^{73}Ge	7.73	2.95 μs	E2	13.3 (100)
		0.499 s	M2	13.3 (100), 53.4 (100)
^{75}As	100	16.8 ms		279.5 (79.5), 303.9 (18.8)
^{77}Se	7.63	17.4 s		161.9 (100)
^{79}Br	50.7	4.86 s		207.2 (100)
^{83}Kr	11.5	1.83 h	E3	9.4 (100), 32.1 (100)
^{87}Sr	7.0	2.80 h		388.5 (100)
^{89}Y	100	16.1 s		909.0 (100)
^{90}Zr	51.4	809 ms		2319.0 (95.2)
^{93}Nb	100	16.1 a	M4	30.8 (100)
^{99}Tc	0	6.01 h		142.6 (99.2)
^{103}Rh	100	56.1 m	E3	39.8 (100)
^{107}Ag	51.8	44.3 s	E3	93.1 (100)
^{109}Ag	48.2	39.6 s	E3	88.0 (100)
^{111}Cd	12.8	48.5 m	M1+E2	150.8 (100), 245.4 (100)
^{113}Cd	12.2 (9E15 a)	14.1 a	E5	263.6 (0.14)
^{113}In	4.3	1.66 h	M4	391.7 (100)
^{115}In	95.7	4.49 h	M4	336.2 (100)
^{117}Sn	7.68	13.6 d	?	156.0 (100), 158.6 (100)
^{119}Sn	8.58	293 d		65.7 (100), 16.0 (100)
^{123}Te	0.91 (1.3E13 a)	120 d	E5	88.5 (100), 159.0 (100)
^{125}Te	7.12	58 d	?	35.5 (100),109.3 (100)
^{129}Xe	26.4	8.89 d		39.6 (100), 196.6 (100)
^{131}Xe	21.1	11.9 d	M4	163.9 (100)
^{135}Ba	6.59	1.20 d	M4	268.2 (100)
^{136}Ba	7.8	308 ms		163.9 (100), 818.5 (100), 1048.1 (100)
^{137}Ba	11.2	2.55 m	M4	661.7 (100)
^{155}Gd	14.8	32.0 ms		13.4 (100), 21.0 (100), 86.5 (98.7)
^{167}Er	23.0	2.27 s	E3	207.8 (100)
^{171}Yb	14.3	5.25 ms	E1	19.4 (100), 75.9 (97.6)
^{176}Yb	12.7	11.4 s (IT>90%, β⁻<10%)		82.1 (100), 96.0 (100), 189.6 (100), 293.0 (100), 389.3 (100)
^{176}Lu	2.59 (3.78E10 a)	3.64 h (β⁻=99.1%, EC=0.1%)		88.3 (100),201.8 (100), 306.8 (100) [from ^{176}Hf]

[a] This list is limited to isotopes having excited eigenstates with half-lives of 1 microsecond or greater. In addition to naturally occurring isotopes a few man made isomers have been included because of their importance in current applications or because of general interest. This list was compiled using data from reference 19 and supplemented using several additional sources presented in §3.4. Although a thorough review of the literature was performed to compile this list it is not necessarily a complete list.
[b] For naturally occurring radioactive isotopes, the half-life of the long-lived state is given in parentheses.

Table 3-1 A partial list of naturally occurring isotopes having isomers. (Continued)

Isotope	Natural Abundance[a] (%)	Isomer Half-Life	Transition Type to Ground	Photons Observed in Isomeric Decay[b] (keV, (Intensity in %))
^{177}Hf	18.6	51.4 m		214.0 (100), 326.7 (76.4), 311.5 (63.9), ...
		1.08 s		228.5 (95.4), 378.5 (63.8), ...
^{178}Hf	27.3	4.0 s		88.9 (100), 93.2 (100), 213.4 (100), 325.6 (100), 426.4 (100)
^{179}Hf	13.6	18.7 s	?	160.7 (100), 214.3 (100)
^{180}Hf	35.1	5.5 h (IT=99.7%, β^-=0.3%)		57.6 (74.1), 93.3 (100), 215.2 (100), 332.3 (100), 443.1 (74.1), 500.6 (25.9)
^{180}Ta	0.012 (1.2E15 a)	> 1.2 x 10^{15} a [Ground = 8.15 h]		93.3 (24.9) [from ^{180}Hf after EC] 103.6 (3.6) [from ^{180}W after β^-]
^{180}W	0.13	5.47 ms		103.6 (100), 234.0 (100), 390.6 (100), 350.9 (100), 450.0 (100)
^{183}W	14.3	5.2 s		102.5 (100), 107.9 (78.6)
^{189}Os	16.1	5.8 h	M3 + E4	30.8 (100)
^{190}Os	26.4	9.9 m		38.9(100), 186.7 (100), 361.1 (100), 502.5 (100), 616.1 (100)
^{191}Ir	37.3	4.94 s		41.9 (100), 129.4 (100)
		5.5 s		41.9 (100), 129.4 (100), 395.1 (100), 420.1 (100), 524.5 (100), 536.0 (100)
^{193}Ir	62.7	10.5 d	M4	80.2 (100)
^{192}Os	41.0	5.9 s		205.8 (61.2), 302.5 (88.2), 453.1 (71.0), 484.6 (61.2), 569.4 (85.9)
^{195}Pt	33.8	4.0 d		30.9 (45), 98.8 (45), 129.5 (100), 129.7 (55)
^{197}Au	100	7.73 s		130.2 (96.7), 279.0 (95.3)
^{199}Hg	16.9	42.6 m		158.4 (100), 374.1 (100)
^{204}Pb	1.4	67.2 m		374.7 (>97.5), 899.2 (97.5), 911.8 (>97.5)
^{207}Pb	22.1	0.81 s		569.7 (100), 1063.7 (100)
^{229}Th	0			0.0035 (100)
^{235}U	0.72	25 m	E3	0.0768 (100)
^{236}Np	0	22.5 h		60 (?)
^{237}Pu	0	0.18 s		145.5 (100)
^{244}Cm	0	34 ms		43.0 (69.9), 99.4 (69.9), 153.0 (69.9), 744.0 (69.9)

3.1.1 Characteristics

Four physical characteristics of an isotope which are of importance in determining suitability for industrial PRE are the natural abundance of the isotope, the half-life of the isomer, the energy and intensity of the principle gamma-ray(s) associated with the decay of the isomer and the cross-section for excitation of the isomeric state. For analytical measurement applications, where the goal is to determine the quantity of some element in a sample, low natural abundance of the isomeric isotope worsens the minimum detectable

[a] For naturally occurring radioactive isotopes, the half-life of the long-lived state is given in parentheses.
[b] Only Intensities > 60% are listed.

amount of the element in comparison with the case where the isomer is the sole naturally occurring isotope. For isotope production applications, a low natural abundance decreases the specific activity which may be achieved in a similar fashion, all other things being the same. In some cases though, use of sample materials enriched in the isomeric isotope might be possible, allowing increased specific activities to be achieved (usually at a significant increase in cost).

While technical difficulties act to set a lower limit on the half-lives of isomers that can be used for PRE applications (§3.3), practical considerations act to set an upper limit on the half-lives of isomers useful for PRE applications. For assay purposes in industrial applications requiring real time or near real time data acquisition, isomeric half-lives must be comparable to the amount of time allotted for measurement in order to acquire sufficient data. This is primarily due to the limited intensity of suitable photon irradiation sources currently available for industrial use. As has been shown in Chapter 2 and will be further demonstrated in following chapters, these photon sources are now capable of producing excited isomeric populations in short lived nuclei which are just capable of satisfying realistic design objectives. For long lived isomeric nuclei to yield similar results in the same measurement times would require photon sources having proportionally greater intensities in relation to the differences in half-life between the short lived and long lived isomers. For applications using isomers, long lived excited isotopes may be similarly difficult if measurements are needed later. Additionally, one of the prime advantages in using isomers, that they decay quickly leaving no long lived radioactive materials behind for handling and disposal, is lost when using isomers having long half-lives.

Examining Table 3-1 and reviewing the decay schemes of isomeric nuclei, two other isomer parameters with relevance to the development of an industrial PRE system become apparent, the relative intensity and energy of the characteristic gamma rays associated with the isomer's decay. For PRE based assay applications the interpretation of the measured isomer decay data must account for the possible attenuation of these characteristic decay photons in the sample matrix. In addition, for many potential industrial PRE applications which involve the measurement and quantification of isomeric materials in bulk materials, such as ore and soil, the attenuation of the decay photons in these materials will also act to constrain the probing depth of the technique, imposing a maximum effective material thickness. The relevance of the intensity of the decay photons to the design of an industrial PRE system is analogous to that of the natural abundance of the isomeric isotope. Just as the time required to determine the amount of some element in a sample increases as the abundance of the isomeric isotope in that sample is decreased, so too does the required measurement time increase if the relative intensity of the decay photons being measured is reduced. Unfortunately, the relative intensity of the decay photon of interest cannot be changed; if the time required to acquire a measurement to the needed precision at a certain decay energy is too long the only options are to either increase the intensity of the irradiation flux, increase the detection efficiency of the measurement system or choose a different decay photon to monitor.

Of course, one very important characteristic is the isomeric excitation cross section. With the understanding of the different transition pathways influencing the population of the isomeric state during and after irradiation presented in Chapter 2, it is clear that both the intensity and spectrum of the irradiating photon source together with the isomeric excitation cross section directly determine the activity of the isomer in the sample. Referring to the theoretical model of the previous chapter for predicting isomeric excitation cross sections, together with a study of the limited experimental photonuclear resonant absorption excitation cross section data in the literature, one notices that in general isomeric excitation cross sections do not vary significantly (within a factor of ~2) in magnitude or in their energy dependence between nuclei. Because of this, industrial systems developed to produce isomers for some secondary uses or to probe materials will be similar in key design parameters irrespective of the actual isomer being excited. Unlike other types of nuclear reactions such as neutron absorption where, within the energy range of typical irradiating sources, strong resonance features often exist, the smooth nature of photonuclear isomeric excitation probabilities as a function of energy coupled with the preferable bremsstrahlung irradiation spectrum makes the results of photonuclear irradiation less dependent on parameter variables such as sample heterogeneity, density and moisture content.

3.1.2 Previous Work

In the design on an industrial PRE system the energy dependence of the isomeric excitation cross section must be known. For some nuclei, experimental work has been carried out to measure this cross section, for these nuclei and others the analytical techniques of Chapter 2 may also be used to either help corroborate this data (which was often reported with little or no indication of uncertainties in the reported values) or to make initial estimates on the values of cross sections for unreported isomers. Reading through the literature on the subject, however, one finds a considerably larger body of information where the energy integrated excitation cross section is reported. [20,21] The most likely reason for this is probably that it is easier to just measure the isomeric activity at different excitation energies than it is to process these data (i.e., using a differencing method for data taken with a bremsstrahlung beam, for example) to back out the continuous energy dependence. Unfortunately, the exact spectrum of the radiation field used to excite the isomers in these studies is rarely reported in these papers either, making the extrapolation and use of reports of integrated isomeric excitation cross sections more useful in a qualitative rather than quantitative fashion for the engineering design of a real industrial PRE system. An example of this type of experimental data is given in Table 3-2. As with the published energy dependent excitation cross sections, the published data in this area rarely includes an indication of the uncertainty in the reported values. Since such data are derived from the specific irradiating photon spectrum, exact calculation of the isomeric excitation rate for different facilities cannot be done. However, as a first step in gauging the promise of a particular industrial concept they can be useful.

Table 3-2 Energy Integrated Isomeric Excitation Cross Sections.[20,21]

| Isotope | Integrated Cross Section ($\times 10^{-26}$ cm^2 keV) ($\pm$ 20%)[a] | | | | | | | | | | |
| | Bremsstrahlung Endpoint Energy (MeV) | | | | | | | | | | |
	1	1.5	2	2.5	3	3.5	4	4.5	5	5.5	6
^{77}Se	——	5	8	12	12	12	20	50	100	120	100
^{79}Br	——	0.2	0.8	3	4	5	7	10	30	50	30
^{89}Y (x 100)	——	15	30	60	50	50	80	150	500	500	500
^{137}Ba	——	0.2	0.8	3	4	5	7	10	30	50	30
^{167}Er	——	20	50	80	80	80	100	160	700	800	700
^{176}Lu	30	30	60	70	100	150	150	300	600	500	800
^{180}Ta	30	30	60	70	100	150	150	300	600	500	800
^{183}W	——	0.2	0.8	3	4	5	7	10	30	50	30
^{191}Ir	——	20	50	80	80	80	100	160	700	800	700
^{197}Au	——	10	15	30	30	40	50	80	200	200	200

A considerable volume of research reporting the isomeric activity induced in samples irradiated by bremsstrahlung beams has amassed over the years. Of particular note is the compilation of data by Goryachev and the experimental results of Kaminishi and Kojima, Otvos et. al. and researchers at the University of Texas at Dallas. [20–24] The published body of work in this area is mainly concerned with the reporting of the PRE activity induced in samples of natural and isotopically enriched elements; the main variables being the energy and current (or power) of the accelerators used and the irradiation and counting times of the experiments. A summary of some of this work is provided in Table 3-3, where the results of bremsstrahlung irradiation with four different endpoint energies are listed. As might be expected by inspecting this previous table, irradiations at different endpoint energies in the 1 to 6 MeV range can result in significant differences in induced isomeric activities. These increases are due to both the opening of new transition pathways as the photon energy is increased, allowing excitation of higher energy discrete states,

---

[a] These values were interpreted from charted data, the 20% uncertainty is due to interpolation of values from the chart. No indication of uncertainty regarding the accuracy of these values is presented in either of the references from which this information was taken.

as well as the smooth increases in the indirect isomeric excitation pathway through compound nuclear states at even higher photon energies.

Another important feature to be garnered from this work is the importance of the relationship between the excited isomers half-life and the duration of the irradiation. Even though a rather high current electron accelerator (1 mA) was used for these experiments, the induced isomeric activity for isotopes having half-lives on the order of a day or longer was quite low. This serves to illustrate both the difficulties associated with the use of industrial PRE for probing/measurement applications involving long lived isomeric states as well as the necessity for long irradiation periods in order to produce high specific activity isomeric materials in these nuclei. Two notable anomalies in this data are ^{87m}Sr and ^{176m}Lu which appear to have rather larger induced activities than might be expected given half-lives and in comparing their reported 3 MeV beam activities with other isomers having similar half-lives. This may stem in part from the opening of a large discrete excitation pathway in these isotopes at some energy below 3 MeV which is absent in the other nuclei. A comprehensive review of the published literature dealing with the isotopic activation of isomers was published by Veres in 1980.[25]

At this point it is worth taking some time to consider the use of resonant photon absorption for the excitation of isomeric eigenstates in radioactive nuclei as well. This process is the same as that for excitation in stable nuclei and it may be modeled using the general transition equation of Chapter 2. However, as one might intuitively expect, energetic eigenstates in radioactive nuclei can also undergo nuclear transformation through decay, a channel which competes with de-excitation through isomeric transition. Since there is little information known about the branching ratios for these competing reactions at higher energy eigenstates, exact calculations are often difficult to perform. Nevertheless, several industrial PRE applications involving the use of radioactive nuclei can be envisioned. One example could be as a method to improve the sensitivity of work focused on determining the concentration of technetium-99 in different matrices; a significant source of the long-term radioactivity in spent nuclear fuel, accurate methods of quantifying the presence of technetium are desired. Due to its long half-life and strong tendency to decay purely by beta emission without an accompanying photon, PRE could serve to dramatically improve the sensitivity of technetium quantification.[26,27,28]

Table 3-3 Normalized isomeric activity in isotopic and natural elemental samples under various irradiation and counting conditions.[23,24]

Isomer/ Element	Known Half-Lives	Induced Isomeric Activity [a]			
		Irradiation Conditions:			
		3MeV T_{irr}=1 h I=1 mA	4 MeV T_{irr}=1 m I=1 mA	5 MeV T_{irr}=1 m I=1 mA	6 MeV T_{irr}=1 m I=1 mA
^{77m}Se	17.4 s	3.78		26.5	
^{79m}Br	4.86 s		32.6		
^{87m}Sr	2.90 h	0.257			0.00612
^{89m}Y	16.1 s	1.27		1.84	
^{103m}Rh	56.1 m	0.00270		0.00408	
Ag	39.8 s, 44.2 s	5.68		3.67	
^{111m}Cd	48.5 m	1.76			0.0102
In	1.658 h, 4.486 h				0.163
^{115m}In	4.49 h	7.62[b]			
Sn	13.6 d, 293 d	0.000270			0.0000102
Ba	0.308 s, 2.552 m, 1.20 d			0.0122	
^{137m}Ba	2.55 m	0.0432			
^{167m}Er	2.27 m	0.0757	100		
^{176m}Lu	3.64 h	0.100			
Hf	1.1 s, 4.0 s, 18.7 s, 51.4 m, 5.52 h, 25.1 d, 31 a			32.6	
^{179m}Hf	18.7 s	100			
W	5.15 s			2.45	
Ir	4.93 s, 6 s, 10.53 d			42.8	
^{191m}Ir	4.94 s, 5.00 s	27.0			
^{195m}Pt	4.02 d	0.0270		0.00612	
^{197m}Au	7.73 s	10.0	87.8		
^{199m}Hg	42.6 m	0.0594			0.00184

[a] Although several papers comparing the induced isomeric activity for different isomers have been published in the literature, there often are important differences in the irradiation conditions between experiments. The information presented here is from two separate experiments; results may be compared within the 3 MeV column or within the 4, 5 and 6 MeV columns. The data in the 3 MeV column are normalized to hafnium; data in the 4, 5 and 6 MeV columns is normalized to erbium.

[b] Data for this isotope may also have included photoactivation results for ^{113m}In.

3.2 RADIATION SOURCE

After deciding that an adequate match exists for the use of an isomer in an application, the first step towards the development of an industrial PRE system is determination of the performance requirements of the irradiation system which will be used. Since the photon excitation probabilities for different isomeric isotopes are similar, the general characteristics of radiation sources desirable for PRE applications are rather constant, irrespective of the actual circumstances of the task. In §3.2.1 various types of photon radiation sources are introduced and compared using criterion pertinent to industrial PRE. Some factors influencing the choice of irradiation source are size, shielding requirements, ease of operation, reliability, stability, safety and cost. Depending upon the application it may be desired to have a system which is transportable (for use as a field assay device) or easily moveable (capable of being installed in industrial facilities as a 'diagnostic appliance'.) The time dependence of the irradiation source may also prove an important factor in the choice of irradiation source, depending upon the half-life of the isotopes of interest and the detector system chosen to carry out analyses, another design choice may be whether to use a steady state or pulsed irradiation system.

Evaluating the characteristics of these different photon sources one ultimately finds that electron accelerator based bremsstrahlung is the best choice, having a large range of applications for which it is well suited. In §3.2.2 a detailed analysis of bremsstrahlung source operational parameters and their importance in the context of an industrial irradiation facility are presented. Understanding these practical aspects in the operation of the PRE irradiation system is important in order to be able to define realistic expectations and limitations for the eventual performance of an industrial system. Applying this information will be important for design studies exploring the use of PRE to produce isotopes for secondary purposes, allowing calculations of induced isomeric activities and specific activities as well as determining processing times. Integration of this knowledge with the information of §3.3, which examines different aspects of radiation detection systems, will be important for PRE probing applications as well where information concerning induced isomeric activities will be needed to ascertain detection and measurement system requirements.

3.2.1 Photon Radiation Sources

There are three general categories into which photon radiation sources may be classified: isotopic sources using one or more radioisotopes, nuclear reactors and sources utilizing particle accelerators. For PRE applications using one of these it is useful to further categorize the sources in terms of their photon spectrums, being either discrete or continuous in energy. In Table 3-4 several important characteristics of these six types of photon sources are presented for comparison. In the sections that follow, the relevance of these characteristics in relation to determining the suitability of each type of source for PRE will be discussed.

Table 3-4 Characteristics of discrete and continuous energy photon sources for industrial PRE.

Operational Parameter	Irradiation Source:					
	Isotopic		Reactor		Accelerator	
	Discrete	Continuous	Discrete	Continuous	Discrete	Continuous
Maximum Photon Energy (Mev)	~2	~2	~10	~2	~10-15	~60
Photon Intensity Depends On:	Source Activity	Source Activity, Scattering	Reactor Power, Reaction	Reactor Power, Reaction, Scattering	Accelerator Energy, Current, Reaction	Accelerator Energy, Current, Target
Source Size	Small	Large	Very Large	Very Large	Variable	Variable
System Size	Small	Large	Very Large	Very Large	Medium	Medium
Portable	Yes	No	No	No	Maybe	Maybe
Shielding Requirements	Standard	Standard	Extensive	Extensive	Standard	Standard – Extensive
Operational Reliability	High	High	Moderate	Moderate	High	High
Spectrum Stability	Very High	Very High	High	High	High	High
Relative Capital Cost	Low	Moderate	Very High	Very High	Moderate	Moderate
Time Spectrum	Continuous	Continuous	Continuous	Discrete/ Continuous	Discrete/ Continuous	Discrete/ Continuous

3.2.1.1   Isotopic – Discrete Energy

Isotopic photon sources emitting photons at one or a few discrete energies are straightforward to use, examples of which are radioisotopes such as cobalt-60 or cesium-137. Some characteristics of this type of source are that they are robust and reliable and do not rely on either human operators or the functioning of mechanical equipment. Another advantage of this type of radiation source is its low cost in comparison with other types of sources. The disadvantage of this type of source rests in the difficulty in finding a source which emits photons matching the energy of an excited eigenstate in the sample being analyzed.

From the physics review of Chapter 2 it is clear that a) for photons to excite a discrete eigenlevel they must exactly match the energy of that level and b) the probability of nuclear excitation through non-resonant processes is quite low. Because of these it is difficult to find a radioisotope suitable for PRE. In principle it would be possible to use an already excited quantity of the isomeric isotope as the irradiation source, however, since for most applications (especially those exciting isomers to conduct material assays in

samples) the lifetime of the isomeric state is small the utility of using the same isotope as the irradiation source is low. Radioisotopes emitting photons very close in energy to an eigenstate in the isomer could also be used in conjunction with some external method of kinetically shifting the energy of the irradiation photons, such as heating the radiation source or placing the irradiation source in a high speed rotor.

The upper energy limit of emitted photons from such sources is in the 2 to 3 MeV range, essentially excluding excitation through the indirect excitation of higher energy eigenlevels in the compound nucleus. Since a high activity source would be required, the design of an industrial PRE system using an isotopic source would require a shielding shutter capable of closing off radioisotope source. A source of this kind would emit photons continuously in time, making the examination of materials with short lived isomeric half-lives difficult in the continuous background of the irradiation source.

3.2.1.2   Isotopic – Continuous Energy

Due to the difficulty in finding isotopic sources emitting photons which are a match in energy for PRE an alternative which has been used is to arrange an isotopic source in a geometry where scattered photons can be used for excitation. Due to their availability for sterilization purposes, the pencils used in very high activity cobalt-60 irradiation systems could be used as the radiation source for industrial photonuclear resonance excitation, for example. In this configuration Compton scattered photons from the radioisotopic source would be the radiation source for PRE rather than the actual photons emitted during the nuclear decay process. Since this source involves a two step process (discrete photon produced in decay, production of continuous photon spectrum after scattering) a high activity source would be required. Several papers exploring isomeric excitation with this type of source have been reported in the literature.[25,29,30] Using these as a guide, an isotopic source using cobalt-60 would likely need to be on the order of thousands of Curies in strength to be useful.

As with the discrete energy isotopic sources, a continuous energy isotopic source would be limited to lower energy photons, less than ~2 MeV or so based upon the availability of the radioisotope. Due to the need for a high activity of the radioisotope and the use of scattered radiation, the geometry of such source would likely require a rather large physical footprint. This could make the installation of a PRE system using this technique difficult in certain situations. This is not only due to the need for a geometrically favorable scattering layout but also because of the shielding needed for such a large assembly. Additionally, a major concern with similar isotopic based sterilization systems is the danger of human intrusion during operation and safety issues associated with reloading.

Some advantages of a continuous energy isotopic radiation source are the stable nature of the radiation source and the relatively easy ability to increase or decrease the intensity of the irradiating photon spectrum due to the modular nature of the individual radioisotopic source pencils. One disadvantage of such a system is the characterization of the radiation spectrum. Due to the extended geometry required to hold the irradiation pencils and the use of the scattered photons it would be difficult to accurately characterize the time integrated photon spectrum seen by the materials being irradiated. For the short term irradiations comprising assay type measurements this could be particularly difficult. Also, because of the large size of the system and the constant need for shielding it is unlikely that a system using this type of radiation source would be transportable.

3.2.1.3   Nuclear Reactor – Discrete Energy [31-35]

Since the efficacy of an industrial photonuclear resonance excitation system depends upon the availability of a high intensity source of photons, some researchers have proposed using the intense neutron flux of a nuclear reactor as a starting point for the generation of the irradiation spectrum. A discrete energy photon source could be generated in this way through the use of any of a number of intermediate neutron target materials where photons are generated through (n,γ) reactions. Using an intermediate neutron absorption

target this approach is similar to the isotopic photon source. However, by continuously creating the photon emitting nuclei through neutron absorption, the lower limit in the allowable lifetime of the decaying isotope is effectively eliminated and the number of candidate isotopes which might be employed is significantly increased. The irradiation photon intensity for a particular reactor will depend upon the neutron flux at the absorber position and the positioning of the sample material with respect to this absorber. As an example of the signal strength that might be expected from a source such as this, one experiment reported in the literature, which used a water moderated reactor having a neutron flux of $4.70 \pm 0.53 \times 10^{11}$ cm^{-2} sec^{-1}, produced NRF signals of ~10,000 counts in 20 minutes using a 7 cm x 7 cm NaI crystal.[34]

The main advantage of a system employing this type of source would be the ability to leverage an existing facilities, when a reactor is already available, without requiring significant modifications. In spite of allowing a wider selection of candidate nuclei for photon production, the difficulty in finding an exact match still exists. For material assay applications, the technical difficulties associated with the incorporation of a reactor based photon source into a practical industrial system are numerous and include: the need for adequate shielding to reduce material activation and to reduce the photon background in the analysis process, as well as difficulties in constructing the reactor in a convenient location, with a geometry suitable for continuous and efficient analysis of the materials. For isomeric isotope production the technical disadvantages of this type of irradiation source are less restrictive, for those cases where a convenient match exists between an isomer and a candidate neutron activation target a reactor might be an attractive source, *especially if a high flux reactor is available.* However, it would be difficult to justify the construction of a new reactor solely for the purposes of isomer production.

Practical considerations which minimize the attractiveness of reactor based systems are of course dominated by cost but also include factors such as reliability (the need to be shutdown for extended periods to perform maintenance, inspections and refueling), variability in the irradiation spectrum and intensity as a function of varying reactor power and the large area needed for a reactor and its associated support facilities. Since it would not be cost effective to build a reactor dedicated to isomer production the reactor based approach would require the modification of an existing reactor. This would limit the use of short-lived isomers produced with this method to the vicinity of the reactor and increase the induced activity of medium-lived isomers needed due to decay losses during transportation.

3.2.1.4   Nuclear reactor – Continuous Energy

Utilizing a photon scattering geometry, as with the continuous energy isotopic photon source, a nuclear reactor could also be used to provide a continuous spectrum of photons for industrial PRE applications. For the same reactor power, and incident neutron flux on target, the intensity of a continuous photon spectrum generated in this way would be less than that of the discrete spectrum. However, this source would be completely general it its applicability for exciting different isomeric isotopes only being limited by the upper energy of the resultant photon spectrum (~2 MeV) and the feeding of excited levels to the isomeric state. The advantages and disadvantages of this type of system are essentially the same as those for the discrete energy reactor based photon system with the additional advantage of being applicable to a broader range of isomeric nuclei. This type of system could be particularly useful for the production of isomeric isotopes for secondary purposes provided a reactor with sufficient power was available to achieve the needed irradiation photon intensity.

3.2.1.5   Accelerator – Discrete Energy

An alternative to the (n,γ) reaction based photon source, a charged particle accelerator, can also be used to produce photons for isomeric photonuclear resonance excitation. For example, protons impinging upon fluorine-19 in the ^{19}F(p,αγ)^{16}O reaction have been used to produce dual energy photon spectrum with 87% of the photons at either 6.91 or 7.12 MeV and 13% of the photons at 6.14 MeV.[36] In this scheme, isomeric excitation takes place indirectly through the formation of a compound nucleus which can then decay to the

isomeric state. Through the judicious choice of incident particle energy and target nucleus, a wide energy range of monoenergetic photons could be similarly produced using a charged particle accelerator. An alternative method of producing monoenergetic photons using a charged particle accelerator is to produce positrons and then accelerate those positrons to some desired energy prior to striking a target and annihilating. The energy of the photon field resulting from this type of arrangement within a specific solid angle would be discrete. Depending only upon the observation angle relative to the original positron beam trajectory and the final energy of the positron beam.

The major advantage of this type of photon source is the ability to vary the energy of the irradiating photon spectrum through either the choice of target materials and manipulation of the incident particle and its energy. The disadvantages of this approach come mainly from the low efficiency of using charged particles to generate photons of the proper energy and the resultant need for high current accelerators. Due to limitations in the availability of high current, commercially proven particle accelerators it is unlikely that isomeric isotope production could be carried out using a particle accelerator. However, if a suitable machine could be identified a discrete energy accelerator based photon source might be viable for material assay applications. A particularly useful advantage of this type of source might be found in the fact that the energy of the photons exciting the isomeric state are significantly different than those measured in the decay of the isomer. Because of this, a wise choice in selecting the irradiation and measurement geometry and adequate shielding might allow the measurement process to take place concurrently with irradiation, allowing analysis of short lived nuclear states but presenting new challenges in maintaining adequate signal to noise ratios at the desired energy.

An accelerator suitable for industrial PRE applications following this scheme would probably be too large to be considered portable. Also, some commercial heavy charged particle accelerators require liquid nitrogen for the operation of their vacuum pumping systems, an industrial PRE design based on this type of photon source might not be appropriate for field deployment in more remote locations. However, under some specific circumstances such as when two interfering isomers are present in a sample material, the ability to vary the energy of the excitation radiation might overcome these obstacles by improving the measured signal to noise ratio by cycling between different incident photon energies having different excitation probabilities for the two isomers.

3.2.1.6   Accelerator – Continuous Energy

As intimated in Chapter 2, an attractive source of photons for PRE work is the bremsstrahlung produced as a result of the slowing down of high energy electrons in high Z materials. As with the continuous energy isotopic source cobalt-60, industrially reliable x-ray sources are currently available from a number of commercial manufacturers for food and medical sterilization purposes. One major advantage of the accelerator based continuous energy photon source over isotopic sources however is the flexibility afforded the designer in choosing the energy range of the irradiating photon spectrum, which is set by choosing the operating energy of the accelerator generating the electrons. Another advantage lies in the fact that the spatial distribution of photons emanating from the high Z electron beam stop (convertor) is highly peaked in the forward direction relative to the incident electron beam rather than being isotropic as is the case for an isotopic source.

Depending upon the power requirements (photon intensity) needed for the accelerator to achieve the desired performance requirements, either a minimum detection limit or minimum quantifable amount (to some accuracy) or required induced isomeric activity or specific activity, the foot print of a x-ray irradiation facility will vary. However, if an irradiation system needs to be installed into small area (e.g., to fit into an existing space on an assembly line), it might be possible to locate many of the accelerator components at a distance from the accelerator and make use of an extended beam line to bring the electrons from the accelerator to a convertor closer to the area to be irradiated. Because of this, along with the anisotropy of a high energy bremsstrahlung field, prudent design in the layout of an industrial PRE facility

using an x-ray source can result in small physical space requirements; eliminating much of the bulk of the shielding required with the distributed pencil sources used in cobalt-60 irradiators.

Since an accelerator based photon source does not involve the use of permanent radioactive materials, another advantage of an x-ray based system is the ability to turn it off. This allows for greater flexibility in the installation of an irradiation facility for material analysis, simplifying both normal operating procedures as well as procedures dealing with problems associated with the sample materials (e.g., they become jammed on a conveyor belt) or a failure of some component of the irradiation system. Unlike the situation with heavy charged particle accelerators, technological advances in the design of electron accelerators have advanced to the level where they are commonly deployed in field applications and require only occasional monitoring by a technician. Additionally, as a proven technology for industrial and medical sterilization, bremsstrahlung x-ray sources have been operated for long periods of time with exceptional reliability (small down time).

3.2.1.7 Comparison of Photon Sources

Some of the strengths and weaknesses of the six types of photon sources listed above, in the context of the design of an industrial photonuclear resonance excitation system, are presented in Table 3-5. The advantages of isotopic photon sources are related to practical issues dealing with their operation (size, reliability, cost, ...); the disadvantages of these sources are an inapplicability for PRE on a physics basis, for discrete sources, and the cumbersome size and a need for very high activities for continuous sources. Based upon the physics of the problem discrete isotopic sources are clearly not an attractive choice for either material assay applications or isotope production, except for possibly a few unique situations. Continuous energy isotopic photon sources could possibly be successfully used for PRE applications; however, the disadvantages associated with this type of source, including the size and need to safely manage an assembly with such a large inherent activity, would restrict its implementation to very specialized situations.

Reflecting on the advantages and disadvantages of reactor based photon sources, the commercial viability of a PRE system chiefly depends upon the pragmatic issue of having access to the source. Technical issues pertaining to the use of discrete and continuous energy reactor based photon sources for PRE are similar to those for isotopic sources, but the inability to justify the cost of this source eliminate its use except when one is already available. Due to the rarity of reactors already equipped as high intensity photon sources, or capable of being modified in this way, reactor based PRE is only likely to be useful for isomer production. For this application, however, considerations dealing with the time involved in the packaging and shipment of the excited product will in most cases limit the list of isomers which could be produced to those having half-lives on the order of days or greater. Referring to Table 3-1, only about 11 isotopes are therefore likely candidates for reactor based PRE.

Due to the broad range of photon energies and intensities achievable, as well as practical considerations such as size, cost, availability, ease of installation and ease of operation, the numerous advantages of accelerator based photon sources, and their comparatively fewer and less severe disadvantages, make them the most logical choice for serving as photon source for typical industrial PRE applications. In particular, electron accelerators are currently available which are capable of producing intense x-ray fields at intensities required for both material assay as well as isomer production. As the production of this type of accelerator increases to satisfy growing market demands for food sterilization material processing their performance and cost indices will improve even further. Only for those unique situations where existing isotopic or reactor based irradiation sources are available with discrete photon spectra of very high intensity will the performance of these other sources exceed accelerator sources for isomeric excitation. For those situations where PRE irradiations may parasitically share an existing isotopic or reactor based irradiation facility, the use of these sources may be practical against the overall more competitive accelerator based photon sources.

Table 3-5 Advantages and disadvantages of photon sources for PRE.

Source & Energy Spectrum		Advantages	Disadvantages
Isotopic	Discrete	– Small size – Reliability – Low cost – May be transportable	– Difficulty in finding matches between decay photons and isomeric levels – Shielding and handling of a long-lived, high activity source – Only capable of exciting one energy level – Limited energy range fails to excite isomers through the compound nucleus
	Continuous	– Capable of exciting multiple energy levels – Use of proven and commercially available sterilization technology – Capability to assemble high activity sources – Reliability	– Extra shielding required to entirely encase the extended radiation source – Handling of a high activity radiation source – Limited energy range fails to excite isomers through the compound nucleus
Nuclear Reactor	Discrete	– If an existing reactor may be used, cost may be low – Using prompt photons created following neutron absorption, higher energy eigenstates may be excited, eliminating the need for an exact match in energy	– Requires a nuclear reactor – Requires a large workforce – A dedicated facility would be expensive – Special care must be taken to avoid neutron activation of sample materials – If measurements must be taken of short-lived isomers background radiation may be high – Difficulty in finding matches between decay photons and isomeric levels at lower energies
	Continuous	– If an existing reactor may be used, cost may be low – Capable of exciting multiple discrete energy levels	– Requires a nuclear reactor – Requires a large workforce – A dedicated facility would be expensive – Special care must be taken to avoid neutron activation of sample materials – If measurements must be taken of short-lived isomers background radiation may be high
Accelerator	Discrete	– The photon energy may be chosen by either selection of the incident article energy alone or in conjunction with locating a target at a particular solid angle – Ability to turn off the radiation source – Can operate continuously or in a pulsed mode	– Although proven to be reliable, most heavy charged particle accelerators have been proven operating records under rugged industrial conditions – The possible requirement for cryogenics – May require skilled workers beyond the technician level – Accelerators with sufficient current to produce satisfactory photon intensities may not be available
	Continuous	– The photon energy range may be selected by choosing the accelerator operating energy – The forward peaked radiation field allows for a concentration of higher energy photons, reducing overall shielding requirements – Compact size may allow portability – Can operate continuously or in a pulsed mode – Uses proven, commercial technology – Excites both discrete eigenlevels as well as the compound nucleus	– Low energy photons in the bremsstrahlung spectrum are ubiquitous and useless for PRE. – High energy bremsstrahlung fields can be difficult to fully characterize

3.2.2 Bremsstrahlung Sources

In this section different characteristics of electron accelerator generated bremsstrahlung are analyzed in the context of using this type of radiation source in an industrial resonant photonuclear isomer excitation system. The analysis presented here is split into two parts, one focusing on general issues related to photon production such as the electron energy and current and the other dealing with performance issues influencing the choice a particular accelerator among several having the same radiation output. By focusing on parameters related to the use of the x-ray field (spectrum, energy, intensity) separately from those dealing with the accelerators performance, a more general understanding is gained of how to determine the optimal choice of accelerator variables for a particular application as well as how to understand the importance of more practical aspects of operating the accelerator such as power requirements, ease of maintenance, scheduled and unscheduled downtime and cost.

3.2.2.1 X-ray Production and Calculation

A good deal of theoretical and experimental research has been reported in the literature concerning the generation of x-ray radiation resulting from the stopping of fast electrons in matter. One of the original examinations of this problem, presented by Bethe and Heitler in 1934, provides a simple analytical expression for determining the probability that an electron starting with some energy E_0 emits a light quantum of some frequency between v and $v + dv$ in a transition to a lower energy state E.[37] Including screening effects in calculating the emission of radiation under the influence of the electric field of a nucleus, their cross section for this interaction has been shown to be quite accurate at higher electron energies. For very high incident electron energies, $E_0 \gg 137 mc^2 Z^{-\frac{1}{3}}$ (e.g., ~16 MeV in tungsten), the cross section may be written as

$$\sigma(v)\,dv = \frac{Z^2}{137}\frac{r_0^2}{E_0^2}\frac{dv}{v}\,4\left[(E_0^2 + E^2 - \tfrac{2}{3}E_0 E)\ln(183\,Z^{-\frac{1}{3}}) + \frac{E_0 E}{9}\right] \qquad \textbf{3-1}$$

where Z is the atomic number of the material stopping the electron and r_0 is the classical electron radius,

$$r_0 = \frac{e^2}{4\pi\varepsilon_0\, m_e c^2}, \qquad \textbf{3-2}$$

where $m_e c^2$ is the rest mass energy of the electron. In terms of the energy of the emitted photon, E_γ, the cross section may be written as[a,38]

$$\sigma(E_\gamma)\,dE_\gamma = \frac{Z^2}{137}r_0^2\frac{dE_\gamma}{E_\gamma}\,4\left\{\left[\frac{4}{3}\left(1 - \frac{E_\gamma}{E_0}\right) + \left(\frac{E_\gamma}{E_0}\right)^2\right]\ln(183\,Z^{-\frac{1}{3}}) + \frac{(E_0 - E_\gamma)}{9}\right\}. \qquad \textbf{3-3}$$

For a real system, however, a more accurate tool must be used to determine the characteristics of the radiation spectrum. In particular, modeling of the radiation field must include a better model of electron

---

[a] *Note*: This non-relativistic expression for the probability of emission of a light quantum of energy E_γ from an electron of energy E_0 yields the bremsstrahlung radiation spectrum for thin targets. In reference 38 there is an error in this equation.

slowing down in the target, it must address complexities associated with the use of thick targets (which completely stop the incident electrons) and it must account for errant scattering of the bremsstrahlung by various components of the irradiation system as well as the sample target itself. One way to do this is to simulate the problem using any one of several numerical simulation routines such as the general Monte Carlo N-particle transport code MCNP.[39,40] Using this program it is relatively easy to simulate the character of the photon spectrum for industrial PRE systems, with accuracies of ~5-10% (which is often better than the uncertainty associated the cross sections used in these calculations, therfore accelerating the design and optimization process for various applications.

3.2.2.2 Intensity

Ideally, the intensity of the irradiation spectrum is solely dependent upon the voltage and current of the incident electron beam or, for a constant voltage accelerator V, the electron beam power P. However, the photon intensity generated using bremsstrahlung at the energies needed for PRE is highly anisotropic and varies as a function of the energy of the photon E_γ. In modeling an irradiation setup using MCNP, one option the user may choose is to calculate the number of photons having an energy between E_γ and $E_\gamma + dE$ per incident electron incident upon some surface. The rate at which photons are produced per incident electron, or the photon production efficiency, $n_\gamma(E_\gamma, E_{e-})$ [photons per incident electron] calculated using MCNP may be converted to the photon intensity $I(E_\gamma)$ [photons per second] by using the accelerator beam current I_{e-} according to

$$I(E_\gamma) = n_\gamma(E_\gamma, E_{e-})I_{e-}$$

3-4

or using the accelerator beam power according to

$$I(E_\gamma) = n_\gamma(E_\gamma, E_{e-})\frac{P}{V} .$$

3-5

Another tabulation of photon intensity which is occasionally useful for understanding the performance of an x-ray irradiation system for a PRE application is the probability that a photon of some energy will pass through a particular volume per incident electron, $i(E_\gamma)$. For some volume element dV in a vacuum this may be easily calculated; however, for attenuating mediums $i(E_\gamma)$ is not so easily determined. Fortunately, using MCNP it is possible to calculate the number of photons passing through some volume element per incident electron using

$$i(E_\gamma) = \frac{n_\gamma(\vec{r}, dV, E_\gamma, E_{e-})I_{e-}}{dV} .$$

3-6

A secondary factor which can influence the intensity of the irradiation field is the thickness of the bremsstrahlung convertor plate. Depending upon the beam power needed for the application, active cooling requirements of the convertor plate may require additional structural support beyond the minimum thickness needed to produce the radiation field. The presence of a liquid coolant might also add to photon attenuation losses in the x-ray production head, further reducing the on target photon intensity. One mechanism which might serve to increase the on target photon intensity is scattering of the incident x-ray field off of various components of the system as well as scattering in the target material itself. The dominant contribution to this scattered radiation will likely result from Compton scattering off of the

primary x-ray beam stop in addition to the side walls and structural components of the system as well from within the target itself, but additional photons produced from pair production in these materials as well as more esoteric scattering mechanisms will also contribute as well.

3.2.2.3 Flux

In most situations a more useful measure of the irradiation field for PRE applications is the localized, energy dependent photon flux $\varphi(\vec{r}, E_\gamma)$ which may be expressed as the average number of photons per cm^2 per second at the position $\vec{r}$ having an energy between E_γ and $E_\gamma + dE_\gamma$. For a real problem involving photon attenuation and scattering in the target material as well as surrounding structures the photon flux is difficult to calculate analytically. Using the MCNP code, however, the volume averaged energy dependent photon flux at some point $\vec{r}$ in space can be readily obtained.

3.2.2.4 Sample Calculation

In order to demonstrate the influence different design parameters related to the development of an industrial PRE system have on the irradiation spectrum, this section examines the photon spectrum generated for a generic physical setup designed for examining materials. This generic system is representative of how a system designed to analyze bulk materials traveling on a conveyor belt in the field. For simplicity at this point, the model does not include an associated radiation measurement system. Starting with the design described below, the irradiation spectrum has been simulated for different positions in the transport channel for various electron energies. Following this, the influence of the convertor plate thickness on the irradiation spectrum is explored. Finally, an estimate is made of the importance of the self shielding of the irradiation field in the target material by calculating the radiation field assuming the presence of 9 cm of rock directly above the measurement plane.

Using MCNP4B, the photon spectrum for these different cases have been simulated at several different incident photon energies for the generic system layout of Figure 3-2. The figure depicts a cross sectional view of a shielded channel in which the material being analyzed would be transported. The simplified lead walls of the channel modeled here are 10 cm thick. Located in the center of the top of the shielding is a cylindrical hole 10 cm in diameter, at the top of the hole there is a 0.1 cm thick tungsten plate which serves as the electron beam stop and is the origin of the bremsstrahlung. In the model the assembly extends 100 cm ahead of and behind the irradiation port (into and out of the paper). An imaginary horizontal slice 39 cm from the bottom of the channel and 1 cm thick is the location at which the photon spectrum was calculated. For most of the calculations the channel is filled with air but for some calculations the material in the 9 cm volume directly above the measurement volume is changed to rock as is the measurement plane itself.
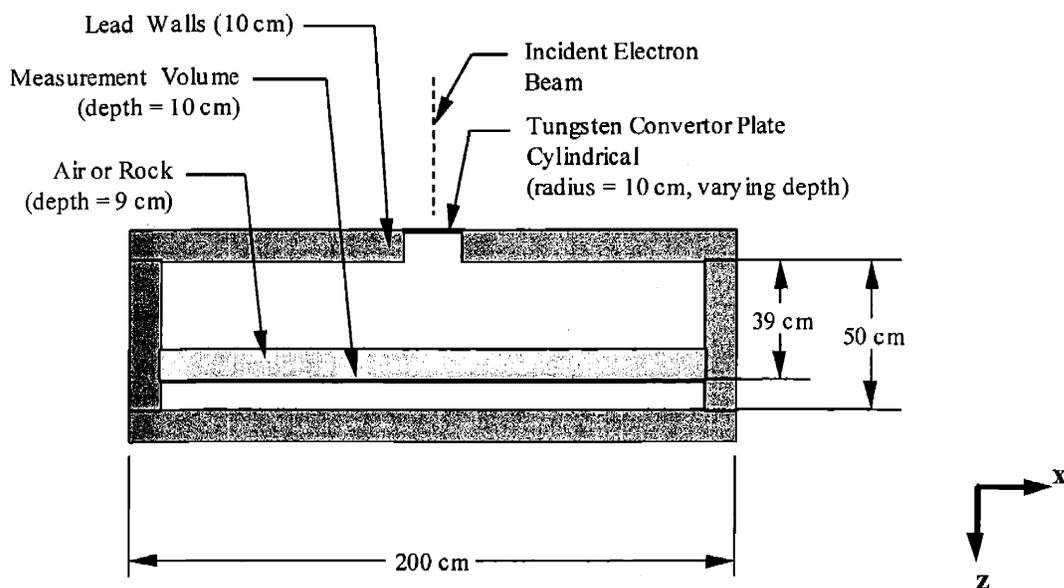
Figure 3-2 Schematic cross section view of the bulk material transport channel studied using MCNP, the rectangular duct extends 100 cm ahead of and behind the irradiation port.

The three major choices to be made concerning the electron accelerator are the beam current, beam energy and the thickness of the beam stop where the bremsstrahlung is generated. The two characteristics of the irradiation field influencing the excitation of isomeric nuclei which these accelerator parameters affect are the photon intensity and energy spectrum. For a constant beam energy, changes in the beam current linearly change the isomeric excitation rate but do not change the energy profile of the irradiation field. Keeping the accelerator beam current constant, changes in the electron energy change both the intensity of the irradiation field as well as the photon energy distribution. At a constant beam energy and current, changes in the thickness of the convertor plate used to stop the electron beam result in small changes in both the photon intensity and energy distribution of the irradiation field in comparison with changes in the beam parameters. These observations are listed in Table 3-6 and are discussed in greater detail below.

Table 3-6 Influence of accelerator beam current, beam energy and convertor plate thickness on the intensity and energy spectrum of the irradiation field.[a]

Accelerator Parameter	Intensity	Energy Spectrum
Beam Current	Strong	Very Weak
Beam Energy	Strong	Strong
Convertor Thickness	Weak	Weak

[a] For electron beam energies less than ~10 MeV.

2 mm Tungsten - On Axis
Generic MCNP Geometry (0.1 MeV bins)
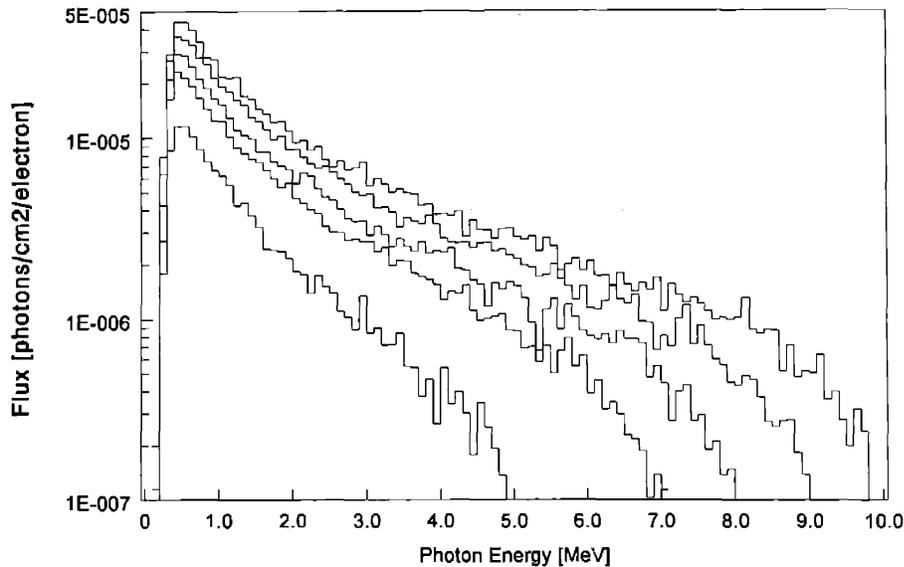
Figure 3-3 Energy dependent photon flux as a function of the incident electron energy determined on the incident beam axis in the measurement plane for electrons incident on a tungsten target 2mm thick.

In Figure 3-3 the relationship between incident electron energy and the irradiation spectrum for the generic irradiation setup of Figure 3-2 is presented. It is clear that as the electron energy is increased the total photon intensity increase and that the number of higher energy photons increases as well, changing the photon energy distribution. Examining the data more closely, one general trend which is observed is that, starting at the lowest photon energy, as the observed photon energy increases the relative number of photons slowly decreases and that as the photon energy begins to approach ~2/3 - 3/4 of the incident electron beam energy the number of photons observed begins to decrease more quickly. This can be seen more clearly in Figure 3-4 where the number of photons observed on the beam axis (normalized to the number of photons observed at the same energy for a 10 MeV beam) has been plotted for incident beam energies of 9, 8, 7 and 5 MeV. Looking at the case of a 9 MeV electron beam, the relative number of photons observed at lower energies is 80-90% that for a 10 MeV beam and slowly decreases with increasing energy up to about 6 MeV, after which the observed number of photons decrease much more rapidly with increasing energy.

For photonuclear resonance excitation, incident radiation fields will probably be limited to a maximum energy no greater than ~10 MeV to limit long term activation. Coupling this with the observation that most photonuclear resonance excitation cross sections are relevant only from ~3-9 MeV, one conclusion which may be reached concerning the selection of the electron beam energy and its relationship to PRE is that the isomeric excitation rate increases more rapidly than a linear rate with beam energy. Noting that many electron accelerators can operate in a constant power fashion (P = Beam Current x Beam Energy), it is more advantageous to operate the machine at the maximum allowable beam energy rather than maximizing the beam current in order to realize the maximal isomeric production.

Relative Photon Intensity
Generic MCNP Geometry (0.1 MeV bins)
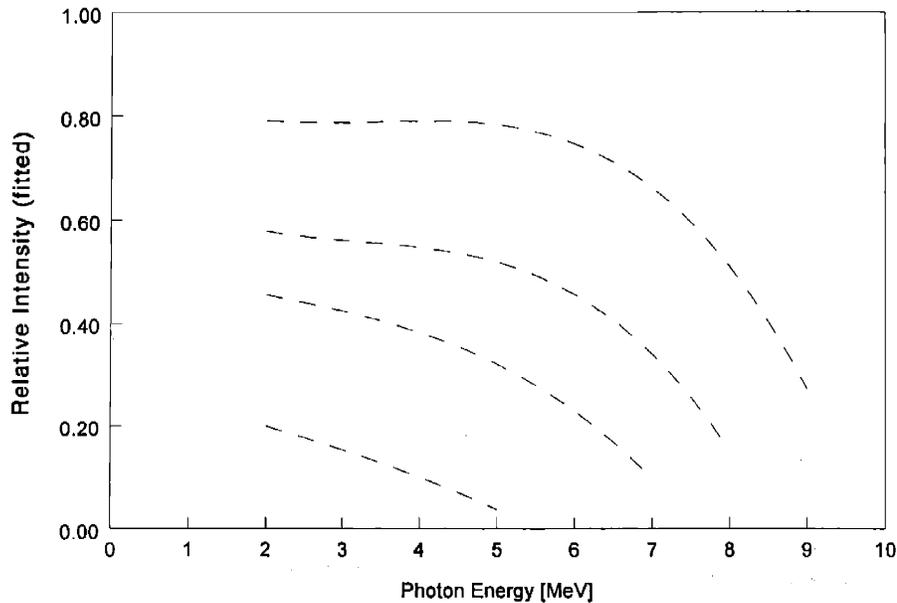
Figure 3-4 Relative number of photons observed at different energies (normalized to the number observed with a 10 MeV beam) for incident electron beam energies of 9, 8 ,7 and 5 MeV.[a]

In Figure 3-5 the differential photon energy flux observed in the measurement plane at different distances from the beam axis resulting from the stopping of 10 MeV electrons in 2 mm of tungsten is presented. From this figure it is apparent that the irradiation field generated using bremsstrahlung is most intense in the forward direction and that the ratio of higher energy to lower energy photons decreases as the distance off the beam axis increases.

In relation to the development of an industrial PRE system, this observation indicates that the highest isomeric activities will be realized in target materials placed directly along the irradiation beam axis, falling within a cone beginning at the bremsstrahlung convertor plate. Since the isomeric activation cross section is more significant in the 3 to 9 MeV energy range, material assay applications will achieve higher sensitivities if the unknown materials are constrained to be within this higher intensity irradiation cone. Isomeric isotope production applications will similarly be optimized of the target materials are placed directly in the center of the irradiation field. Depending upon the photon attenuation characteristics of the target material, this implies that the maximum achievable isomeric activity will be realized in a target material which is narrow and deep rather than one which is broad and shallow.

---

[a] The information presented in this figure has been fitted to simplify comparisons between different cases. This fitting reduced the need for highly accurate (and time intensive) Monte Carlo calculations since only the general trend between differing electron beam energies was of interest. More accurate calculations of this sort could provide an interesting method for calibrating accelerator beam energies as well as helping to benchmark MCNP4B for this type of calculation.

10 MeV Electrons - 2 mm Tungsten

Generic MCNP Geometry (0.1 Mev bins)
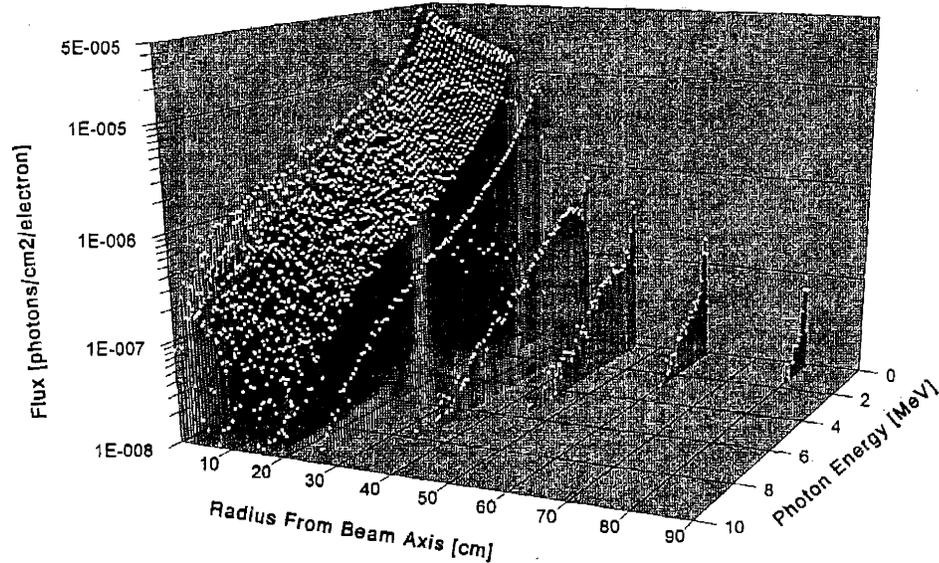
Figure 3-5 Energy dependent photon flux as a function of position in the measurement plane
determined along the x direction starting at the incident beam axis in the measurement plane
for 10 MeV electrons incident on a tungsten target 2 mm thick.

The convertor plate thickness is a critical design parameter because of thermal hydraulic considerations
regarding the need to remove the energy deposited in the convertor plate as the electrons are stopped.
Traditional methods of cooling bremsstrahlung targets include convective cooling of the back plate using
air, water or some other low density fluid or the use of multiple thin plates in a sandwich arrangement with
a cooling fluid being passed in between the plates. In Figure 3-6 below, the differential photon flux
calculated on the beam axis in the measurement plane (using MCNP4B) is presented for different tungsten
convertor plate thickness ranging from 1 to 5 mm.[41,42] Except for a slight bias towards the 1mm convertor
plate in the 0 to 0.5 MeV energy range, the photon intensity generated using the 1 and 2 mm convertor
plates is essentially the same for the entire irradiation spectrum.[43] For thicker covertor plates, the generated
photon spectrum remains essentially the same over the entire irradiation spectrum as well but the overall
photon intensity is observed to decrease slightly but not in proportion to the corresponding increase in
target thickenss.

For the development of an industrial PRE irradiation system, the maximum possible induced isomeric
activity will depend upon the tungsten convertor plate thickness in a similar fashion to its dependence upon
beam current. Since isomeric activity is related to beam current in a one-to-one fashion but is related to
convertor thickness in a weaker way, the optimal irradiation beam intensity will be achieved by
maximizing the beam current at the expense of requiring a slightly thicker convertor plate in order to
accommodate some sort of heat removal system. Reviewing the results of Figure 3-6, the 2 mm thick
convertor plate appears to be an optimal thickness to use for preliminary calculations for the design of an
industrial PRE system. Tungsten of this thickness is approximately one attenuation length for photons of
300 keV, as can be seen in this figure. Consequently, there is relatively little difference in the 2 – 10 MeV
region of the spectra at different convertor plate thicknesses. In addition to the cooling methods described
above, which are essentially 2-dimensional cooling techniques removing heat from one or both faces of the
convertor plate, more advanced volumetric cooling schemes (such as the use of a porous material with

some cooling fluid or the use of a high density liquid metal as the convertor) could allow the thickness of the convertor assembly to be reduced.

10 MeV Electrons - On Beam Axis
Generic MCNP Geometry (0.1 MeV bins)
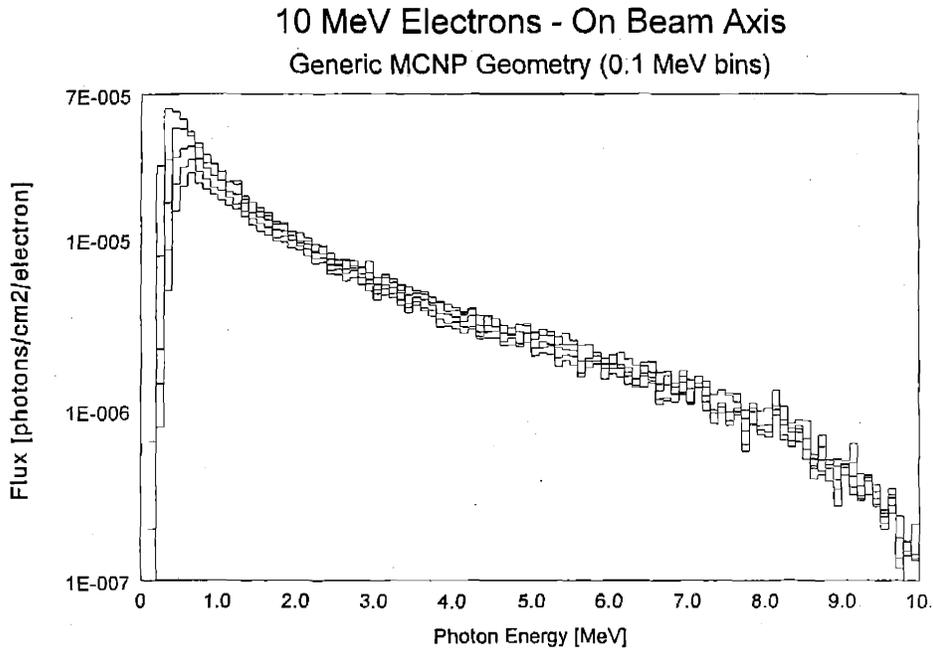
Figure 3-6 Energy dependent photon flux, as a function of the tungsten convertor plate thickness, determined on the incident beam axis in the measurement plane for 10 MeV electrons.

As one final investigation of the properties of the irradiation field, a simulation was carried out to examine the effects of photon attenuation on the irradiation field intensity and energy spectrum. In order to do this, the generic irradiation geometry used in the examples above was modified by changing the 9 cm of material directly above the measurement plane as well as the measurement plane itself from air to a mixture representing a generic igneous rock. The composition of the rock used for these calculations is given in Table 3-7, the density of the mixture was taken to be 2.5 g/cm^3. By making this change, the simulation may be thought of as representing an irradiation set-up designed to analyze some bulk material passing on a conveyor belt travelling through the shielded channel of the problem. For example, this could represent an installation designed to analyze ore to identify the presence of gold in the ore or the set-up could represent a an installation designed to analyze a potentially contaminated soil to determine the presence of heavy metals such as arsenic, cadmium, mercury or lead.

Table 3-7 Chemical composition of the igneous rock used in the generic model. [44]

Compound	Composition (%)
SiO_2	59.14
TiO_2	1.05
Al_2O_3	15.34
Fe_2O_3	3.08
FeO	3.80
MgO	3.49
CaO	5.08
Na_2O	3.84
K_2O	3.13
H_2O	1.59[a]
P2O5	0.30
CO2	0.10
BaO	0.06
	100

The photon flux measured on the beam axis in the measurement plane using a 10 MeV beam with a 2 mm tungsten convertor is presented in Figure 3-7 for the rock irradiation case described above and, for comparison, the case where the channel is filled only with air. As can be seen in Figure 3-7, the spectral nature of the irradiation photon flux in the measurement plane is essentially unchanged by the inclusion of rock in the channel. The overall photon intensity, however, is uniformly decreased for the rock case from ~2 to 10 MeV. At lower energies, the relative photon flux in the rock case exceeds that for the case with air only. This increase can be attributed to the increased generation of lower energy photons in the rock volume due to photon scattering. Unfortunately, the increase in photons at lower energies is not particularly helpful for the purposes of photonuclear resonance excitation due to the lack of a significant isomeric excitation cross section at these energies.

---

[a] Note: The value for water was taken as 1.59% rather than the 1.15% listed in the reference simply to round the total composition to 100%.

Air and Rock - On Axis
Generic MCNP Geometry (0.1 MeV bins)
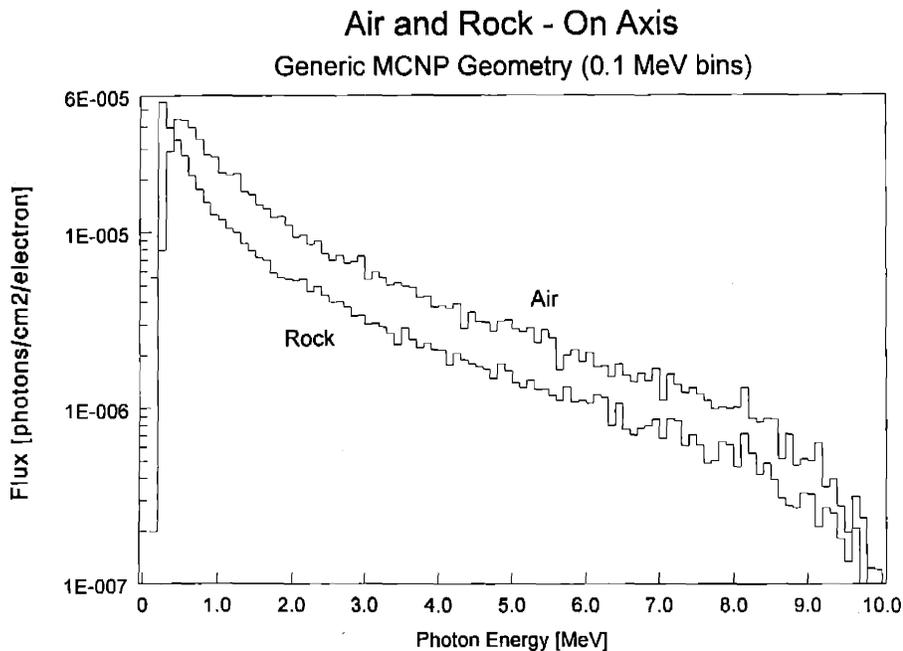
Figure 3-7 Energy dependent photon flux with the inclusion of 9 cm of igneous rock determined along the x direction starting at the incident beam axis in the measurement plane, also composed of igneous rock.

Photonuclear resonance excitation applications aimed at producing high activity samples for secondary purposes are likely to be small in size in order to maximize the specific activity of the materials produced. In these instances, attenuation of the irradiation beam in the target sample is not likely to be a significant factor; for cases involving dense materials where attenuation is important it may be possible either to use multiple irradiation beams or to rotate the material in order to achieve high isomeric activities having a uniform distribution in the sample. For applications aimed at using PRE to analyze materials, photon attenuation in the sample will be an important aspect of the design. For the situation described here, the photon flux at the bottom of the irradiation plane is attenuated to approximately two thirds of the flux incident upon the top surface of the rock. Because of this, the sensitivity of this system will vary as a function of depth in the rock.

When considering the attenuation of the irradiation field in the design of a material assay application, therefore, it would be most desirable to arrange things in such a way that the irradiation flux inside the material was uniform in the material. One way this might be achieved would be to use two bremsstrahlung beams irradiating the target from opposite directions, another might be to use one beam directed into the material along the direction of travel of the material. For analysis applications aimed at exciting longer lived isomers where grab samples must be taken rather than carrying out measurements in real time, it might be possible to rotate the sample to achieve a uniform total irradiation dose. An important additional aspect of the problem which must be considered is the attenuation of the isomeric decay photons as they exit the material being analyzed. With isomeric decay photons typically being less than 0.5 MeV, the sensitivity of the measurement system will be position sensitive within the material volume due to attenuation of these photons as well. Considering attenuation of both the irradiation and decay photons in the target material, one possible method of optimizing the system sensitivity would be to irradiate the material using tow beams (one positioned along each edge of the conveyor belt) and then to use detectors positioned above and below the target material.

3.2.2.5   Timing

Depending upon the performance requirements for a particular application, the choice of whether to use a continuous or pulsed irradiation source may be important in the design of an industrial PRE facility designed to analyze materials. One such case is when the half life of the isomer being excited is very short with respect to the time available to move the material from the irradiation location to a place for measurement. For a situation such as this, the measurement system must be located in close proximity to the sample material in order to acquire an adequate signal before the isomer decays and therefore the measurement system must be close to the radiation source as well. A pulsed radiation source would be particularly useful here because it would allow measurements to be taken between pulses, in the absence of the background radiation associated with the source (including direct bremsstrahlung from the convertor, scattered radiation from the system and target and electrical radio frequency interference from the accelerator electronics), thus improving the signal to noise ratio for the isomeric decay signal in comparison with measurements including accelerator generated noise. If the radiation measurement system can withstand continuous irradiation while operating in a data collection mode (the characteristics of radiation detectors under irradiation are discussed in §3.3) then a simple switching gate could be used to stop data collection during pulses. Otherwise, more sophisticated gating circuitry might be required to switch the radiation detection equipment on and off between accelerator pulses.

When the half life of the isomeric state being excited is not so short that measurements must be taken between pulses, however, a pulsed radiation source may still be desirable. For example, one possible problem which might be addressed using PRE techniques is the analysis of gold bearing ore to identify or maybe quantify the presence of gold.   Although the isomeric state of gold has a half life of 7.73 seconds, a pulsed machine might still be desirable because it would allow the detectors to be placed closer to the area where the gold activity would be highest, close to the bremsstrahlung source. For material assay applications involving the excitation of longer lived isomeric states or for applications aimed at producing isomers for secondary purposes either pulsed or continuous radiation sources could be used with equal ease.

The physics describing the excitation of a nucleus to an isomeric state is independent of whether the excitation source is pulsed or continuous in nature. However, for a pulsed radiation source the equations for determining the isomeric activity in a sample as a function of time do not take into account the timing of the irradiation process. The accelerator duty cycle, D, is defined as the ratio of the duration of a pulse to the time between successive pulses,

$$D = \frac{t_{on}}{t_{on} + t_{off}} .$$

3-7

If the isomer decay rate λ is of the same order as the pulse frequency f then a significant fraction of the excited nuclei will decay in between pulses. For this situation the actual timing of the irradiation source must be used in determining the induced activity along with the actual irradiation flux, which is proportional to the accelerator current and thus the accelerator beam power P. If the isomer half life is large in comparison with the pulsing period, then the total time of the irradiation may be used in conjunction with the average accelerator power,

$$\overline{P} = PD .$$

3-8

to determine the isomeric activity in the sample at some time during or after irradiation.

3.2.2.6 Reliability

One critical performance aspect for all types of industrial instrumentation is that of reliability. In order for a PRE system to be attractive to an end user it must be capable of operating reliably for long periods of time without the need for continuous maintenance or technical support. Fortunately, commercially available electron accelerators have been employed in other industries such as plastic and wood pulp processing as well as for the growing e-beam based food sterilization industry. Because of this, industrial grade high power electron accelerators are available from a number of sources. Since the performance requirements for the accelerators used in these other industries are already high it seems likely that an already available commercial machine could be identified for use in an industrial PRE application.

3.2.2.7 Stability

For material assay applications another important operational parameter is the stability of the electron beam over time. Besides issues regarding the reliability of the system itself and the on time of the machine, it would be desirable to have an irradiation system which maintains a constant beam current and energy over time. As discussed above, the energy distribution of the irradiation spectrum generated using bremsstrahlung is highly dependent upon the endpoint energy of the electrons incident on the convertor plate. Because of this, applications involving the excitation of short lived isomers where material quantification is desired will be highly sensitive to short term transients in the beam energy. While it may be possible to include a real time diagnostic to monitor the irradiation field, it is generally difficult to accurately characterize a high intensity bremsstrahlung beam. If a beam diagnostic is employed, the system performance may not be capable of meeting material throughput demands when the isomeric isotopes being excited are short lived and large volumes of material must be analyzed. As a best case, instabilities in the irradiation spectrum will either alter the accuracy and minimum detectable limits for the target or require a feedback system to adjust the material feed rate.

In material assay applications where longer lived (relative to fluctuations in the irradiation field) isomeric eigenstates are being excited or long term irradiations are being carried out for isotope production, issues regarding beam stability are less important. Since a high degree of beam stability, or the added instrumentation needed to monitor beam instabilities, will likely add to the cost associated with the development of an industrial PRE system, this may be an area where significant savings can be made in the size, complexity and cost of such a system.

3.2.2.8 Cost

In the final analysis of the attractiveness on an industrial PRE system for some application the two questions which must be answered in the affirmative are a) does it work? and b) is it the price right? The answers to these two questions depend, of course, on what the performance goals for the system are. Starting with a clear objective, the answer to the first question should be straightforward – either the system will or will not be able to achieve the desired performance objectives such as material analysis rate, minimum detectable limit, minimum determinable limit, accuracy and precision. Answering the second question may not be quite so easy. For a system designed to irradiate some target to produce a specific amount of isomeric activity in that target for sale, an economic analysis may be carried out to determine the relationship between the capital costs of the system and the corresponding rate of return for that investment based upon a market analysis for the use of the excited material. When the irradiated end product will not be sold but rather is intended to be used in some process, the cost of producing the isomeric material using PRE may be compared to the cost of acquiring through existing or other proposed sources.

When the PRE application involves the assay of a material, however, it may be more difficult to assess the value of the system. Only a handful of technologies can be used to carry out a material analysis in bulk materials on an industrial scale and these have only really seen commercialization for a few applications such as on-line coal analysis or radioactive material cleanup. Additionally, due to the limited number of

isomeric isotopes few if any of the existing bulk material analysis applications would be suitable for PRE analysis. Because of this, most of the PRE based material analysis applications which can be envisioned are new and can not be compared with existing or competing analytical procedures on a simple capital cost basis. In light of this, the acceptable price for an industrial PRE system, to make it an economically desirable part of some process, will include factors such improvements in overall material throughput and quality control, reductions in environmental emission, decreases in downstream processing requirements and changes in personnel requirements for processes downstream of the material analysis.

The radiation source will constitute a significant fraction of the initial capital investment for an industrial PRE system. Additional costs will be associated with material handling equipment and shielding, and possibly enriched isotopic materials for isomeric isotope production applications and radiation measurement instrumentation for material assay applications. In comparison with other methods of producing a radiation source suitable for PRE, electron accelerator based bremsstrahlung is the most desirable source for the broadest array of applications. Because of the extensive and still growing use of high power electron accelerators in different industrial settings, it seems likely that a "commercial off the shelf" (COTS) accelerator can be found for most PRE system designs. Further, it seems likely that a commercially available accelerator can be located for most applications which will demonstrate satisfactory performance and operational characteristics, at a cost which is reasonable in terms of the capital costs typically associated with mid-sized industrial scale projects.

3.3 DETECTION AND MEASUREMENT SYSTEM

The third aspect in the design of a practical system for photonuclear resonance excitation applications that must be considered is the selection of components used for detecting and measuring the decay radiation emitted during the de-excitation of the PRE excited isomeric nuclei. This is particularly relevant for material assay applications but is also relevant to simple isomeric isotope production applications since the induced isomeric activity will have to be determined to verify that production goals have been met as well as for quality assurance and quality control purposes. The data acquisition system must be capable of operating for extended periods of time without maintenance, possibly in rugged and aggressive physical environments (temperature, humidity, dust, moisture, shock, etc.). Additionally, the measurement system may need to exhibit a good degree of stability in counting efficiency and energy resolution over long periods of time so that the stability of the irradiation field over time can be monitored and to allow for correct interpretation of sample and standard data sets. Examining the list of candidate isomeric nuclei, it is evident that in general a system must be capable of carrying out measurements from approximately 0.2 to 2 MeV depending upon the specific application. For portable systems, or for systems to be installed in places of limited size, the detection system size may be important. Depending upon the sensitivity requirements of the measurement system as well as the background radiation at the intended place of operation, detector size may also be important due to background shielding considerations.

There are two basic measurement schemes that might be employed in a PRE application: gross measurement of the isomeric activity produced in a sample and counting of the induced isomeric activity in an irradiated sample in some predefined energy region. When little or no incidental activity is expected during the measurement process (or when this incidental activity level is unchanging) a straightforward gross activity measurement may be made and used in conjunction with a correlation with a known standard material to determine the induced isomeric activity in the sample. When significant background radiation or interference is expected during the measurements, a more elaborate measurement scheme involving the use of either lower energy photon discrimination or an energy window must be employed. For these applications, detectors with satisfactory energy resolution for the problem must be selected. There are several types of x- and gamma-ray detectors which could be employed in a PRE system including gas filled detectors, solid state detectors, and liquid scintillator and solid scintillator detectors.

For these four detector types, some of the advantages and disadvantages associated with their implementation into an industrial PRE system are discussed in Table 3-8 below. Because of their price,

durability, size, detector efficiency and availability, the detector types which are most likely to be useful for the largest array of applications are solid scintillator detectors. For real time assembly-line material assay applications involving isomers having half lives on the order of seconds, where *little* background radiation is expected and no PRE induced interfering radiation will be generated, gas filled detectors and liquid and organic scintillator detectors operating in a gross counting mode should prove quite useful. When isomers having longer half lives are being created and the situation permits moving the target material from the irradiation area to a separate analysis area, solid state detectors may be useful, especially when very close interfering radiation signals are present in the sample. For most applications, however, including those requiring good timing resolution (involving isomers having half-lives less than a second), or for applications requiring photon energy discrimination or energy spectroscopy, inorganic scintillator detectors are probably the best choice.

Due to their broad appeal for PRE applications, different functional attributes of inorganic scintillator detectors are discussed in greater detail in the following sections. In particular, issues related to the operation of these detectors to measure small signals in close proximity to the high intensity irradiation sources needed for photonuclear resonance excitation are discussed. For applications where other types of detectors would be equally suitable, the design challenges related to their implementation in a PRE system are straightforward and similar to other industrial radiation measurement problems.

In §3.3.1 a brief summary is presented of several different types of inorganic scintillators which are available or under development. Following this, §§3.3.2.1 through 3.3.2.8 discuss different operating characteristics of scintillator detectors which are relevant to their implementation in an industrial PRE facility. In spite of the large variety of different scintillator materials, for most applications the well proven and reliable NaI based scintillator is the best choice. For situations requiring more demanding performance requirements, some of the newer rare-earth oxyorthosilicate detectors are promising. In §3.3.3 a comparison of these different detector types, based upon reported performance characteristics as well as experimental testing between the two is presented.

Table 3-8 Comparison of different types of photon detectors applied to PRE applications.

Detector Type	Advantages	Disadvantages
Gas	– Can be made in large and unusual sizes – Cheap in comparison with solid state and solid scintillator detectors on a volume basis – Simple and durable – Can achieve good energy resolution	– Low gas densities imply the need for large detector volumes or high pressures to achieve high detection efficiencies – Large detector volumes increase detector shielding requirements and can lead to higher background counting rates – Can be sensitive to changes in temperature
Solid State	– Excellent energy resolution – Compact size and high density – Excluding associated electronics and cryogenics, easy to shield	– May require cryogenic support – Typically restricted to small detector volumes due to manufacturing constraints – Expensive, may be very expensive to monitor large areas – May be highly sensitive to environmental variables
Liquid Scintillator	– Can be made in large and unusual sizes – Cheap in comparison with solid state and solid scintillator detectors on a volume basis – Simple and durable – Might be capable of achieving good measurement sensitivities for lower isomeric decay energies	– Poor energy resolution – Large detector volumes increase detector shielding requirements and can lead to higher background counting rates – Can be sensitive to changes in temperature – Low light collection efficiency
Solid Scintillator	– Smaller detector units can be arranged into larger detector volumes relatively easily – Cheap in comparison with solid state detectors on a volume basis – High density detector materials can be used, reducing the detector volume needed	– Expensive in comparison with gas and liquid scintillator detectors – Short term exposure to radiation bursts can temporarily alter detector performance – Exposure to radiation for long periods of time can result in long term damage to the detector

3.3.1 Types of Inorganic Scintillators

A great deal of research and development work has focused on creating and studying inorganic scintillator crystals. Of the hundred or so different variants that have been reported in the literature, however, only a relatively small number of such scintillators have made their way to general commercial production and sale. Much of the work in the area was focused on developing detectors for high-energy physics

instrumentation but a considerable effort has also been focused on developing detectors for industrial applications such as well-logging and for the space program.

There are several broad categories of inorganic scintillators including crystals based on alkali halogens (LiF, NaI, KI and CsI), alkaline halogens (CaF_2 and BaF_2), yttrium aluminate (YAG) ($Y_3Al_5O_{12}$), yttrium aluminum perovskites (YAP) ($YAlO_3$), germanates ($Bi_4Ge_3O_{12}$), heavy metal halogens (CeF_3), heavy metal tungstates ($CdWO_4$, $PbWO_4$ and $ZnWO_4$) and rare-earth oxyorthosilicates (Gd_2SiO_5, Lu_2SiO_5 and Yb_2SiO_5). With the various crystals, small quantities of dopants are often added to improve the radiative properties (e.g., light yield, radiation length, radiation hardness) and physical properties (e.g., maleability, hygroscopicity) of the scintillator. The choice of dopant depends upon the type of crystal, thallium being the most common for the halogens and cerium most common for the oxyorthosilicates.

A comprehensive list of currently available inorganic scintillator materials along with their physical and scintillation properties is provided in Table 3-9 below. The source for the data in this table comes from a large number of technical papers published over the last forty years. (See references 45 through 88.) In many cases, the physical and scintillation properties for a particular type of crystal depend not only upon the main crystal but also the concentration of various contaminants and dopants in the crystal. Because of this there is some variation in the reported performance of some crystals between researchers; the values given in Table 3-9 are those found to be most representative of published values.

Of the materials listed in the Table 3-9 the sodium iodide scintillator is by far the most widely used. The NaI based radiation detector has been proven as an all around choice for a broad array of applications from medical imaging to industrial logging applications. For the analysis of scintillator materials NaI is commonly used as a benchmark for comparisons of various performance characteristics. However, for many applications specific engineering restrictions and performance goals require a detector material demonstrating significantly different behavior than NaI. Some of the reasons research has been carried out to develop these alternative scintillator materials include the need for detectors having a higher electron densities (better photon sensitivity per unit volume), the need to develop more durable crystals capable of withstanding rough handling and shocks, the need for crystals having faster response times and the need for crystals that can operate in high radiation environments.

Table 3-9 Comparison of typical properties of inorganic scintillators suitable for PRE.

	Properties	NaI:Tl	CsI:Tl	BaF	CeF	CdWO	PbWO:?	YAG:Ce	YAP:Ce	BGO	BSO	GSO:Ce 1 mol%	LSO:Ce 0.22%	YSO:Ce
												Type of Detector		
Physical	Chemical Formula	NaI	CsI	BaF_2	CeF_3	$CdWO_4$	$PbWO_4$	$Y_3Al_5O_{12}$	$YAlO_3$	$Bi_4Ge_3O_{12}$	$Bi_4Si_3O_{12}$	Gd_2SiO_5	Lu_2SiO_5	Yb_2SiO_5
	Density (g/cm³)	3.67	4.51	4.89	6.16	7.90	8.28	4.57	5.37	7.13	6.80	6.71	7.35	4.54
	Hardness (Mohs)	2	2	3	4	4-4.5		8.5	8.6	5	5	5.7		
	Melting Point (°C)	651	621	1280	1443	1272	1123	1970	1875	1050	1030	1900	>2000	
	Linear Coef. of Thermal Expansion (10^{-5}/K)	4.75	5	1.84				8-9	4-11	7		4-12		
	Cleavage	(100)	none	(111)	(0001)	(010)		None	None	None	None	(100)	None	
	Hygroscopic	Strong	Slight	Slight	No	No		No	No	No	No	No	No	
Radiative	Peak Emission (nm)	415	540	220/310	375	470	420/480	550	370	480	480	440	420,440?	420
	Decay Constant (ns)	230	1050	0.6 620	30	5000	10 40	70	25(98%) 246(2%)	5.2(2%) 45(9%) 279(89%)	2.4(6%) 26(12%) 99(82%)	30-60,56 600	40	37, 82
	Refractive Index [a]	1.85	1.78	1.49	1.68	2.25		1.82	1.95	2.15	2.06	1.85	1.82	
	Radiation Length, X_o (cm)	2.59	1.86	2.03	1.66	1.06	0.85	3.5	2.7	1.12	1.15	1.38	1.14	
	Total Light Yield at 300 K (10^3 Photons/MeV)	38	52	20/4		12		8	10, 19.7	8.2		8-10	~30	
	Light Yield (w.r.t. NaI)	100	120-140	5/16	40-50	30-50	Low	15	40	7-20		20-25	54-76	25
	10-90% Rise Time (ns)	500	4000	3000		20000				800		< 100		
	Resolution, $\Delta E/E$ [b] (%)	6-7	~7	~11		~8			6.7-11	9-10	10-15	~8	7.5-10.3	
	Afterglow (%/ms)	0.5-5.0/3	0.1-0.8/6			0.005/3		<0.005/6	<0.005/6	0.005/3		<0.005/6	Low	
	Radiation Hardness (rad)	10^3	10^3	10^{6-7}	10^{5-6}	10^{5-8}				10^{4-5}	10^{5-6}	10^9	10^8	
Economic	Price ($/cc)[c, d]	1-2	2	2.5	[3]	10	20			5			[50]	

[a] At peak emission wavelength.
[b] For a ^{137}Cs source.
[c] Relative to NaI at this time (2000).
[d] Expected mass-produced price in [ ].

3.3.2 Operational Parameters

Having narrowed the choice of detector material to an inorganic scintillator on the basis of size, detector density (sensitivity), ease of operation and price, the choice among the different types of these scintillators must be made with the end goal of assembling a system capable of achieving measurement speeds and accuracies of interest in industrial applications. However, a commercial PRE system must also be competitively priced, with the value of the information to the owner exceeding the cost of the PRE system. Depending upon the specifics of the particular application, some of the criteria which will be most important in choosing the detector material will be: the detection efficiency of the scintillator, the light output of the scintillator, short term decay properties of the crystal following interaction with a high energy photon, long term decay properties of the crystal following exposure to radiation, the rate of degradation of the crystals performance due to prolonged exposure to high doses of radiation, the stability of the crystal performance due to environmental influences, cost and availability.

3.3.2.1 Detection Efficiency

In order to carry out measurements quickly, detection efficiency is a critical selection criteria. Since one of the key driving factors defining accelerator selection is the need for high incident x-ray fluxes (to compensate for the small isomeric activation cross-sections) it will be important to limit accelerator current requirements by having a detection system capable of measuring as much of the isomeric decay radiation signal as possible. Because of this, the detector system should be designed to cover as large a solid angle from the sample as possible. This can be achieved by either using large crystals, such as is often done with NaI, for example, or by placing multiple small crystals together.

In addition to solid angle, the electron density of the detector is also a critical factor. Higher density crystals are better able to stop energetic photons, thus increasing the detection efficiency. For the same stopping capability, higher density detectors are smaller in size than lower density detectors. This helps reduce the overall detector system size and thus limits the mass and volume of shielding materials needed, a factor that may be of particular importance in PRE systems intended to operate in the field. Also, by minimizing the detector volume and using higher density materials, the total noise in the data stream can be improved with respect to larger, lower density detectors by reducing the active volume of radioimpurities in the crystal (such as K and Lu), thus reducing the natural background signals and signals.[a] Using a high density detector material will improve the signal to noise ratio by maximizing the full energy transfer from the photon to the detector by reducing energy loss out of the crystal due to Compton scattering and annihilation escape.

Scintillator density will be a particularly important parameter regarding detector efficiency when dealing with higher energy photons. At lower energies NaI performs quite well (e.g., as used in medical imaging cameras designed to image the 140 keV photons from the decay of ^{99m}Tc); at higher energies trends in industrial radiation instrumentation have shifted towards the use of higher density scintillators despite increases in cost (e.g., the use of BGO and now LSO to measure the 511 keV photons for PET instrumentation.)

Based upon density, the best choice of scintillator for a PRE system would be either CdWO, BGO or one of the heavy-metal oxyorthosilicates such as GSO or LSO.

---

[a] For two detectors made of the same material, simply reducing the detector volume while maintaining the same radioimpurity concentraion will not result in an improvement in the signal to noise ratio.

3.3.2.2 Light Properties: Light Yield & Wavelength

Following interaction in the crystal, the production of light by the scintillator and the subsequent transmission of that light to the photocathode of an associated photomultiplier or to a photodiode are critical phenomena that must be looked at in comparing scintillators. A crystal which produces less light is not as desireable as one with a higher light yield because the observed signal to noise ratio is in general less and, as mentioned, relatively small signals are expected in PRE measurements. The wavelength of the light emitted from the crystal following the absorption of ionizing radiation must a) be capable of escaping the crystal to reach the photocathode and b) be able to induce electron emission in the photocathode. The degree to which the emitted light penetrates the crystal is essentially incorporated into the crystal light yield, for a particular size. Depending upon the wavelength, care must be taken in selecting a photodetector sensitive over the same spectral range. A wide variety of photodetector systems, both photomultiplier tubes as well as photodiodes, is available to match the crystals of Table 3-9, thus wavelength is not of great concern in the selection of a scintillator for PRE except perhaps for BaF_2.

Examining the crystals found in Table 3-9, NaI or LSO would be the detector material of choice. After these two, there are a number of crystals having relative light yields in the 30-50% range, with most of the others having relative light yields of ~20% or lower.

3.3.2.3 Decay Constant

When ionizing radiation enters a scintillator it interacts with the electrons in the crystal. The light generated as these electrons de-excite in the crystal structure then interacts in an associated photon detector to register the initial ionizing radiation event, the number of such interactions being related to the energy of the incident ionizing radiation. The characteristic time it takes for these quick lattice de-excitations is referred to as the decay constant of the crystals. Scintillators may have multiple decay constants as indicated in Table 3-9; in those cases more than one wavelength of photon is emitted from a decaying crystal. Typical decay constants range anywhere from 0.01 to 5 microseconds. For investigations measuring short-lived excitations, such as NRF, where very high radiation fields might be expected, detector decay constant would be important.

Since most isomeric nuclei likely to be analyzed using PRE have half-lives on the order of 1000 microseconds or longer and relatively small signal strengths are expected, crystal decay constants are not of particular importance for PRE applications – unless the detector is overloaded by an initial high-intensity burst of radiation.

3.3.2.4 Energy Resolution

The energy resolution of the detector system may be important in some situations particularly when interfering sources of radiation are important (either natural of due to other isomeric nuclei in the target.) In order to increase the signal to noise ratio, the use of energy windows to focus on the radiation associated with the decay of the isomeric state may also prove useful. Referring to the table above, NaI is found to have the best energy resolution of the common scintillator materials while the more exotic (more complicated) crystal structures such as YAG, YAP and the rare earth oxyorthosilicates demonstrate the worse energy resolution, down by as much as ~2X.

For those situations where energy resolution is an important requirement, NaI appears to be the best choice of scintillator crystal. However, considering other parameters such as crystal sensitivity and density, energy resolution will not likely be the most important parameter in most situations.

3.3.2.5 Afterglow

Another potentially important property in the selection of a scintillator material for PRE applications is afterglow. Afterglow is a measure of the residual light (or energy) within the crystal following exposure to a light source. In NaI, for example, experiments have shown that as much as 5% of the ultraviolet signal strength in a crystal following exposure to ionizing radiation can be expected after more than 3 milliseconds. In part, afterglow can be thought of as a long-lived decay component of the crystal. However, due to the long lifetime of afterglow radiation, spectral measurements do not result in a clean photopeak but rather result in an asymmetric background continuum biased towards lower energies. For a PRE measurement, where small signals are expected and high signal to noise ratios are important, afterglow in a crystal may be problematic, especially if the crystals are exposed to high radiation fields (direct exposure to the irradiation field).

Based on afterglow, crystals such as YAG, YAP, GSO and LSO are ideal choices for PRE instrumentation.

3.3.2.6 Radiation Hardness

Depending upon the measurement requirements for a particular application as well as constraints such as available space and cost, various components of a PRE measurement system might be arranged in such a way that that they are exposed to high radiation doses, high radiation dose rates and large, varying electromagnetic fields. Of course, the long term ability of the system to survive and operate consistently and within nominal operating parameters under these conditions is a must. The ability of the scintillator to withstand large radiation doses is termed radiation hardness and has been extensively studied for many crystal types. Empirical measurements of the light output of crystals following exposure to varying photon radiation doses indicates that, for most crystals, prolonged exposure slowly decreases light output up to some critical dose and then quickly decreases as the integrated dose is increased beyond that value. As indicated in Table 3-9, the iodinated scintillators are comparatively poor in terms of radiation hardness (limited to total doses less than $\sim10^3$ rad) while CdWO, BGO and the rare earth oxyorthosilicate GSO demonstrate excellent radiation hardness properties up to as much as 10^9 rad.

For installations where the crystal material will be subjected to direct exposure to the irradiation field, detectors made of crystals demonstrating good radiation hardness characteristics, such as CdWO, BGO, GSO and LSO, are an ideal choice.

3.3.2.7 Stability

Due to temperature changes in the ambient environment, the efficiency of scintillator based radiation detectors can change.[59,89] Experimental investigations of this influence have shown, however, that in the temperature range from $\sim0°$ C to $\sim80°$ C, scintillator crystals such as NaI and BGO demonstrate a linear variation in signal output with temperature. Because of this, for PRE applications where large temperature swings are expected, it should be possible to develop an empirical correlation for the detector system. Depending upon the circumstances, it may be possible to employ an active cooling system to maintain the detector system at a constant temperature irrespective of the ambient temperature in order to avoid this problem.

When exposed to large radiation fields, an additional signal instability can arise due to problems associated with the use of photomultiplier tubes. In particular, excessively large radiation pulses can lead to the temporary distortion of the electromagnetic fields employed in the dynode structure of the photomultiplier tube because of screening effects associated with the large number of electrons generated at the higher voltage, later stage dynodes. This effect has been reported in the literature and is referred to as the Malter effect. When high intensity, continuous radiation sources are used there are relatively few methods of dealing with the Malter effect other than reducing the incident photon intensity (reducing the size of the crystal associated with the photomultiplier tube) or accepting the degraded performance and attempting to

104

compensate for fluctuations using some sort of pre-determined correlations. Neither of these alternatives is desirable because they both lead to a higher signal to noise ratio and thus increase the minimal determinable isomeric activity level and degrade the precision of the activity determination.

When high intensity, pulsed radiation sources are used, one particularly useful solution to the Malter effect is the use of an electronic gating circuit to temporarily disable the photomultiplier during the pulse so that excessive electron densities are never achieved. Since the Malter effect is only likely to be relevant when the radiation detector is exposed to the irradiation field directly and because this situation is only likely to occur when very short half-lived isomers are being excited, the use of a pulsed radiation source together with pulsed gating circuitry should prove to be a useful solution in most situations. Experimental investigations of the use of pulsed gate circuitry will be discussed in some detail in the next chapter.

Concerning the stability of the radiation detection system, the use of an empirically determined correlation between the ambient temperature and the counting rate may prove useful in situations where the temperature is expected to change significantly over time. When counting instabilities due to the Malter effect are expected, either a gating circuit may be used or else perhaps a an alternative to the photomultiplier, a photodiode could be used.

3.3.2.8 Price

In a general comparison of detector materials such as this, it is difficult to compare different scintillator materials on the basis of cost. Generally speaking, the older scintillator materials such as NaI, CsI and BaF are the cheapest scintillators, costing a few dollars per cubic centimeter. The use of the denser crystal BGO in nuclear instrumentation such as CAT and PET imaging systems has led to its commercial availability as well, costing from \$5 to \$10 per cc. As the use of BGO in these applications increases its price may decrease but it is unlikely that they will ever be as low as for NaI. Future use of even denser crystals such as GSO and LSO in nuclear medical applications may reduce their prices as well (>\$10 per cc) but they will likely remain at the high end of scintillator materials for many years.

Based upon cost, NaI is the best choice of scintillator material when the measurement system must cover large areas. For installations requiring only small measurement areas, higher density crystals such as BGO, GSO or LSO may be the best choice. Although they are more expensive, their higher detection efficiencies may allow for cost savings in the irradiation system by reducing the photon flux required to achieve a particular detection sensitivity.

3.3.3 Conclusions

From the sections above it appears that, depending upon the particular circumstances, detector systems for industrial PRE applications can essentially be classified into one of two different groups. When very short lived isomers are being created the detector systems will be small, located in very close proximity to the irradiation source, and the source for these applications will be pulsed. In this case, premiums will be placed upon detector performance characteristics such as high detection efficiency, short decay constants, low afterglow and good radiation hardness. The best detectors for these applications will be BGO and the rare earth oxyorthosilicates. When the PRE application is creating isomers with half lives sufficiently long enough to allow the materials to be moved from the irradiation area to a separate area (e.g., on a material conveyor belt), the detector system will need to be large enough to monitor the moving, excited materials for a sufficiently long time to acquire an adequate signal. In this case, premiums will be placed upon detector performance requirements such as detection efficiency, stability and cost. The best detector for these applications is NaI.

3.4 REFERENCES

[1] Fuller, E. G. and Hayward, E., "Nuclear Elastic Scattering of Photons," Phys. Rev. **101**, (692-700) 1956.

[2] Hayward, E. and Fuller, E. G., "Photon Self-Absorption and Scattering by the 15.1-MeV Level in C^{12}," Phys. Rev. **106**, (991-995) 1957.

[3] Garwin, E.L., "Gamma-Ray Excitation of the 15.1-MeV Level in C^{12}," Phys. Rev., **114** (143-154) 1959.

[4] Langhoff, H., "Resonance Fluorescence in Re^{187}," Phys. Rev. **135**, (B1-B8) 1964.

[5] Robinson, S. W., et. al., "Gamma-Ray Widths of the 3.00-MeV Level of Al^{27} and the 3.13-MeV Level of P^{31}," Phys. Rev. **174**, (1320-1323) 1968.

[6] Rasmussen, V. K. and Swann, C. P., "Gamma-Ray Widths in C^{13}, Li^6, and P^{31}," Phys. Rev. **183**, (918-923) 1969.

[7] Metzger, F. R., "Electric Dipole Transitions from the 2.6-MeV Septuplet in Bi^{209}," Phys. Rev. **187**, (1680-1682) 1969.

[8] Metzger, F. R., "Width of the 2.186-MeV 1- Level in Nd^{144}," Phys. Rev. **187**, (1700-1704) 1969.

[9] Sowerby, B. D., "A New Method of Element Analysis Using Nuclear Resonance Scattering of Gamma Rays," Nucl. Instr. Meth. **94**, (45-51) 1971.

[10] Treml, K. and Langhoff, H., "The Slowing Down of Atoms with Energies of E<10 eV in Crystals," Z. Physik **B25**, (123-129) 1976.

[11] Ellis, W. K., et. al., "Bulk Analysis For Copper and Nickel In Ores Using Gamma-Ray Resonance Scattering," Proc. Nucl. Tech. And Mineral Resources 1977, (499-520) 1977

[12] Muckenheim, W., et. al., "Nuclear Resonance Fluorescence in 238U and a New Approach to Doppler-Shift-Attenuation Using High Speed Rotation," Z. Phys. A – Atoms and Nuclei **300**, (43-46) 1981.

[13] Palathingal, J. C., "Nuclear Resonance-Fluorescence Analyser of Ores and Surfaces," Capture Gamma-Ray Spectroscopy and Related Topics-1984, AIP Conf. Proc. No. 125, (847-850) 1984.

[14] Kehlenbeck, G., "The Slowing-Down of Low-Energy Recoil Atoms in Solids and Liquids Investigated by Nuclear Resonance Fluorescence," Z. Phys. B – Cond. Matter **66**, (147-151) 1987.

[15] Heil, R. D., et. al., "Observation of Orbital Magnetic Dipole Strength in the Actinide Nuclei ^{232}Th and ^{238}U," Nucl. Phys. **A476**, (39-47) 1988.

[16] Margraf, J., "Photoexcitation of Low-Lying Dipole Transition in ^{236}U," Phys. Rev. C **42**, (771-774) 1990.

[17] Govaert, K., et. al., "Polarized Bremsstrahlung Nuclear Resonance Fluorescence Set-Up At the 15 MeV Linac In Gent," Nucl. Instr. Meth. A **337**, (265-273) 1994.

[18] Ohgaki, H., et. al., "Linearly Polarized Photons From Compton Backscattering of Laser Light for Nuclear Resonance Fluorescence Experiments," Nucl. Instr. Meth. A. **353**, (384-388) 1994.

[19] R. B. Firestone, "Table of Isotopes CD-ROM," S. Y. Frank Chu, CD-ROM editor, Eighth Edition. v1.0, (1996).

[20] Anderson, J. A., et. al., "Nuclear Photoactivation Cross Sections for Short-Lived Isomeric States Excited With A 6 MeV Linac," Nucl. Instr. Meth. **B40/41**, (452-454) 1989.

[21] Carroll, J. J., et. al., "Accelerated Deay of ^{180m}Ta and ^{176}Lu In Stellar Interiors Through (γ,γ') Reactions," Astrophysical Journ. **344**, (454-459) 1989.

[22] Goryachev, B. I., "Cross-Sections of Photonuclear Reactions Tabulated Data," At. Energy Rev. **3**, (71-148) 1964.

[23] Kaminishi, T. and Kojima, C., "Production of Nuclear Isomers from Stable Nuclides with Bremsstrahlung," Jap. J. App. Phys. **2**, (399-405) 1963.

[24] Otvos, J. W, et. al., "Photoactivation and Photoneutron Activation Analysis," Nucl. Inst. Meth. **11**, (187-195) 1961.

[25] A. Veres, "Gamma Activation of Nuclear Isomers and Its Applications," At. Energy. Rev. **18**, 271-328 (1980).

[26] Sekine, Yoshihara, Nemeth, Lakosi and Veres, "A New Detection Method of ^{99}Tc By Nuclear Excitation," J. Radioanal. Nucl. Chem., Articles **130**, 269-278 (1989).

[27] Sekine, Yoshihara, Lakosi, Nemeth and Veres, "Integral Cross Section of the ^{99}Tc$(\gamma,\gamma')^{99m}$Tc Reaction in the 15-50 Mev Energy Region," Appl. Radiat. Isot. **42**, 149-153 (1991).

[28] Yagi, Sekine and Yoshihara, "Detection Limit of Technetium in ^{99}Tc$(\gamma,\gamma')^{99m}$Tc Radioactivation Analysis in the Presence of Molybdenum," J. Radioanal. Nucl. Chem., Letters **155**, 433-443 (1991).

[29] A. Veres and I. Pavlicsek, "Nuclear Photoactivation Analyses By Means Of An 80-kCi ^{60}Co γ-Radiation Source," J. Radioanal. Chem. **3**, 25-28 (1969).

[30] Veres, Pavlicsek, Csuros and Lakosi, "Nuclear Excitation by g Rays of Radioactive Sources," Acta Physica Academiae Scientiarum Hungaricae **34**, 97-104 (1973).

[31] B. Arad et. al., "Studies of Highly Excited Nuclear Bound Levels Using Neutron Capture Gamma Rays," Phys. Rev. **133**, B684-B700 (1964).

[32] G. Ben-David et. al., "Further Study of Nuclear Resonant Scattering Using Neutron-Capture Gamma Rays," Phys. Rev. **146**, 852-860 (1966).

[33] R. B. Begzhanov and S. M. Akhrarov, "Investigation of Highly Excited Levels of Nuclei with the Aid of Neutron-Capture Gamma Rays," JETP Letters **10**, 26-28 (1969).

[34] R. B. Begzhanov and S. M. Akhrarov, "Resonance Scattering by Certain Nuclei of γ Rays from Radiative Capture of Thermal Neutrons," Bull. Acad. Sci. USSR Phys. Ser. **35**, 120-123 (1972).

[35] O. Shahal and R. Moreh, "Recent Developments in Nuclear Scattering of Capture Gamma Rays," AIP Conf. Proc. No. 125, Capture Gamma-Ray Spectroscopy and Related Topics – 1984, S. Raman, ed., 179-191 (1984).

[36] J. R. Huizenga and R. Vandenbosch, "Photoexcitation of the Isomeric States of Cd^{111} and In^{115} with Mono-Energetic Gamma Rays," Nucl. Phys. **34**, 457-460 (1962).

[37] H. Bethe and W. Heitler, "On the Stopping of Fast Particles and on the Creation of Positive Electrons," Proc. Roy. Soc. **A146**, 83-112 (1934).

[38] M. G. Davydov and V. A. Shcherbachenko, "Selecivity of γ-Activation Analysis," Atomnaya Energiya **27**, 205-208 (1969).

[39] MCNP v.4B Code Package, Radiation Shielding Information Center, Oak Ridge National Laboratory, USA.

[40] J. F. Briesmeister, ed., MCNP – A General Monte Carlo N-Particle Transport Code Version 4B, LA-12625-M, Version 4B Manual, Los Alamos National Laboratory, USA, March 1997.

[41] H. W. Koch and J. W. Motz, "Bremsstrahlung Cross-Section Formulas and Related Data," Rev. Mod. Phys. **31**, 920-955 (1959).

[42] S. Lindenstruth, "Measurements and Simulations of Low Energy, Thick Target Bremsstrahlung Spectra," Nucl. Instr. Meth. Phys. Res. **A300**, 293-296 (1991).

[43] H. Bethe and W. Heitler, "On the stopping of Fast Particles and on the Creation of Positive Electrons," Proc. Roy. Soc. **146**, 83-112 (1934).

[44] D. R. Lide, ed., *Handbook of Chemistry and Physics, 72nd Edition*, CRC Press, 14-7 (1991).

[45] Storey, Jack and Ward, "The Fluorescent Decay of CsI(Tl) for Particles of Different Ionization Density," Proc. Phys. Soc. **72**, 1-8 (1958).

[46] C. F. G. Delaney and A. M. Lamki, "Long-Lived Phosphorescent Components in NaI(Tl) and CsI(Tl)," Int. J. App. Rad. Isotop. **19**, 169-170 (1968).

[47] S. Keszthelyi-Landori and G. Hrehuss, "Scintillation Response Function and Decay Time of CsI(Tl) to Charged Particles," Nucl. Instr. Meth. **68**, 9-12 (1969).

[48] P. E. Francois and D. T. Martin, "Phosphorescent Components in CsI(Tl) and CsI(Tl)," Int. J. App. Rad. Isotop. **21**, 687 (1970).

[49] Koicki, Koicki and Ajdacic, "The Investigation of the).15 s Phosphorescent Component of NaI(Tl) and Its Application in Scintillation Counting," Nucl. Instr. Meth. **108**, 297-299 (1973).

[50] Crannell, Kurz and Viehmann, "Characteristics of Cesium Iodide for Use As a Particle Discriminator for High-Energy Cosmic Rays," Nucl. Instr. Meth. **115**, 253-261 (1974).

[51] Moszynski, Gresset, Vacher and Odru, "Timing Properties of BGO Scintillator," Nucl. Instr. Meth. **188**, 403-409 (1981).

[52] M. Laval, et. al., "Barium Fluoride – Inorganic Scintillator for Subnanosecond Timing," Nucl. Instr. Meth. **206**, 169-176 (1983).

[53] S. L. Wen and C. F. He, "A New Approach to the Radiation Hardness of BGO," Nucl. Instr. Meth. **219**, 333-335 (1984).

[54] H. Grassmann, et. al., "Improvements in Photodiode Readout for Small CsI(Tl) Crystals," Nucl. Instr. Meth. **A234**, 122-124 (1985).

[55] E. Sakai, "Recent Measurements on Scintillator-Photodetector Systems," IEEE Trans. Nucl. Sci. **NS-34**, 418-422 (1987).

[56] Holl, Lorenz and Mageras, "A Measurement of the Light Yield of Common Inorganic Scintillators," IEEE Trans. Nucl. Sci. **35**, 105-109 (1988).

[57] Yin, Wei, Shen and Xie, "A New BGO Crystal with Higher Radiation Hardness," Nucl. Instr. Meth. **A275**, 273-276 (1989).

[58] Woody, Levy and Kierstead, "Slow Component Suppression and Radiation Damage in Doped BaF_2 Crystals," IEEE Trans. Nucl. Sci. **36**, 536-542 (1989).

[59] G. F. Knoll, *Radiation Detection and Measurement*, John Wiley and Sons, Inc., 1989.

[60] Melcher, Schweitzer, Utsu and Akiyama, "Scintillation Properties of GSO," IEEE Trans. Nucl. Sci. **37**, 161-164 (1990).

[61] M. Kobayashi and M. Ishii, "Excellent Radiation-Resistivity of Cerium-Doped Gadolinium Silicate Scintillators," Nucl. Instr. Meth. **B61**, 491-496 (1991).

[62] M. Kobayashi, et. al., "Cerium Fluoride, A Highly Radiation-Resistive Scintillator," Nucl. Instr. Meth. **A302**, 443-446 (1991).

[63] Yanovzky, Chizhov and Skorikov, "BGO Crystals – Radiation Hard Scintillators," Nucl. Instr. Meth. **A309**, 596-597 (1991).

[64] Suzuki, Tombrello, Melcher and Schweitzer, "UV and Gamma-Ray Excited Luminescence of Cerium-Doped Rare-Earth Oxyorthosilicates," Nucl. Instr. Meth. **A320**, 263-272 (1992).

[65] C. L. Melcher and J. S. Schweitzer, "Cerium-Doped Lutetium Oxyorthosilicate: A Fast, Efficient New Scintillator," IEEE Trans. Nucl. Sci. **39**, 502-505 (1992).

[66] M. Kobayashi and M. Ishii, "Effect of Cerium Doping on the Radiation Hardness of Gadolinium Silicate Gd_2SiO_5," Nucl. Instr. Meth. B **82**, 85-90 (1993).

[67] Ziegler, Rogers, Selivanov and Sinitzin, "Characteristics of the New $YAlO_3$:Ce Compared With BGO and GSO," IEEE Trans. Nucl. Sci. **40**, 194-197 (1993).

[68] S. C. Sabharwal, et. al., "Thermoluminescence and Transmission Recovery of Gamma Irradiated $Bi_4Ge_3O_{12}$ Single Crystal," Nucl. Instr. Meth. **A329**, 179-182 (1993).

[69] M. Ishii, et. al., "Research and Development of Ce-Doped GSO Scintillation Crystals," SPIE **2305**, 68-79 (1994).

[70] R.-Y. Zhu, "Crystal Gamma-Ray Detectors for High Energy Physics," SPIE **2305**, 80-97 (1994).

[71] Yin, Feng and Hu, "Doping Effect and Mechanism of Radiation Damage of Bismuth Germanate ($Bi_4Ge_3O_{12}$) Crystals," Ferroelectrics **151**, 287-298 (1994).

[72] H. Suzuki, et. al., "The Role of Gadolinium in the Scintillation Processes of Cerium-Doped Gadolinium Oxyorthosilicate," Nucl. Instr. Meth. A **346**, 510-521 (1994).

[73] Kobayashi, Ishii, Usuki and Yahagi, "Cadmium Tungstate Scintillators With Excellent Radiation Hardness and Low Background," Nucl. Instr. Meth. A **349**, 407-411 (1994).

[74] S. Baccaro, et. al., "Scintillation Properties of YAP:Ce," Nucl. Instr. Meth. A **361**, 209-215 (1995).

[75] Kobayashi, Ishii, Harada and Yamaga, "Bismuth Silicate $Bi_4Si_3O_{12}$, A Faster Scintillator Than Bismuth Germanate $Bi_4Ge_3O_{12}$," Nucl. Instr. Meth. A **372**, 45-50 (1996).

[76] M. Moszynski, "Timing Properties of GSO, LSO and Other Ce Doped Scintillators," Nucl. Instr. Meth. A **372**, 51-58 (1996).

[77] A. Fyodorov, et. al., "Progress In $PbWO_4$ Scintillating Crystal," Radiat. Meas. **26**, 107-115(1996).

[78] S. K. Sahu, et. al., "Radiation Hardness of Undoped BGO Crystals," Nucl. Instr. Meth. A **388**, 144-148 (1997).

[79] Taulbee, Rooney, Mengesha and Valentine, "The Measured Electron Response Nonproportionality of CaF_2, BGO, LSO and GSO," IEEE 0-7803-3534-1/97, 326-330 (1997).

[80] M. E. Casey, et. al., "Investigation of LSO Crystals for High Spatial Resolution Positron Emission Tomography," IEEE 0-7803-3534-1/97, 1029-1033 (1997).

[81] S. Yamamoto, "LSO and GSO: Performance Evaluation for PET," Radioisotopes **46**, 265-271 (1997).

[82] C. W. E. van Eijk, "Development of Inorganic Scintillators," Nucl. Instr. Meth. A **392**, 285-290 (1997).

[83] D. Konishi, et. al., "Full Energy Peak Efficiency of GSO(Ce) Detectors for Gamma-Rays," IEEE 0-7803-4258-5/98, 829-832 (1998).

108

[84] H. Ishibashi, et. al., "Scintillation Performance of Large Ce-Doped Gd_2SiO_5 (GSO) Single Crystal," IEEE 0-7803-4258-5/98, 838-841 (1998).

[85] R.Y. Zhu, et. al., "A Study on the Radiation Hardness of Lead Tungstate Crystals," IEEE Trans. Nucl. Sci. **45**, 686-691 (1998).

[86] M. Tanaka, et. al., "Applications of Cerium-Doped Gadolinium Silicate Gd2SiO5:Ce Scintillator to Calorimeters in High-Radiation Environment," Nucl. Instr. Meth. A **404**, 283-294 (1998).

[87] S. C. Sabharwal and Sangeeta, "Study of Growth Imperfections, optical Absorption, Thermoluminescence and Radiation Hardness of $CdWO_4$ Crystals," J. Crystal Growth **200**, 191-198 (1999).

[88] S. Baccaro, "Recent Progress in the Development of Lead Tungstate Crystals," IEEE Trans. Nucl. Sci. **46**, 292-295 (1999).

[89] Melcher, Schweitzer, Liberman and Simonetti, "Temperature Dependence of Fluorescence Decay Time and Emission Spectrum of Bismuth Germanate," IEEE Trans. Nucl. Sci. **NS-32**, 529- (1985).

Chapter 4

METHOD CAPABILITIES AND EXPERIMENTS

In Chapter 2 the basic principles underlying the excitation of nuclei with photons leading to the formation of nuclear isomeric states was presented. After a discussion of the different photonuclear interactions which take place for photon energies less than ~50 MeV, a detailed analysis was presented of the physics describing the resonant absorption of photons by nuclei and the decay of the excited nuclear states resulting from this process to isomeric states including a theoretical model for evaluating the energy dependent cross section for the formation of isomeric states in nuclei resulting from resonant photon absorption. This information was then used to develop a mathematical model for calculating the activity of an isomeric species in a sample of material being irradiated by energetic photons. Building upon this understanding of the physics underlying the resonant absorption of photons by nuclei leading to the creation of isomeric nuclei, Chapter 3 explored the three different building blocks of an industrial system designed to carry out PRE, namely the isomer, the excitation radiation and the system designed to measure the decay of the isomer. Combining the knowledge of the physics of the photonuclear resonant excitation process with the insights gained in analyzing the different components of an industrial photonuclear resonance excitation (PRE) system, this chapter examines how well an industrial PRE system would be expected to operate, focusing on performance goals which might be realistically expected from industrial systems designed to excite isomeric nuclei.

The analysis of §4.1 discusses the use of PRE to generate high activity isomeric materials focusing on the relationship between the irradiation field, the duration of the irradiation and the total and specific isomeric activity in the target. Following this, §4.2 considers the use of PRE for material assay applications where estimates of sensitivity such as the minimum detectable limit and minimum quantifiable limit for trace amounts of isomers in bulk materials are introduced together with their relationship to the quantity of material being analyzed and the analysis processing rate. In order to demonstrate the efficacy of the PRE process for isomeric excitation and to investigate potential problems associated with its implementation a series of experimental investigations have been carried out. Section 4.3 summarizes this experimental work and presents several practical issues dealing with photonuclear resonance excitation which are relevant to the design of an industrial material assay system based upon PRE.

4.1   ISOMER PRODUCTION

As with other radioisotopes, isomeric isotopes could find applications in a variety of applications. Some examples include the use of isomers in tracer studies exploring material transport, for diagnostic medical imaging and for therapy. Isomers might also find use as isotopic radiation sources for industrial purposes. In comparison with conventional radioisotopes, either naturally occurring or artificially made, isomeric nuclei might be particularly useful for some applications. One reason why the use of isomeric isotopes might be advantageous could be the ability to produce and deliver short-lived isotopes for field applications. Currently, radioisotopes which are used in the field at a plant or factory are limited to short lived isotopes produced using isotopic generator pairs (e.g., ^{99}Mo-^{99m}Tc), medium or long lived isotopes generated at nuclear reactors or long lived naturally radioactive elements. Since a system designed to produce isomers would be relatively small and could be portable, short lived isomers that are not currently available from isotopic generators might find uses in places currently unable to procure radiotracers. In some cases PRE generated isomers might be able to fill niche markets because some elements having isomeric states might not otherwise be available; their use could also help to expand existing applications or open new tracer applications.

Generally speaking, the most important aspect related to the production of radioisotopes for industrial purposes is the maximization of specific activity of the product. Of secondary concern for industrial uses but equal concern for medical applications is the minimization of radioimpurities in the product. For isomers produced through the PRE process, specific activity and radioimpurity concentration are both governed by the energy spectrum of the irradiation spectrum. Higher endpoint energy electron beams increase the overall photon intensity at all energies, increasing the maximum achievable specific activity. As the photon intensity at energies greater than the neutron and proton binding energies is increased, the radioimpurity concentration may begin to build up due to the opening of (γ,n) and (γ,p) reactions channels.

4.1.1   System Parameters

In order to determine the performance level an industrial PRE isomer production system might be expected to meet, numerical simulations have been carried out to determine the nature of a bremsstrahlung generated irradiation spectrum for a system configuration typical of what might be used to produce high specific activity isomeric samples. The geometry of the model used for this analysis is given in Figure 4-1 below and consists of a lead cube having sides 20 cm long with a 2 cm diameter hole entering the cube from the center of one face and extending to the cube's mid-plane. The bremsstrahlung is generated using a 10 MeV electron beam which impinges upon a 2 mm tungsten plate located at the opening of the cylindrical channel. In the figure, the isomer production region is defined as the area inside the cavity extending from 3 cm to 6 cm from the convertor plate. Within this area, the photon flux was calculated within annular slices of depth 0.1 cm and having radial thicknesses of 0.1 cm, forming a series of concentric annular rings stacked upon each other.

112

6 cm
5 cm
4 cm
3 cm

Lead
Shielding

Tungsten
Convertor
Plate

Incident
Eectron
Beam

Isomer
Production
Region

Scale: ⊢⊣
1 cm
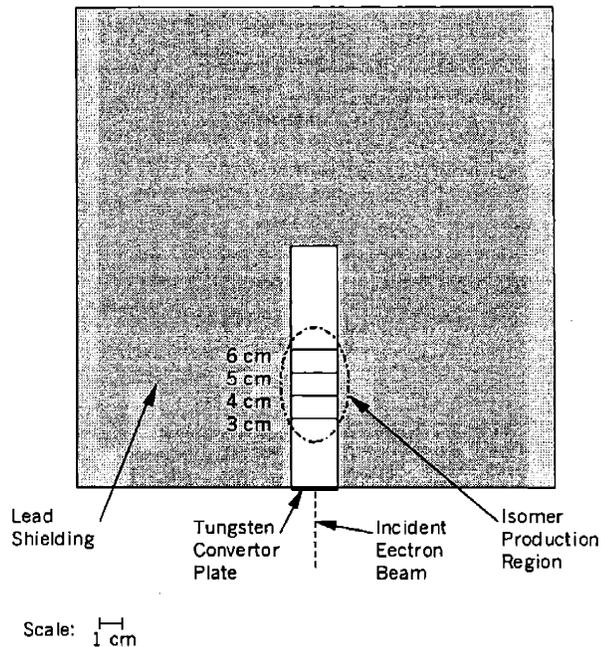
Figure 4-1 Schematic drawing of an idealized irradiation system (modeled using MCNP4B) for producing isomeric isotopes for secondary purposes.

The material within the hollow core for these calculations was taken as air. The production area location has been defined at a location near to the convertor plate in order to utilize the region of space having the highest photon intensity. The average photon flux in the production region from 3.0 to 3.1 cm in a disk having a radius of 0.1 cm centered co-axially with the beam axis is depicted in Figure 4-2; the flux values in this figure are totaled over 0.1 MeV bins. At 4 MeV, the photon flux was calculated to be approximately 6×10^{13} quanta/cm^2/sec/mA per MeV. As will be seen in the next section, this photon flux is capable of producing samples having equilibrium specific activities on the order of mCi per gram or greater per mA of beam current for many isomers.

Photon Flux at 3.0 cm From Convertor Face
(Averaged within r=0.1cm)
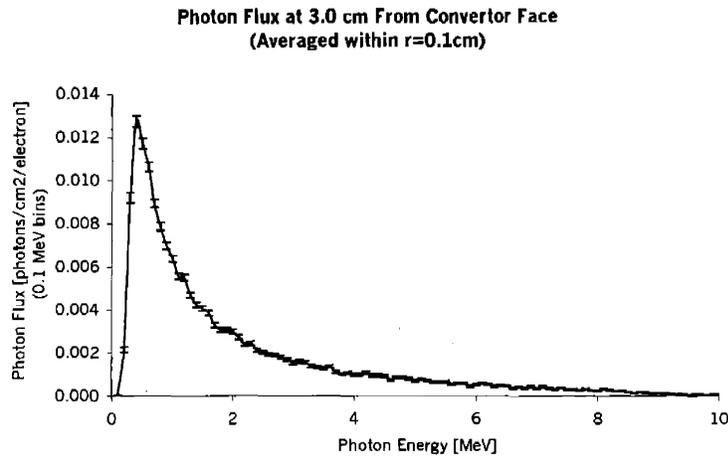
Figure 4-2 Photon flux averaged from 3.0 cm to 3.1 cm within a circle of 0.1 cm centered on the beam axis calculated for the sample geometry of Figure 4-1 with an incident electron beam of 10 MeV and a tungsten convertor plate 2 mm thick.

One aspect of high activity isomer production that might be of interest in some applications is the uniformity of the irradiation spectrum, and thus the activity distribution within the product. In Figure 4-3 intensity plots of the photon flux distribution within the production region are given at photon energies ranging from 1 to 10 MeV (in 0.1 MeV bins) as well as the total photon flux distribution at energies from 0.1 to 10 MeV. (The color shading in these figures is linear in magnitude with the maximum intensity in the depth range from 3.0 to 3.1 cm on the beam axis and the minimum intensity occurring in the depth range from 5.9 to 6.0 cm at the outmost radial slice from 0.9 to 1.0 cm.) In these contour plots, the statistical precision of the Monte Carlo calculations at higher energies is on the order of 10% of the plotted values, in comparison with precisions better than 1-2% at 1 MeV. The reason for the differences in precision is a result of the relative difference in the total number of photons at the two energies.

Progressing from 1 MeV, Figure 4-3 a), through 10 MeV, Figure 4-3 j), the flux gradient in the radial direction at lower energies is observed to be less than that at higher energies. The ratio of the photon flux on axis to that along the edge of the isotope production region from 3.0 to 3.1 cm at 1 MeV is 2.88 ± 0.08, at 5 MeV the ratio is 3.69 ± 0.30 and at 9 MeV the ratio is 6.43 ± 1.28. At the far end of the production region however, from 5.9 to 6.0 cm, the flux ratios are 1.71 ± 0.09, 1.53 ± 0.26 and 2.04 ± 0.76, respectively. The photon flux intensities at 1 through 10 MeV are also shown in Figure 4-4. As can be seen more clearly in this figure, at the 3.0 to 3.1 cm distance the general trend in flux distribution at different energies is the same up to ~9-10 MeV. The reason for the differences between flux ratios at the two ends of the production region is primarily due to the forward peaked, cone-beam like geometry of bremsstrahlung radiation at these energies and the spreading out of the radiation as the distance from the convertor plate is increased. At lower energies the total photon flux throughout the isomer production region is also supplemented by radiation scattered off the inside walls of the shielding.

a)

10 MeV Electrons - 2 mm Tungsten
1 MeV Photon Energy (0.1 MeV bin)
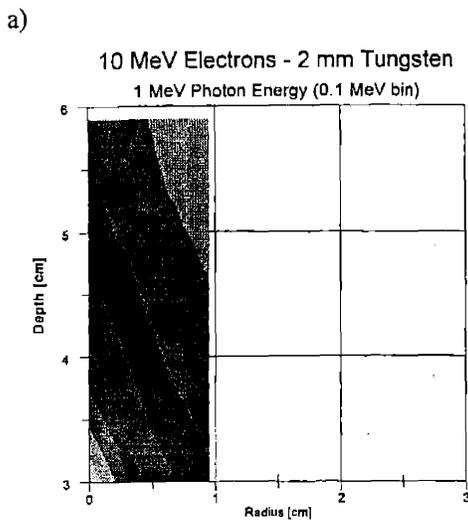
$\varphi = 6.38\text{E-}3 - 1.03\text{E-}3 \ [\text{photons/cm}^2/\text{electron}]$

c)

10 MeV Electrons - 2 mm Tungsten
3 MeV Photon Energy (0.1 MeV bin)
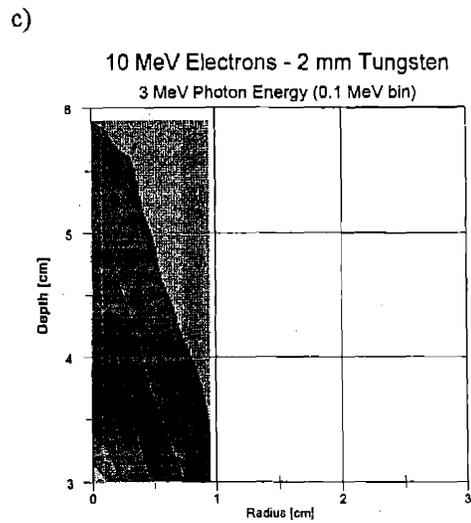
$\varphi = 1.52\text{E-}3 - 2.19\text{E-}4 \ [\text{photons/ cm}^2/\text{electron}]$

b)

10 MeV Electrons - 2 mm Tungsten
2 MeV Photon Energy (0.1 MeV bin)
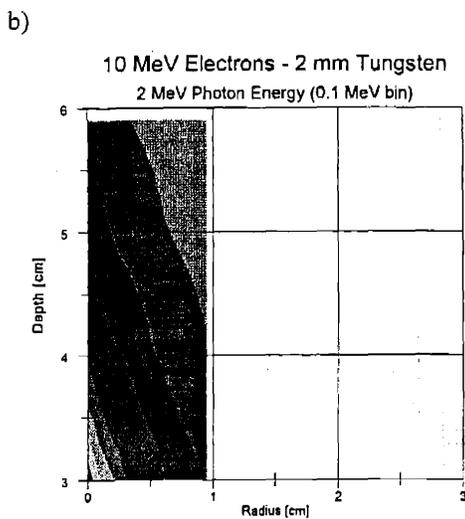
$\varphi = 2.96\text{E-}3 - 4.14\text{E-}4 \ [\text{photons/ cm}^2/\text{electron}]$

d)

10 MeV Electrons - 2 mm Tungsten
4 MeV Photon Energy (0.1 MeV bin)
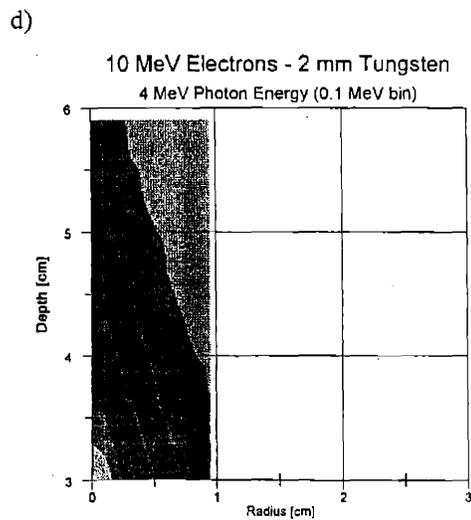
$\varphi = 9.84\text{E-}4 - 1.31\text{E-}4 \ [\text{photons/ cm}^2/\text{electron}]$

Figure 4-3 Photon flux within 0.1 MeV bins in the isomer production region of Figure 4-1 generated using 10 MeV electrons incident upon a 2 mm tungsten target at photon energies of from 1 to 10 MeV and the total photon flux in the same region for photons ranging in energy from 0.1 to 10 MeV.[a,b]

---

[a] Each change in color shading represents a one tenth change of the flux range indicated at the bottom of each figure.

[b] Using the Monte Carlo technique there is an uncertainty associated with all calculated values. In general, the magnitude of the uncertainty associated with a particular value decreases as the number of event histories modeling the phenomenon increases. For bremsstrahlung calculations, uncertainties in the photon flux at higher energies are always higher than those for lower photon energies because there are more low energy photons generated per incident electron than there are at higher energies. Because of this, statistical variation in the plots of photon flux in these figures increases with energy. This effect is clearly seen in the photon energy bins from 7 MeV to 10 MeV. As can be seen, variations on the order of 5 – 15% occur at these energies where the photon flux rate is the lowest (indicating the forward peaked nature of high energy bremsstrahlung), in the outer radial region of the target.

e)

10 MeV Electrons - 2 mm Tungsten
5 MeV Photon Energy (0.1 MeV bin)
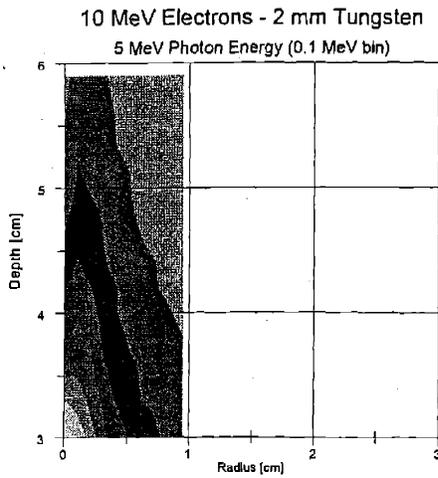
$\varphi = 6.88E\text{-}3 - 9.07E\text{-}5$ [photons/ cm^2/electron]

g)

10 MeV Electrons - 2 mm Tungsten
7 MeV Photon Energy (0.1 MeV bin)
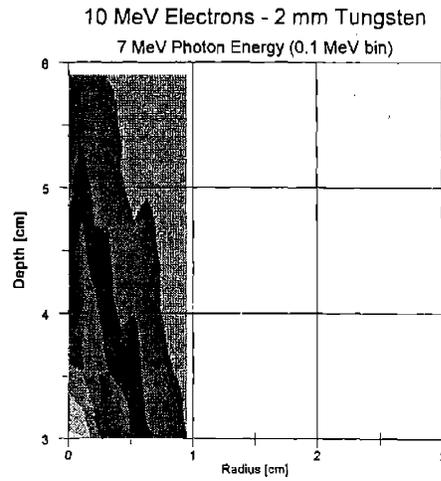
$\varphi = 3.34E\text{-}4 - 4.64E\text{-}5$ [photons/ cm^2/electron]

f)

10 MeV Electrons - 2 mm Tungsten
6 MeV Photon Energy (0.1 MeV bin)
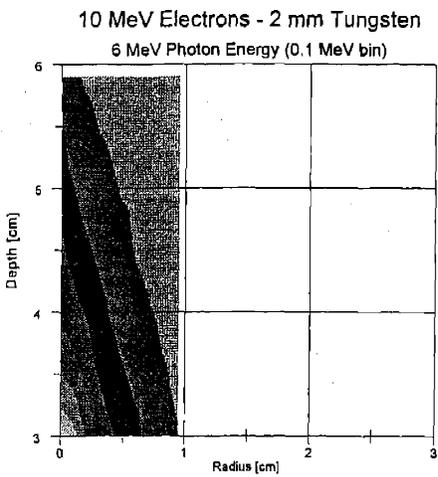
$\varphi = 5.07E\text{-}4 - 6.47E\text{-}5$ [photons/ cm^2/electron]

h)

10 MeV Electrons - 2 mm Tungsten
8 MeV Photon Energy (0.1 MeV bin)
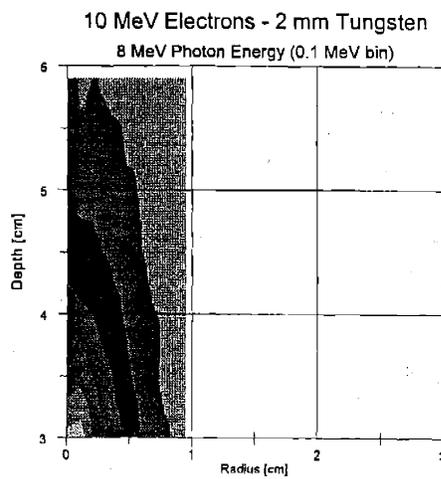
$\varphi = 2.22E\text{-}4 - 3.22E\text{-}5$ [photons/e cm^2/lectron]

Figure 4-3 (con't)

i)

10 MeV Electrons - 2 mm Tungsten

9 MeV Photon Energy (0.1 MeV bin)
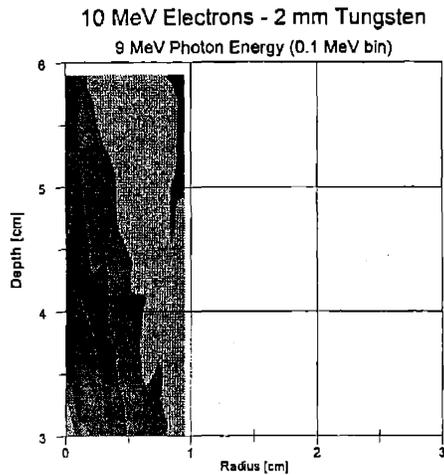
$\varphi = 1.24E-4 - 1.48E-5$ [photons/ cm^2/electron]

j)

10 MeV Electrons - 2 mm Tungsten

10 MeV Photon Energy (0.1 MeV bin)
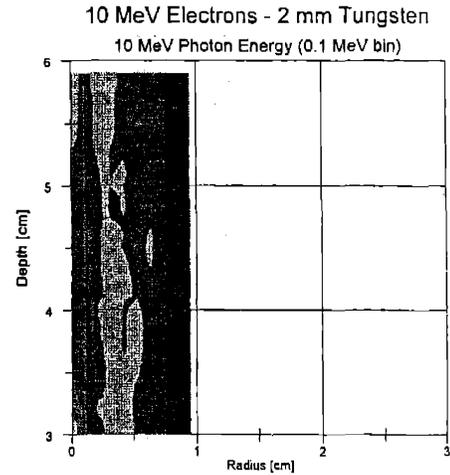
$\varphi = 3.34E-5 - 9.36E-7$ [photons/ cm^2/electron]

k)

10 MeV Electrons - 2 mm Tungsten

All Photons (0-10 MeV)
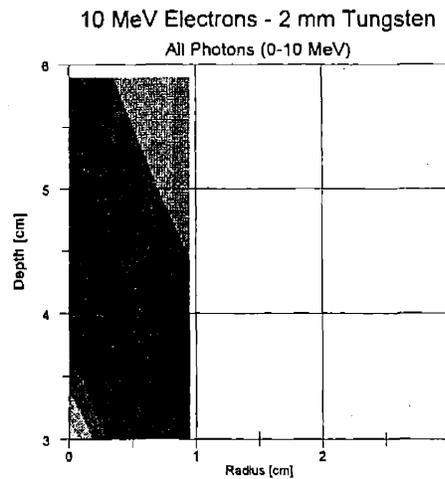
$\varphi = 0.175 - 0.0278$ [photons/ cm^2/electron]

Figure 4-3 (con't)

The nature of this distribution suggests that in order to achieve the highest specific activity in a target it must be placed as close to the convertor plate as possible. However, if a homogeneous activity distribution is desired in the sample it should be held in such a fashion that it can be rotated both along and transverse to the incident beam axis. Additionally, if a reduction in specific activity can be tolerated, removing the target to greater distances from the convertor plate or introduction of a preliminary scatterer may also be useful in improving the activity distribution within the target. Referring to the discussion in Chapter 3 on the importance of the electron beam energy on the irradiation spectrum, a more homogeneous spectrum might also be achieved using a lower energy beam. While this might be desirable for other reasons as well (i.e., reducing shielding requirements or reducing induced background radiation resulting from higher energy photonuclear reactions), obvious drawbacks are a) a reduction of photon flux at all energies and b) loss of those highest energy photons for which the isomeric excitation cross section is the largest.

Photon Flux Angular Distribution
for Different Photon Energies
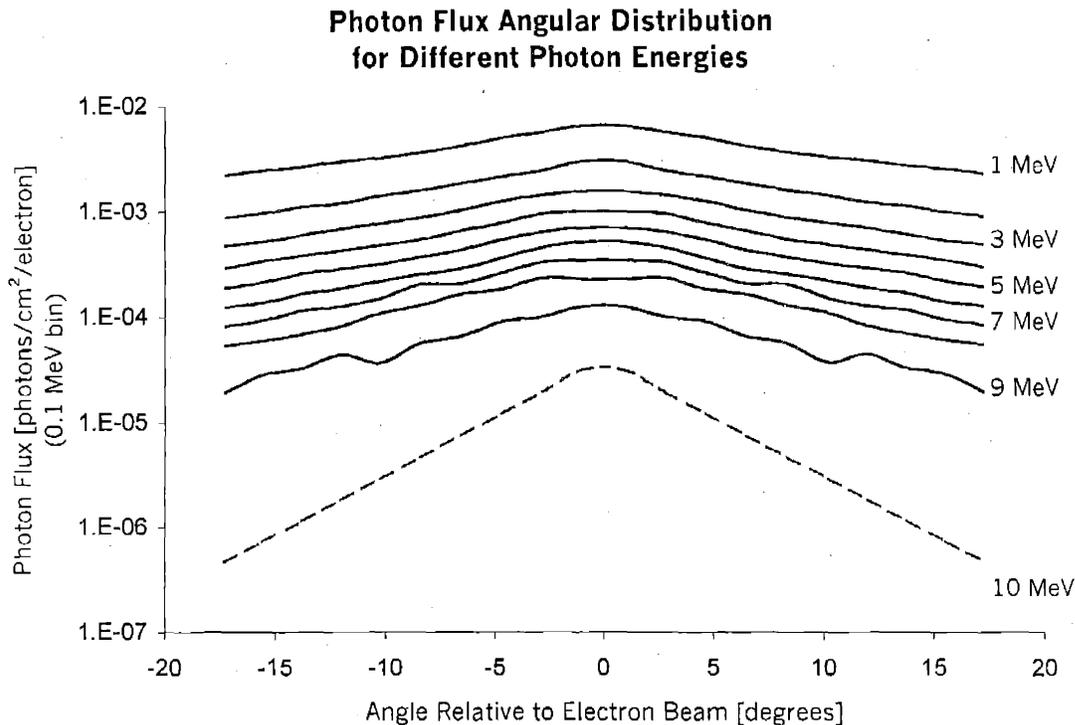
Figure 4-4 Angular dependence of the photon flux distribution at 3 cm generated using a 10 MeV electron beam and 2 mm tungsten convertor plate at photon energies from 1 MeV to 10 MeV in 0.1 MeV bins. (The values at 10 MeV have been smoothed.)

In the diagram of the idealized isomer production irradiation setup, the gap between the convertor plate to the beginning of the isomer production region was included to allow for the possibility that it might be necessary to magentically sweep electrons passing through the convertor plate away from the isomeric target. For example, 10 MeV electrons impinging upon a 2 mm thick tungsten convertor plate would emerge from the opposite face with an energy of ~1 MeV as a result of collisional losses within the convertor. Using a magnetic sweeping system with a magnetic flux density of 1 Tesla, 1 MeV electrons would have an orbital radius of 4.85 mm. Additionally, at higher beam powers it might be desired to alter the convertor plate geometry in order to install some sort of active cooling system. Both of these design changes would require additional space but would not be expected to significantly alter the irradiation spectrum. The effects of these improvements upon the irradiation spectrum could be easily accounted for by reanalyzing the problem and including the relevant structures needed to remove the electron beam and/or cool the convertor. Along the same lines, depending upon the target sample physical properties such as density and melting point and its size and the intensity of the irradiation spectrum, it might also be necessary to actively cool the target too.

The attenuation of the irradiation spectrum within the target sample itself is another important phenomenon which must be accounted for. For small target volumes the change in the photon spectrum and flux within the target in comparison with the calculations presented above is not likely to be greater than a factor of 2 under most circumstances but this change is still significant for most situations. Since the alteration of the photon flux and spectrum resulting from self attenuation within the target is completely dependent upon the target material it is not practical to examine the nature of this effect in a completely general fashion but rather it must be addressed uniquely for every situation. Among other aspects of judging the method capabilities of using PRE to produce isomers, in §4.1.2 this effect is studied for the specific case of radiation attenuation in an indium target.

118

4.1.2 Method Capabilities

As stated above, for the application of photonuclear resonance excitation to produce isomeric isotopes the principle criterion to judge the design of a system is the specific activity of the product which can be produced. The determination of the specific activity of an isomer achievable by a particular system is only really dependent on one design variable, the irradiation source. While the physics governing the excitation process is the same for all isotopes, examination of the data of the few isomers for which the PRE cross section exists indicates that most isomeric excitation cross sections are similar in magnitude and energy dependence. This suggests that a system designed to irradiate a sample until equilibrium is achieved will produce a product having, to within an order of magnitude, the same specific activity regardless of the isotopes involved. Realizing this, the sections below examine the particular case where indium-115m is produced by irradiating an enriched indium-115 target using the generic irradiation system design of Figure 4-1.

4.1.2.1 Induced Activity

To characterize the capability of PRE to produce high specific activity isomer samples, this section explores the use of PRE to create indium-115m. The decay scheme of indium-115m is shown in Figure 4-5 below. Natural indium is comprised of indium-113 (4.3 %) and indium-115 (95.7 %). Indium-113 also has an isomeric eigenstate, at 391.7 keV, which has a half-life of 1.66 h. With a high natural abundance, a medium duration half-life and the moderate energy and nearly monochromatic nature of the radiation associated with the decay of indium-115, this isotope exhibits many characteristics that might be desirable for isomer applications.
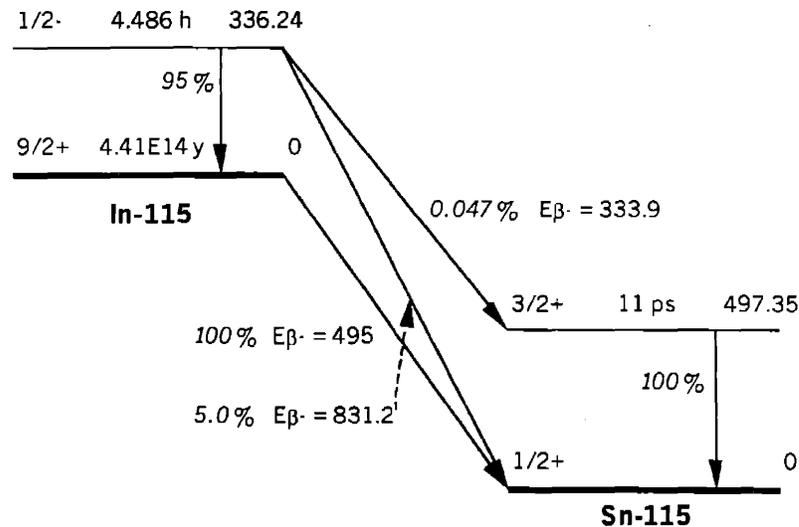
Figure 4-5 Decay scheme of the isomeric state of indium-115.[1]

The isomeric excitation cross section for indium-115m, determined experimentally using a bremsstrahlung irradiation source and the photon difference method, is given in Figure 4-6; as with most reported isomeric excitation cross section values there is no indication of the precision of the results reported in this paper.[2] The cross section displays the characteristics typical of isomeric excitation cross section including a smooth increase in magnitude from about 2 to 8 MeV and a decrease in magnitude at greater energies, attributable to the opening of the (γ,p) reaction channel at 6.804 MeV and the opening of the (γ,n) reaction channel at

9.039 MeV. The overall magnitude of the cross section is also in the typical range expected for isomeric excitation cross sections, peaking in the one to two millibarn range.

Indium-115 PRE Cross Section
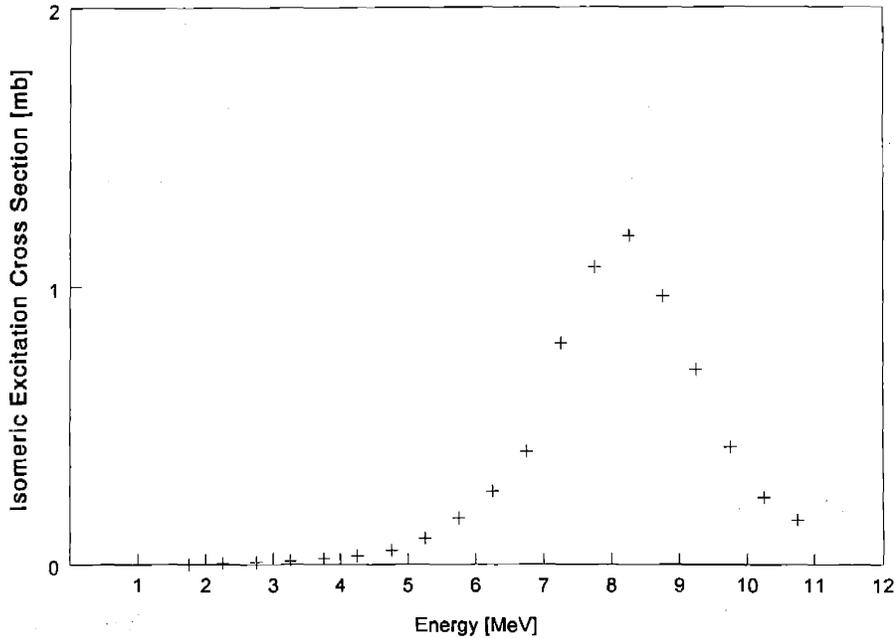
Figure 4-6 Photonuclear resonance excitation cross section for $^{115}In(\gamma,\gamma')^{115m}In$.[2]

Comparison of Flux Distribution
On Axis - 3.0 to 3.1 cm - (1 MeV bins)

─────── Air   ─ ─ Indium
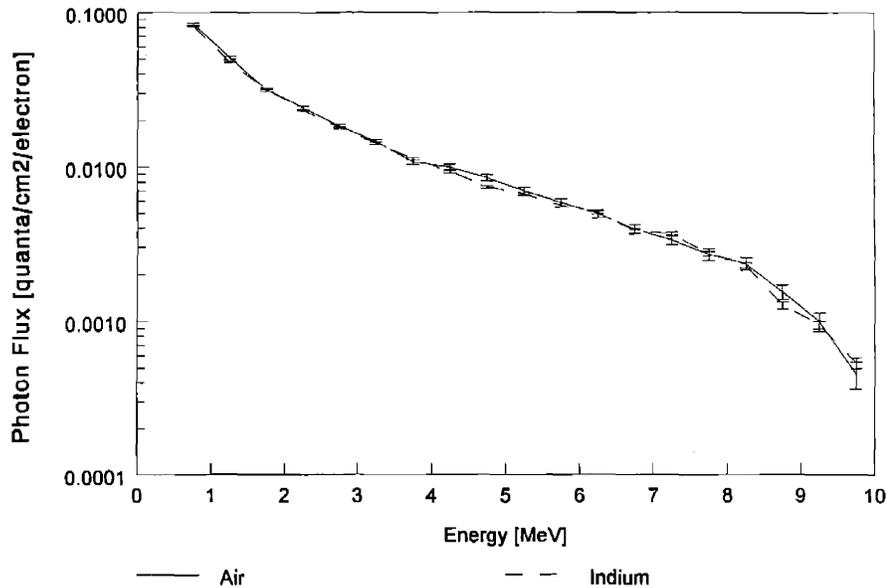
Figure 4-7 Comparison of the photon flux spectrum in air and an indium production target at a depth of 3.0 to 3.1 cm in the production region along the beam axis (flux values in 1 MeV bins).

Comparison of Flux Distribution
On Axis - 3.9 to 4.0 cm - (1 MeV bins)
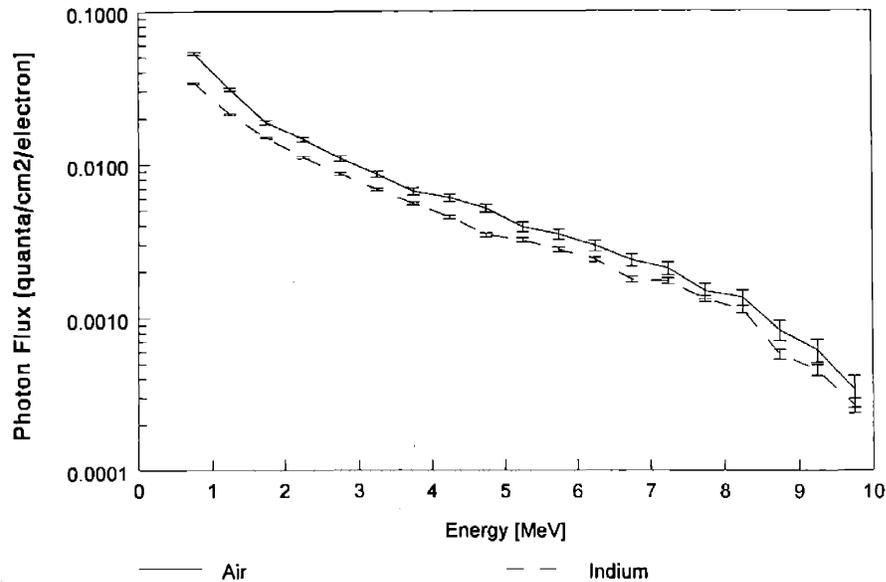
Figure 4-8 Comparison of the photon flux spectrum in air and an indium production target at a depth of 3.9 to 4.0 cm in the production region along the beam axis (flux values in 1 MeV bins).

For this analysis calculations were carried out to determine the isomeric indium-115 activity in a cylindrical target of enriched indium (100% In-115) with a radius of 0.1 cm and length 1.0 cm, having a density of 7.31 grams/cm^3 (total mass 0.230 grams), located along the irradiation beam axis in the irradiation geometry of Figure 4-1, at a distance of from 3.0 to 4.0 cm from the front face of the convertor plate. The photon flux within the indium was determined using MCNP4B, the experimentally determined excitation cross section from reference 2 was used. Examining Figure 4-7 and Figure 4-8, the difference in the intensity of the photon flux within the sample target when consisting of air and indium is not very large.

The equilibrium indium-115m activity and specific activity in the ten segments of the sample target are tabulated in Table 4-1 below. Since no information is available concerning the uncertainty of the cross section values used for these calculations, the numbers in the table are not reported with uncertainty values and as such should be taken as rough estimates only (the uncertainty in the calculated activities due to the statistics of the Monte Carlo calculation is less than 5%). It is important to note that the total equilibrium activity of the product is a) the total intensity of an isotropic source and not flux value and b) that, to relate the activity to photon intensity or flux, requires a correction factor of 0.95 due to the branching ratio of the isomeric state.

One aspect of this approach, however, which might be advantageous under certain circumstances is the non-destructive nature of the process. By not requiring any chemical or physical processing after the irradiation period, metallic sample targets could potentially be recycled one or more times depending upon the response of the material to cyclic irradiation. An important caveat, however, is the fact that irradiation of indium-115 under these conditions will also produce the unstable isotope indium-114 due to (γ,n) reactions. If the existence of this contaminant in the product was troublesome the electron beam energy would have to be reduced to less than the indium-115 neutron separation energy (9.039 MeV).

Table 4-1 Equilibrium indium-115m activity in a sample target irradiated using 10 MeV bremsstrahlung in the isomer production region from 3.0 to 4.0 cm, radius 0.1 cm.

Region in Target [cm]	Activity [Bq/mA]	Activity [mCi/mA]	Specific Activity [Bq/g/mA]	Specific Activity [mCi/g/mA]
0.0 – 0.1	8.92×10^6	0.241	3.89×10^8	10.5
0.1 – 0.2	8.22×10^6	0.222	3.58×10^8	9.67
0.2 – 0.3	7.54×10^6	0.204	3.28×10^8	8.87
0.3 – 0.4	6.92×10^6	0.187	3.01×10^8	8.14
0.4 – 0.5	6.36×10^6	0.172	2.77×10^8	7.49
0.5 – 0.6	5.86×10^6	0.158	2.55×10^8	6.90
0.6 – 0.7	5.41×10^6	0.146	2.36×10^8	6.37
0.7 – 0.8	5.00×10^6	0.135	2.18×10^8	5.89
0.8 – 0.9	4.62×10^6	0.125	2.01×10^8	5.44
0.9 – 1.0	4.30×10^6	0.116	1.87×10^8	5.06
Total:	6.32×10^7	1.71		
Average:			2.75×10^8	7.43

4.1.2.2   Production Schedules

Some decisions which must be made concerning the production of isomers in industrial quantities include the timing of the irradiation and the geometry of the material placement during irradiation. As with other nuclear activation techniques, the buildup of the indium activity (assuming that the gound state population of the isomeric isotope may be assumed constant) is given by the familiar relationship of Eq. 4-1.

$$A(t) = A_{equilibrium} \left(1 - e^{-\lambda t}\right) \qquad \qquad \textbf{4-1}$$

For the irradiation of indium in the example above, the activity buildup in the target would reach its equilibrium value, 1.71 mCi, after ~31 hours as shown in Figure 4-9.

Indium-115m Specific Activity Buildup
Length = 3.0 to 4.0 cm , Radius = 0.1 cm
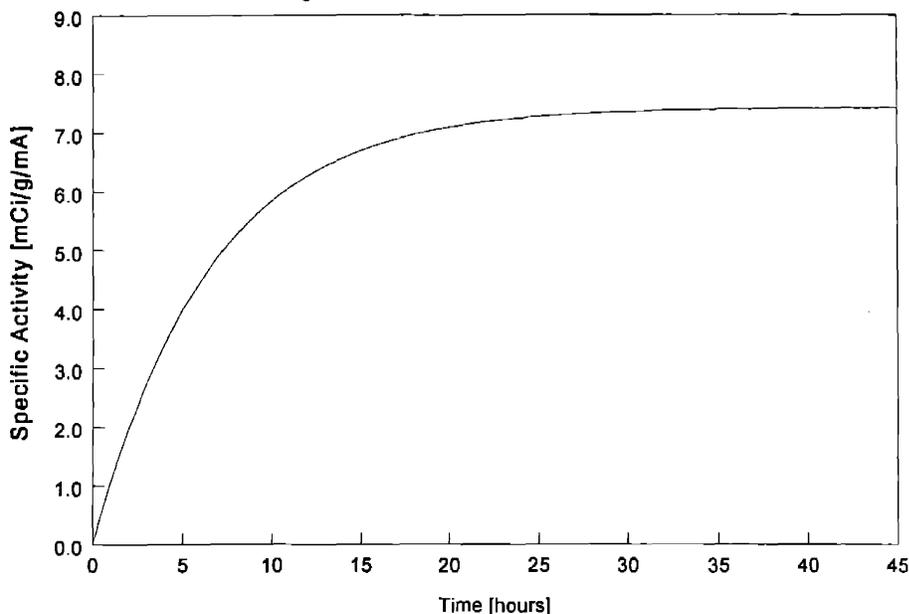
Figure 4-9 Buildup of [115m]In activity in a sample target extending from 3.0 cm to 4.0 cm in the isomer production region and having a radius of 0.1 cm.

The irradiation geometry in the example above does not, however, use the irradiation field in an efficient way. In comparison to the total photon intensity, only a small fraction of the irradiation field passes through the sample target and as discussed above, most of these photons pass through the target without causing isomeric excitation (either scattering within the target or passing through it with no interaction at all). It would be better if a production scheme could be used which did a better job at exploiting more of the available irradiation field.

As seen in Table 4-1, the difference in induced activity between 3.0 cm and 4.0 cm is approximately a factor of two. This trend is a result of the decrease in photon flux within the sample at greater and greater depths which stems from both the natural decrease in intensity as the distance from the source is increased (the divergence of the photon beam) and the attenuation of photons within the sample. However, in the region behind and to the side of the sample target the irradiation photon flux is still high. If a lower specific activity product was acceptable it would be possible irradiate a larger sample volume to produce either a higher total activity product or high specific activity product at a faster rate. Referring to Figure 4-3 and Figure 4-4 it is clear that it would be more desirable to expand the target in the radial direction rather than making it deeper since at all energies the rate of decrease of the photon flux is less radially outward from the beam axis than it is as a function of depth.

There are a variety of irradiation schemes which one might consider when using a high energy photon beam to produce radioisotopes. For the indium-115m production case, it might be useful to use an irradiation geometry similar to that depicted in Figure 4-10 where the central sample target is nestled within an array of future targets. The production schedule for this arrangement would involve the insertion of a cold target into position 1 and then cycling it through positions 2 through 6, after which it would be moved to the central position for the last portion of the irradiation. Examining Figure 4-3 and Figure 4-4, the photon intensity from 3.0 to 4.0 cm in the radial region from 0.1 to 0.3 cm is found to be approximately 75% of that in the central region. Extrapolating this value to an equilibrium activity for indium samples in the outer ring yields a value of 1.28 mCi/mA.
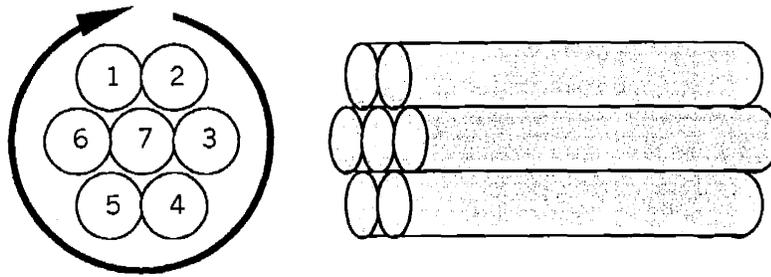
Figure 4-10 Multiple target irradiation geometry for sequential product production.

Assuming that it would be desirable to have a 24 hour production schedule, the maximum product activity which could be produced using a single irradiation target is 1.67 mCi/mA, corresponding to a maximum specific activity in the target of 7.26 mCi/g/mA. In comparison, a cyclic irradiation scheme based on 6 hour irradiations would yield sample targets having a total activity of 1.54 mCi/mA every six hours, corresponding to a maximum specific activity in the target of 6.69 mCi/g/mA. Thus, the cyclic process yields 92% of the activity of a standard 24 hour irradiation but takes only one quarter the time. Summing together the total activity in each of the four consecutive targets present at the end of one day, 2.48 mCi/mA is available. The relationship between the build up of activity in a single target irradiated on the beam axis for 24 hours, the activity in a single target as it goes through each of the seven cyclic position over 42 hours, and the total activity of the output product of a cyclic irradiation scheme summing together four consecutive samples is shown in Figure 4-11.

Contrasting this with a standard irradiation, the cyclic production schedule is found to produce a total product having approximately 50% more activity than that from a standard scheme after 24 hours. However, it should be noted that the specific activity in this case, at 2.69 mCi/g/mA, is significantly less than that for the standard case. As one final observation, if instead of a cyclic rotation the total and specific activity in all seven targets is summed together after 6 hours of irradiation, the total activity is found to be 5.68 mCi/mA and 3.53 mCi/g/mA. After 24 hours, these values are 9.17 mCi/mA and 5.69 mCi/g/mA, respectively. From this analysis the relevant conclusions are that if the chief desire is to produce a high specific activity target, the use of a cyclic production schedule is the best choice, but if the objective is to produce a product with the maximum activity, a standard irradiation of a sample of larger mass is best. In addition, depending upon the circumstance, the quicker throughput of a cyclic production scheme might prove to be advantageous.

Indium-115m Activity Buildup
Standard vs. Multi-Target
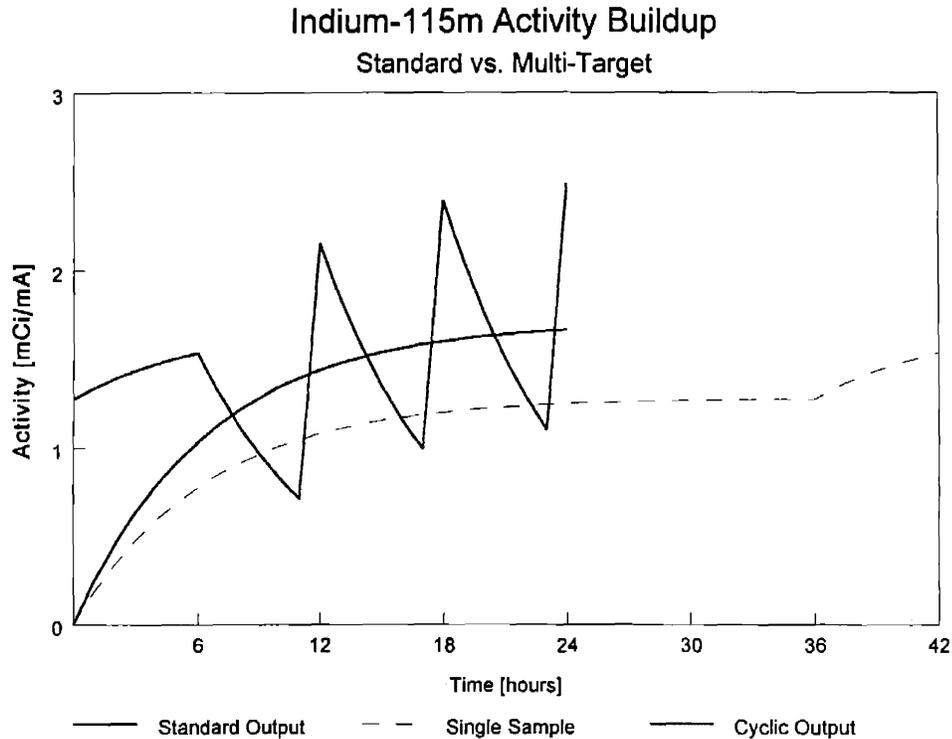
Figure 4-11 Indium-115m activity using different production schemes.

4.2 MATERIAL ASSAY

With the availability of reliable, high power electron accelerators a second application of photonuclear resonance excitation which is worth exploring is the interrogation of materials. Depending upon the circumstances, it might be desirable to analyze a sample to determine whether isomeric material is present or, taking things further, actual quantification of the amount of isomeric material present in the sample might be needed. This section examines issues related to the use of PRE to analyze bulk materials. In §4.2.1 the basic parameters of an industrial PRE material assay system are discussed. In §4.2.2 the capabilities of an industrial assay system such as detection sensitivity, material quantification limits and material throughput are explored.

4.2.1 System Parameters

As with the use of PRE to produce high activity sources of isomers, the energy spectrum and intensity of the irradiation field is an important parameter which must be known when assessing the performance of a PRE based material assay system. Depending upon the requirements for a particular application, a material assay system would involve the examination of either small samples or large, bulk materials. In addition, depending upon the application it might be required that analyses be carried out continuously or it may be possible to operate in a batch fashion. A brief overview of some potential PRE assay applications along with the parameters associated with them is provided in Table 4-2.

Table 4-2 System parameters associated with various PRE material assay applications.

Application	Nature of Sample	Timing
Mining – *Assay of precious metal content in ore*	In mining applications, the ideal assay system would be capable of analyzing unprocessed ore, a bulk material.	Analyzing large quantities of bulk materials, such as ore, requires a system capable of carrying out measurements within a few seconds.
Environmental Restoration – *Assay of heavy metal content in soil for hazardous waste clean up* *Assay of technetium in soil for nuclear waste analysis*	For environmental restoration a field deployable system capable of analyzing small grab samples might be desired for site characterization while bulk material analysis might be desired during processing.	A system designed to aid in site characterization would probably not require measurement times less than several minutes. Bulk soil analyzers would require faster analysis times but would not likely need to be as fast as those for mining.
Science and Engineering – *Assay of isomeric isotopes in materials*	In the analysis of materials the range of possible sample sizes is large.	Regardless of sample size, analysis time is not likely to be a critical constraint for these applications.

For practical reasons it would of course be desirable to have a system which could analyze samples of any size to assay arbitrarily small quantities of isomeric material with absolute precision, and which could do this instantaneously. Since this can not be done, choices must be made regarding the selection of the radiation source and detector to assemble a system which is capable of achieving real performance objectives while meeting constraints of cost, size and complexity. For applications where the processing speed must be fast, the sensitivity of the measurement system will be primarily limited by the amount of time available for irradiation and measurement. These systems will be the most demanding in terms of accelerator current and detection efficiency requirements. For applications involving the analysis of smaller samples where measurement time is not a limiting factor, smaller accelerators and less efficient detectors might be acceptable, helping to reduce the cost and size of these systems.

When examining big samples a particularly important parameter which must be accounted for is the self-attenuation of the isomeric decay photon(s) within the sample matrix, which is relevant because of its impact on detection efficiency. For homogeneous samples with a uniform distribution of isomeric material, the effects of self-attenuation may be corrected for numerically, using MCNP for example. When the sample is inhomogeneous but the isomeric material is still distributed uniformly, a radiographic transmission measurement of the sample could be used to determine the materials 3-dimensional attenuation coefficient and using this information together with numerical modeling it would again be possible to correct for signal attenuation in the sample and to determine the correct detection efficiency. For the case of an inhomogeneous sample containing a non-uniform distribution of isomeric material (such as gold in ore), however, numerical modeling could only be used to determine a worst case estimate of the detection efficiency. Because of this, material assays for the latter case would be limited to reporting minimum concentrations rather than absolute concentrations.

A third important parameter relevant to the detection and quantification of isomeric signals is the background radiation associated with their measurement. As is illustrated in the following section, both

the magnitude of the background signal as well as its uncertainty affect the sensitivity and precision of measurements in activation analysis. Because of this an industrial system must be designed a) to reduce the background signal to an acceptably low level and b) to determine the background radiation signal with a high degree of precision. Background radiation for this type of analysis can be categorized into two groups, radiation originating from naturally occurring radiation and radiation induced in the sample as a result of the irradiation of nuclei other than the isomeric species.

To account for naturally occurring radiation there are two options. If this category of background radiation is essentially constant (constant concentration of natural radiogenic isotopes in the sample) then it should be possible to characterize its intensity with good precision before the system is put into operation. In this case, a constant value would be used for all analyses. If the natural background radiation in not constant within the sample material, a pre-irradiation background measurement would need to be carried out either prior to irradiation or after irradiation after the isomeric signal has decayed. For real time processing applications this solution would require additional radiation detection instrumentation. For batch analyses the same detector could be used to acquire both the background and isomeric signals (increasing the overall evaluation time) or a second detector could be used. To account for background radiation resulting from the irradiation process, the use of energy discriminating detector could be used to differentiate radiation signals of different energies. Depending upon how close in energy the two signals are, however, the detector choice for the system might be limited. An alternative for discriminating between natural and induced background radiation and isomeric radiation of similar energy might be to carry out a time analysis of the total signal to separate the different components if there was a difference in the half-lives of their signals. A third alternative which shows promise is to evaluate the total measured energy spectrum and then to decompose it using elemental libraries associating each source of radiation with a spectrum rather than an intensity at a particular energy.[3]

4.2.2 Method Capabilities

In previous sections different aspects of an industrial PRE system such as the characteristics of the irradiation spectrum and factors influencing the choice of irradiation and detector systems have been addressed. Building upon this information, the analytical tools for analyzing the capabilities of a material assay system are outlined below. Specifically, in §4.2.2.1 the method of determining the sensitivity of an industrial PRE material assay system, as defined by the decision limit, detection limit and determination limit of a particular isomer in a sample is derived using the general approach for activation analysis outlined by Currie, which is introduced in the Appendix.[4] In §4.2.2.2 the relationship between system sensitivity and material throughput is presented in the context of a PRE system designed to analyze bulk materials in real time.

4.2.2.1 Material Detection and Quantification and Its Uncertainty

The mathematical formalism for treating uncertainty in nuclear analytical techniques is presented in the Appendix. Having developed general expressions for the decision, detection and determination limits in general, the next step is extend these expressions for use in PRE analyses of isomers. Determination of κ, the proportionality constant relating the amount of mass m_S which leads to a signal S, for a particular measurement system and isomer requires information about the radiation detector's overall efficiency for recording the characteristic photon(s) associated with the decay of the isomer. This efficiency includes both geometrical factors related to the size and configuration of the detectors and physical factors including the attenuation of characteristic photons before reaching the detector and the detectors inherent detection efficiency at the characteristic photon energy. For PRE assay applications the goal is, of course, to determine the total quantity of a particular isotope present in a sample, not just the quantity of the excited isotopes present. This may be incorporated into the definition of κ as well by including the information such as the duration of the irradiation, the production ratio of excited nuclei to total isomeric nuclei at the end of irradiation, the amount of time between the end of irradiation and the beginning of the measurements and the duration of the measurement. Including these factors, κ may be defined using

$$\kappa = \varepsilon(E,\vec{r})\,P(\varphi(E,\vec{r}),\sigma(E),\lambda,t_{irr})\,D(\lambda,t_{decay})\,T(\lambda,t_{meas}) \qquad \textbf{4-2}$$

where

$\varepsilon(E,\vec{r})$ = absolute detection efficiency [counts per isomeric decay]

$P(\varphi(E,\vec{r}),\sigma(E),\lambda,t_{irr})$ = production ratio at end of irradiation [nuclei excited per gram of isomeric isotope]

$D(\lambda,t_{decay})$ = decay of isomer after irradiation and prior to measurement = $e^{-\lambda t_{decay}}$

$T(\lambda,t_{meas})$ = total fraction of excited nuclei present at the beginning of the measurement period which decay = $1 - e^{-\lambda t_{meas}}$.

The isomer production ratio at some point $\vec{r}$ in a material depends upon the irradiation flux $\varphi(E,\vec{r})$ at $\vec{r}$ and the isomeric excitation cross section $\sigma(E)$, both of which are dependent upon the energy of the photons involved in the process, the isomer decay probability λ and duration of the irradiation, t_{irr}. The term accounting for the decay of the isomer in between the end of irradiation and the start of the measurement depends upon the decay probability λ and the decay period, t_{decay}. The term accounting for the total fraction of nuclei present at the beginning of the measurement period which decay depends upon the decay probability λ and the duration of the measurement, t_{meas}.

For PRE the isomer production ratio may be taken from the equation for $dN_i(t)/dt$ from Chapter 2,

$$\frac{dN_i(t)}{dt} = -\frac{\Gamma_i}{\hbar}N_i(t) + \sum_{j=i+1}^{k}\frac{\Gamma_{ji}}{\hbar}N_j(t) + \left(\int_0^{E_{max}} \sigma_{0\to i}^{abs}(E)\varphi(E,\vec{r})dE + \int_{E_{cont}}^{E_{max}} \sigma_{0\to i}^{abs*}(E)\varphi(E,\vec{r})dE \right)N_0(t),$$

$$\textbf{4-3}$$

by solving for $N_i(t)$ at some position $\vec{r}$ in the sample. If the feeding of the isomeric state from the natural decay of discrete higher energy eigenstates is neglected the second term of Eq. (4-3) may be discarded. Further, making the approximation that the groundstate population may be assumed to be nearly constant, $N_0(t) = N_0$, the calculation of the isomeric isotope population immediately after irradiation becomes straightforward to carry out and is found to be

$$N_i(t) = \frac{\sigma_{0\to i}^{abs}(E_i)\varphi(E_i,\vec{r}) + \int_{E_{cont}}^{E_{max}}\sigma_{0\to i}^{abs*}(E)\varphi(E,\vec{r})dE\; N_0}{\Gamma_i/\hbar}(1 - e^{-\Gamma_i/\hbar\, t_{irr}}). \qquad \textbf{4-4}$$

The production ratio at the end of irradiation is thus given by

$$P(\varphi(E,\vec{r}),\sigma(E),\lambda,t_{irr}) = \frac{N_i(t)}{N_0\,M/N_{av}} = \frac{\sigma_{0\to i}^{abs}(E_i)\varphi(E_i,\vec{r}) + \int_{E_{cont}}^{E_{max}}\sigma_{0\to i}^{abs*}(E)\varphi(E,\vec{r})dE}{\lambda\,M/N_{av}}(1 - e^{-\lambda t_{irr}}), \qquad \textbf{4-5}$$

where M represents the molar mass of the isomeric isotope [grams per mole] and N_{av} is Avogrado's number [atoms per mole]; the decay probability $\Gamma_i/\hbar$ has been replaced by λ. The term accounting for the decay of isomeric nuclei in between the end of irradiation and the start of measurement is written as

$$D(\lambda, t_{decay}) = e^{-\lambda t_{decay}}.$$

4-6

The term accounting for the total number of isomeric nuclei that decay during the measurement period is written as

$$T(\lambda, t_{meas}) = 1 - e^{-\lambda t_{meas}}.$$

4-7

The term representing the absolute detection efficiency for registering a particular characteristic isomeric decay photon, $\varepsilon(E, \vec{r})$, must be known in order to relate a measured signal to the mass of isomeric material present in a sample. There have been several reports investigating methods to determine the absolute detection efficiency for activation analysis involving large samples.[5,6,7,8,9] In the most general sense, the absolute detector efficiency may be written as

$$\varepsilon(E, \vec{r}) = \frac{S}{\Omega(\vec{r}) F(E, \vec{r}) A(\vec{r})},$$

4-8

where $\Omega(\vec{r})$ represents the solid angle from the source subtended by the detector, $F(E, \vec{r})$ represents various energy dependent factors accounting for such things as attenuation of photons in the source and probability of photon absorption in the detector and $A(\vec{r})$ represents the isomeric activity in the sample at the position $\vec{r}$. Unfortunately, it is impossible to determine $\varepsilon(E, \vec{r})$ analytically for a bulk sample containing an unknown, heterogeneously distributed source of activity. One approach to dealing with this for industrial PRE assay applications is to calculate a worst case detector efficiency for the activity distribution having the smallest efficiency and then to use this as a lower bound for the quantification of isomeric material in the sampler (i.e., producing a result indicating that the amount of isomeric material in the sample is greater than or equal to some value at some maximum degree of uncertainty.) For less ambiguous situations, with homogeneously distributed activities where the bulk material matrix for different samples may be assumed to be constant, tools such as Monte Carlo modeling techniques may be used to determine the absolute detection efficiency. In the next chapter investigating PRE applications the determination of the detection efficiency for an industrial assay application will be discussed.

Taking these individual components together, κ maybe written as

$$\kappa = \varepsilon(E, \vec{r}) \frac{\sigma_{0 \to i}^{abs}(E_i) \varphi(E_i, \vec{r}) + \int_{E_{cont}}^{E_{max}} \sigma_{0 \to i}^{abs*}(E) \varphi(E, \vec{r}) dE}{\lambda M / N_{av}} (1 - e^{-\lambda t_{irr}}) e^{-\lambda t_{decay}} (1 - e^{-\lambda t_{meas}}).$$

4-9

With an expression for κ, it is possible to determine the mass of isomeric isotope in a sample corresponding to the critical level, m_C, the determination level, m_D, the quantification level, m_Q, and to the net signal derived for an unknown sample, m_S:

$$m_C = \frac{L_C}{\kappa} = \frac{k_\alpha (\mu_B + \sigma_B^2)^{1/2}}{\kappa},$$

4-10

$$m_D = \frac{L_D}{\kappa} = \frac{k_\alpha(\mu_B + \sigma_B^2)^{1/2} + \frac{k_\beta^2}{2}\left\{1 + \left[1 + \frac{4 k_\alpha(\mu_B + \sigma_B^2)^{1/2}}{k_\beta^2} + \frac{4 k_\alpha^2(\mu_B + \sigma_B^2)}{k_\alpha^2 k_\beta^2}\right]^{1/2}\right\}}{\kappa}, \qquad \text{4-11}$$

$$m_Q = \frac{L_Q}{\kappa} = \frac{\frac{k_Q^2}{2}\left[1 + \left(1 + \frac{4\sigma_0^2}{k_Q^2}\right)^{1/2}\right]}{\kappa} \qquad\qquad \text{4-12}$$

and

$$m_S = \frac{S}{\kappa}. \qquad\qquad \text{4-13}$$

In order to design a PRE assay system one must decide whether the objective is to simply identify the presence of isomeric material in a sample above some minimum concentration or to quantify the amount of isomeric material in a sample. With this, the next step is to decide on the precision required for the analysis, either in the rate of false negative and positive decisions for the case of material detection or in the quantification of material for material assays. Using this decision, an iterative procedure may be applied to optimize the selection of the irradiation source and detector configuration so as to achieve the desired material analysis goals. Examples of threshold determination applications include the detection of contraband materials and the assaying of ores for sorting purposes while applications aimed at measuring trace quantities of materials would like be more quantitative in nature.

4.2.2.2   Material Throughput

In addition to the precision to which material detection and quantification can be done, another analysis goal likely to be imposed upon a PRE system is material throughput. Material throughput in this context refers to the maximum rate at which material can be analyzed; throughput is a particularly important consideration for an assembly line system. Currently, most analytical procedures used to determine elemental concentrations in bulk materials rely on grab sampling and laboratory analysis. Although such procedures do not come close to providing a 'real time' analysis of the materials, they do not generally inhibit the material process flow rate either. The most desirable situation for an industrial PRE system would be one where the measurement process could be installed without reducing the material throughput of an already existing process. A system capable of analyzing materials at a predetermined rate, e.g., the rate at which material is processed along a conveyor belt, implies an externally defined limit on the amount of time allowed for irradiation and measurement and is constrained by the irradiation source and detector efficiency. As an example a layout for such a system is depicted in Figure 4-12, where a conveyor belt is used to transport material through an irradiation field and then in between three pairs of detectors.

Examining the equations of §4.2.2.1, it is clear that the production ratio for this case would be more useful if written in terms of the belt velocity rather than irradiation time. Taking the speed of the conveyor belt to be v and using the relationships

$$x = vt \quad \rightarrow \quad t = x/v, \qquad\qquad \text{4-14}$$

it is convenient to rewrite Eq. 4-5 as

$$P(\varphi(E,\frac{x}{v},y,z),\sigma(E),\lambda,t_{irr}) =$$

$$\sum_{x=-x'}^{x'} \frac{\sigma_{0\to i}^{abs}(E_i)\varphi(E_i,x,y,z)+\int_{E_{cont}}^{E_{max}}\sigma_{0\to i}^{abs*}(E)\varphi(E,x,y,z)dE}{\lambda M/N_{av}}(1-e^{-\lambda\frac{x}{v}})e^{-\lambda(x_1-x)/v}dx$$

4-15

a) *Top View*

c) *Side View*

b) *Time Line*
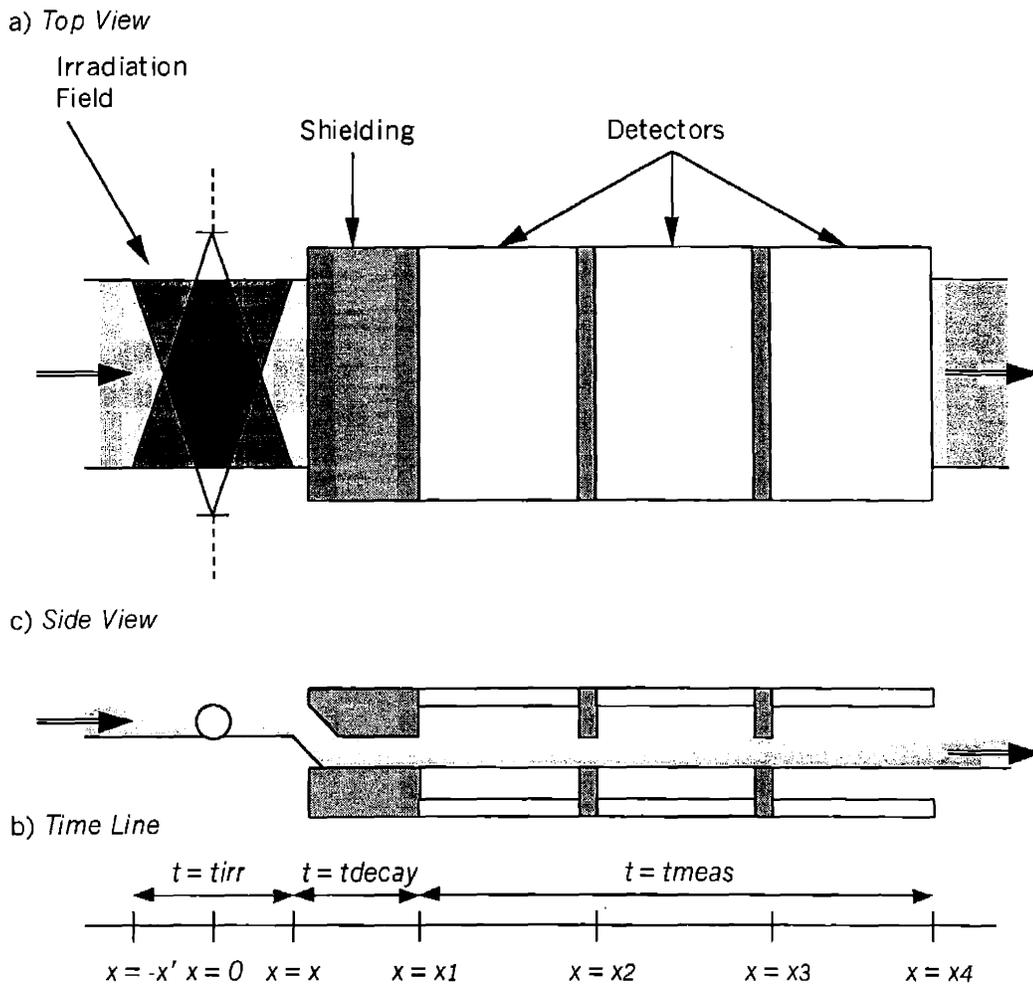
Figure 4-12 An example of how a system using PRE to analyze material passing along a conveyor belt might be designed. Two opposing bremsstrahlung beams are used to irradiate material on the belt at position $x = 0$. The radiation associated with the decay of the isomer is measured in the detectors centered at positions x_1, x_2 and x_3.

In a similar fashion the relation for the total number of nuclei which decay during the measurement period may be rewritten as

$$T(\lambda, t_{meas}) = 1 - e^{-\lambda(x_4 - x_1)/v}.$$

Examining the problem in this way provides a clearer understanding of how the sensitivity of an on-line assays system depends upon the material processing speed. Using similar reasoning the sensitivity of a system designed to analyze very short lived isomers, where the measurement instrumentation must be positioned in the same location as the irradiation source, may also be derived.

In the figure above, the detector array is shown comprised of three individual detector pairs. Depending upon the process speed and the half-life of the isomer being analyzed, it might be desirable to use multiple detectors in a configuration similar to this to reduce the sample size being analyzed. The motivation for this comes from the observation that for the photon energies likely to be encountered in most PRE assay applications, the spatial detection efficiency in the detector will tend to drop off rather quickly as the distance from the source increases, primarily due to self-attenuation in the sample. In practice, this fact could be exploited by summing the output signal from separate detector pairs (D1, D2 and D3 in this case) in series fashion,

$$(S + B) = (S + B)_{D1} \Big|_{t=(x_2-x_1)/v}^{t=x_1/v} + (S + B)_{D2} \Big|_{t=(x_3-x_2)/v}^{t=x_2/v} + (S + B)_{D3} \Big|_{t=(x_4-x_3)/v}^{t=x_3/v} \cdot$$

Depending upon the geometry of the layout, this could provide a comparable net signal to that recorded using just one large pair of detectors covering the same area and would be easier to assemble from an engineering perspective, using small modular detector units. Additionally, analyzing variations in the gross signal of the summed detector array would also provide information regarding the presence of isomeric material in the ore.

4.3   EXPERIMENTS

In support of the goals of this project experimental work has been carried out to explore the photonuclear resonant excitation process, to discover practical engineering issues which might preclude its industrial implementation and to identify solutions to these problems. A description of the facilities for these experiments is provided in §4.3.1. Unfortunately, a lack of versatility in much of the available equipment severely limited the ability to carry out a complete experimental investigation of the physics of the photonuclear resonance excitation process or its application to the wide array of situations for which it could be used. Some of these limitations include the fact that the electron accelerator was only capable of operating at one fixed energy, it was not possible to measure the beam current directly, the beam power was low in comparison with requirements for industrial applications (50 μA average versus ~ 5 mA average) and that the physical space for conducting experiments was constrained by the design of the facility and the presence of other diagnostic instrumentation.

In §4.3.2 experiments aimed at demonstrating the use of PRE to excite an isomeric isotope are discussed. Additionally, a discussion of attempts at using these same facilities to examine the decay of prompt excited nuclear states created using PRE (also called nuclear resonance fluorescence) is included in this section. Following this, §4.3.3 explores a number of potential pitfalls related to the practical implementation of PRE for industrial purposes including the degradation of the isomeric signal due to scattered photon radiation, background radiation, afterglow in the scintillator crystal and methods for dealing with these problems. In §4.3.4 the use of a simple photomultiplier gating circuit in conjunction with the pulsed electron accelerator of these experiments and how it can help to resolve many of the problems associated with the analysis of PRE isomeric signals is discussed.

4.3.1 Facilities and Equipment

The accelerator used for the experiments described below was located at the MIT Bates Linear Accelerator Center in Middleton, Massachusetts. The machine is a fixed current, fixed energy MINAC-6 linear electron accelerator manufactured by Schonberg Research Corporation, Santa Clara, CA. A detailed description of the accelerator's specifications and performance have been reported elsewhere, a summary is included in Table 4-3 for reference.[10,11,12] This commercially available accelerator is sold primarily for use as a high intensity, high energy X-ray source for conducting radiographic measurements of large objects such as bridge and building structural components. Although the accelerator is field portable, at the Bates Laboratory the accelerator has been mounted in a shielded experimental room. The primary research objectives for the facility are studies aimed at exploring the application of high energy x-ray computed tomography for the study of phenomena related to the cooling of molten metals and the detection of phase transitions in metals between the liquid and solid state. In support of these studies, the facility includes a dedicated tomographic detector array and its related electronics. Unfortunately, restrictions imposed upon the system in its configuration for tomography, including the irradiation beam geometry and the amount of physical space available, limit the usefulness of the facility to a rather restrictive region of experimental investigations relevant to the study of PRE and in particular its application towards industrial purposes.

Table 4-3 Engineering specification of the MINAC-6 accelerator.

Beam Energy	6 ± 0.5 MeV
Beam Pulse Rate	180 pulses per second
Beam Pulse Duration	4 µs
Beam Pulse Rise and Fall Time	0.5 µs
Peak Beam Current (During Pulse)	50 mA
Average Beam Current	50 µA
Peak Beam Power	300 kW
Average Beam Power	300 W
Duty Cycle	0.001
Accelerator Frequency	X-band (9303 MHz)

The accelerator's x-ray head incorporates a tungsten cone-beam collimator 9.52 cm long (3.75 inches) and 11.43 cm in diameter (4.5 inches) that has a 32° degree opening. For the experiments discussed in §4.3.3, a cone shaped lead insert with a coaxial 0.70 cm diameter hole (0.275 inches) was inserted in the collimator, creating a pencil beam collimator 0.70 cm in diameter. An additional 2.54 cm (1 inch) pencil beam tungsten collimator was placed directly next to the lead insert and next to this a lead pencil beam collimator 10.16 cm (4 inches) thick, each of these collimators was 0.70 cm (0.275 inches) in diameter. Finally, a 10.16 cm (4 inches) collimator of lead with a diameter of 2.54 cm (1 inch) was used as the outermost region of collimation. Along the sides and above, below and behind the accelerator head lead shielding of at least 15.24 cm (6 inches) was used.

Following preliminary proof-of-principle experiments carried out using a well-type NaI detector, radiation measurement were done using one of three scintillator crystals: a small NaI detector, a large NaI detector and a GSO detector. Information relevant to the operation of these 3 detectors is summarized in Table 4-4. The two NaI detectors each manufactured by Bicron and are permanently coupled crystal – photomultiplier tube (PMT) pairs. The GSO detector was assembled at MIT using a high purity crystal from Hitachi chemical Company, Ltd. together with a standard PMT in the normal fashion.[13] All three of the detectors used the same pair of voltage dividing bases; one operating in an ordinary configuration and the other operating in an externally gated mode, which is discussed in more detail in §4.3.4.

Table 4-4 Characteristics of the three radiation detectors.[a]

Parameter	Detector		
	Small NaI	Large NaI	GSO
Operating High voltage	-1300 V	-1300 V	-1300 V
Dimensions			
Diameter	3.81 cm (1.5 inches)	7.62 cm (3 inches)	2.54 cm (1 inch)
Length	1.27 cm (0.5 inches)	7.62 cm (3 inches)	10.16 cm (4 inches)
Resolution			
at 661.7 keV	10.9 %	9.74 %	6.11 %

Data acquisition was performed using standard NIM based spectroscopy hardware units. For all of the experiments using this experimental setup the detector axis was horizontal and placed so that its axis was orthogonal to the pencil beam axis with the front face of the detector positioned approximately 5.08 to 7.62 cm (2-3 inches) from the pencil beam axis. High voltage was supplied to the detector through a 15.24 m cable (50 feet) from a NIM based high voltage unit located in the accelerator control room. The detector output was connected to an amplifier after passing through a linear gate, both of which were powered using a standard NIM rack (no special electromagnetic or lead shielding) located in the accelerator vault using a 1.83 m (6 foot) cable from the detector to the gate. The linear gate was operated in an anti-coincidence mode with the accelerator's trigger pulse; this resulted in turning off the signal entering the vault amplifier approximately 2 µs prior to the accelerator beam pulse and turning it back on again approximately 11 µs later, 4µs after the end of the accelerator beam pulse. The output from the vault amplifier was connected to a second amplifier in the control room via a 15.24 m cable (50 feet). A PC based analog-to-digital (ADC) convertor and 1024 channel multichannel (MCA) analyzer was used for final data acquisition and energy spectrum data analysis. In addition to MCA operation, multichannel scaling (MCS) mode data acquisition was also possible, allowing the total signal intensity to be summed within successive time intervals.

4.3.2 Proof of Principle

As a first examination of the photonuclear excitation process, experiments were carried out to irradiate a gold foil (10.9 g) using the metal casting experimental facilities at the Bates Laboratory. The experimental setup for this experiment used the accelerator in its original configuration for tomographic measurements rather than the altered shielding design described above. In this configuration, the irradiation field was dispersed in a fan-beam, the gold foil was completely placed in the beam. After irradiation for greater than two minutes, to bring the induced isomeric gold activity to equilibrium, the accelerator was immediately shut off and the gold foil was manually moved from within the accelerator vault to a shielded well-type NaI detector located outside. Typical transfer times were from 11 to 14 seconds; measurements were carried out using an ADC operating in MCS mode for a total data acquisition period of 60 seconds. An example of the time spectra acquired from these experiments is presented in Figure 4-13.

---

[a] The GSO crystal used for this experiment was graciously provided on loan by Prof. J. Schweitzer, University of Connecticut.
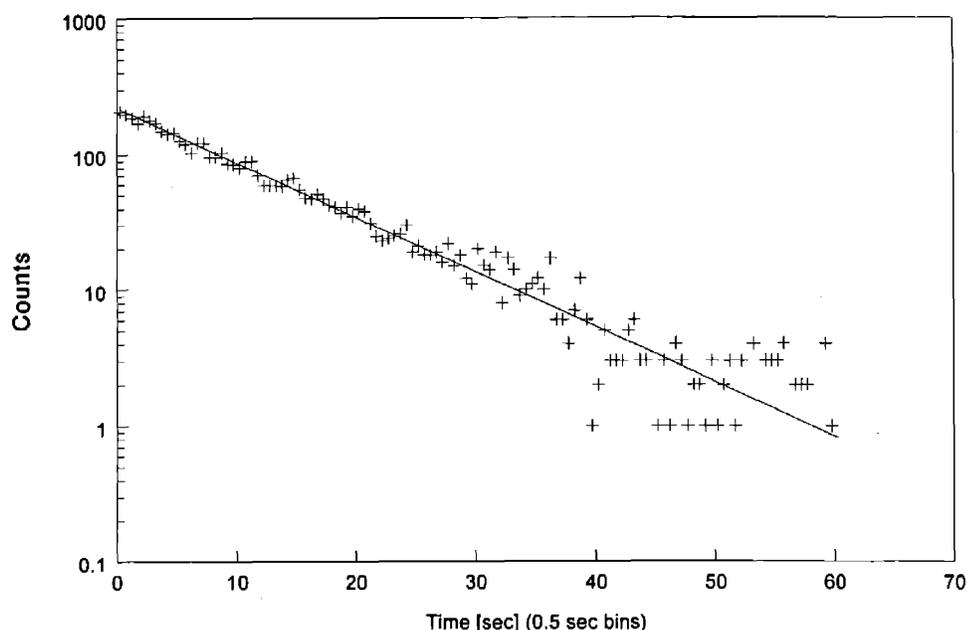
Figure 4-13 Measurement of the decay of ^{197m}Au (+ for data, − a fit to the data).

In the above figure the fitted line was derived from a series of three similar experiments, one of these sets of data is also plotted (+ signs). The background signal was acquired over a long period of time and was 2.06 ± 0.06 counts per bin (i.e., counts per ½ second) and was subtracted from the data that are plotted. To minimize the background signal the MCA's lower level and upper level discriminators were adjusted so that only counts from the 279.1 keV decay photon of ^{197m}Au were measured. The isomeric gold half-life determined from these data was 7.51 ± 0.30 seconds, which is in agreement with the accepted value of 7.73 seconds.

Although similar experiments have been reported in the literature elsewhere, these particular experiments were useful because they demonstrated first hand the simplicity of using a simple, industrial electron accelerator for photonuclear resonance excitation of isomeric nuclei.[14,15,16] Unfortunately, the relatively low beam current of the accelerator used for these experiments imposed a rather large minimum detection limit for the gold analysis. Using the Currie criterion outlined earlier, measurements carried out in this way for 40 seconds would have a critical mass of 16.6 mg (± 16.6 mg) and a minimum detectable mass of 80.1 mg (± 32.5 mg), assuming a false positive rate of less than 25% and a false negative rate of less than 1% (k_α = 0.675, k_β = 2.325). However, from these data a crude estimate can be made to determine a lower limit on the detectable mass which could be achieved with a 6 MeV machine irradiating small samples which are measured using a similar well counter.

A significant fraction of the induced gold activity in the above experiment was wasted during the transfer period. If a system could be devised which had a transfer time of 1 second, a gold foil could be irradiated to equilibrium and then measured for ~12 additional seconds, almost tripling the total registered signal strength. In this case the critical mass concentration (that is, the ratio of the mass of gold in a sample to the mass of the sample, which for this comparison has similar density and photon attenuation characteristics to gold) would be 31.1 μg/g (± 31.1 μg/g) and the minimum detectable mass concentration would be 148.4 μg/g (± 58.7 μg/g) *per mA of beam current*, with the same criterion. In light of these calculations, which are based upon rather simple preliminary experimental investigations, PRE seems to show promise as an

135

analytical tool. Based upon this conclusion it was decided to carry out further analysis of the problem and therefore this dissertation.

4.3.3 Isomer Excitation and Problems

Following the initial set of experiments above, the accelerator beam geometry was modified as described in §4.3.1 and the detector and its associated pre-amplification electronics were moved inside the accelerator vault. Initially, a series of experiments was carried out using the modified setup to assess the feasibility of using the MINAC-6 accelerator to perform nuclear resonance fluorescence (NRF) experiments, following irradiation procedures outlined in the literature.[17-21] A considerable amount of work was carried out exploring different detector shielding configurations; however, using the limited resources available for this project it was not possible to demonstrate the prompt resonant absorption and decay photons by nuclei. The primary reason for the inability to register NRF photons was the excessive background signal recorded during the beam pulses. Contributions to this extraneous background signal included both scattered low energy photons, which were found to be ubiquitous within the vault during the beam pulse, as well as RF interference induced in the photomultiplier assembly and vault based electronics due to the pulsing of the accelerator. Contributing factors to the poor signal to noise ratio for these measurements included the limited size of the detector used for these experiments (3x3 NaI), the low duty cycle – high peak current of the accelerator and the processing speed of the MCA.

Recognizing the advantages of being able to collect data with the smallest transit time possible but acknowledging the inability to collect a useable signal during the irradiation pulse, the third batch of experiments was aimed at investigating the isomeric signal which could be measured immediately after the end of irradiation using a detector located in close proximity to the target during irradiation. For these experiments the detector photomultiplier HV was off during the irradiation. Although the isomeric signal could be resolved in this configuration, a significant degradation in the detector system's performance was observed in comparison with the system's capabilities when operated away from the accelerator environment. The results of these experiments are discussed in the sections below.

In summary, as with the NRF experiments, problems resulting from the high photon flux incident on the crystal during the irradiation pulse were observed and include those relevant to energy measurements – discrete interferences and low energy noise (§4.3.3.1), those relevant to temporal measurements – the time dependence of the above phenomena (§4.3.3.2) and, when the high voltage was on at the same time as the accelerator, the stability of the detector over time – changes in the detector gain (§4.3.3.3). Measurements taken during and after accelerator pulses indicated the presence of long term 'ringing' effects in the detector assembly. This pickup effect in the signal lines in the vault together with crystal phenomena (i.e., afterglow) were the likely causes of the observed low energy noise and long term decaying signal which were observed. When the high voltage was applied to the PMT during irradiation, charge collection problems associated with the PMT dynode structure was the likely cause of gain fluctuations.

The low energy noise and part of the decaying signal problem was eliminated by using of a lower level discriminator on the ADC. Gain changes could be avoided by not applying high voltage during irradiation. Except for gain changes, it was noted that measurements could actually be acquired in the interval between accelerator pulses. In order to do this, however, a method of rapidly switching the PMT voltage on and off was required. A discussion of the gating circuitry employed to do this is presented in §4.3.4.

4.3.3.1 Low Energy Noise – The Detector and Electrical Interference

One problem which was observed in energy spectra taken during these experiments was an excessive level of low energy noise. This low energy noise can be seen clearly in Figure 4-14 where a comparison is presented of the background energy spectrum measured by the GSO detector after the accelerator has been on for 60 seconds when a) there was no scattering material in the irradiation beam and b) the case when a gold foil scattering target was in the irradiation beam. For both cases, the detector HV was turned off during the irradiation. One possible reason why the low energy noise was recorded only when a scattering material was present in the beam is afterglow in the scintillator crystal. However, GSO is well known for

136

its low afterglow and fast recovery following exposure to high photon intensity sources and, as demonstrated in Figure 4-16, the time associated with the decay of the low energy noise component of the spectrum seems to be too long to be explained solely by afterglow. Another possibility could be residual effects in the PMT such as phosphorescence in the photomultiplier tube structure or charge buildup on the photocathode.[22,23, 24]

GSO Detector - Low Energy Noise
Irradiation = 60 sec, Decay = 3 sec
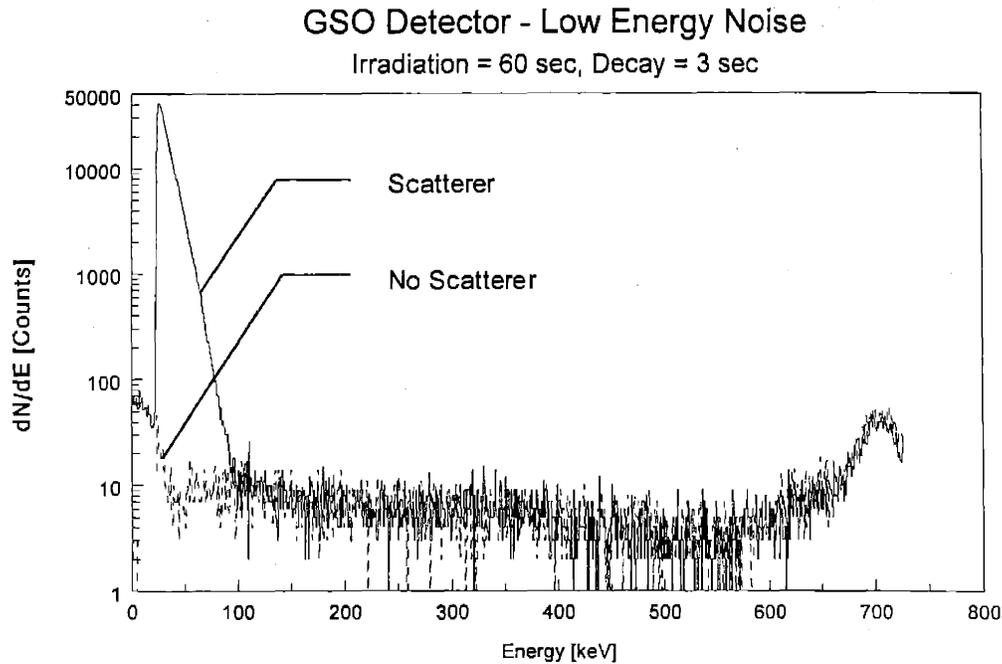
Figure 4-14 Comparison of the GSO detector background energy spectra taken for 30 seconds. (The accelerator was on for 60 seconds during which time the detector high voltage was off. The time between the end of irradiation and start of counting was 3 seconds. The dotted spectrum represents the case when nothing was in the beam, the other represents the case when a dense scattering material was in the beam.)

When a radiation detector is operated in the vicinity of high frequency electronics, significant electromagnetic interference can result. More specifically, nuclear instrumentation which is operated in close proximity to the radio frequency modulator and accelerating structure of an electron accelerator is especially susceptible to RF pickup interference in the detector, its signal processing electronics and the cabling associated with these. In Figure 4-15 a photograph of the voltage signals from the radiation detector (when there was no high voltage applied to the photomultiplier tube) and the accelerator triggering pulse, both measured in the control room, is presented. Trace 1 is a nominal +5 V, 11 μs, 180 Hz pulse generated in the control room which triggers the beginning of each accelerator beam pulse. The accelerator beam pulse begins ~1 ms after this pulse and can be recognized in Trace 1 by the onset of large, high frequency spikes in the signal. The accelerator pulse duration is approximately 4 μs, which coincides with the end of the main RF interference in Trace 1. The detector signal, Trace 2, has been delayed 2 μs so that it can be seen together with Trace 1, the signal amplification for Trace 2 is the same as that used for acquiring all of the spectra in the experiments described in §4.3.3.
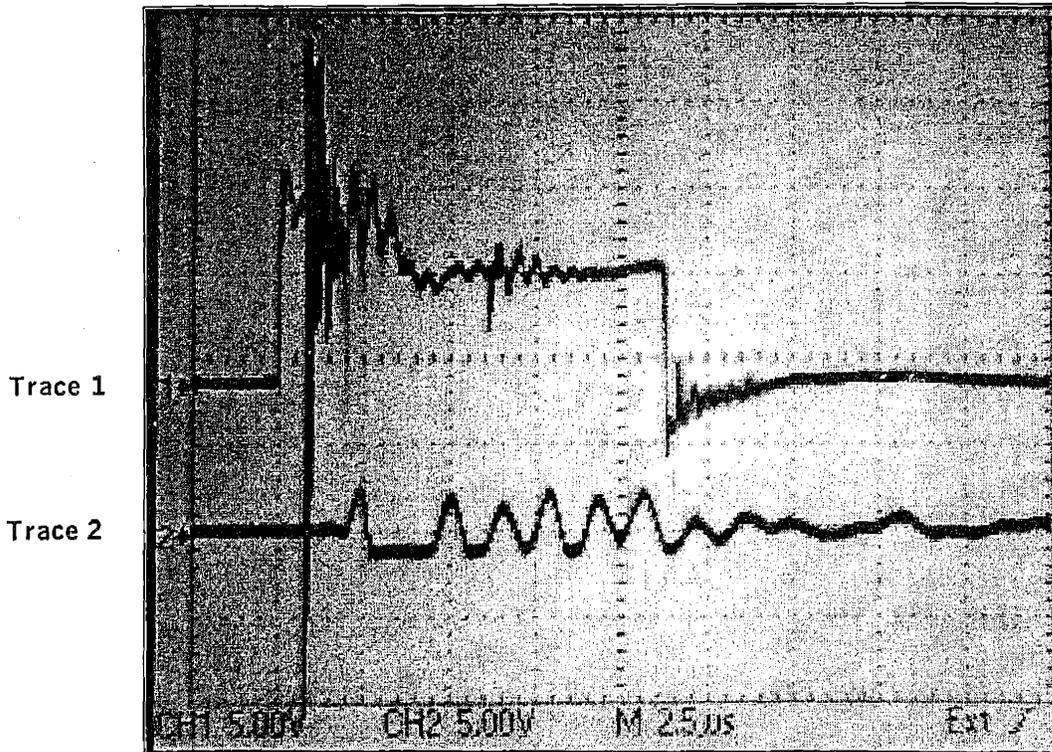
Trace 1

Trace 2

Figure 4-15 Voltage signals: Trace 1 is the accelerator trigger pulse, Trace 2 is the detector signal with the HV off (delayed +2 ms to allow better viewing).

Since the PMT high voltage was off for the above measurement and no scattering material was placed in the irradiation beam, the voltage fluctuations evident in Trace 2 are attributed to electromagnetic interferences occurring in the accelerator vault.[25,26] Oscillating voltage fluctuations were also observed to continue for up to several seconds at the end of irradiation during experiments with a scattering target when the HV was on during irradiation. Further investigations of this problem led to the conclusion that the major source of low energy noise in the detector signal was due to transient voltages in the electronics resulting from this rapid application of high voltage to the PMT. One method to address these problems, described in Ref. 26, is to construct an electromagnetic shielded cage around the detector electronics that are near the accelerator. Another approach described in that reference is to use special purpose, rapid switching constant voltage sources for the PMT circuitry. However, a less expensive and more flexible alternative is to incorporate a high voltage gating switch into the PMT itself.

In summary, there are several possible sources which might contribute to the low energy noise component of the signal measured from the radiation detector in these experiments. Afterglow can be minimized by choosing a resistant scintillator material and designing a system to reduce backscattered radiation to a minimum. If further research found residual noise due to phosphorescence or charge buildup in the PMT to be a significant contributing source to the low energy noise one option might be to choose a different model of PMT with a faster recovery time and with less susceptibility to charge buildup. An optimized measurement geometry that minimized backscattered radiation from surrounding materials would also help reduce these effects. In order to minimize noise resulting from RF interferences with the accelerator, more sophisticated electromagnetic shielding of the detector, detector electronics and the signal cables could be employed. Additionally, digitization of the signal within the accelerator vault would help by reducing noise pickup in the long cable connecting the vault NIM equipment to the control room and by reducing problems associated with pulse reflections within this cable. Finally, noise associated with the rapid increase in voltage in the PMT dynode structure could be avoided by selectively altering the voltage of only

part of the PMT during irradiation and then returning the PMT to its standard voltage level in a more controlled manner at the end of irradiation (§4.3.4).

4.3.3.2   Decaying Background Signal

Related to the problem of low energy noise in the energy spectrum is the time dependence of the signal immediately after the irradiation pulse. This is particularly important for applications where short-lived isomers are being examined. In Figure 4-16 three MCS mode time spectra are presented, all of which were taken immediately after the end of irradiation. The bottom trace was taken when no target material was present, the middle trace was taken with a scattering target of a few grams (a gold foil) and the top trace was taken with a massive scattering target (a lead brick). For the case with no target present the signal rate quickly approaches an asymptotic level which, on a longer time scale, was observed to slowly decay away within a few seconds. The two traces taken with a target demonstrate two distinct trends. Immediately after irradiation a short decay component is present (this is also seen in the no target case) which is then followed by a longer period decay component. The rate of decay of the short decay component suggests that this is not likely related to afterglow in the crystal. However, there clearly is a relationship between the interaction of radiation in the crystal (i.e., the intensity of the scattered radiatio, which is related to the mass of the scattering target) and the decaying signal. Other than afterglow, a second possibility is that the decaying signal observed in the time spectra is related to phosphorescence in the PMT itself, which might also be the source of the longer decay component as well. (Although both gold and lead have isomeric states, the isomeric activity induced in the targets with this accelerator is too weak to be observed in the short time periods of these measurements.) The use of alternative PMT materials with less phosphorescence response together with minimizing extraneous scattered radiation into the detector are two suggestions for dealing with this problem.

An additional potential source of time varying background signal during short term irradiations is the decay of stimulated isomeric nuclei in accelerator shielding materials. In particular, both tungsten and lead have isomeric isotopes with half-lives on the order of seconds. For the experiments performed here, no interference is expected from the tungsten comprising the pencil beam collimator due to the fact that over eight inches of lead was placed between this tungsten and the detector. Also, in the experimental layout used for these experiments the detector was not in a direct line of sight of lead directly exposed to the beam either and no characteristic lead isomeric decay photons were ever observed. Interference from lead shielding could pose a problem in the design of an industrial system though. One method of dealing with this issue would simply be to use non isomeric materials (e.g., iron) as the shielding. Due to the significant difference in density between lead and iron, though, a more practical approach might be to still use lead or tungsten as the primary shielding material and then use a thinner secondary shield of iron around the detector to attenuate isomeric photons from the primary shield.

GSO Detector - Decaying Signal
Irradiation = 60 sec, Decay = 3.8 msec
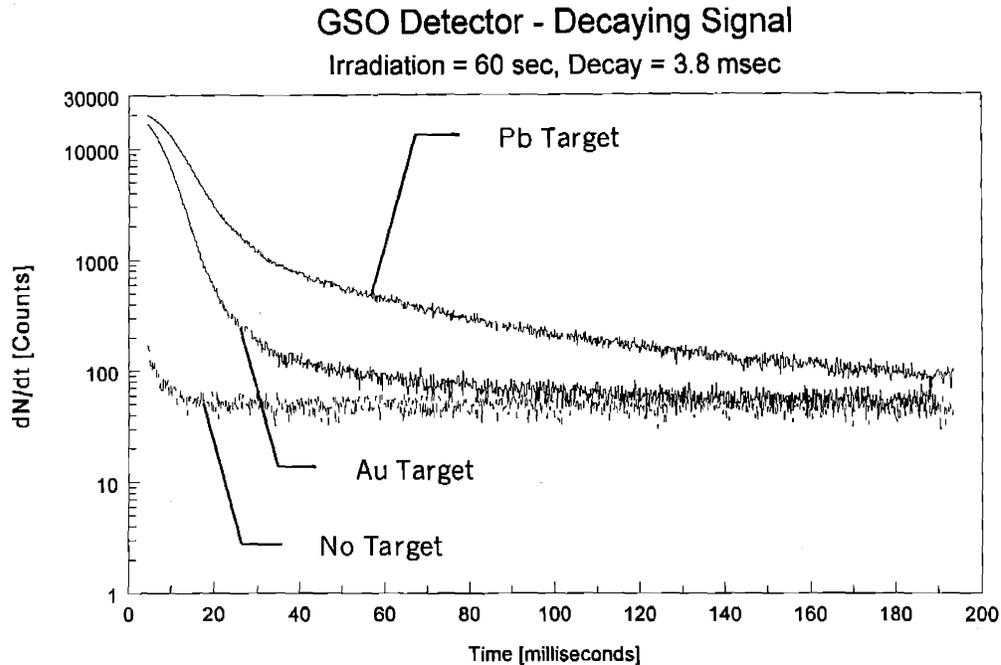
Figure 4-16 Comparison of the GSO detector signal after the detector high voltage is turned on following a 60 second irradiation with different target materials in the irradiation beam.

4.3.3.3   Gain Changes

A third problem that was encountered in this set of experiments was that after an irradiation with a dense target material the gain of the detector system changed. This can be seen in Figure 4-17 where two energy spectra taken with the 3x3 NaI detector are plotted. (The top spectrum has been multiplied by a factor of 10 to help distinguish differences between the two.) In the figure, the bottom spectrum was taken with no target material in the irradiation beam while the upper spectrum was taken with a Au target in the beam. The peak in the upper spectrum at 279 keV is the isomeric decay signal from gold. In this figure, the gain of the two high energy peaks (from a constant source of ^{182}Ta near the detector) is observed to have decreased by ~1%. At first it was thought that this phenomenon was a result of the Malter effect, which acts to distort the gain of a PMT at high count rates ($>10^5$-10^6 counts per second) due to thermal and electrical problems in the dynode structure.[27-32] However, since the PMT voltage was off during the irradiation this effect would be limited since the high count rate would only result from the effects of afterglow. Additionally, most reports of distortions resulting from the Malter effect typically refer to an increase in again, although some indicate a decrease . The causes of the small gain change (which was consistent and repeatable) remains unclear.

NaI Detector - Shift In Gain
Irradiation = 60 sec, Decay = 4 sec
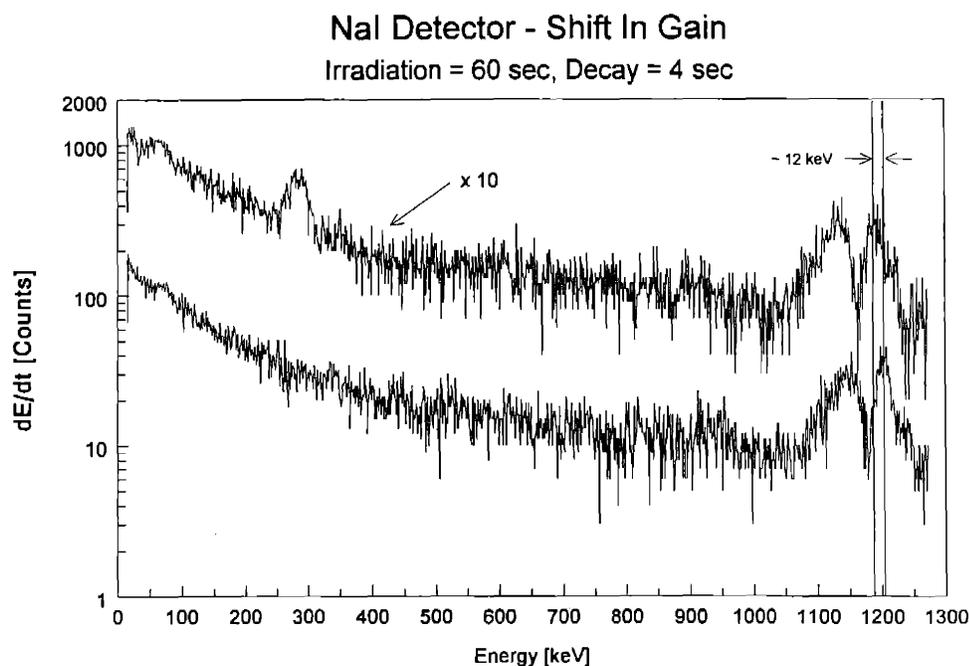
Figure 4-17 Comparison of NaI detector response before and after exposure to a high intensity photon source (a Au scattering target in the beam). Comparison between the top and bottom traces indicates the decrease in gain resulting when a Au target was in the beam. Top – Au target in beam, multiplied by x10 to allow comparison; Bottom – no target in beam.

The effects of small, reproducible gain changes on the order of ~1% can be compensated for in analytical measurements. However, in scaling an irradiation and measurement system up from the laboratory to industrial scale, it is possible to imagine a case where large photon fluxes on the crystal could lead to significant gain changes resulting from the Malter effect. Realizing this, it was decided to focus the next set of experimental investigations on incorporating a fast switching high voltage gating circuit into the PMT. In addition to allowing a rapid power up for the PMT and thus reducing the largest source for long term, low energy noise in the measurements by eliminating the manual HV supply, the use of the gating circuitry described in the next section significantly increases the number of isomeric isotopes that can be studied using PRE, lowering the minimum isomeric half-life for analyses from a few seconds to a few milliseconds or less.

4.3.4 Gating Circuitry

There have been a number of reports describing the use of gating circuitry for photomultiplier tubes.[33 – 42] Despite the general simplicity of photomultiplier tubes, however, the number of different approaches taken to gate a PMT on and off reflected in this literature is large. Some approaches involve the use of high precision, fast switching power supplies to control the voltage of one or more dynodes while others emphasize the importance of the focusing grid or the photocathode bias itself. Besides the use of multiple external power supplies some techniques employ solid state switching circuitry including transistors and diodes to control the gating while some simpler designs discuss the use of simple resistor-capacitor or battery circuits.

After a thorough review of these different options the gate design for this work was taken from research using photomultiplier tubes to study luminescence and fluorescence in the biological and chemical

sciences.[43-47] This gating circuit is designed for use with a negatively biased tube and works by holding the focusing grid bias at a constant +80 V with respect to the photocathode and pulsing the first dynode between +80 V (PMT = on) and –246 V (PMT = off). In addition to excellent performance characteristics including fast switching response, low noise and high signal attenuation in the off state, this circuit is simple, robust and cheap to construct. A complete description of its design and an assessment of its performance capabilities has been published elsewhere.[46]

By using a gated PMT, it was possible to collect isomeric decay data during an irradiation with the pulsed MINAC-6 accelerator (actually in between pulses). In Figure 4-18 the energy spectrum acquired using the NaI 3x3 detector together with the gated PMT when analyzing the decay spectrum of ^{197m}Au (T½ = 7.73 sec) is presented. In Figure 4-19 a similar plot is given for measurement of the decay spectrum of ^{75m}As (T½ = 16.8 msec). In the two figures the lower trace is background while the upper trace is the signal with the target in place. As can be seen, low energy noise has not been eliminated in these spectra. The reason for the difference in magnitude of this noise between the two plots is that the arsenic target was significantly larger than the gold (~3 cm along the beam axis versus ~2mm for the gold) and, because of the length of the arsenic sample, a portion of the sample extended beyond the center line of the detector closer to the accelerator (increasing the energy of Compton scattered photons entering the detector originating within this end of the target).
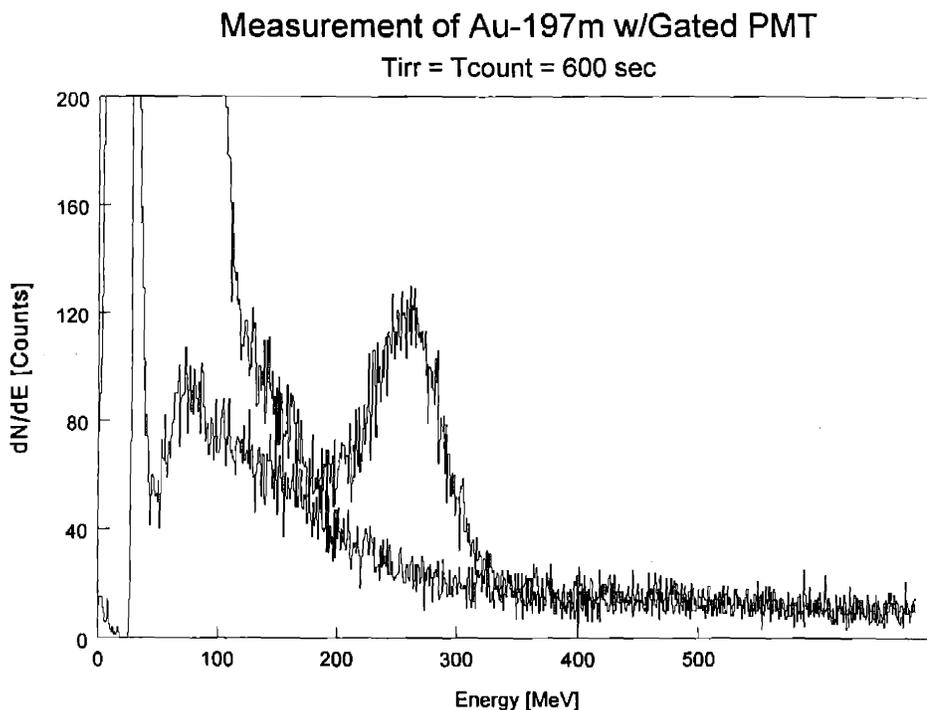
Figure 4-18 Energy spectra of Au-197m acquired during irradiation
using a gated photomultiplier tube.

Measurement of As-75m w/Gated PMT
Tirr = Tcount = 600 sec
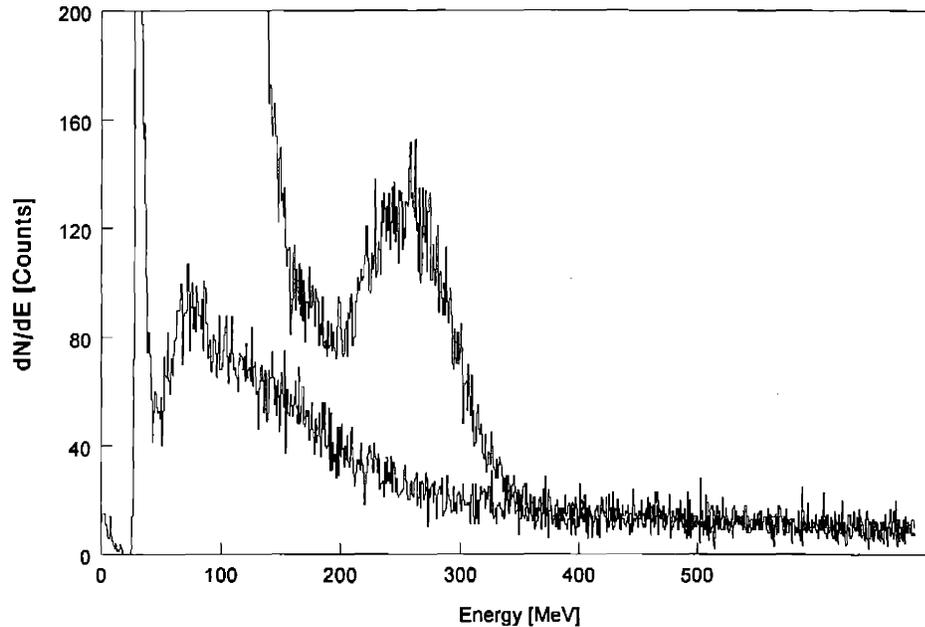
Figure 4-19 Energy spectra of As-75m acquired during irradiation using a gated photomultiplier tube.

Although a gated photomultiplier has been used elsewhere to examine the decay of isomeric nuclei during a pulsed irradiation, this is the first demonstration of its use: employing robust, inexpensive components; to collect energy spectral data; to sum differential energy data from multiple pulses or to conduct measurements without the use of extensive physical electromagnetic and radiation shielding. In short, these experiments have helped to demonstrated the ability to evolve the use of photonuclear resonance isomeric excitation from the use of research grade equipment in the laboratory setting to equipment and facility conditions likely to be encountered in dealing with industrial applications.

4.4 REFERENCES

[1] R. B. Firestone, *Table of Isotopes CD-ROM*, S. Y. Frank Chu, CD-ROM editor, Eighth Edition, v1.0, (1996).

[2] Bogdankevich, Lazareva and Nikolaev, "Inelastic Scattering of Photons by Indium-115 Nuclei," Sov. Phys. JETP **4**, 320-327 (1957).

[3] SpIDer Computer code v4.1, Western Kentucky University Nuclear Group, (1997).

[4] L. A. Currie, "Limits for Qualitative Detection and Quantitative Determination: Application to Radiochemistry," Anal. Chem. **40**, 586-593 (1968).

[5] T. Nakamura, "Monte Carlo Calculation of Efficiencies and Response Functions of NaI(Tl) Crystals for Thick Disk Gamma-Ray Sources and Its Application to Ge(Li) Detectors," Nucl. Inst. Meth. **105**, 77- (1972).

[6] T. Nakamura, "Monte Carlo Calculation of Peak Efficiencies and Respose Functions of Coaxial-Type Ge(Li) Detectors for Disk Gamma-Ray Sources," Nucl. Inst. Meth. **131**, 521- (1975).

[7] S. Taczanowski, "Correction for the Neutron and Gamma Attenuation Effects In 14 MeV Beutron Activation Analysis," Nucl. Inst. Meth. **144**, 299- (1977).

[8] R. B. Galloway, "Corection for Sampl Self-Absorption in Activity Determination by Gamma Spectrometry," Nucl. Inst. Meth. In Phys. Res. **A300**, 367- (1991).

[9] R. M. W. Overwater, *The Physics of Big Sample Instrumental Neutron Activation Analysis*, Dissertation, Delft Technological University, Delft, The Netherlands, (1994).

[10] I. M. Jureidini, *A Design for a High Energy X-Ray Computed Tomography Sensor for the Study of Solidification Fronts in Aluminum*, S.M. Dissertation, Nuclear Engineering Department, Massachusetts Institute of Technology, Cambridge, MA, (1997).

[11] I. M. Jureidini, *Design and Performance of a Compact High-Energy Computed Tomography system for the study of Metal Solidification*, Ph.D. Dissertation, Nuclear Engineering Department, Massachusetts Institute of Technology, Cambridge, MA, (1998).

[12] M. M. Hytros, *Development of a High-Energy X-Ray Computed Tomography Sensor for Detecting the Solidification Front Position in Aluminum Casting*, Ph.D. Dissertation, Department of Mechanical Engineering, Massachusetts Institute of Technology, Cambridge, MA, (1999).

[13] W. R. Leo, *Techniques for Nuclear and Particle Physics Experiments*, Springer-Verlag, (1992).

[14] J. A. Anderson, et. al., "Nuclear Photoactivation Cross Sections for Short-Lived Isomeric States Excited With A 6 MeV Linac," Nucl. Instr. Meth. **B40/41**, 452-454 (1989).

[15] Tonchev, Harmon and King, "Application of Low Energy Photon Spectroscopy in Isomer Production of Hf, W, Ir, Pt, Au and Hg using (γ,γ') Reactions," Nucl. Instr. Meth. Phys. Res. A **422**, 510-512 (1999).

[16] Tonchev, Harmon and Brey, "Analysis of Ore Samples Employing Photon Activation of the Metastable States of Gold and Silver," Nucl. Instr. Meth. Phys. Res. A **422**, 926-928 (1999).

[17] Robinson, Swann and Rasmussen, "Gamma-Ray Widths of the 3.00-MeV Level of Al^{27} and the 3.13-MeV Level of P^{31}," Phys. Rev. **174**, 1320-1323 (1968).

[18] V. K. Rasmussen and C. P. Swann, "Gamma-Ray Widths in C^{12}, Li^{6}, and P^{31}," Phys. Rev. **183**, 918-923 (1969).

[19] F. R. Metzger, "Electric Dipole Transitions from the 2.6-MeV Septuplet in Bi^{209}," Phys. Rev. **187**, 1680-1682 (1969).

[20] J. Margraf, et. al., "Photoexcitation of low-lying dipole transitions in ^{236}U," Phys. Rev. C. **42**, 771-774 (1990).

[21] K. Govaert, et. al., "Polarised Bremsstrahlung Nuclear Resonance Fluorescence Set-Up at the 15 MeV Linac in Ghent," Nucl. Instr. Meth. Phys. Res. A **337**, 265-273 (1994).

[22] S. N. Makeev et. al., "Study of Photomultiplier Anode-Current Variation with Pulse Gamma-Neutron Irradiation," translation from Pribory i Tekhnika Eksperimenta (Russian) **6**, 135-137 (1985).

[23] S. N. Makeev, et. al., "Variation of Photomultiplier Anode Current for Continuous and Pulsed Gamma Radiation," translation from Pribory i Tekhnika Eksperimenta (Russian) **1**, 160-163 (1986).

[24] S. N. Makeev, et. al., "Study of Photomultiplier Anode-Current variation With Pulse Gamma-Neutron Irradiation," translation from Pribory i Tekhnika Eksperimenta (Russian) **6**, 135-137 (1985).

[25] J. J. Carroll, "Excitation and De-excitation of Selected Nuclear Isomers Through (gamma,gamma') Reactions," Ph.D. Dissertation, University of Texas, Dallas (1991).

[26] C. Hong, "Measurements of Short-Lived Isomers With A Gated Detector," Ph.D. Dissertation, University of Texas Dallas, (1993).

[27] A. K. Gupta and N. Nath, "Gain Stability In High-Current Photomultiplies At High Variable Counting Rates," Nucl. Instr. Meth. **53**, 352-354 (1967).

[28] C. Weitkamp, et. al., "Count-Rate Dependence of the Gain of RCA 7046 Photomultipliers for Fixed Dynode Potentials," Nucl. Instr. Meth. **61**, 122-124 (1968).

[29] M. Yamashita, "Observation of a Hysteresis Effect In Rate-Dependent Photomultiplier Gain Variations," Nucl. Instr. Meth. **142**, 435-437 (1977).

[30] D. K. Li, V. G. Epishev and T. D. Radaeva, "The Effect of Ionizing Radiation On A Photomultiplier," translation from Pribory i Tekhnika Eksperimenta (Russian) **2**, 170-172 (1985).

[31] A. S. Belousov, et. al., "Stability of Scintillation Spectrometer With NaI(Tl) Crystal and FEU-49 Photomultiplier At high Count Rates," translation from Pribory i Tekhnika Eksperimenta (Russian) **3**, 49-52 (1985).

[32] V. N. Evdokimov and M. I. Mutafyan, "Short-Term Instability and Stabilization of Photomultiplier Gain," translation from Pribory i Tekhnika Eksperimenta (Russian) **4**, 134-138 (1986).

[33] J. P. Glore, "Equipment for Experiments with Activities Having Half-Lives In the Range From 10μsec to 1 sec," Los Alamos Report LA-2152, (1958).

[34] R. R. Fullwood and R. W. Hockenbury, "Neutron Inelastic Scattering Measurements with a Gated Photomultiplier," Nucl. Instr. Meth. **77**, 245-248 (1970).

[35] R. R. Fullwood, "A Bistable Symmetrical Photomultiplier Gate Using Integrated Circuits," Nucl. Instr. Meth. **95**, 509-513 (1971).

[36] M. Rossetto and D. Mauzerall, "A Simple Nanosecond Gate for Side Window Photomultipliers and Echoes in Such Photomultipliers," Rev. Sci. Instr. **43**, 1244-1246 (1972).

[37] M. Yamashita, "Photomultiplier Gate With Gating Times Larger Than A Few Microseconds," Rev. Sci. Instr. **45**, 956-957 (1974).

[38] Rosen, Robrish and Jan de Vries, "Design Of A Simple and Inexpensive Analog Gate," Rev. Sci. Instr. **46**, 1115-1116 (1975).

[39] J. J. Ramirez and L. W. Kruse, "Gated Scintillator-Photomultiplier Neutron Detector for Time-of-Flight Measurements in the Presence of a Strong X-Ray Background," Rev. Sci. Instr. **47**, 832-835 (1976).

[40] H. Sang Lee, et. al., "Gated Photomultiplier Response Characterization for DIAL Measurements," App. Optics **29**, 3303-3315 (1990).

[41] M.C. Piton, "An 'On'-Gated Photomultiplier Circuit for the Determination of Phosphorescence Lifetimes," Rev. Sci. Inst. **61**, 3726-3728 (1990).

[42] D. J. Creasey, et. al., "Fast Photomultiplier Tube Gating System for Photon Counting Applications," Rev. Sci. Inst. **69**, 4068-4073 (1998).

[43] Yoshida, Jovin and Barisas, "A High-Speed Photomultiplier Gating Circuit for Luminescence," Rev. Sci. Inst. **60**, 2924-2928 (1989).

[44] T. M. Yoshida, "Measurement of Protein Rotational Diffusion Using Time- and Frequency-Domain Polarized Fluorescence Depeletion," Ph.D. Dissertation, Colorado State University (1989).

[45] J. R. Herman, "Development of Laser Optical Instrumentation for Luminescence Measurements in Biological Systems," Ph.D. Dissertation, Colorado State University (1991).

[46] J. R. Herman, et. al., "Normally On Photomultiplier Gating Circuit with Reduced Post-Gate Artifacts for Use in Transient Luminescence Measurements," Rev. Sci. Inst. **63**, 5454-5458 (1992).

[47] T. R. Londo, "Theoretical and Instrumental Developments in the Measurement of Integral Membrane Protein Dynamics," Ph.D. Dissertation, Colorado State University (1992).

Chapter 5

CASE STUDIES

This Chapter presents two case studies examining the application of photonuclear resonance excitation isomeric nuclei for industrial purposes. Throughout the proceeding chapters numerous examples have been given of potential industrial applications of the PRE process including isomer production for medical and industrial purposes and material analysis and assay activities. Since this area of low energy nuclear physics has received relatively little engineering-based attention it seems likely that many other uses of short and medium lived isomers will be envisioned in the future as well. In the past, research exploring this field has often failed to consider both the physics and the engineering issues relating to PRE application. In this Chapter, a concerted effort has been made to take into account practical issues related to design in order to produce a fair analysis of the PRE based systems discussed.

The eight elements listed in Table 5-1 are classified a hazardous materials per US CFR 261.24 and as such are regulated by the Environmental Protection Agency. A material containing one or more of these elements is classified as a hazardous material if water is capable of leaching away the particular element at concentrations greater than those specified. Coincidentally, all of these regulated elements has an isomeric isotope with a half-life of less than an hour, except for chromium. Because of this, a PRE based analytical tool could be used in the analysis of potentially hazardous materials to determine the concentrations of As, Ba, Cd, Pb, Hg, Se and Ag.

Table 5-1 Characteristics of hazardous wastes – maximum
concentration of contaminants for the toxicity characteristic.[1]

Constituent	Isomeric Isotopes	Half-Life	Regulatory Level [mg/L][a]
Arsenic	^{75}As	16.8 ms	5.0
Barium	^{135}Ba	1.20 d	100
	^{136}Ba	308 ms	
	^{137}Ba	2.55 m	
Cadmium	^{111}Cd	48.5 m	1.0
	^{113}Cd	14.1 a	
Chromium	none	———	5.0
Lead	^{204}Pb	67.2 m	5.0
	^{207}Pb	0.81 s	
Mercury	^{199}Hg	42.6 m	0.2
Selenium	^{77}Se	17.4 s	1.0
Silver	^{107}Ag	44.3 s	5.0
	^{109}Ag	39.6 s	

In §5.1 a system designed to analyze materials to quantify the amount of arsenic in the material is presented. A carcinogenic substance, arsenic has found use in large scale industrial processes for well over a century and, as a result of this use, it has been identified in ground and drinking water around some of these sites at extremely high concentrations (greater than 0.5 % – 1 %). Environmental remediation of contaminated industrial sites is time consuming and expensive. One of the more time consuming aspects of this process is site characterization, when a map of the site is made detailing the extent of the contamination. Often, large numbers of soil samples must be taken at varying locations and depths in order to accurately characterize a site. Typical analytical measurements conducted to quantify the amount of arsenic in a sample are time consuming, requiring elaborate sample preparation and subsequent analysis at a distant laboratory using complex and expensive equipment. The design presented in §5.1 is small and could be made transportable by using a medium sized utility truck. Analysis using this system would require minimal sample preparation, essentially just placing the material into a suitable container and weighing it. Additionally, minor modifications could be made in the base design presented in §5.1 to conduct measurements of successive samples quickly or to allow for the analysis of core samples taken from a site.

Using the system described in §5.1 to measure the presence of arsenic or other heavy metals in solid environmental samples, measurements of liquid samples might also be possible. Using extraction chromatography techniques developed for the processing of spent nuclear fuel and nuclear waste, small resin bed columns can be designed that have very high affinities for different elements depending upon their electronic structure. If a water sample was poured through one of these columns, those elements for which the resin in the column was designed to capture would be arrested within the column. This technique could be used to produce a concentrated sample for analysis. While this technique could also be used as a preconcentration tool for more conventional analytical methods, the entire column could be placed in a PRE based instrument for analysis, eliminating the need for further chemical processing to return the concentrated element(s) to solution for extraction and analysis.

Besides the analysis of relatively small sized samples described in §5.1, another potential application of isomeric analyses is to analyze larger samples at fast rates. An ideal application for this approach to PRE is the analysis of potentially gold bearing ore to determine if the concentration of gold in the ore exceeds some predetermined value. Currently, analytical analyses of gold ore are made using flame assay measurements conducted at laboratories. Because of the limitations of this process, only very small

[a] Concentrations of elements in liquid samples are most often reported in units of mg/L. If the density of the liquid is the same as water, these values are equivalent to the µg/g, or ppm, units used in reporting elemental concentrations in solid materials.

samples of material may be tested at a time and often the amount of time between when a sample is collected and when the results of its analysis are complete is several hours. These two drawbacks of the current process make it essentially impossible to analyze the large quantities of ore which are mined daily at a site to accurately characterize its quality in anything close to real time.

A system designed to analyze gold ore is presented in §5.2. Due to peculiarities in the distribution of gold within ore, and the mining process itself, most of the ore exiting a mine contains no gold at all. Since the gold extraction process involves extensive physical and chemical processing of the ore, considerable savings could be made by classifying the ore grade prior to processing. The challenges related to the design of a system capable of carrying out these measurements, conducting isomeric analyses of the 7.73 second isomer of gold of a fast moving sample in real time are large. However, unlike the material assay case studied in §5.1, for this application the gold concentration in the ore doesn't necessarily have to be measured. Instead, a decision must be made of whether or not the amount of gold in the ore exceeds some preset limit. Additionally, only the false negative error rate must be low. Since all of the ore is being processed using current techniques, the false positive error rate for these measurements is not as important. Depending upon the total cost of production, which will of course vary from mine to mine, a reduction in the ore processing volume of 80 to 90% paired with a reduction in the total gold recovery rate of 5 to 10%, could prove to be an economically favorable improvement. Further, significant benefits would also be realized by reducing the volume of mined material sent through the entire gold extraction process, minimizing the use of hazardous materials and the production of acidic, cyanide laced mine tailing wastes.

5.1 ANALYSIS OF SOIL/ROCK TO QUANTIFY ARSENIC

To demonstrate the use of photonuclear resonance excitation as an environmental measurement tool this section evaluates a system designed to quantify the amount of arsenic in an unknown soil or rock sample. As the first step in this analysis, calculations were carried out to determine the energy dependent isomeric excitation cross section for the $^{75}As(\gamma,\gamma')^{75m}As$ reaction according to the procedures outlined earlier in Chapter 2. Since this cross section has not been reported in the literature the conclusions of this study must be based on these theoretical cross section. Referring to the accuracy these calculations have been shown to have for the cases shown earlier, the final results should be expected to be accurate to within ~50%.

The giant dipole resonance parameters used for these calculations were taken from Figure 5-1. Since the only data available for arsenic's GDR cross section are combined (γ,n) and $(\gamma, n+p)$ the GDR maximum energy was estimated to be 16.2 MeV, the width 4.5 MeV and the maximum was taken as 97.2 millibarns. The neutron binding energy for arsenic is rather high, at 10.244 MeV. Because of this, the isomeric excitation cross section is expected to increase continuously up until ~10 MeV. The theoretical excitation cross section used for this analysis is shown in Figure 5-2.

$$^{75}As(g,n)^{74}As \ + \ ^{75}As(g,n+p)^{73}Ge$$
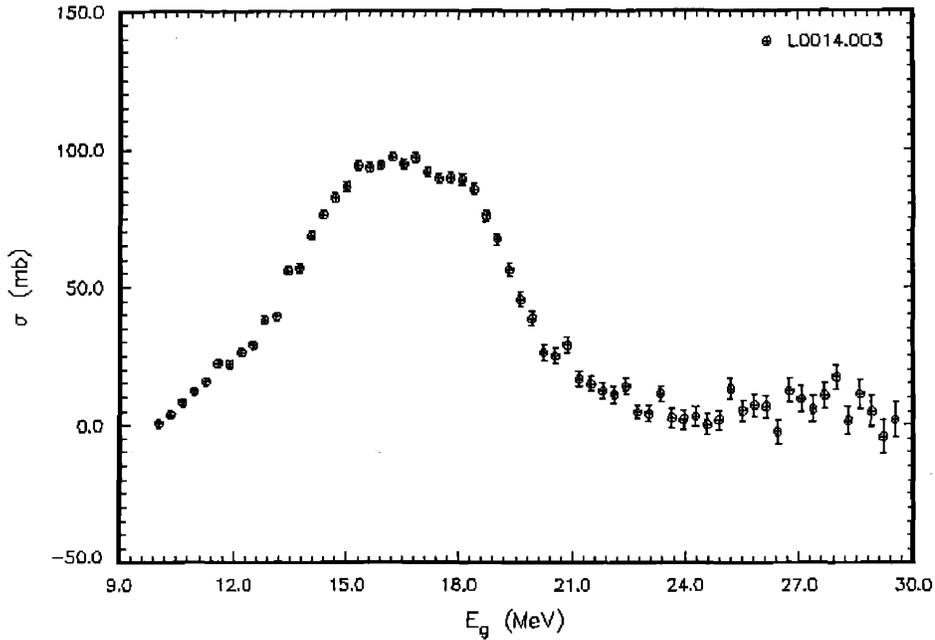
Figure 5-1 Experimental GDR photoneutron cross section for arsenic.[2]

As-75 Isomeric Excitation Cross Section
(Theoretical)
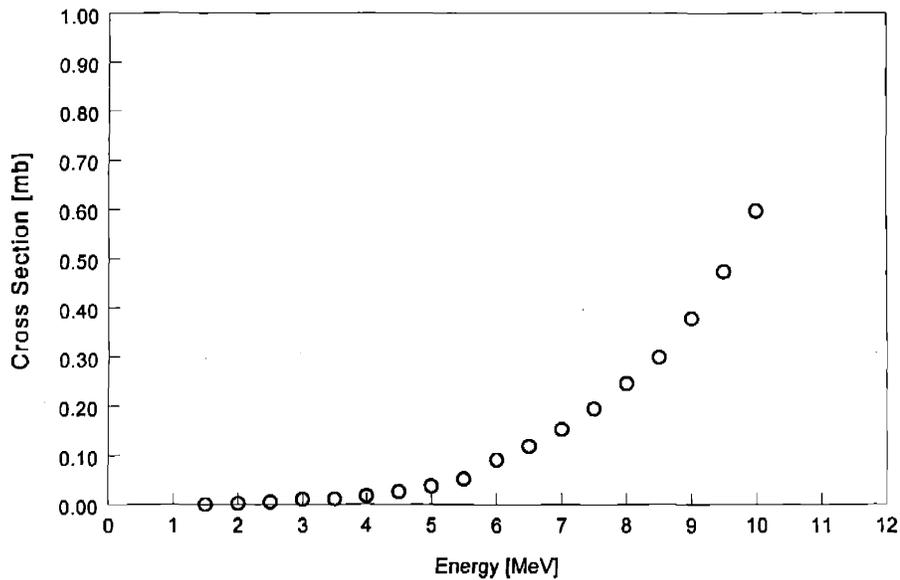
Figure 5-2 Isomeric excitation cross section calculated for As-75.

The irradiation source for this example is a 10 MeV bremsstrahlung field. Following from the discussions in previous chapters, the reason for this choice of irradiation source should be obvious. In short, they include reliability, intensity, mobility and cost. The 10 MeV energy is chosen to maximize the induced

isomeric activity in the sample while minimizing induced activity due to other photonuclear reactions. The detector system for this case study is comprised of eight NaI crystals, each of which is a cube measuring 10.16 cm (4 inches) on a side. A schematic diagram of the instrument's layout is given in Figure 5-3. In this figure, an electron beam 0.5 cm in diameter impinges upon a 2 mm thick tungsten convertor plate from the top. An eight inch long lead and iron collimator is used to create a roughly pencil beam like irradiation field aligned coaxially with a cylindrical soil or rock sample [diameter: 2.54 cm (1 inch), length: 5.08 cm (2 inches)] centered 25.4 cm (10 inch) from the convertor plate. The 8 NaI detectors are arranged in a horizontal plane centered with the sample being analyzed. Beyond the sample is a 22.86 cm (9 inch) deep, 5.08 cm (2 inch) wide beam dump. In order to reduce the background activity in the detector array resulting from the 67.2 minute isomer of ^{204}Pb and the 0.81 scond isomer of ^{207}Pb used in the collimator, 2.54 cm (1 inch) of iron has been used along the inside surfaces of the shielding along all surfaces which shine upon the detector.
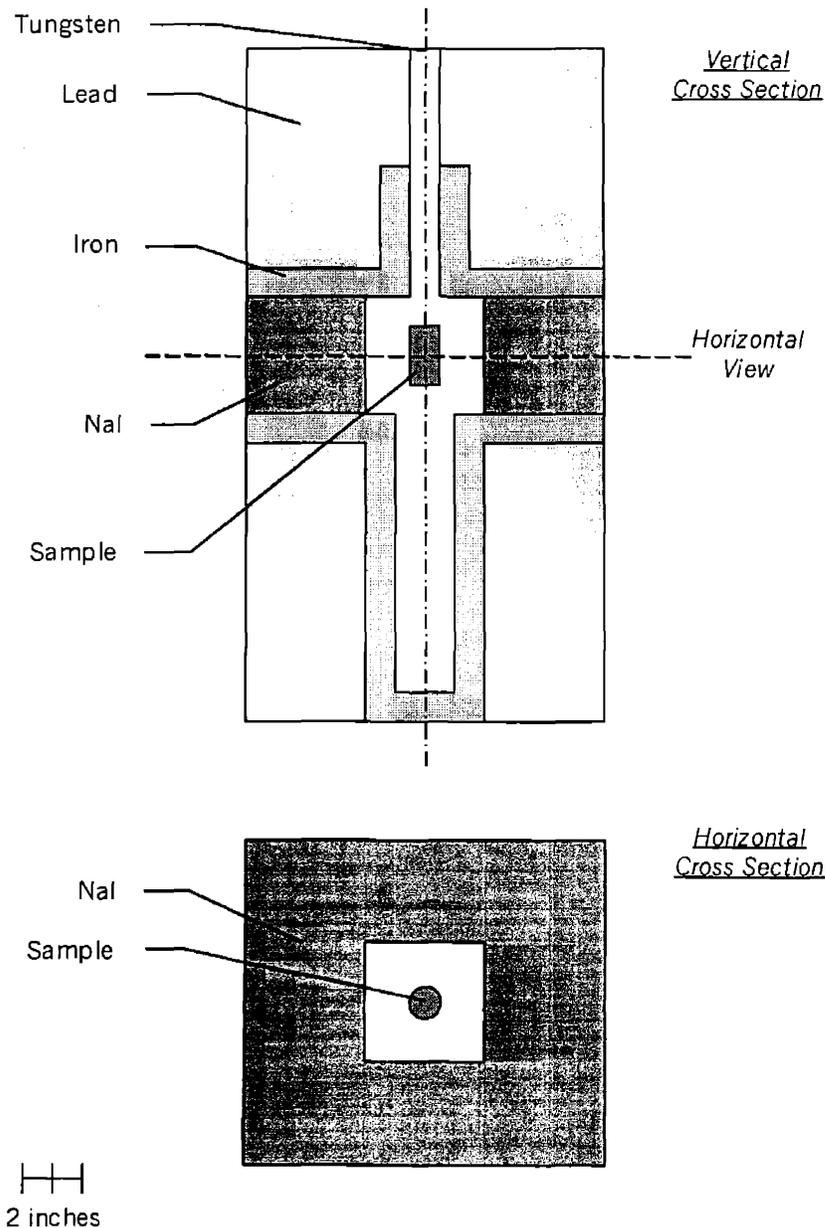
Figure 5-3 Material assay configuration.

Photon Attenuation Coefficient
Igneous Rock
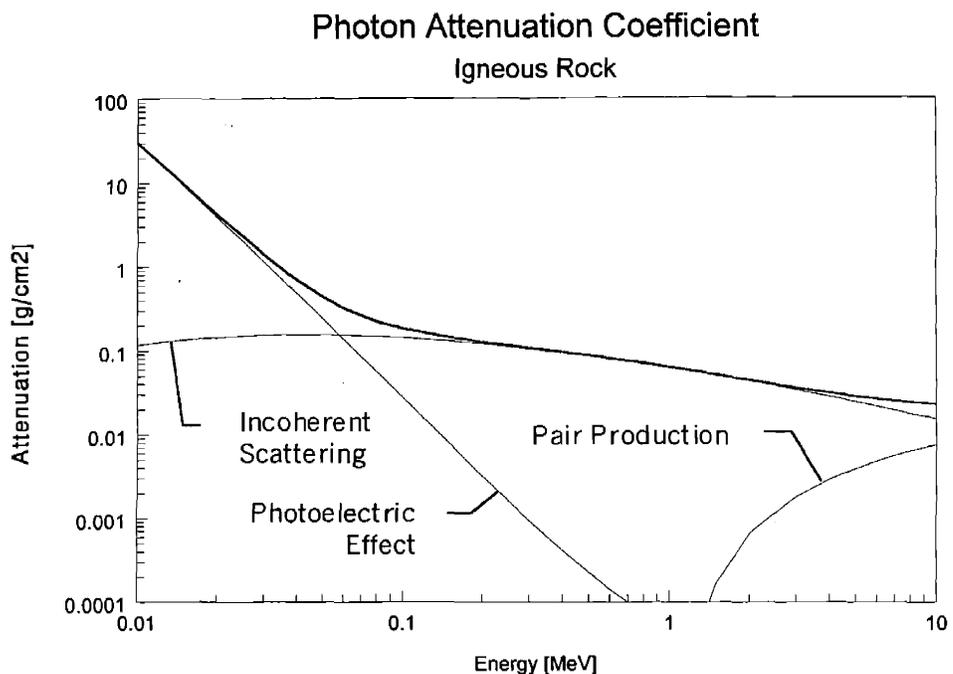
Figure 5-4 Total photon attenuation coefficient and its components for igneous rock.

Photon Attenuation Coefficient
NaI
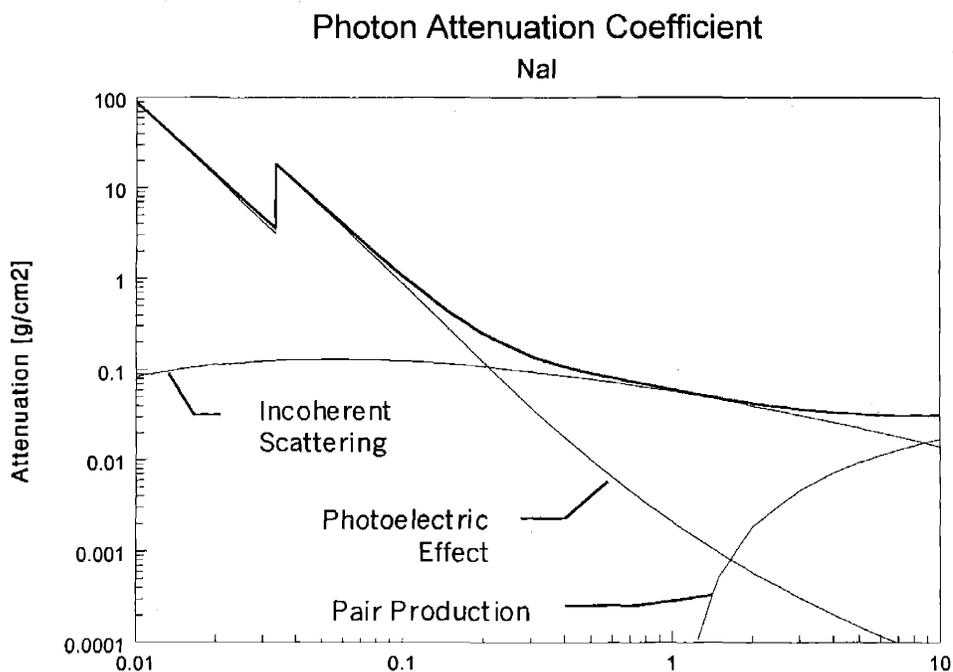
Figure 5-5 Total photon attenuation coefficient and its components for NaI.

For this example, the sample material has been taken to be the generic igneous rock described earlier in Chapter 4, the density was taken as 2 grams per cm^3. The bulk composition and density of the material is important because of the possibility of self absorption of the 279.5 keV principle isomeric decay signal from arsenic.[3,4] These assumptions of the bulk material composition and density are overly conservative

estimates of a typical sample that would be analyzed in this fashion (soil versus rock) and thus, without a real sample to use as a baseline, the calculations will overstimate the importance of sample self shielding and therefore underestimate the sensitivity of this system. In Figure 5-4 the photon attenuation coefficient for the sample material is given. In Figure 5-5, the photon attenuation coefficient for the NaI detectors is provided as well. The dimensions of the NaI crystal were choosen to maximize the total absorption of the principal arsenic decay photon of 279.5 keV, which occurs 79.5% of the time.

In Figure 5-6, the induced equilibrium isomeric activity in the sample is presented as a function of the position within the sample. Calculations were performed based upon a position dependent irradiation spectrum within the sample calculated using MCNP4B. The energy dependent photon flux was calculated to a statistical accuracy of better than 5% uncertainty in 100 keV energy bins from 100 keV to 9 MeV and to better than 15% from 9 to 10 MeV. The photon flux was calculated in 0.508 cm (0.2 inch) slices along the depth of the sample in a central core region of 0.762 cm (0.3 inch) radius and an outer annular region from 0.762 cm (0.3 inch) radius to 1.27 cm (0.5 inch) radius.

Equilibrium Arsenic Activity
Core & Outer Annulus
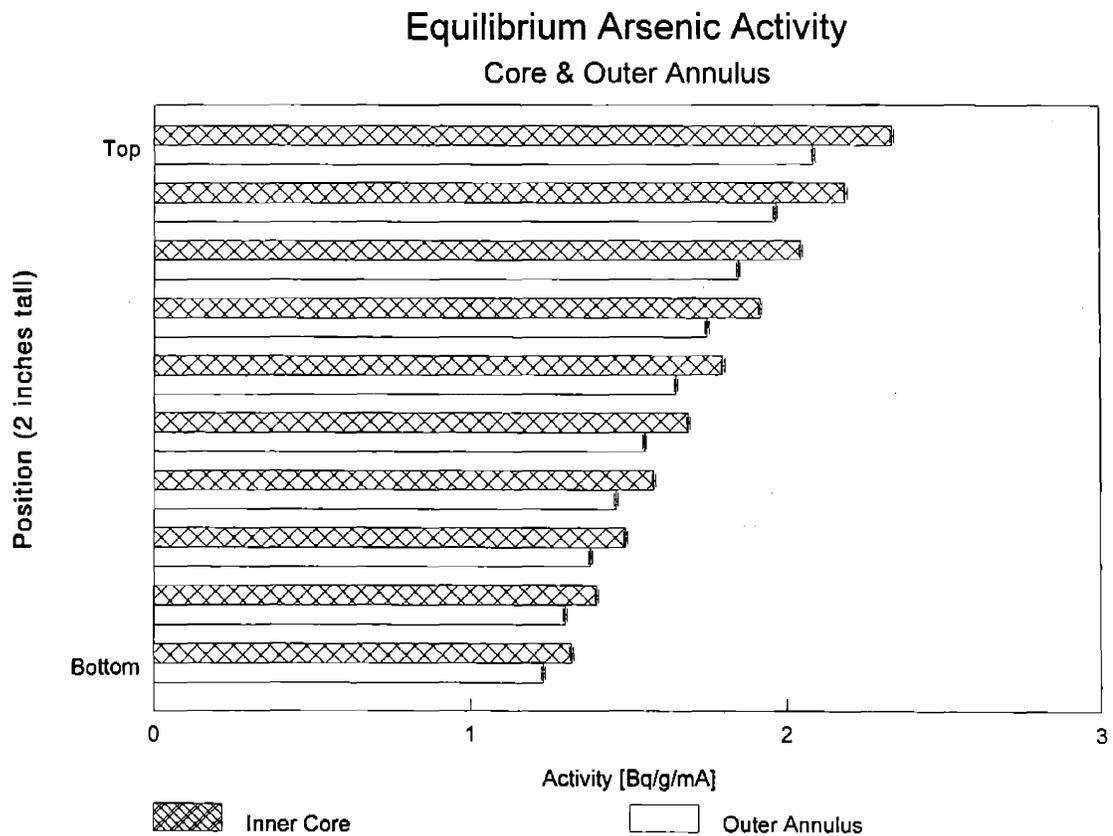
Figure 5-6 Equilibrium isomeric arsenic activity within a homogeneous rock sample having an arsenic concentration of 1 ppm.

Having calculated the induced isomeric activity in the sample, the next step in this analysis is to determine the absorption efficiency of the detector array for measuring the full energy of the arsenic decay photon. This was done using the same sample model used in the above calculations and assuming a uniformly distributed source of arsenic within the sample.[5,6] The results of this calculation are presented in Figure 5-7. As can be seen, there is a slight difference in the full photopeak absorption efficiency along the length of the sample. The influence of self shielding can be noticed by comparing the detection efficiency of the inner and outer regions of the sample, the average difference is ~5% while the detection efficiency averaged over the entire sample is 45%.

279.5 keV Detection Sensitivity
Volume Source - Core & Outer Annulus
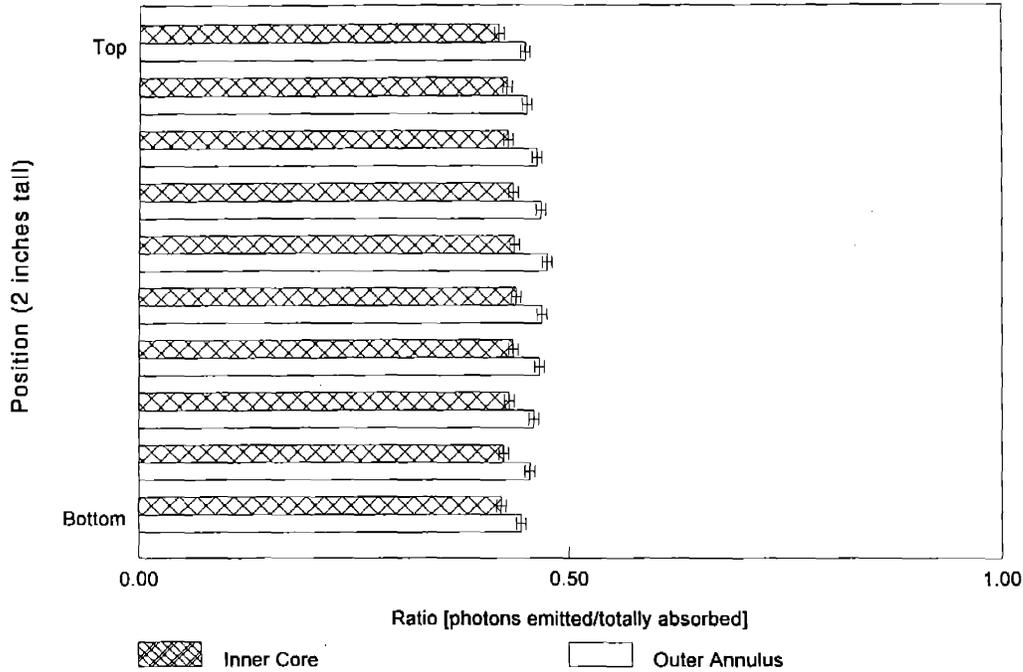
Figure 5-7 Full energy absorption efficiency for 279.5 keV photons originating from different positions within a low density igneous rock sample calculated using MCNP4B.

Having calculated the induced activity in a sample and the efficiency of the detector array, the final step is to carry out a parametric analysis of the measurement sensitivity of the system for this type of sample in terms of the accelerator current and the sample background count rate. Referring to the equations of Chapter 4, the acceptable false positive and false negative measurement errors will both be set at 5% such that $k_\alpha = k_\beta = 1.645$. As a baseline for analysis, the quantification limit will be set at the minimum amount of material which can be analyzed with a standard deviation, σ_Q, of 10% or better. For these values the equations for L_C, L_D and L_Q are reduced to

$$L_C = 2.33\sqrt{\mu_B}$$

5-1

$$L_D = 2.71 + 4.65\sqrt{\mu_B}$$

5-2

and

$$L_Q = 50\left[1 + \left(1 + \frac{\mu_B}{12.5}\right)^{1/2}\right]$$

5-3

where μ_B is the mean background counting rate, having a standard deviation $\sigma_B = \sqrt{\mu_B}$.[7] For a specific accelerator current and background count rate, the measured isomeric signal increases linearly as the duration of the measurement is increased while the minimum signals corresponding to the detection and determination limits increases at a rate proportional to the square root of the measurement time, as does the

154

standard deviation in the determination of the arsenic. In Table 5-2 the values of L_C, L_D and L_Q evaluated for different background counting signals are presented.

Table 5-2 Relationship between the background signal and L_C, L_D and L_Q ($\sigma_Q < 10\%$).

| Background Signal σ_B [counts]	Critical Level Signal L_C [counts]	Determination Level Signal L_D [counts]	Quantitative Level Signal L_Q [counts]
0	0	3	100
10	7	17	117
50	16	36	162
100	23	49	200
500	52	107	370
1,000	74	150	500
5,000	165	332	1051
10,000	233	468	1465

Looking first at Figure 5-6, the equilibrium activity in the sample (with an arsenic concentration of 1 ppm) is found to be 86 Bq per mA of beam current. The probability that the decay of isomeric arsenic will lead to a 279.5 keV photon is 79.5%, so the effective 279.5 keV activity is 68 Bq per mA. Taking the average full photopeak absorption efficiency to be ~45% (a rough interpretation of Figure 5-7), the approximate absorption rate in the detector array is 31 counts per second. Examining this in light of Table 5-2, one sees that it would take 3.8 seconds to collect 117 signal counts, and thus it would take 3.8 seconds to analyze a sample of 1 ppm arsenic to an accuracy of 10% when the background count rate was 2.6 counts per second. At a higher background count rate, it would take ~ 47.2 seconds to collect 1465 signal counts which is the amount of time needed to measure a sample of 1 ppm arsenic to within 10% uncertainty in a background count rate of ~211 counts per second.

The material quantification limit depends upon the specified measurement accuracy and the background counting rate. In order to estimate the background count rate that might be expected for this system, measurements were carried out to characterize the background count rate of a 4 x 4 x 4 inch NaI crystal shielded by 2 inches of ordinary lead. A plot of the differential energy spectrum of this detector for a background measurement of 300 seconds is provided in Figure 5-8. The average background count rate in the 150 keV wide region of interest centered at the 279.5 keV decay photon energy of arsenic is 24.4 ± 0.3 counts per second. Using this for a baseline estimate of background, the 8 detector assembly of the measurement system described here would be 195 counts per second. In addition to the inherent background count rate of the measurement system, background radiation in the detection system might also result from the presence of naturally radioactive materials in the sample, other isomeric isotopes in the sample, as a result of (γ,n) and (γ,p) photonuclear reactions in the sample and due to radiation effects in the crystal (e.g. afterglow resulting from the interaction of radiation scattered from the sample during each beam pulse). Since natural lead contains an isomeric isotope, the inside of the measurement area of the system is lined with iron to attenuate isomeric lead photons.

For most situations, no natural background radiation is expected to be in the sample. In order to verify this, a sample of contaminated soil from the Industri-Plex Superfund site in North Woburn, Massachussetts was measured using the same detector described above. The soil at this site is contaminated with a variety of volatile organic compounds including benzene and toluene as well as the heavy metals arsenic, chromium and lead. Neutron activation analysis measurements were performed using a small sample of the soil and indicated that the arsenic concentration was 3554 ± 62 ppm. A 300 second background measurement of the soil resulted in a count rate in the region of interest of 24.3 ± 0.3 counts per second, which is statistically the same as the natural background counting rate of the detector. As with other nuclear based analytical techniques, calibration of the isomeric activation technique described here would be most conveniently performed using a comparative technique and a sample prepared with a known arsenic concentration and

having a similar material matrix to the unknown samples being analyzed to simulate self-attenuation effects within the sample.

Shielded 4 x 4 x 4 inch NaI Detector
Background Measurement - 300 seconds
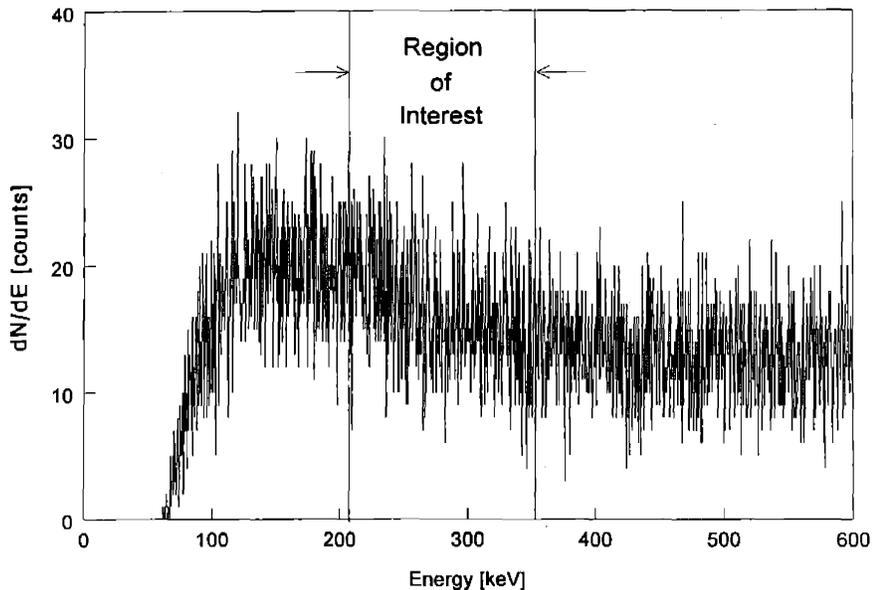
Figure 5-8 **The background differential energy spectrum taken with a shielded 4 inch NaI detector over 300 seconds, the region of interest is 150 keV wide, centered at the isomeric arsenic decay photon energy of 279.5 keV.**

Examining the elemental components of the igneous rock used in this analysis, an estimate may be made of the degree to which potential photonuclear reactions in the sample might lead to increases in the systems background radiation. In Table 5-3, all of the isotopes present in the igneous rock at an atom fraction greater than 0.1% are listed together along with their respective neutron and proton separation energies and the daughter products that might be generated when these isotopes are irradiated with a 10 MeV bremsstrahlung beam. As can be seen, the only major constituent that might lead to an increase in the arsenic signal background count rate is Mg-24, which comprises 0.9% of the material. If further investigations indicated that this radiation source was problematic, corrective measures could be employed by either subtracting the new background using spectroscopic analysis techniques or by taking advantage of the discrepancy between the arsenic and magnesium half-lives and taking background measurements intermittently during the arsenic analysis by turning the accelerator off for short periods of time, waiting for the isomeric arsenic to decay, and then measuring the background.

If afterglow or some other detector related phenomenon was troublesome, even when using a detector system which is well shielded from the primary source, gating circuitry to avoid PMT based effects during the beam pulse and a collimated beam dump to reduce back scattering effects, alternatives might be to change the detector system design to use more resilient (and more costly) detector materials such as those described in Chapter 3. Additionally, a less efficient detector design might be employed by increasing the distance between the detectors and the sample or moving the sample further away from the beam convertor, thus reducing the maximum energy of photons which can be Compton scattered from the target and still interact in the crystal. Finally, a smaller sample might be used to reduce the intensity of photons scattered into the detector array.

Table 5-3 Neutron and proton separation energies of the major igneous rock constituents together with the daughter products of resulting from reactions exceeding a 10 MeV threshold.

Isotope	Atom Fraction	Separation Energy [MeV]		Daughter Product, T ½ & Photon Energy
		S_N	S_P	
H-1	0.172	——	——	
O-16	0.616	15.7	12.1	
Na-23	0.018	12.4	8.8	Stable
Mg-24	0.009	7.0	10.6	Mg-23, 11.32 sec, $E_\gamma = 439.8$ keV
Mg-25	0.001	7.3	12.1	Stable
Mg-26	0.001	11.1	14.1	
Al-27	0.037	13.1	8.3	Stable
Si-28	0.105	17.2	11.6	
Si-29	0.005	8.5	12.3	Stable
Si-30	0.004	10.6	13.5	
K-39	0.008	13.1	6.4	Stable
K-41	0.001	10.1	7.8	Stable
Ca-40	0.010	15.6	8.3	Stable
Fe-54	0.001	13.4	8.8	Mn-53, 3.7 x 10^6 yr, no photons
Fe-56	0.008	11.1	10.2	

A more detailed analysis may be performed by taking into account variations in the induced activity as well as the position dependent detection efficiency within the sample. In Figure 5-9 the time dependence of the system's sensitivity is plotted for beam currents of 0.1, 0.5, 1 and 5 mA with a photopeak background count rate of 100 counts per second. A similar plot is provided in Figure 5-10 for a background count rate of 500 counts per second. These background count rates were chosen as upper and lower limit bounds of the background count rate which might be expected for an industrial system, based upon the 195 cps rate deduced using a single 4 inch cube NaI detector.

The use of higher current accelerator beams would results in a more sensitive analytical instrument, with the count rate increasing linearly with current increases and thus required measurement time decreasing linearly. Additionally, higher background count rates degrade the sensitivity of measurements using the system. For the cases analyzed here it is clear that a 1 mA accelerator would be ideally suited for use in all situations, even those with high background count rates. For applications where the measurement goal is less than the technically challenging 1 ± 0.1 ppm level addressed here, lower energy accelerators might also be found to be satisfactory. If a target sensitivity of 100 ppm was acceptable, a much lower current accelerator would be acceptable. Additionally, if a less sensitive measurement system was acceptable a lower energy electron beam might also be acceptable.

The average concentration of arsenic in the Earth's crust is ~1-2 ppm. In light of this, the above analysis of a PRE based system intended for analyzing contaminated soils does not adequately reflect the usefulness of such a system based upon realistic performance goals. As a more realistic assessment of the performance of a system designed to analyze environmental samples of highly contaminated materials, calculations have been performed to determine the analysis time required to quantify the quantity of arsenic in a sample to a concentration of 100 ppm with an error of less than 10%. Depicted in Figure 5-11, the results of these calculations indicate that relatively low current accelerators could potentially be used for the analysis of environmental samples at concentrations of interest when analyzing potentially contaminated materials. For example, a 50 microamp accelerator could be employed to carry out useful analyses of contaminated soil samples from the Industri-Plex site with measurement times of less than a minute per sample.

PRE Analysis of Arsenic in Soil/Rock
Variable Beam Current, BKD = 100 cps
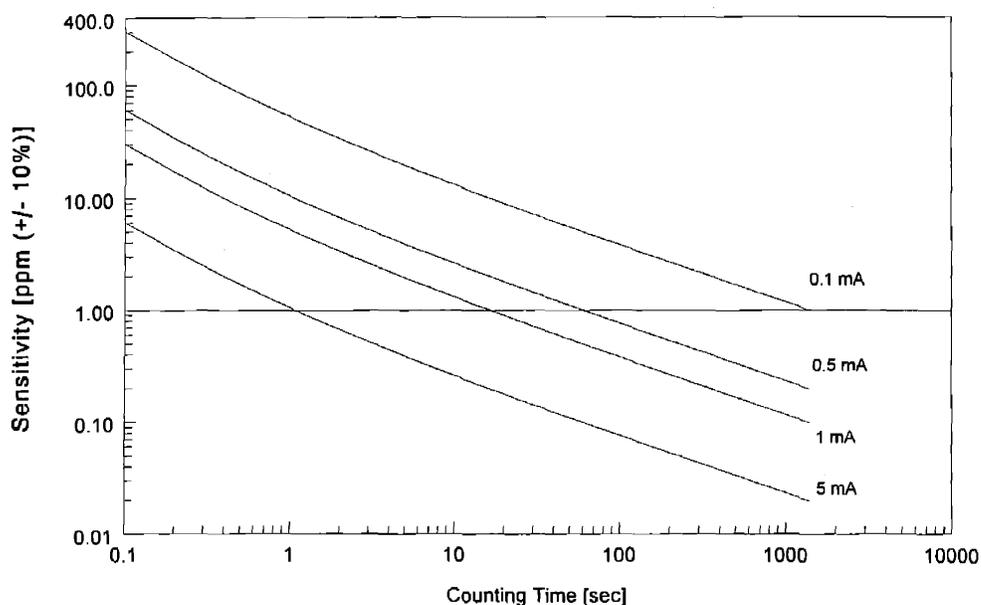
Figure 5-9 Minimum concentration of arsenic that can be quantitatively determined to within ±10% using the system outlined in this section with a photopeak background count rate of 100 counts per second at beam currents of 0.1, 0.5, 1 and 5 mA.

PRE Analysis of Arsenic in Soil/Rock
### Variable Beam Current, BKD = 500 cps
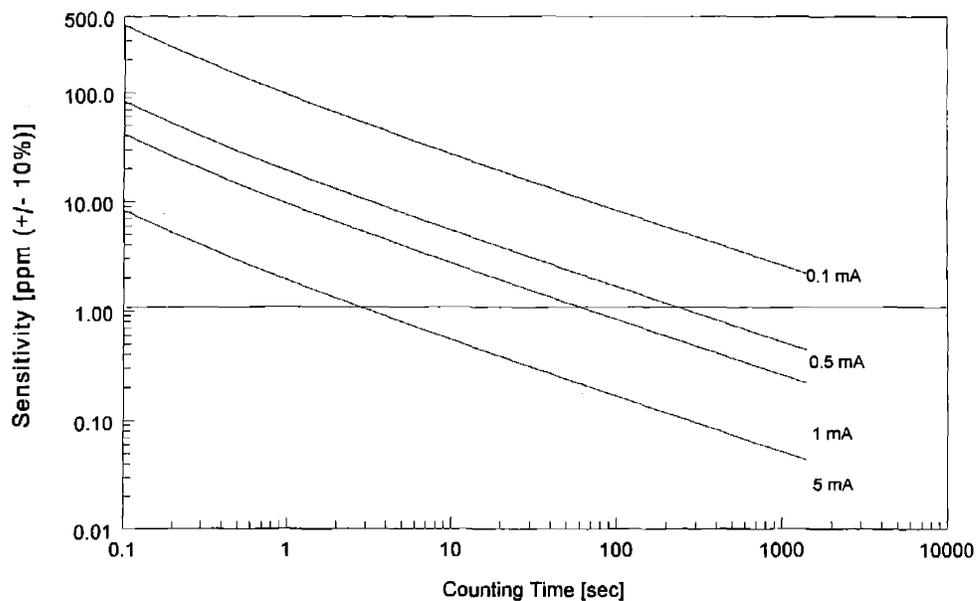
Figure 5-10 Minimum concentration of arsenic that can be quantitatively determined to within ±10% using the system outlined in this section with a photopeak background count rate of 500 counts per second at beam currents of 0.1, 0.5, 1 and 5 mA.

158

PRE Analysis of Arsenic in Soil/Rock
Variable Beam Current, BKD = 1000 cps
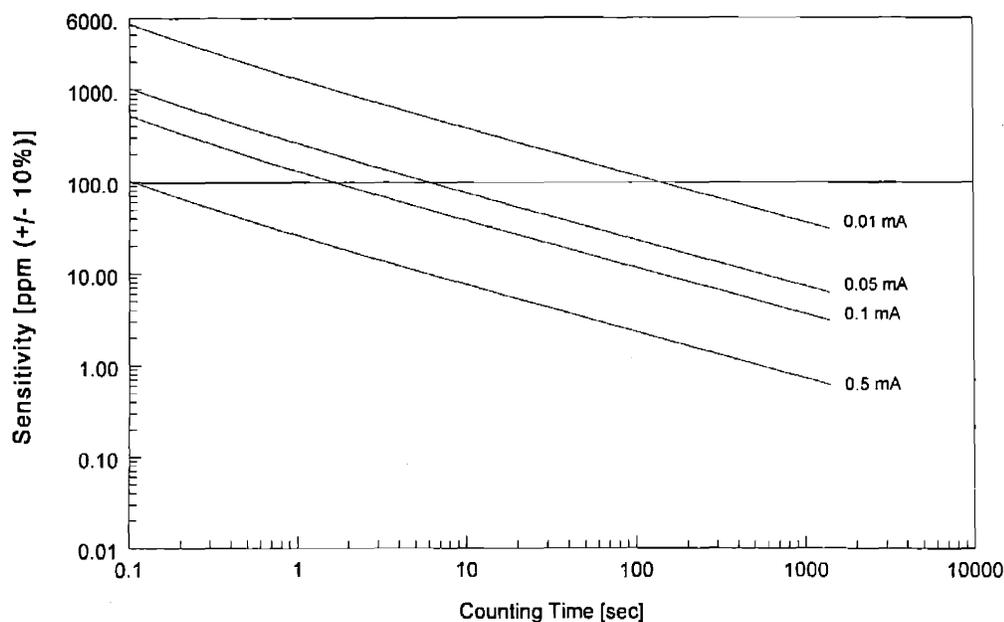
Figure 5-11 The time required to analyze a sample such that concentrations greater than 100 ppm can be quantified with less than 10% error with a photopeak background count rate of 1000 counts per second at beam currents of 0.01, 0.05, 0.1 and 0.5 mA.

Before concluding this section, it is important to return to a discussion of some of the assumptions that went in to this analysis and which have a significant impact on the evaluation of the system. The largest single source of uncertainty in the analysis above is the isomeric excitation cross section. Although the theoretical model which was used to determine this cross section has been shown to be accurate to within ~10% for several other nuclei, it is possible that the actual cross section might differ from the one used here by more than this amount. A 10% variation in the cross section would lead to a similar variation in the measured decay activity and would have a similar impact on the counting time required to achieve a particular sensitivity. Smaller sources of uncertainty include the irradiation intensity and full photopeak absorption efficiency which were calculated using Monte Carlo techniques. Statistical uncertainties in these values were generally less than 5% in magnitude, differences in these values also lead to changes in the system's ultimate sensitivity in a linear fashion. Finally, the assumption of an igneous rock matrix having a density of 2 g/cm^2 probably results in an overly conservative estimate of self-attenuation effects within the sample and thus lowers the calculated absorption efficiency from that which would actually be found in the analysis of soil.

5.2 ANALYSIS OF ORE TO IDENTIFY THE PRESENCE OF GOLD

The second PRE application which will be explored in depth is the analysis of ore travelling along a conveyor belt to determine if it contains gold above some specified amount. The motivation for this analysis is the realization that, due to the peculiarities of the mining process, a relatively large fraction of the gold recovered from most mines is found in only a small fraction of the excavated ore. A useful companion to this analysis is a report from South Africa exploring the use of neutrons to excite the isomeric state of gold using the $^{197}Au(n,n')^{197m}Au$ reaction.[8] In Figure 5-12 from this report, a plot is presented of the nature of the distribution of gold within a typical ore from the Vaal Reef area of South Africa. The abscissa of this figure is the cut-off level for a hypothetical sort of this type of ore, three

variables are plotted on the ordinate. The Grade plot represents the grade of the ore obtained when a sort is carried out to discard all ore having a gold concentration less than the cut-off value; if no sorting is carried out (cut-off equals zero) the grade value is simply the ratio of the mass of all of the gold removed from the mine divided by the mass of all of the ore removed from the mine. The gold recovered plot indicates the fraction of gold removed from the mine which is sent for further processing (eventually recovered and sent to market) at different cut-off values. The mass recovered plot indicates the fraction of the total ore excavated from the mine which is sent for further processing at different cut-off values.
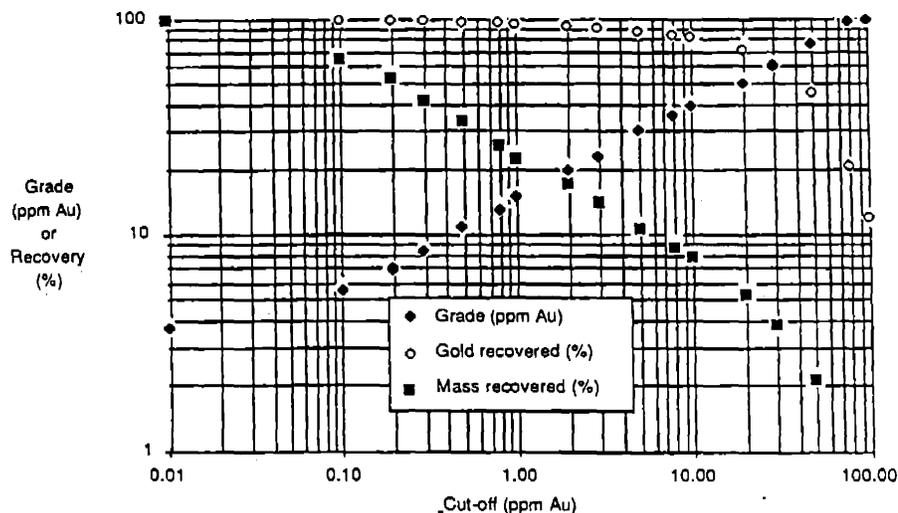
Figure 5-12 Variation of the grade of the sorted fraction, the percentage of gold recovered and the percentage of the total mass of ore remaining after sorting, as a function of the cut-off grade for an ideal sort of an ore with a log-normal gold distribution.[8]

From this information rich plot an interesting trend is observed; approximately 95.3% of the gold can be recovered from a mine of this type of ore by only processing about 25% of the ore, a cut-off level of 1ppm. The problem, of course, is to know which 25% of the rocks to keep and which 75% of the rocks to discard. At a cut-off of 10 ppm, the gold recovery fraction has fallen to 82% but the ore mass sent on for processing has decreased to about 8%. Depending upon the relationship between overhead fixed costs, processing related costs and the price of gold, significant savings could potentially be realized by a commercial mining venture by incorporating ore sorting into the mine's operation. If a system could be acquired at a cost on the order of the financial savings made in one year, such a system would seem to be a reasonable capital investment.

Clearly, in attempting to analyze gold ore to determine if gold is or is not present above some threshold value, there are many variables which will be unique to the particular circumstances of each mine. Some of these variables, and their values that are used in the following analysis, include:

- *The density of the ore during analysis.* Since a major component of most ores is silica, the density of gold ore is often taken to be 2.7 g/cm^3, this is the value used here. Of course, this value will vary at each mine.
- *The material processing rate.* A typical processing rate might be on the order of 100 tons per hour but this value could vary significantly at different mines. In the analysis below, the irradiation parameters were chosen such that the cross sectional area of the ore traveling on a conveyor belt is 10.16 cm by 5.08 cm (4 inches wide, 2 inches deep). At a processing rate of 100 tons per hour, this corresponds to a belt velocity of 200 cm/sec. For the purposes of this analysis, the porosity is taken as zero, which is of course unrealistic. In reality, the porosity probably lies somewhere around 25%, corresponding to a belt speed of 300 cm/sec.

160

— *The gold distribution in the excavated ore.* As the ore is transferred from the excavation site to the processing area, what is its distribution on the conveyor belt? Is the gold highly localized within individual rocks or more generally distributed in small sections of ore on the belt. The unit distance along the conveyor belt in the analysis below is 10 cm (1.393 kg). In terms of this, the questions is whether 1 ppm (μg/g) in a unit section such as this corresponds to one 1.393 mg gold nugget or several smaller particles of gold. For the analysis presented here, gold particles are taken to be on the order of 275 μg, indicating ~5 particles per unit distance per ppm of gold.[8] In the analysis below, activation and detector sensitivity calculations are based upon a homogeneous gold distribution. Because of this, measurement uncertainty at the 1ppm level might be higher than the values indicted but should be accurate at levels of ~10 ppm or greater (>50 particles) where the homogeneous approximation is more realistic.

Because a number of generalizations must necessarily be incorporated into this analysis, the applicability of the system described below to any particular mine is limited. Instead, what the reader should take from this case study is an understanding of the *relationship* between different factors such as the material processing rate, the accelerator beam current and the detector measurement efficiency.

A schematic diagram of the irradiation set up for this problem is presented in Figure 5-13. The top view in the figure shows the ore bed, 4 inches wide, passing in between two opposing 1 meter long, 2 mm thick convertor plates.[a] A 10 MeV accelerator (not shown) is used to generate a high current electron beam which is then split into two beams (each 1 cm in diameter), each of which is then redirected in to the plane of motion and perpendicular to the ore and rapidly swept back and forth along the convertor plates. The side view in the figure shows the bremsstrahlung irradiation field from one of the convertor plates. The bottom view is an end view from within the ore downstream (or upstream) of the irradiation region showing the two convertor plates, the incident electron beams an the opposing irradiation fields.

---

[a] The convertor plates, which are used to stop the electron beam and thus generate the bremsstrahlung irradiation spectrum, are arranged in this configuration to allow for a simple passive convective cooling scheme to be employed along the outside face of each plate. However, if an active convertor plate cooling scheme was used the overall area of each convertor plate could be reduced.

a) Top View

Convertor Plates ─   Irradiation Region

Ore

b) Side View

c) End View

Irradiation Region

Electron   Electron
Beam   Beam

Ore
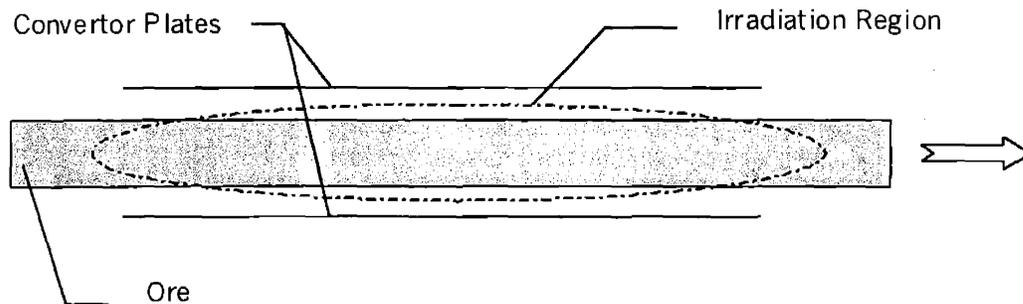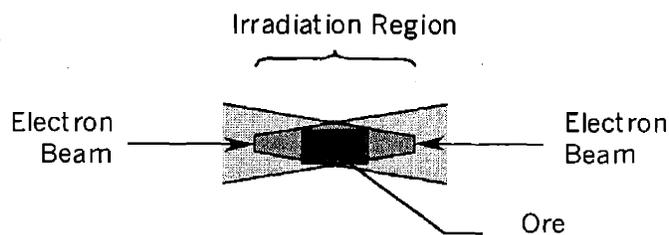
Figure 5-13 Gold ore irradiation geometry.

The irradiation spectrum within the ore was calculated using MCNP4B in 0.1 MeV energy bins, statistical uncertainties were less then 5% at energies from 0.1 to 9.5 MeV and from 5 to ~10% from 9.5 to 10 MeV. Within the ore, 24 sample regions were defined, creating four 1 inch thick horizontal layers and 6 vertical columns, two columns 1 inch wide in the middle section and two columns 0.5 inches wide on each edge. Sample cells were taken in 10 cm lengths from 50 cm prior to the irradiation, through the 100 cm of the irraiation region and then another 50 cm past the irradiation region. Signficant use was made of the symmetry of the geometry to reduce the complexity of the problem. In Figure 5-14 a contour plot is shown of the energy dependent photon intensity within the ore in the middle region along the top and bottom edges. Similar plots are shown in Figure 5-15 and Figure 5-16 for the regions indicated to the side of each plot.

Photon Flux [photons/cm2/electron]

Ore Irradiation (0.5 Mev bins)
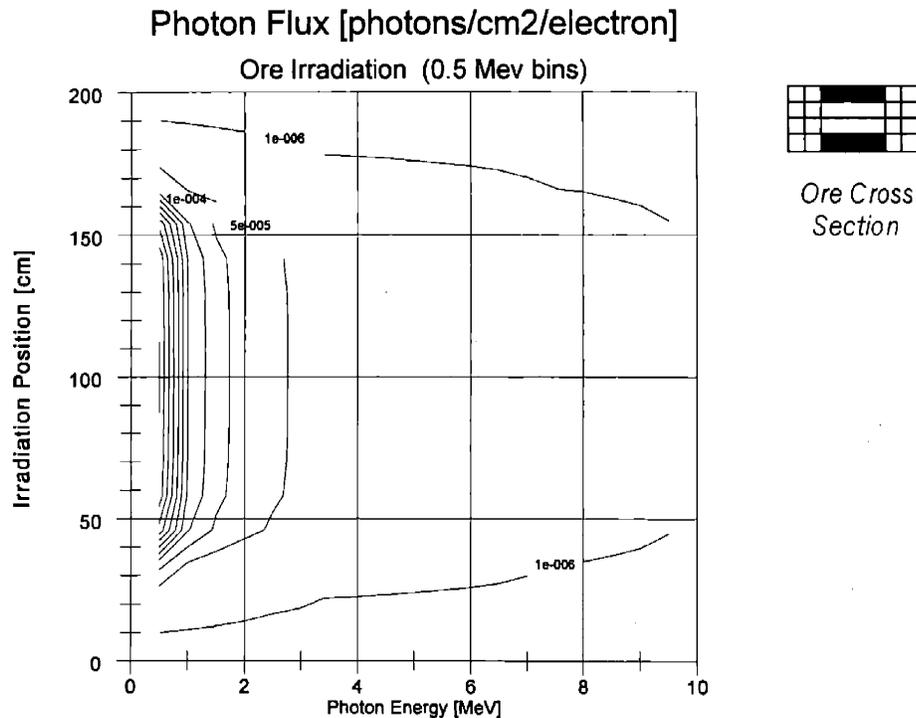
Figure 5-14 Energy dependent isoflux contours (photons/cm²/electron) within the ore at the top (and bottom) middle region of the ore as a function of the ore position along the conveyor belt. (Convertor plates located on both sides from 50 to 150 cm.)

Photon Flux [photons/cm2/electron]

Ore Irradiation (0.5 Mev bins)
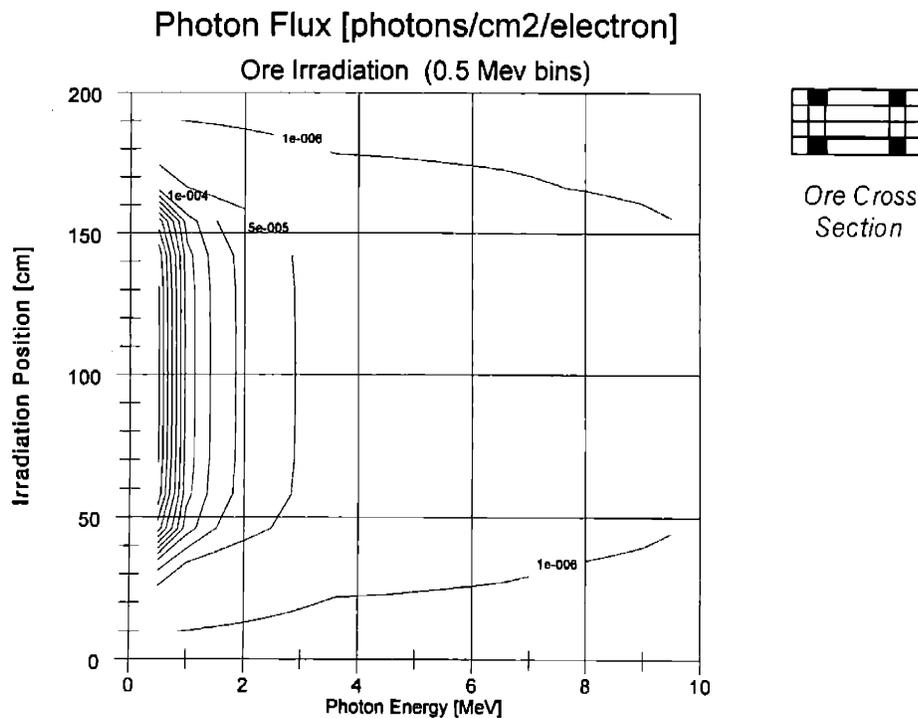
Figure 5-15 Energy dependent isoflux contours (photons/cm²/electron) within the ore at the top (and bottom) region of the ore, from 2.54 cm to 3.81 cm transverse to the conveyor belt, as a function of the ore position along the conveyor belt. (Convertor plates located on both sides from 50 to 150 cm.)

Photon Flux [photons/cm2/electron]

Ore Irradiation (0.5 Mev bins)
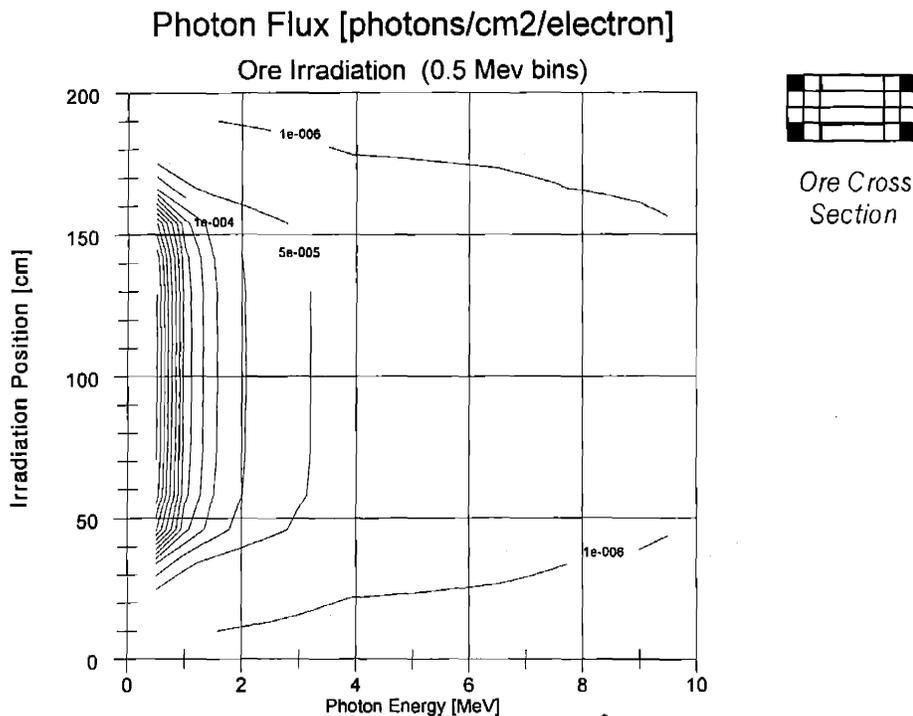
Figure 5-16 Energy dependent isoflux contours (photons/cm²/electron) within the ore at the top (and bottom) region of the ore, from 2.54 cm to 3.81 cm transverse to the conveyor belt, as a function of the ore position along the conveyor belt. (Convertor plates located on both sides from 50 to 150 cm.)

As can be seen, the photon intensity within the irradiation region is uniform to better then 10% at all energies and falls off by several orders of magnitude within 20 cm of the start and end of the irradiation region. The two 1 meter long convertor plates were chosen to accommodate the large heat removal requirements encountered when using high current electron beams. Overall, there is approximately a 4.5% reduction in induced isomeric activity within the ore at the end of irradiation in comparison with what would be expected using two opposing, 1 cm diameter stationary electron beams at the end position.[a]

In Figure 5-17 the energy dependent photon flux calculated in the upper 1 inch deep wide row (and lower 1 inch deep row) within the ore is shown for three different transverse positions, namely, a 0.5 inch thick column along the outer edges, the next 0.5 inch column in from the first column, and the 2 inch thick central column. A similar plot is shown in Figure 5-18, the difference in this case being that the flux is averaged over a 2 inch thick horizontal slice through the middle of the ore. Both plots are calculated in the center of the irradiation region. Examining each figure individually, the benefit of using use two opposing irradiation beams can be seen by noting the small difference in intensity over all energies between the outer edge central region. Comparing the two figures, the benefit of using a diffuse irradiation beam (1 cm diameter) can be seen by noting the small difference in intensity between the same transverse positions in the upper/lower slices and the middle slice. Since the gold distribution within the ore on the scale of the conveyor belt unit volumes discussed here is essentially random, it would be desirable to achieve an intense, uniform irradiation spectrum throughout the ore. Due to the inherent angular spread of the forward peaked bremsstrahlung beam and the effect of attenuation of the beam as it passes through the ore, however, it is essentially impossible to achieve a uniform photon flux throughout the ore using a single irradiation beam. As seen in the figures below, a two beam irradiation geometry is useful because it results in a roughly uniform photon spectrum within the ore (~ a factor of 2). Since the measurement system detection efficiency (discussed below) is lowest in the middle of the ore, further analysis of the irradiation

---

[a] The decrease in overall isomeric gold activity produced in the ore between these two cases is a result of the decay of some of the isomeric gold that is produced throughout the irradiation after it has traveled over the 1 meter length of the irradiation area.

beam configuration, incorporating site specific parameters for a particular mine, might lead to the design of an irradiation system with an effectively uniform activity measurement parameter (incorporating both activation and measurement efficiency) throughout the ore travelling along a conveyor belt.

Ore Irradiation Flux Comparison
Top/Bottom (0.5 MeV bins)
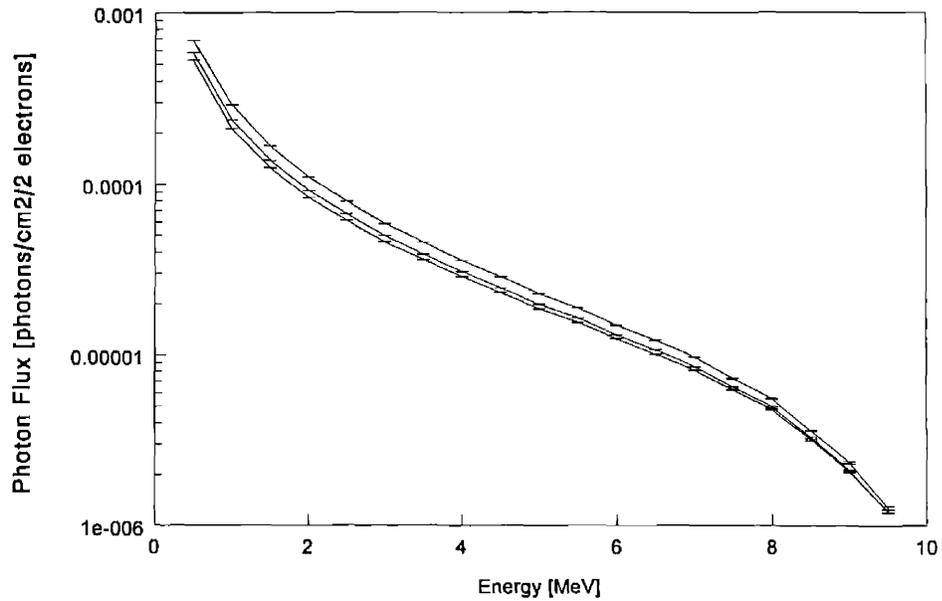
Figure 5-17 Energy dependent photon flux in 1 inch deep rows on the top and bottom edges in three regions: top trace – 0.5 inch columns along the edges nearest the convertor plates, middle trace – 0.5 inch columns closer to the center of the ore, bottom trace - a 2 inch wide column in the center.

Ore Irradiation Flux Comparison
Middle (0.5 MeV bins)
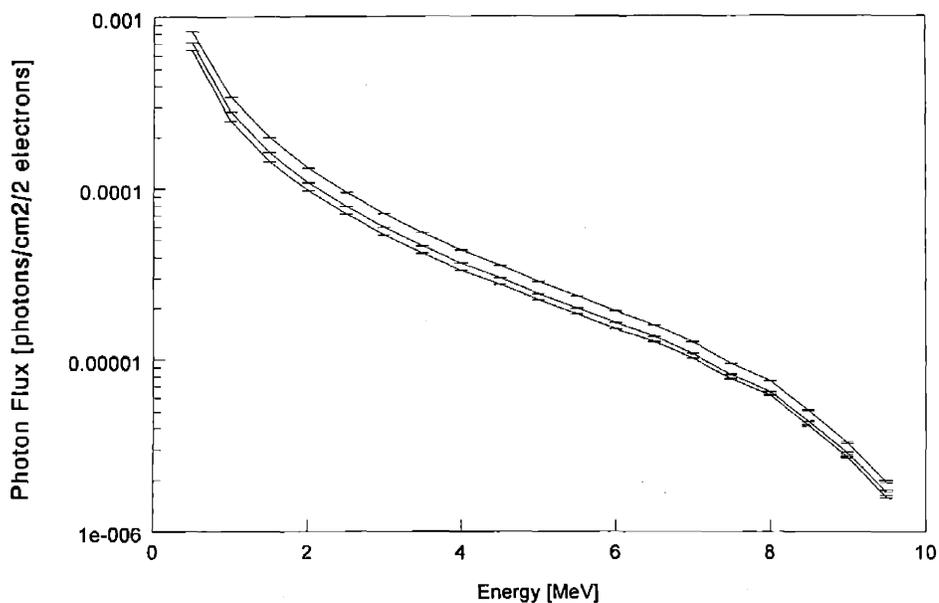
Figure 5-18 Energy dependent photon flux in a 2 inch deep rows in the middle in three regions: top trace – 0.5 inch columns along the edges nearest the convertor plates, middle trace – 0.5 inch columns closer to the center of the ore, bottom trace - a 2 inch wide column in the center.

After considering the details of the irradiation process, the next issue to address is the radiation measurement system. A schematic view of the measurement system designed for the case studied here is presented in Figure 5-19. After travelling through the irradiation region, the ore passes through a small channel a thick (50 cm) shielding wall and enters an array of NaI detectors. The detector array is comprised of five detector segments that are 4 inches thick, each segment consists of a 4 x 4 x 4 inch NaI crystal centered above and below the ore at a distance of 1 inch from the ore and a 4 x 4 x 8 inch NaI crystal on each side of the ore with 1 inch gap from the ore.

166

a) Side View

NaI Detector Arrays

Irradiation
Region

1   2   3   4   5

Ore

Shielding
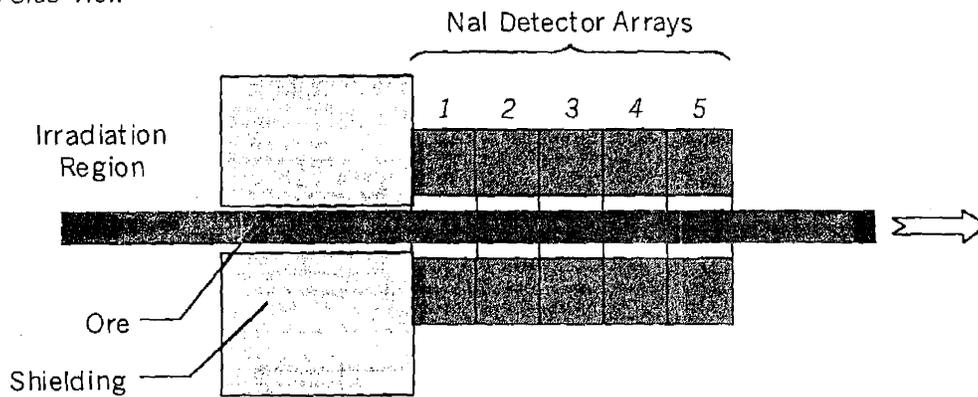
b) Detector Array Cross Section View (x2)
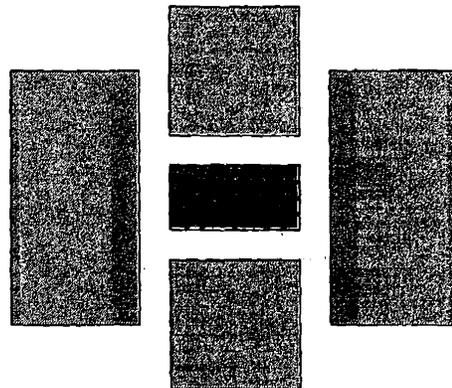
Figure 5-19 Schematic view of the radiation measurement system. Figure a) is a side view of the system and shows the ore passing from the irradiation region through a shielded area and then entering an array of NaI detectors a thick shielded. A cross sectional view of the detector array is seen in figure b).

For the 16 small cross sectional regions in the ore, the complete photon absorption efficiency of each of the five segments in the detector array was calculated for the 16 small cross sectional regions in the ore indicated in the above figure. As with the photon flux calculations, the detection efficiency was calculated for ore sections 10 cm long. In order to determine the photopeak count rate of the detector array as a unit ore segment (10 cm x 2 in x 4 in.) passes through it, calculations were conducted in a step-wise fashion in linear increments of 2.5 cm. In Figure 5-20, the calculated photopeak detection efficiency of the total detector array is presented together with the detection efficiency for each of the five detector segments. The detection efficiency averaged over the entire ore segment as it passes through the array is seen to reach a nearly constant level of 32% when it is in the middle of the array. Looking at the contribution of individual detector segments to the detection sensitivity it is apparent that no more than three individual detector segments provide a substantial contribution to the detection efficiency at any one time.

Ore Detector Array Efficiency
Total Array & Individual Detectors
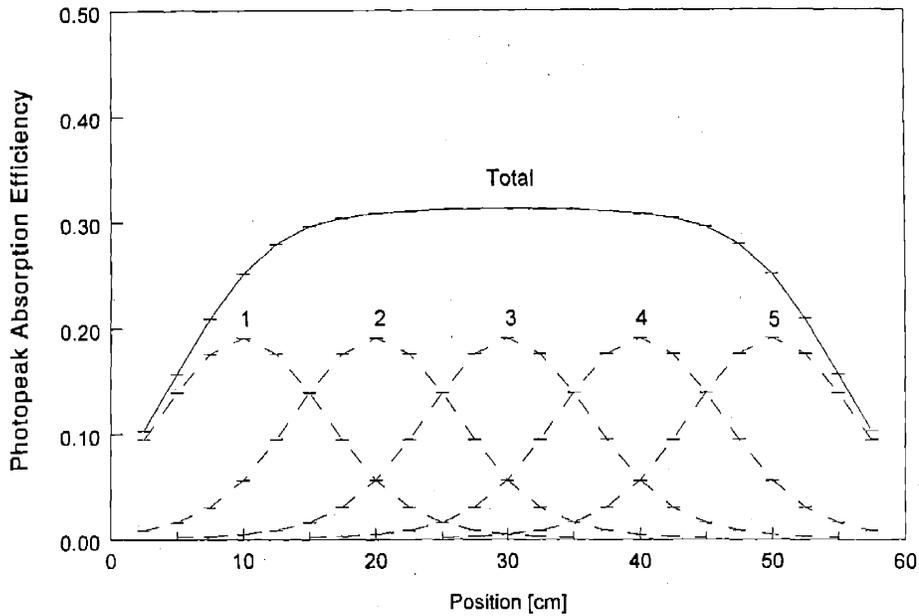
Figure 5-20 Detector array photopeak absorption efficiency in each of the five detectors and the total array, averaged over a cross section of the conveyor belt, as it passes through the array calculated using MCNP4B with a position resolution of 2.5 cm.

In the next figure, the detector array detection efficiency is presented for the best and worst of the measurement volumes calculated within the ore sample as well as the average value for comparison. The best detection efficiency, 41%, occurs at the outer corners or the ore, where the effect of self-attenuation of the gold isomeric photon is the smallest. The worst detection efficiency occurs in the middle 2 in. x 1 in. region of the ore, where the average detection efficiency is 24%. The oscillations in the detection efficiency observed for the worst case are a result of discontinuous nature of the detector array, being composed of individual detector segments. An examination of the detection efficiency of each detector segment to photons originating in the middle of the ore shows a much narrower response function as a function of position of the belt than the overall response function averaged over the entire ore body.

Ore Detector Array Efficiency
Best - Average - Worst
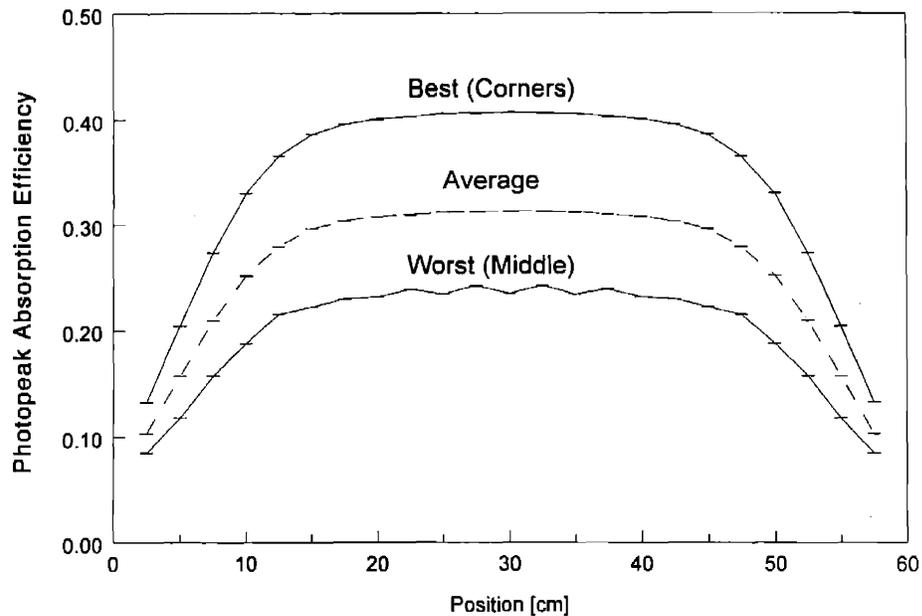
Figure 5-21 Detector array total photopeak absorption efficiency as function of the ore position along the conveyor belt for the best, average and worst cases.

The two design variables that must be optimized for on-line assay measurements are the material processing rate and the material determination limit. The principle factors influencing these are the intensity and spectrum of the irradiation source and the background counting rate in the detector array. As the material processing rate is increased, the total measurement time decreases. In Figure 5-22 the product of the detection efficiency and isomeric signal strength is plotted as the ore passes through the detector array for different conveyor belt speeds. At very slow processing speeds the effect of the decay of the isomeric gold is dominant and the useful length of the array is reduced because the isomeric signal is significantly decreased by the time it reaches the farthest detector segments to be measured. As the belt speed is increased beyond ~100 cm/sec, however, the total measurement time becomes short with respect to the rate of decay of the isomeric signal and, as can be seen in the figure, the loss of isomeric signal due to decay becomes negligible. Since the material processing rate is essentially set by requirements of the mine, the two methods of increasing the measured isomeric signal are to increase the irradiation strength (by using additional accelerators or accelerators of high current) or to increase the measured isomeric signal. At high processing speeds one method of increasing the measured signal would simply be to use a larger detector array. If one assumes a price of $2 per cm^3 for detector system, the detector array would cost ~$60,000. At high processing rates, the use of a second detector array would thus result in a detector system cost of ~$120,000. From the equation for L_D above, one sees that when the detector array is doubled, and thus the measured signal is essentially doubled, the signal required to identify the presence of gold in the ore with false positive and false negative error rates less than 5% is increased by only a factor of 1.4. Using 4 detector arrays, the improvement ratio between the measured signal and the required signal is greater than a factor of 2. Thus, an increased cost of $180,000 in the measurement system is equivalent to a doubling of the irradiation source intensity. Beyond 4 or 5 detector arrays, however, decreases in the isomeric signal due to simple decay become important at belt speeds of 500 cm/sec or less, thus there is a limit to the size of the detector array which can be used.

Absorption Efficiency & Decay
Various Processing Speeds
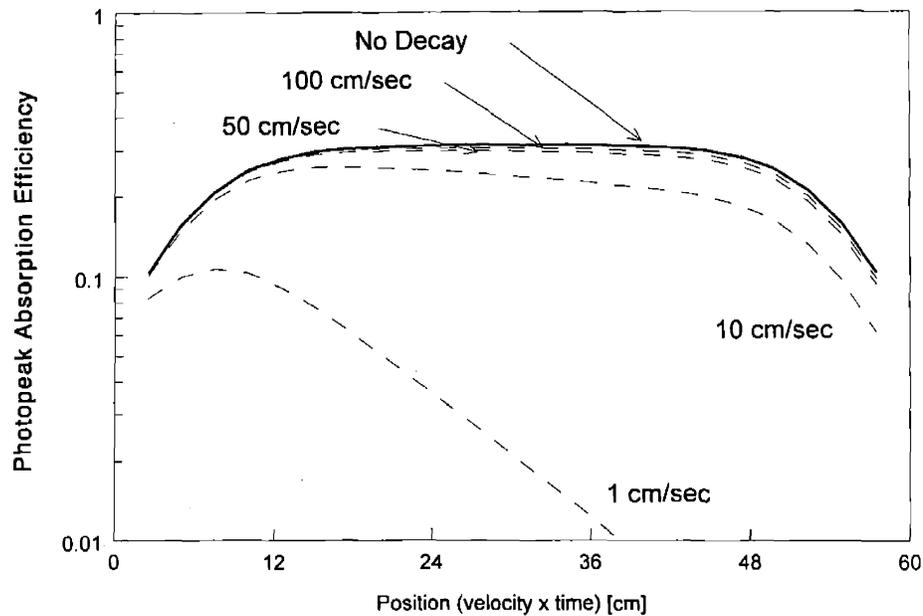
Figure 5-22 The combined effect of absolute detection efficiency and the decay of the isomeric signal for processing speeds, or conveyor belt speeds, of 1, 10, 50 and 100 cm per second.

As in the material analysis case of arsenic, the background count rate is a critical factor affecting the performance of this system. Using the 25 counts per second benchmark described earlier, each segment of a well shielded detector array might be expected to have a background count rate of 150 counts per second while each detector array might be expected to have a background count rate of 750 counts per second. If naturally radioactive materials are present in the ore, the background count rate would of course be higher. Additionally, background radiation could be introduced due (γ,n) or (γ,p) photonuclear reactions taking place within the ore. Referring to Table 5-3, photonuclear reactions occurring in an ore having similar components to that of igneous rock are not likely to lead to a significant background spectrum.

In Figure 5-23, the signal required for determination of the presence of a homogeneous distribution of 1 ppm gold in a unit ore volume is presented along with the measured signal, both of which have been determined as a function of the belt velocity where an optimistic background count rate of 500 counts per second was used. In this figure, the values for these two quantities have been plotted for systems employing 1, 2, 3 or 4 detector arrays arranged in series. As mentioned above, the discrete nature of the distribution of gold at this low concentration level would likely limit the smallest quantifiable ore volume to something larger than the unit volume described here. As can be seen, at belt speeds between 200 and 300 cm per second, a system designed using a 1 mA accelerator would be incapable of meeting the minimum analysis requirements for the analysis of gold ore at concentrations of 1 ppm.

Uniform Gold Distribution In Ore
Signal and Detection Level
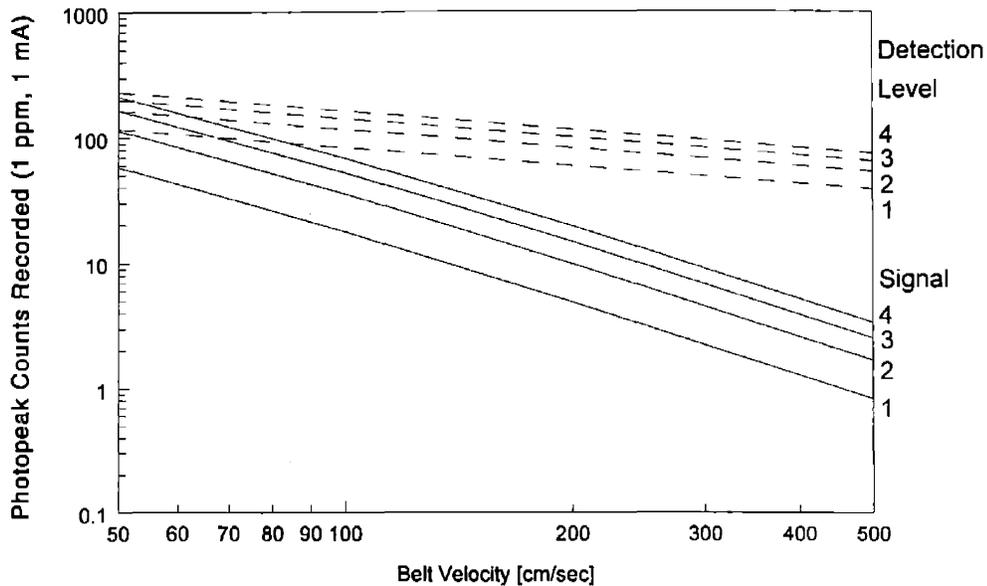
Figure 5-23 The isomeric gold signal (per 10 cm of length on the belt) measured at various conveyor belt velocities using 1, 2, 3 or 4 detector banks and the corresponding minimum detection level signals assuming a homogeneous gold distribution in the ore, a 1 mA accelerator and a *500 count per second* background in each detector bank.

In light of the discussion at the beginning of this section, however, and the information presented in Figure 5-12, a more realistic performance goal for an ore analysis system might be an instrument capable of sorting ore at a cut-off level of ~5-10 ppm gold – a decrease in total gold recovery of somewhere from 11 to 18% but a reduction in processed ore volume in the range of 89 to 92%. In Figure 5-24 the signal levels required for detection of 5 ppm of gold with false positive and false negative detection limits of 5% and a background count rate of 500 cps per detector array are plotted (dashed lines) together with the isomeric signal (solid lines) expected to be measured for a system using a 10 mA accelerator at various belt velocities. Similar information is presented in Figure 5-25 for a system with a background count rate of 1000 cps. Using the cases with background count rates of 500 and 1000 cps as upper and lower case bounding estimates for a real system the results presented here suggest that a photonuclear resonance excitation based isomeric assay system could be used as the measurement tool for assaying gold ore for sorting.

Uniform Gold Distribution In Ore
5 ppm, 10 mA, BKD = 500 cps
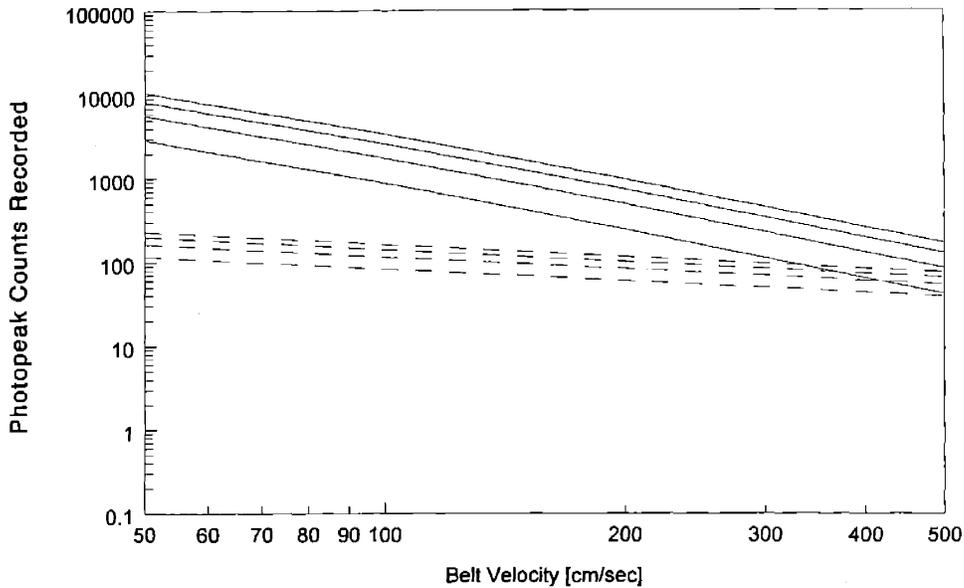
Figure 5-24 The isomeric gold signal (per 10 cm of length on the belt) measured at various conveyor belt velocities using 1, 2, 3 or 4 detector banks and the corresponding minimum detection level signals assuming a homogeneous gold distribution in the ore, a 10 mA accelerator and a *500 count per second* background in each detector bank.

Uniform Gold Distribution In Ore
5 ppm, 10 mA, BKD = 1000 cps
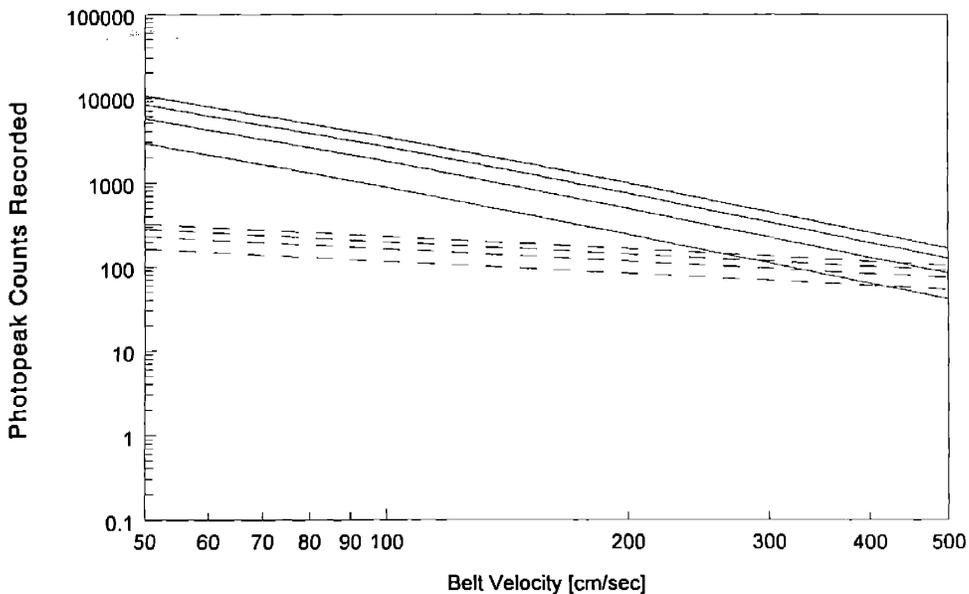
Figure 5-25 The isomeric gold signal (per 10 cm of length on the belt) measured at various conveyor belt velocities using 1, 2, 3 or 4 detector banks and the corresponding minimum detection level signals assuming a homogeneous gold distribution in the ore, a 10 mA accelerator and a *1000 count per second* background in each detector bank.

172

5.3 REFERENCES

[1] US 40 CFR 261.24

[2] B. L. Berman, et. al., "Photoneutron Cross Sections for As75, Ag107, and 133Cs," Phys. Rev. **177**, 1745 (1969). Plot from the National Nuclear Data Center, Brookhaven National Laboratory.

[3] R. B. Galloway, "Correction for Sample Self-Absrption in Activity Determination by Gamma Spectrometry," Nucl. Instr. Meth. Phys. Res. **A300**, 367-373 (1991).

[4] S. Taczanowski, "Correction for the Neutron and Gamma Attenuation Effects in 1 MeV Neutron Activation Analysis," Nucl. Inst. Meth. **144**, 299-309 (1977).

[5] T. Nakamura, "Monte Carlo Calculation of Efficiencies and Response Functions of NaI(Tl) Crystals for Thick Disk Gamma-Ray Sources and Its Application to Ge(Li) Detectors," Nucl. Instr. Meth. **105**, 77-89 (1972).

[6] T. Nakamura, "Montecarlo Calculation of Peak Efficiencies and Response Functions of Coaxial-Type Ge(Li) Detectors for Disk Gamma-Ray Sources," Nucl. Instr. Meth. **131**, 521-527 (1975).

[7] L. A. Currie, "Limits for Qualitative Detection and Quantitative Determination: Application to Radiochemistry," Anal. Chem. **40**, 586-593 (1968).

[8] J. I. W. Watterson, "A Theoretical Study of the Sorting of Witwatersrand Gold Ore," Report No. SRCNS 86/03, Schonland Research Centre for Nuclear Science, University of the Witwatersrand, South Africa 1986.

Chapter 6

SUMMARY

Although the phenomenon of photonuclear resonance excitation has been known for over 60 years it has yet to be transformed from an experimental nuclear physics technique to a commercial application. This is not for lack of trying; as pointed out in earlier chapters there have been several proposed uses for photonuclear resonance excitation. In some cases, these design ideas failed because of technical difficulties related to the process itself or because the systems failed to either demonstrate consistent performance characteristics or to show promise of doing so. [1-5] (For example, a system designed to analyze gold ore concentrations requiring the construction of a nuclear reactor at the mine dedicated for this purpose.) In other instances, the reason these industrial systems failed to reach any level of commercial realization stems from a clear lack of understanding on the designers part of the performance characteristics needed. (For example, a system designed to analyze individual gold rocks at a rate of a few per minute while actual mines have material throughput rates greater than 100 tons per hour.)

In this dissertation, the focus has been to develop the tools and methodology needed for designing industrial PRE systems. However, in order to help a designer to avoid mistakes such as those discussed above, the design framework presented herein provides an engineering based approach for making decisions a) to simply determine whether a particular idea is feasible and b) to make optimal choices among various components of a proposed system in the context of the basis upon which the systems ultimate

commercial desirability will be based. Regarding the second of these two points, for systems designed to produce high activity sources of isomeric isotopes (mCi/gram per mA) emphasis is placed on showing the relationship between accelerator energy and current, beams stop/convertor plate thickness, target geometry and location and the induced isomeric activity. For systems designed to analyze materials in order to identify and/or quantify the presence of isomeric elements in them, this dissertation suggests how the value of these same system components can be compared as well as the detection efficiency of an associated detector system. In approaching this subject in the general way done here, if specific information regarding the cost of various system components is collected, from manufacturer quotes for example, straightforward analysis can then be carried out to determine the cost for a system capable of producing a product of some set activity within a given amount of time or, conversely, the best system that can be acquired given fixed limits on resources such as space, weight or cost.

In order to design a system using photonuclear resonance excitation for some industrial application, specific information regarding the excitation of the isomer, the generation of the radiation used for excitation and, in some cases the radiation detection system, must be known. Due to a lack of adequate information concerning isomeric excitation cross sections, a theoretical model has been developed for calculating isomeric excitation cross sections for nuclei. This provides an important tool for assessing the quality of existing data and greatly expands the number of isomeric isotopes for which systems can be designed. Concerning the radiation source, a comprehensive comparison of potential radiation sources has been compiled. Although bremsstrahlung sources are the most suitable photon sources for the widest number of applications, this review helps to illuminate those particular situations where already existing radiation sources (either reactor based or radioisotopic based sources) might be used. Additionally, parametric analyses have been performed to understand particular design characteristics related the generation of x-rays in the energy range needed for PRE.

Regarding the detector system, analyses have been separated into two parts. Since inorganic scintillators are the most likely candidates for use in industrial systems, a summary of existing information related to their performance under circumstances similar to those to be encountered in most PRE applications has been presented. Additionally, since this area is the most technically challenging aspect in the development of PRE based analytical systems, experimental research has focused on examining this behavior to better understand difficulties associated with its implementation and to develop strategies for overcoming these difficulties. In the second part, parametric analyses have been carried out for two different cases dealing with PRE based measurement systems. Although these systems are based on NaI detector systems, the important parameter relevant to allowing the optimization of the two systems is simply the overall detector efficiency. Because of this, the results could easily be extracted to other inorganic scintillator materials or to other types of detectors altogether by using their appropriate detection efficiencies and background count rates for each instance. Additionally, by following the framework presented in each of the two cases the direction for expanding the studies carried out to determine the usefulness of additional detector types can be plainly seen.

6.1 CONCLUSIONS

(1) Theoretical analyses based upon the use of statistical nuclear structure models for calculating photon induced isomeric excitation cross sections, resulting from the absorption of photons at energies less than nucleon binding energies, have been carried out for several isomers. The results of these calculations agree with experimentally reported values for several isomers reported in the literature to within a factor of 2 or less over all energies less than nucleon binding energies. As a method for exploring the validity of different theories dealing with nuclear structure, these results indicate that a fully developed treatment of the problem incorporating neutron and proton boil off as well as photofission could prove to be a useful new tool in the field of low energy nuclear physics. Concerning the assessment of proposed PRE applications and the preliminary development of PRE systems, this theoretical tool provides a valuable method for building confidence in what is often questionable existing cross section values published in the literature and the only means for approaching problems involving the excitation of isomers for which no data exists at all.

(2) Although only a relatively small number of isomeric nuclei have previously been identified as useful for practical applications, a review of the available data regarding isotopes having half-lives greater than 1 microsecond yields a large number of isomers which could find use in industrial applications. One reason that little research has been published regarding the use of many of these isotopes might stem from a lack of adequate data, while in some cases the short half-lives of some isomers may have led to their dismissal because they were thought to be too short to use. In either case, new uses for many of these isomers may be possible, as suggested earlier in the identification of hazardous waste.

(3) For most situations the low cost, small physical foot print, ease of operation, continuous and high intensity photon spectrum and lack of long term radiation associated with bremsstrahlung radiation sources makes accelerator generated irradiation fields the ideal choice for PRE applications. However, for those situations where existing reactor or radioisotopic radiation sources are available these might also prove to be useful for PRE irradiation.

(4) For most situations the high density, moderate energy resolution and comparatively low cost of NaI scintillator detectors makes these a good choice for use in PRE measurement applications. However, in those cases where design constraints require direct exposure of the detector system to the irradiation field, the higher cost of more exotic scintillators such as GSO or LSO may be overcome by their ability to perform better in these environments. Additionally, as the development of room temperature solid state detectors with high resolution, high densities and large volumes begins to yield these materials at reasonable prices for commercial applications, they may also prove to be useful for PRE applications.

(5) A PRE based system designed to produce high activity isomeric samples could be expected to produce materials with specific activities on the order of a few millicurries per gram per milliamp of beam current using a 10 MeV beam. Additionally, using creative product irradiation geometries, significant reductions in irradiation times can be achieved in comparison with simply placing a target in a stationary position for irradiation. One example of such an improved production scheme is to rotate targets about a central beam axis to allow activity buildup and then to transfer the target to a central position for final irradiation. As an example, using a 'six-shooter' technique for a 24-hour production cycle of ^{115m}In, individual samples could be completed every 6 hours, each of which contained 92% of the isomer product collected from a single sample irradiated for the entire 24-hours in the central position.

(6) Using a statistical error analysis method, it is possible to simplify the design issues regarding the development of a PRE system to identify the importance of different design parameters on the sensitivity of PRE based analytical techniques. In doing so, it is possible to make decisions regarding the choice of accelerator and detector in terms of their impact upon the performance of the system and in the context of the design parameters required by the end user.

(7) A PRE based system canbe built that would be suitable for the analysis of environmental samples to quantify their arsenic concentration. With a detection sensitivity of 1 ppm ($\pm$ 10%) and a NaI based detector system having an average detection efficiency of ~45%, a 1 mA (10 MeV) accelerator would be needed to acquire data with measurement times less than a few minutes. For a system designed to measure samples with higher concentrations (>100 ppm), a much lower current accelerator could be used to yield the same precision.

(8) A PRE based system could be designed for the assay of gold content in ore to determine if the grade of ore within a small volume of ore exceeded some preset value. At a preset value of 1 ppm, the accelerator current required for such a system would likely exceed that of currently available commercial accelerators. However, at a preset value of 5 ppm a 10 MeV electron accelerator having an average current on the order of 10 mA could be expected to yield satisfactory measurement results at a processing rate of 100 tons of ore per hour. Additionally, significant improvements in the performance of a gold analysis system could likely be achieved by optimizing the design features of the irradiation and measurements systems to the specific performance requirements of a particular mine.

6.2 RECOMMENDATIONS FOR FUTURE WORK

Three major avenues of research can be identified as logical extensions of the work presented in this dissertation. As described in the section below, work in any of these areas would be of value in itself by expanding our physics and engineering knowledge base in the general field of nuclear engineering. However, taken together research in the areas outlined below would lead to the development of the facilities and expertise needed to design, build, test and assess engineering concepts related to the industrial application of photonuclear resonance excitation as well as the development radiation based systems in general.

6.2.1 Theory

Although the tools developed to analyze isomeric excitation cross sections are useful for the applications described in this dissertation, it would be helpful to incorporate isomeric excitation into a larger analytical or computational physics model to address other photon based phenomena. In particular, inclusion of the effects of reaction competition as photon energies increase and neutron and proton emission channels are opened would be extremely useful. Also, including competition with photofission would be helpful for modeling PRE isomeric excitation in heavy nuclei. While numerical physics package codes have been developed for predicting photonuclear interactions at energies near the giant dipole resonance, the analysis of isomeric yield ratios resulting from nucleon absorption has received the majority of attention related to the nuclear physics of isomer formation and comparatively little work deals with photon excitation of isomers.

6.2.2 Basic Experimental Science and Engineering

Experimental information related to the excitation of nuclei during photon irradiation is limited. Of the numerous stable isotopes with isomeric eigenstates, only a small hand full have been analyzed in a deliberate fashion to determine their photon excitation cross sections. Of those few isomers that have been analyzed, the published literature is sparse and the errors associated with their reported cross section measurements often are unknown. Regarding the production of radiation using electron accelerators, room for significant improvement still exists in the development of experimental techniques for accurately measuring the position dependence of the energy spectrum of the irradiation field and in using this information in the validation of radiation transport codes for calculating bremsstrahlung radiation. Concerning the operation of energy analyzing radiation detectors near particle accelerators and in the presence of high dose rate pulsed and continuous radiation fields, there is also considerable room for improvement in design. Due to the importance of maximizing the signal to noise ratio in nuclear analytical applications, this is a particularly important area.

6.2.3 Development of a Demonstration and Testing Facility

Development of an experimental testing facility incorporating a variable current, variable energy, high resolution electron accelerator with a variable duty cycle and a large shielded experimental bay for conducting experiments would yield a highly versatile tool for the investigation of problems having industrial relevance. Relatively little of the existing knowledge in the area of low energy nuclear physics has been leveraged for industrial purposes, those few cases where nuclear science has been commercialized have shown great societal benefits. In light of this, such an experimental facility would present a rare opportunity to conduct meaningful research in a poorly studied area nuclear physics which might also lead to the development of new technologies of benefit. In addition to providing a versatile facility for conducting basic experiments in the area of photonuclear physics, such a facility would also allow laboratory scale experiments of industrial applications dealing with photon activation, nuclear resonance fluorescence, isomer excitation and photonuclear transformation to be assembled. These would serve as preliminary proof-of-principle demonstrations for use in moving design concepts from academia to industry.

178

6.3 REFERENCES

[1] Y. N. Bourmistenko, "Gamma-Activation Installation for Fast Determination of Gold and Its Accompanying Elements in Ore Samples," Isotopenpraxis 17, 241-243 (1980).

[2] B. N. Rybkin et. al., "Analysis of Geological Samples or Gold and Silver by the Method of Spectral Ratios," trans. from Atomnaya Energiya 66, 42-44 (1989).

[3] I. A. Miransky et. al., "Multielemental Automated INAA System for Gold Ore Samples," J. Radioanal. Nucl. Chem, Articles 168, 329-336 (1993).

[4] T. K. Magagula, "The Production of Nuclear Isomers by the (n,n') Reaction and Its Application to Selective Activation Analysis," M.S. Dissertation, University of the Witwatersrand, Johannesburg, South Africa (1998).

[5] Tonchev, Harmon and Brey, "Analysis of Ore Samples Employing Photon Activation of the Metastable States of Gold and Silver," Nucl. Instr. Meth. Phys. Res. A 422, 926-928 (1999).

APPENDIX

Throughout the literature on the subject of activation analysis many ideas have been presented on how to choose to describe the sensitivity of analytical measurements. A very good review article on the subject was published by Currie in 1968; it is the formalism presented in this paper that is used here to analyze the sensitivity of PRE for material assay work.[1,2] Specifically, three distinct criteria are used to quantify the quality of an analytical measurements ability to determine the presence of some material in a sample; these are the decision limit, the detection limit, and the determination limit. The decision limit, L_C, is defined as the minimum measured signal (less background) for which the analyst can report something has been detected. The detection limit, L_D, is defined as the minimum measured signal (less background) which the analyst expects to lead to detection. The determination limit, L_Q, is the minimum measured signal (less background) above which quantitative analysis may be carried out to some specific level of precision deemed satisfactory.

Industrial PRE measurements can be split into two categories: a) indentification of the presence of the isomer in a sample and b) quantification of the amount of the isomer in a sample. For the first case, where the measurement goal is to determine if isomeric material is present in a sample above some minimum level, the performance of a PRE measurement system will be judged in part by the detection limit of the system, i.e., the system will be capable of determining whether or not the amount of isomeric material in the sample exceeds some predefined amount. For applications where simple identification of the presence

of isomeric material in a sample is insufficient and an estimate of the quantity of isomeric material in the sample is needed, the system performance will be related to the determination limit of the system, representing the smallest quantity of material in a sample which can be quantified within some precision deemed satisfactory for the situation.

As pointed out by Currie, the literature on the subject of statistical and analytical measurements has been confused with a myriad of definitions dealing with the science of detection, quantification and assay. So as not to further muddle the subject, the following table contains the nomenclature which will be used here, taken directly from Currie. For this analysis, the gross signal refers to the data (number of counts) collected by the PRE measurement system when measuring the decay photons of the isomeric isotope following irradiation. The "blank" signal refers to a measurement taken, under identical irradiation and measurement conditions, of a sample identical to that in the gross measurement case but without any isomeric material. The blank measurement is thus a procedure blank for the analysis and is often referred to as the background signal.

Table A - 1 Statistical analysis nomenclature.[1]

Blank Signal Terms :	μ_B	Blank signal limiting mean (or "true" mean)
	B	Observed blank signal value
	σ_B	Blank measurement standard deviation
Gross Signal Terms:	μ_{S+B}	Gross signal limiting mean
	$S+B$	Observed gross signal value
	σ_{S+B}	Gross measurement standard deviation
Net Signal Terms:	$\mu_S = \mu_{S+B} - \mu_B$	Net signal limiting mean
	$S = (S+B) - B$	Calculated net signal value
	$\sigma_S = (\sigma_{S+B}^2 + \sigma_B^2)^{1/2}$	Calculate net standard deviation

Regarding the assay of a sample to determine whether or not isomeric material is present, the problem may be attacked from two opposite points of view: *a priori* – Prior to a measurement, using information about the performance of the radiation measurement system, an estimate may be made of the minimum true signal, μ_S, which is expected to yield a sufficiently large derived net signal, S, that it will be detected and *a posteriori* – Following a measurement, a decision must be made to determine if the derived net signal, S, is large enough that one may conclude that $\mu_S > 0$. To begin, the *a posteriori* problem is taken first. For this case, one first begins by defining the two errors associated with *a posteriori* problems; namely,

Error of the first kind – A false positive, occurring with a probability α, where no isomeric material is present in the sample but the conclusion is that isomeric material *is* present

and

Error of the second kind – A false negative, occurring with a probability β, where isomeric material is present in the sample but the conclusion is that isomeric material *is not* present.

The value of α is decided upon by the analyst and is used together with the standard deviation of the net signal for a sample with no isomeric material ($\mu_S = 0$) to determine a critical level, L_C, for the derived

signal. If a derived signal S is less than L_C, then the sample is reported to not contain the isomeric material, with a confidence probability of $1 - \alpha$.

With this definition of L_C, which sets the level below which a net signal must be in order for the material to be classified as not containing isomeric material, a second critical level may defined. In this case, a detection level L_D is exactly defined so that the probability distribution of possible outcomes (when measuring a sample having a true mean value L_D) intersects L_C so that the fraction of measurements $1 - \beta$ corresponds to the correct decision of "material present". In addition to the probability, β, the standard deviation of the net signal (for a sample with some amount of isomeric material D) is also needed to define the detection level, L_D. If a derived signal S is greater than L_D, then the sample is reported to contain an amount of isomeric material equivalent to or greater than the amount D, with a confidence probability of $1 - \beta$. If the net signal is greater than L_C but less than L_D, then a report of "no material present " will have a probability of being wrong which exceeds α and a report of "material present" will have a probability of being wrong which exceeds β.

The acceptable values for α and β are decided upon by the designer of the assay system after taking into account the requirements of the user and practical limitations in the selection of system components. The relationship between α and β and the critical and detection limits are shown graphically in Figure A-1 and Figure A-2. In these figures, taken from Currie, W(S) represents the probability that the net signal S will be observed for a measurement. The area under the curve in each figure is exactly equal to one. In Figure A-1 there *is no* isomeric material present to be detected and the true mean value of measurements of this sample, μ_S, is zero. However, due to statistical fluctuation, there is a probability that measurements of this sample will generate a net signal. The standard deviation of the net signal associated with this measurement, σ_S, for the special case when no isomeric material is present, is written $\sigma_0 = \sigma_S$. In Figure A-2 there *is* a small amount of isomeric material to be detected and the true mean value of measurements of this sample is such that $\mu_S = L_D$, where L_D is the measured signal corresponding to the amount D, called the detectable limit. Again, however, there is a probability that a measurement will result in an error (indicating the absence of material). The standard deviation σ_S associated with the net signal S acquired from measurement of a sample containing a small amount of material D is written $\sigma_D = \sigma_S$.
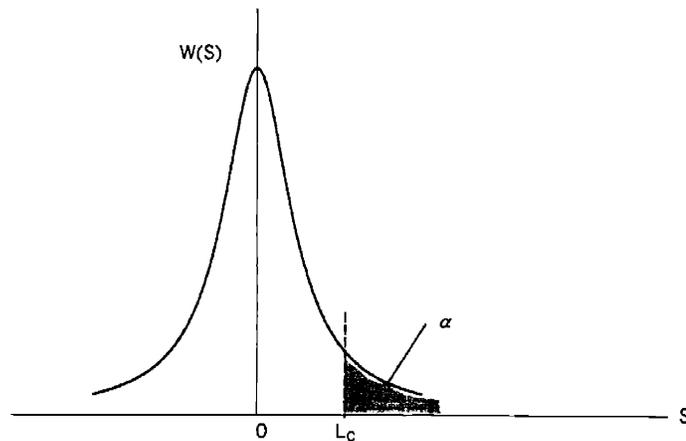
Figure A-1 The relationship between the decision limit L_C and the acceptable false positive error probability α for measurements of a sample with no isomeric material with a standard deviation in measurement of σ_0.[1]
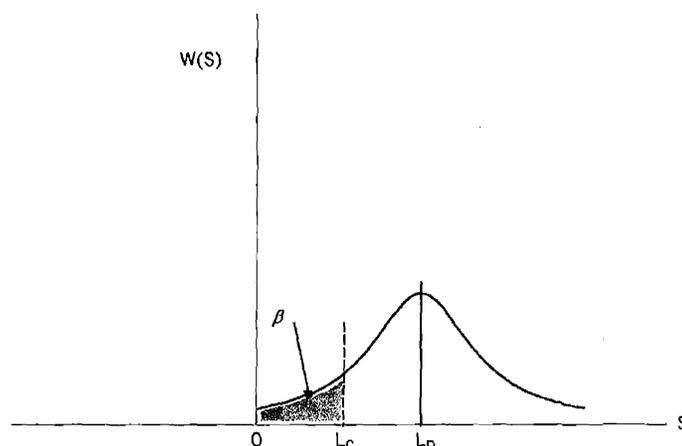
Figure A-2 The relationship between the detection limit L_D, the decision limit and the acceptable false negative error probability β for measurements of a sample with isomeric material with a standard deviation in the measurements of σ_D.[1]

The mathematical relationship for the critical level may be written as

$$L_C = k_\alpha \, \sigma_0,$$

           A-1

and for the detection limit,

$$L_C = L_D - k_\beta \, \sigma_D$$

or

$$L_D = L_C + k_\beta \, \sigma_D.$$

           A-2

For these definitions, k_α and k_β have been introduced so that L_C and L_D can be determined by inspection of a standard normal distribution (which has a total area under the curve of 1 and a standard deviation of 1). The value of k_α corresponds to the abscissa's value such that the area under the curve for values greater than k_α equals α and k_β corresponds to the abscissas value such that the area under the curve for values greater than k_β equals β. Since a standard normal distribution is used for these calculations, the values of k_α and k_β must be multiplied by the corresponding standard deviations for the two cases, σ_0 and σ_D, respectively.[3,a]

The third criteria that may be set is the quantitative limit, L_Q, which corresponds to the minimum net signal (and thus the minimum quantity of isomeric material) which may be measured and quantified to within a pre-specified precision. In this instance, an amount of isomeric material Q, which when analyzed by the radiation measurement system has a true mean net signal $\sigma_S = \sigma_Q$, will by definition have a quantified standard deviation of $1/k_Q$, which follows from the definition;

$$L_Q = k_Q \, \sigma_Q.$$

           A-3

---

[a] A useful table for calculating values of k_α and k_β may be found in reference 3.

In Figure A-3 the relationship between the critical limit, detectable limit and quantitative limit is shown. Depending upon the magnitudes of α and β (and thus k_α and k_β) and k_Q, the minimum net signal needed for measurements to be within one of the three regions will change.
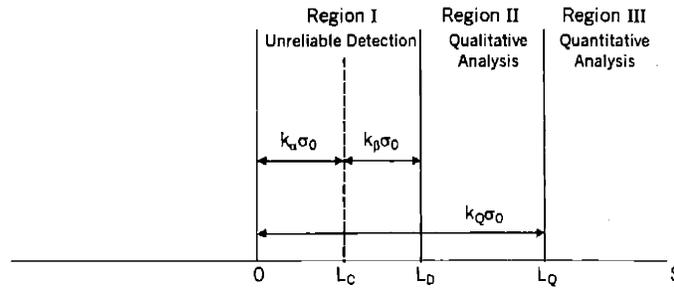

Figure A-3 The regions of unreliable detection, qualitative analysis and quantitative analysis for analytical measurements.[1]

Incorporating simplifications arising from the Poisson nature of the radioactive decay process being observed in PRE, the equations for the three signal limits may be rearranged to illustrate their relationship with the measurement systems background radiation (the blank sample): [1]

$$L_C = k_\alpha \, (\mu_B + \sigma_B{}^2)^{1/2} \, ,$$ **A-4**

$$L_D = L_C + \frac{k_\beta^2}{2}\left\{1 + \left[1 + \frac{4\,L_C}{k_\beta^2} + \frac{4\,L_C^2}{k_\alpha^2\,k_\beta^2}\right]^{1/2}\right\}$$ **A-5**

and

$$L_Q = \frac{k_Q^2}{2}\left\{1 + \left[1 + \frac{4\,\sigma_0^2}{k_Q^2}\right]^{1/2}\right\} .$$ **A-6**

These equations assume that the blank radiation signal is well known; this might not always be the case for industrial PRE applications. It is possible, for instance, that the bulk material matrix containing the isomeric material being analyzed might also contain a heterogeneous and changing background radiation signal simply due to naturally radioactive elements present in the sample. One simple remedy for this type of problem, however, would be to measure the bulk material natural background prior to irradiation. For applications where the PRE system is designed to analyze materials continuously, on a conveyor belt for example, this solution would require a second set of radiation detectors upstream of the material irradiation in addition to the downstream measurement system.

Another reason for variations in the blank signal could stem from the presence of a second isomer in the sample which contributes to the isomeric signal of interest. In this case, a more sophisticated approach must be taken to adequately separate out the interference signal from the signal of interest. If the strength of the interference signal is constant for the bulk material, then a more elaborate complete method of defining the blank signal could be carried out which also included the interference. If the interference strength was also variable, then a more complicated signal processing approach would be needed to resolve the unknown signal from the interference. For example, a set of well constructed pure reference

backgrounds could be used to deconvolve the unknown and interference signals from a spectrum. Alternatively, it might be possible to exploit variations in the PRE cross sections for the two isomers using a dual energy bremsstrahlung spectrum to isolate one signal from the other.

Once the detection limits have been set using the system blank counting statistics and the desired operational performance criteria, it is necessary to develop a relationship for determining the actual amount, or mass, of isomeric material present in the sample, m, and the derived net signal S for an unknown measurement as well as for the special cases corresponding to the critical limit, determination limit and quantification limit. In general, the derived net signal may be related to the mass of isomeric material present according to

$$m_S = \frac{1}{\kappa} S$$

A-7

where κ is a proportionality constant relating the amount of mass m_S which leads to a signal S. The standard deviation in the calculated mass of isomeric material is

$$\sigma_{m_s} = \frac{1}{\kappa} \sigma_S = \frac{1}{\kappa} (\sigma_{S+B}^2 + \sigma_B^2)^{1/2}.$$

A-8

As with other activation analysis techniques, there are two approaches to solving this problem, either a) the factor κ may be determined exactly using specific knowledge of the irradiation and detection system or b) the factor κ may be determined in a comparitive manner by comparing the measurement results of an unknown sample to those obtained from the analysis of a reference sample containing a known amount of isomeric material.

[1] L. A. Currie, "Limits for Qualitative Detection and Quantitative Determination: Application to Radiochemistry," Anal. Chem. 40, 586-593 (1968).
[2] P. Kruger, *Principles of Activation Analysis*, Wiley-Interscience, New York, 368-375 (1968).
[3] R. Tallarida, *Pocket Book of Integrals and Mathematical Formulas, 2nd Edition*, CRC Press, 1992.

BIBLIOGRAPHY

CHAPTER 1

1) F. Isaev and L. P. Kudrin, "Diagnosis of Dense Plasma by Means of Resonance Scattering of Gamma Rays," High Temperature **6**, 737-740 (1968).

2) B. D. Sowerby, "A New Method of Element Analysis Using Nuclear Resonance Scattering of Gamma Rays," Nucl. Instr. Meth. **94**, 45-51 (1971).

3) Sowerby, Ellis and Greenwood-Smith, "Bulk Analysis for Copper and Nickel In Ores Using Gamma-Ray Resonance Scattering," Report IAEA-SM-216/4, Nuclear Techniques and Mineral Resources Proceedings, 499-521 (1977).

4) Wielopolski, Vartsky and Cohn, "Possible Application of Nuclear Resonance Fluorescence to Study Surface Effects," J. Appl. Phys. **54**, 5449-5450 (1983).

5) J. C. Palathingal, "Nuclear Resonance-Fluorescence Analyser of Ores and Surfaces," Capture Gamma-Ray Spectroscopy and Related Topics – 984, AIP Conference Proceedings No. 125, 847-850 (1984).

6) D. J. S. Findlay, "Applications of Photonuclear Reactions," Nucl. Instr. Meth. Phys. Res. **B50**, 314-320 (1990).

7) W. Bertozzi, "Explosives Detection Using Resonance Fluorescence of Bremsstrahlung Radiation," United States Patent No. 5,115,459, May 19, 1992.

8) W. Bertozzi, "Detection of Explosives and Other Materials Using Resonance Fluorescence, Resonance Absorption, and Other Electromagnetic Processes With Bremsstrahlung Radiation," United States Patent No. 5,420,905, May 30, 1995.

9) Marsden, Mansanti and Sass, "Innovative Methods For Precious Metals Recovery in North America," Mining Engineering, 1144-1151 September (1993).

10) G. M. Bernard, "Andacollo Gold Production – Ahead of Schedule and Under Budget," Mining Engineering, 42-47 August (1996).

11) W. R. Yernberg, "Santa Fe Pacific Gold Targets Million Ounces/Year Production," Mining Engineering, 39-43 September (1996).

12) R. L. Lawson, "The United States," Mining, Annual Review, 70-75 (1996).

13) J. I. W. Watterson, "A Theoretical Study of the Sorting of Witwatersrand Gold Ore," Report No. SRCNS 86/03, Schonland Research Centre for Nuclear Science, University of the Witwatersrand, South Africa 1986.

14) Korotaeva, prokopchukand Emets, "Is It Possible to Optimize the Blending of Gold-Bearing Ore Samples," trans. from Zhurnal Analiticheskoi Khimii 40, 1230-1236 (1985).

15) E. T. Bramlit, "Plutonium Mining for Cleanup," Health Physics 55, 451-53 (1988).

16) J. R. Chen et. al., "Determination of the Occurrence of Gold in an Unoxidized Carlin-Type Ore Sample Using Synchrotron Radiation," Nucl. Instr. Meth. Phys. Res. B22, 394-400 (1987).

17) J. Shukla and K. S. Pitre, "Eectrochemical Analysis of Gold in Ore," Analyst 121, 79-81 (1996).

18) B. de Celis, "X-Ray Fluorescence Analysis of Gold Ore," Applied Spectroscopy 50, 572-575 (1996).

19) B. David and C. Widham, "Statistical Control for the Production of Assay Laboratory Standards," Mining Engineering, 73-76 March (1996).

20) Y. N. Bourmistenko, "Gamma-Activation Installation for Fast Determination of Gold and Its Accompanying Elements in Ore Samples," Isotopenpraxis 17, 241-243 (1980).

21) B. N. Rybkin et. al., "Analysis of Geological Samples or Gold and Silver by the Method of Spectral Ratios," trans. from Atomnaya Energiya 66, 42-44 (1989).

22) A. Miransky et. al., "Multielemental Automated INAA System for Gold Ore Samples," J. Radioanal. Nucl. Chem, Articles 168, 329-336 (1993).

23) T. K. Magagula, "The Production of Nuclear Isomers by the (n,n') Reaction and Its Application to Selective Activation Analysis," M.S. Dissertation, University of the Witwatersrand, Johannesburg, South Africa (1998).

24) Tonchev, Harmon and Brey, "Analysis of Ore Samples Employing Photon Activation of the Metastable States of Gold and Silver," Nucl. Instr. Meth. Phys. Res. A 422, 926-928 (1999).

25) D. Clifford, "Stacking Systems In Heap Leaching," Mining Magazine, 90-95 August (1996).

26) T. Mudder et. al., "Lab Evaluation of an Alternative Heap-Leach Pad Closure Method," Mining Engineering, 1007-1014 November (1995).

27) "Handling Tailings, South African Experience, At Home and Abroad, and Work in Tajikistan," Mining Magazine, 90-95 February (1997).

28) S.G. Vick, "Tailings Dam Failure at Omai in Guyana," Mining Engineering, 34-37 November (1996).

29) R. G. Robins, "The Stability of Arsenic In Gold Mine Processing Wastes," Precious Metals: Mining, Extraction and Processing, Kudryk, Corrigan and Liang, eds., The Metallurgical Society of AIME, 241-249 (1984).

30) P. Breban et. al., "Etude Des Possibilites D'Utilisation Analytique Des Isomeres Nucleaires Produits Par Reactions (γ,γ') Entre 6 et 8 MeV," Nucl. Instr. Meth. 158, 205-215 (1979).

31) R. Brey et. al., "The Possibility of Photon Activation Analysis of Radionuclides at Environmental-Levels," 6th International Conference on Nuclear Engineering, ICONE-6456 (1998).

32) Tonchev, Harmon and King, "Application of Low Energy Photon Spectroscopy in Isomer Production of Hf, W, Ir, Pt, Au and Hg Using (, ') Reactions," Nucl. Instr. Meth. Phys. Res A 422, 510-512 (1999).

33) Petrov, Trubachyev and Khan, "Processing of Solutions, Formed at Destruction Lewisite, With production of Arsenic Sulphide," 6th CBW Protection Symposium, Stockholm, Sweden, May (1998).

34) Vettese, Asselineau and Dhermain, "Neutron Activation Analysis Techniques To Identify Arsenic In Chemical Weapons," 5th International Symposium On Protection Against Chemical and Biological Warfare Agents, Stockholm, Sweden, June (1995).

35) Robinson, Swann and Rasmussen, "Gamma-Ray Widths of the 3.00-MeV Level of Al^{27} and the 3.13-MeV Level of P^{31}," Phys. Rev. **174**, 1320-1323 (1968).

36) F. R. Metzger, "Width of the 2.186-MeV 1- Level in Nd^{144}," Phys. Rev. **187**, 1700-1704 (1969).

CHAPTER 2

37) P. A. M. Dirac, The Principles of Quantum Mechanics, Fourth Edition, Oxford University Press, Oxford, 1958.

38) H. A. Bethe and G. Placzek, "Resonance Effects in Nuclear Processes," Phys. Rev. **51**, 150 (1937).

39) H. A. Bethe, "Nuclear Physics B. Nuclear Dynamics, Theoretical," Rev. Mod. Phys. **9**, 220 (1937).

40) G. B. Collins et. al., "Nuclear Excitation of Indium by X-Rays," Phys. Rev. **55**, 507 (1939).

41) G. B. Collins and B. Waldman, "Energy Distribution of Continuous X-Rays from Nuclear Excitation," Phys. Rev. **59**, 109 (1941).

42) E. Guth, "Radiative Transition Probabilities in Heavy Nuclei, Excitation of Nuclei by X-Rays," Phys. Rev. **59**, 325-331 (1941).

43) B. Waldman and M. L. Wiedenbeck, "The Nuclear Excitation of Indium by X-Rays and Electrons," Phys. Rev. **63**, 60 (1943).

44) M. L. Wiedenbeck, "The Nuclear Excitation of Silver and Cadmium," Phys. Rev. **67**, 92-97 (1945).

45) M. L. Wiedenbeck, "The Nuclear Excitation of Rhodium," Phys. Rev. **67**, 267-268 (1945).

46) J. M. Blatt and V. F. Weisskopf, Theoretical Nuclear Physics, John Wiley & Sons, Inc., New York, 1952.

47) F. R. Metzger, "Resonance Fluorescence in Nuclei," Progress In nuclear Physics, O. R. Frisch, ed., Vol. 7, Pergamon Press (1959).

48) P. Axel, "Electric Dipole Ground-State Transition Width Strength Function and 7-MeV Photon Interactions," Phys. Rev. **126**, 671 (1962).

49) Boivin, Cauchois and Heno, "Photoactivation Nucleaire Du 77Se, 107,109Ar, 111Cd, 115In et 199 Hg," Nucl. Phys. **A137**, 520-530 (1969).

50) C. B. Collins et. al., "Activation of 115Inm by Single Pulses of Intense Bremsstrahlung," Phys. Rev. C **38**, 1852-1856 (1988).

51) J. A. Anderson et. al., "Nuclear Photoactivation Cross Sections for Short-Lived Isomeric States Excited with a 6 MeV Linac," Nucl. Instr. Meth. Phys. Res. **B40/41**, 452-454 (1989).

52) J. J. Carroll et. al., "Excitation of 123Tem and 125Tem Through (γ,γ') Reactions," Phys. Rev. C **43**, 897-900 (1991).

53) V. V. Lomonosov and S. B. Sazonov, "Temporal Theory of Resonant Gamma-Ray Scattering from a Nuclear Isomer: Calculation of Scattering Interaction Time," JETP **80**, 45-49 (1995).

54) V. I. Vysotskii, "Controlled Spontaneous Nuclear γ Decay: Theory of Controlled Excited and Radioactive Nuclei γ Decay," Phys. Rev. C **58**, 337-350 (1998).

55) Sowerby, Ellis and Greenwood-Smith, "Bulk Analysis for Copper and Nickel in Ores Using Gamma-Ray Resonance Scattering," Report IAEA-SM-216/4, Nuclear Techniques and Mineral Resources Proceedings, 499-521 (1977).

56) G. Kehlenbeck et. al., "The Slowing-Down of Low Energy Recoil Atoms in Solids and Liquids Investigated by Nuclear Resonance Fluorescence," Z. Phys. B **66**, 147-151 (1987).

57) W. Muckenheim et. al., "Nuclear Resonance Fluorescence in 238U and a New Approach to Doppler-Shift-Attenuation Using High Speed Rotation," Z. Phys. A **300**, 43-46 (1981).

58) P. Axel and J. D. Fox, "Implications of the Photonuclear Effect in Zr^{90}," Phys. Rev. **102**, 400-414 (1956).

59) T. Ericson and V. Strutinski, "On Angular Distributions in Compound Nucleus Processes," Nucl. Phys. **8**, 284-293 (1958).

60) T. Ericson and V. Strutinsky, "On Angular Distributions in Compound Nucleus Processes," Nucl. Phys. **9**, 689-690 (1958/59).

61) T. Ericson, "A Statistical Analysis of Excited Nuclear States," Nucl. Phys. 11, 481-491 (1959).

62) K. J. Le Couteur and D. W. Lang, "Neutron Evaporation and Level Densities in Excited Nuclei," Nucl. Phys. **13**, 32-52 (1959).

63) J. R. Huizenga and R. Vandenbosch, "Interpretation of Isomeric Cross-Section Ratios for (n,γ) and (γ,n) Reactions," Phys. Rev. **120**, 1305-1312 (1960).

64) R. Vandenbosch and J. R. Huizenga, "Isomeric Cross-Section Ratios for Reactions Producing the Isomeric Pair $Hg^{197,197m}$," Phys. Rev. **120**, 1313-1318 (1960)

65) J. L. Need, "Analysis of the Energy Dependence of the Isomer Ratio in the $Sn^{120}(p,\alpha)In^{117,117m}$ Reaction," Phys. Rev. **129**, 1302-1307 (1963).

66) Vandenbosch, Haskin and Norman, " Isomer Ratios for Y87,87m and the Spin Dependence of the Nuclear Level Density," Phys. Rev. **137**, B 1134-1144 (1965).

67) N. D. Dudey and T. T. Sugihara, "Statistical-Model Analysis of Isomeric Ratios in (α,xn) Compound Nuclear Reactions," Phys. Rev. **139**, B 896 (1965).

68) W. B. Walters and J. P. Hummel, "Studies of Isomeric Yield Rations in the Production of Sc44, Mn52, and Y87 by Photonuclear Reactions," Phys. Rev. **150**, 867-876 (1966).

69) PSR-125/GNASH-FKK Code Package, Radiation Shielding Information Center, Oak Ridge National Laboratoy, USA.

70) J. Kopecky and M. Uhl, "Test of Gamma-Ray Strength Functions In Nuclear Reaction Model Calculations," Phys. Rev. C **41**, 1941-1955 (1990).

71) C. Bloch, "Theory of Nuclear Level Density," Phys. Rev. **93**, 1094-1106 (1954).

72) W. D. Myers and W. J. Swiatecki, "Anomalies in Nuclear Masses," Arkiv For Fysik **36**, 343-352 (1966).

73) Wapstra, Audi and Hoekstra, "Atomic Masses From (Mainly) Experimental Data," Atomic Data and Nuclear Data Tables **39**, 281-287 (1988).

74) P. E. Nemirovsky and Yu. V. Adamchuk, "Neutron and Proton Pair Interaction Energy," Nuclear Phys. **39**, 551-562 (1962).

75) J. M. B. Lang and K. J. Le Couteur, "Statistics of Nuclear Levels," Proc. Phys. Soc. A **67**, 585-600 (1954).

76) T. D. Newton, "Shell Effects on the Spacing of Nuclear Levels," Can. J. Phys. **34**, 804-829 (1956).

77) G. W. Cameron, "Nuclear Level Spacings," Can. J. Phys. **36**, 1040-1057 (1958).

78) D. W. Lang, "Nucleon Correlations and Nuclear Level Densities," Nucl. Phys. **42**, 353-366 (1963).

79) U. Facchini and E. Saetta-Menichella, "level Density Parameter values From Neutron and Proton Resonances," Energia Nucleare **15**, 54-62 (1968).

80) V. Ignatyuk, G. N. Smirenkin and A. S. Tishin, "Phenomenological Description of the Energy Dependence of the Level Density Parameter," Sov. J. Nucl. Phys. **21**, 255-257 (1975).

81) N. N. Abdelmalek and V. S. Stavinsky, "Semi-Expirical Formula for Nuclear Level Density and Fission Asymmetry," Nuclear Phys. **58**, 601-610 (1964).

82) N. D. Dudey and T. T. Sugihara, "Statistical-Model Analysis of Isomeric Ratios in (, x n) Compound Nuclear Reactions," Phys. Rev. **139**, B 896-904 (1965).

83) W. P. Ponitz, "A Gamma-Ray Cascade Model for the Calculation of Average -Ray Multiplicities and Isomeric Cross Section Ratios," Zeit. Physik **197**, 262-275 (1966).

84) R. B. Firestone, "Table of Isotopes CD-ROM," S. Y. Frank Chu, CD-ROM editor, Eighth Edition. v1.0, (1996).

85) S. S. Dietrich and B. L. Berman, "Atlas of Photoneutron Cross Sections Obtained With Monoenergetic Photons," Atomic Data and Nucear Data Tables **38**, 199-338 (1988).

86) E. Silva and J. Goldemberg, "Inelastic Scattering of Photons in Y89," Phys. Rev. **110**, 1102-1103 (1958).

87) M. L. Wiedenbeck, "The Nuclear Excitation of Krypton and Rhodium," Phys. Rev. **68**, 237-239 (1945).

88) Bogdankevich, Lazareva and Moiseev, "Inelastic Scattering of Photons on Rh103 Nuclei," Sov. Phys. JETP **12**, 853-856 (1961).

89) P. Kruger et. al., "Excitation of Isomeric States In Rh103 and In115 by Electrons," Nucl. Phys. **62**, 584-592 (1965).

90) J. Safar et. al., "^{103Rhm} Production By Inelastic Gamma Scattering in the Giant Dipole Resonance Region," Phys. Rev. C **44**, 1086-1090 (1991).

91) Meyer-Schützmeister and V. L.Telegdi, "Inelastic Scattering of Photons from Au197," Phys. Rev. **100**, 961 (1955).

92) L. Meyer-Schützmeister and V. L.Telegdi, "Inelastic Nuclear Scattering of Photons by Au197," Phys. Rev. **104**, 185-190 (1956).

93) E. V. Tkalya, "γ Decay of Isomeric Nuclei in an Intense External Field: The Role of Giant Dipole Resonances," Sov. J. Nucl. Phys. **49**, 992-994 (1989).

94) J. J. Carroll et. al., "Accelerated Decay of 180Tam and 176Lu In Stellar Interiors Through (, ') Reactions," The Astrophysical Journal **344**, 454-459 (1989).

95) B. Collins et al., "The Gamma-Ray Laser – Status and Issues in 1988," Laser and Particle Beams **7**, 357-367 (1989).

96) B. Collins et. al., "Resonant Excitation of the Reaction ^{180}Ta^m(γ,γ')180Ta," Phys. Rev. C **42**, R1813-R1816 (1990).

97) B. Collins et. al., "Status and Issues in the Development of a γ-Ray Laser. II. Giant Resonances for the Pumping of Nuclei," Laser and Particle Beams **11**, 43-54 (1993).

98) S. Olariu and A. Olariu, "Induced Emission of γ Radiation From Isomeric Nuclei," Phys. Rev. C **58**, 333-336 (1998).

99) S. Olariu and A. Olariu, "Power Densities for Two-Step γ-Ray Transitions From Isomeric States," Phys. Rev. C **58**, 2560-2562 (1998).

100) K. Pisk et. al., "Nuclear Excitation by the Inelastic Photoelectric Effect," Phys. Rev. C **25**, 2226-2230 (1982).

101) Ljubičić et. al., "Photoactivation Investigations With ^{115}In," Phys. Rev. C **23**, 2238-2244 (1981).

102) M. Krěmar et. al., "Photoactivation of ^{111}Cd," Phys. Rev. C **25**, 2097-2099 (1982).

103) M. Krěmar et. al., "Photoactivation of Isomeric Levels in ^{113}In and ^{87}Sr," Phys. Rev. C **33**, 293-295 (1986).

104) J. A. Anderson, "Activation of ^{111}Cd^m By Single Pulses of Intense Bremsstrahlung," Phys. Rev. C **38**, 2838-2842 (1988).

105) M. Krěmar et. al., "Resonant and Nonresonant Contributions to the Photoactivation of ^{111}Cd," Phys. Rev. C **41**, 771-774 (1990).

106) P. Von Neumann-Cosel et. al., "Comment on 'Resonant and Nonresonant Contributions to the Photoactivation of ^{111}Cd,'" Phys. Rev. C **44**, 554-558 (1991).

107) M. Krěmar et. al., "Reply to "Comment on 'Resonant and Nonresonant Contributions to the Photoactivation of ^{111}Cd,''" Phys. Rev. C **47**, 906-909 (1993).

108) S. Batkin, "Compton Excitation of Nuclear Levels," Sov. J. Nucl. Phys. **29**, 464-469 (1979).

109) L. Spruch and G. Goertzel, "Magnetic Internal Compton Coefficients in the Born Approximation," Phys. Rev. **94**, 1671-1678 (1954).

110) S. Batkin and M. I. Berkman, "Excitation of Low-Lying Nuclear States by Synchrotron Radiation," Yadernaya Fiz. **32**, 972-977 (1980).

111) V. Tkalya et. al., "Processes of the Nuclear Isomer ^{229m}Th (3/2+, 3.5 ± 1.0 eV) Resonant Excitation by Optical Photons," Physica Scripta **53**, 296-299 (1996).

112) R. Horvat et. al., "Nuclear Excitation During Pair Production," Phys. Rev. C **29**, 1614-1616 (1984).

113) G. Fuller and E. Hayward, "Nuclear Elastic Scattering of Photons," Phys. Rev. **101**, 692-700, (1956).

114) R. Moreh, "Studies of Fundamental Photon Scattering Processes Using n-Capture Gamma-Rays," Nucl. Inst. Meth. **166**, 91-103 (1979).

115) P. Papatzacos and K. Mork, "Delbrück Scattering Calculations," Phys. Rev. D **12**, 206-218 (1975).

116) M. Schumacher and P. Rullhusen, "Delbrück and Rayleigh Scattering Below 5 MeV," Nucl. Inst. Meth. **166**, 85-90 (1979).

117) Schumacher, Rullhusen and Baumann, "Nuclear Compton Scattering at Intermediate Energies," Il Nuovo Cimento **100**, 339-356 (1988).

118) Kahane, Moreh, and Shahal, "Interferences Between Rayleigh, Delbrück and Nuclear Resonance Scattering Processes," Phys. Rev. C **28**, 1519-1526 (1983).

CHAPTER 3

119) Fuller, E. G. and Hayward, E., "Nuclear Elastic Scattering of Photons," Phys. Rev. **101**, (692-700) 1956.
120) Hayward, E. and Fuller, E. G., "Photon Self-Absorption and Scattering by the 15.1-MeV Level in C12," Phys. Rev. **106**, (991-995) 1957.
121) Garwin, E.L., "Gamma-Ray Excitation of the 15.1-MeV Level in C12," Phys. Rev. **114**, (143-154) 1959.
122) Langhoff, H., "Resonance Fluorescence in Re^{187}," Phys. Rev. **135**, (B1-B8) 1964.
123) Robinson, S. W., et. al., "Gamma-Ray Widths of the 3.00-MeV Level of Al^{27} and the 3.13-MeV Level of P^{31}," Phys. Rev. **174**, (1320-1323) 1968.
124) Rasmussen, V. K. and Swann, C. P., "Gamma-Ray Widths in C^{13}, Li^6, and P^{31}," Phys. Rev. **183**, (918-923) 1969.
125) Metzger, F. R., "Electric Dipole Transitions from the 2.6-MeV Septuplet in Bi^{209}," Phys. Rev. **187**, (1680-1682) 1969.
126) Metzger, F. R., "Width of the 2.186-MeV 1- Level in Nd^{144}," Phys. Rev. **187**, (1700-1704) 1969.
127) Sowerby, B. D., "A New Method of Element Analysis Using Nuclear Resonance Scattering of Gamma Rays," Nucl. Instrum. Meth. **94**, (45-51) 1971.
128) Treml, K. and Langhoff, H., "The Slowing Down of Atoms with Energies of E<10 eV in Crystals," Z.Physik **B25**, (123-129) 1976.
129) Ellis, W. K., et. al., "Bulk Analysis For Copper and Nickel In Ores Using Gamma-Ray Resonance Scattering," Proc. Nucl. Tech. And Mineral Resources 1977, (499-520) 1977
130) Muckenheim, W., et. al., "Nuclear Resonance Fluorescence in ^{238}U and a New Approach to Doppler-Shift-Attenuation Using High Speed Rotation," Z. Phys. A – Atoms and Nuclei **300**, (43-46) 1981.
131) Palathingal, J. C., "Nuclear Resonance-Fluorescence Analyser of Ores and Surfaces," Capture Gamma-Ray Spectroscopy and Related Topics-1984, AIP Conf. Proc. No. 125, (847-850) 1984.
132) Kehlenbeck, G., "The Slowing-Down of Low-Energy Recoil Atoms in Solids and Liquids Investigated by Nuclear Resonance Fluoescence," Z. Phys. B – Cond. Matter **66**, (147-151) 1987.
133) Heil, R. D., et. al., "Observation of Orbital magnetic Dipole Strength in the Actinide Nuclei ^{232}Th and ^{238}U," Nucl. Phys. **A476**, (39-47) 1988.
134) Margraf, J., "Photoexcitation of Low-Lying Dipole Transition in ^{236}U," Phys. Rev. C **42**, (771-774) 1990.
135) Govaert, K., et. al., "Polarized Bremsstrahlung Nuclear Resonance Fluorescence Set-Up At the 15 MeV Linac In Gent," Nucl. Instrum. Meth. A **337**, (265-273) 1994.
136) Ohgaki, H., et. al., "Linearly Polarized Photons From Compton Backscattering of Laser Light for Nuclear Resonance Fluorescence Experiments," Nucl. Instrum. Meth. A. **353**, (384-388) 1994.
137) R. B. Firestone, "Table of Isotopes CD-ROM," S. Y. Frank Chu, CD-ROM editor, Eighth Edition. v1.0, (1996).
138) Anderson, J. A., et. al., "Nuclear Photoactivation Cross Sections for Short-Lived Isomeric States Excited With A 6 MeV Linac," Nucl. Instrum. Meth. **B40/41**, (452-454) 1989.
139) Carroll, J. J., et. al., "Accelerated Deay of 180mTa and ^{176}Lu In Stellar Interiors Through (γ,γ') Reactions," Astrophysical Journ. **344**, (454-459) 1989.
140) Goryachev, B. I., "Cross-Sections of Photonuclear Reactions Tabulated Data," At. Energy Rev. **3**, (71-148) 1964.
141) Kaminishi, T. and Kojima, C., "Production of Nuclear Isomers from Stable Nuclides with Bremsstrahlung," Jap. J. App. Phys. **2**, (399-405) 1963.
142) Otvos, J. W, et. al., "Photoactivation and Photoneutron Activation Analysis," Nucl. Inst. Meth. **11**, (187-195) 1961.
143) Veres, "Gamma Activation of Nuclear Isomers and Its Applications," At. Energy. Rev. **18**, 271-328 (1980).

144) Sekine, Yoshihara, Nemeth, Lakosi and Veres, "A New Detection Method of 99Tc By Nuclear Excitation," J. Radioanal. Nucl. Chem., Articles **130**, 269-278 (1989).

145) Sekine, Yoshihara, Lakosi, Nemeth and Veres, "Integral Cross Section of the $^{99}Tc(\gamma,\gamma')^{99m}Tc$ Reaction in the 15-50 Mev Energy Region," Appl/ Radiat. Isot. **42**, 149-153 (1991).

146) Yagi, Sekine and Yoshihara, "Detection Limit of Technetium in $^{99}Tc(\gamma, \gamma')^{99m}Tc$ Radioactivation Analysis in the Presence of Molybdenum," J. Radioanal. Nucl. Chem., Letters **155**, 433-443 (1991).

147) Veres and I. Pavlicsek, "Nuclear Photoactivation Analyses By Means of an 80-kCi ^{60}Co γ - Radiation Source," J. Radioanal. Chem. **3**, 25-28 (1969).

148) Veres, Pavlicsek, Csuros and Lakosi, "Nuclear Excitation by g Rays of Radioactive Sources," Acta Physica Academiae Scientiarum Hungaricae **34**, 97-104 (1973).

149) B. Arad et. al., "Studies of Highly Excited Nuclear Bound Levels Using Neutron Capture Gamma Rays," Phys. Rev. **133**, B684-B700 (1964).

150) G. Ben-David et. al., "Further Study of Nuclear Resonant Scattering Using Neutron-Capture Gamma Rays," Phys. Rev. **146**, 852-860 (1966).

151) R. B. Begzhanov and S. M. Akhrarov, "Investigation of Highly Excited Levels of Nuclei with the Aid of Neutron-Capture Gamma Rays," JETP Letters **10**, 26-28 (1969).

152) R. B. Begzhanov and S. M. Akhrarov, "Resonance Scattering by Certain Nuclei of γ Rays from Radiative Capture of Thermal Neutrons," Bull. Acad. Sci. USSR Phys. Ser. **35**, 120-123 (1972).

153) O. Shahal and R. Moreh, "Recent Developments in Nuclear Scattering of Capture Gamma Rays," AIP Conf. Proc. No. 125, Capture Gamma-Ray Spectroscopy and Related Topics – 1984, S. Raman, ed., 179-191 (1984).

154) J. R. Huizenga and R. Vandenbosch, "Photoexcitation of the Isomeric States of Cd^{111} and In^{115} with Mono-Energetic Gamma Rays," Nucl. Phys. **34**, 457-460 (1962).

155) H. Bethe and W. Heitler, "On the Stopping of Fast Particles and on the Creation of Positive Electrons," Proc. Roy. Soc. **A146**, 83-112 (1934).

156) M. G. Davydov and V. A. Shcherbachenko, "Selecivity of γ -Activation Analysis," Atomnaya Energiya **27**, 205-208 (1969).

157) MCNP v.4B Code Package, Radiation Shielding Information Center, Oak Ridge National Laboratoy, USA.

158) J. F. Briesmeister, ed., MCNP – A General Monte Carlo N-Particle Transport Code Version 4B, LA-12625-M, Version 4B Manual, Los Alamos National Laboratory, USA, March 1997.

159) H. W. Koch and J. W. Motz, "Bremsstrahlung Cross-Section Formulas and Related Data," Rev. Mod. Phys. **31**, 920-955 (1959).

160) S. Lindenstruth, "Measurements and Simulations of Low Energy, Thick Target Bremsstrahlung Spectra," Nucl. Instr. Meth. Phys. Res. **A300**, 293-296 (1991).

161) H. Bethe and W. Heitler, "On the Stopping of Fast Particles and on the Creation of Positive Electrons," Proc. Roy. Soc. **146**, 83-112 (1934).

162) D. R. Lide, ed., Handbook of Chemistry and Physics, 72nd Edition, CRC Press, 14-7 (1991).

163) Storey, Jack and Ward, "The Fluorescent Decay of CsI(Tl) for Particles of Different Ionization Density," Proc. Phys. Soc. **72**, 1-8 (1958).

164) F. G. Delaney and A. M. Lamki, "Long-Lived Phosphorescent Components in NaI(Tl) and CsI(Tl)," Int. J. App. Rad. Isotop. **19**, 169-170 (1968).

165) S. Keszthelyi-Landori and G. Hrehuss, "Scintillation Response Function and Decay Time of CsI(Tl) to Charged Particles," Nucl. Instr. Meth. **68**, 9-12 (1969).

166) P. E. Francois and D. T. Martin, "Phosphorescent Components in CsI(Tl) and CsI(Tl)," Int. J. App. Rad. Isotop. **21**, 687 (1970).

167) Koicki, Koicki and Ajdacic, "The Investigation of the 0.15 s Phosphorescent Component of NaI(Tl) and Its Application in Scintillation Counting," Nucl. Instr. Meth. **108**, 297-299 (1973).

168) Crannell, Kurz and Viehmann, "Characteristics of Cesium Iodide for Use As a Particle Discriminator for High-Energy Cosmic Rays," Nucl. Instr. Meth. **115**, 253-261 (1974).

169) Moszynski, Gresset, Vacher and Odru, "Timing Properties of BGO Scintillator," Nucl. Instr. Meth. **188**, 403-409 (1981).

170) M. Laval, et. al., "Barium Fluoride – Inorganic Scintillator for Subnanosecond Timing," Nucl. Instr. Meth. **206**, 169-176 (1983).

171) S. L. Wen and C. F. He, "A New Approach to the Radiation Hardness of BGO," Nucl. Instr. Meth. **219**, 333-335 (1984).

172) H. Grassmann, et. al., "Improvements in Photodiode Readout for Small CsI(Tl) Crystals," Nucl. Instr. Meth. **A234**, 122-124 (1985).

173) E. Sakai, "Recent Measurements on Scintillator-Photodetector Systems," IEEE Trans. Nucl. Sci. **NS-34**, 418-422 (1987).

174) Holl, Lorenz and Mageras, "A Measurement of the Light Yield of Common Inorganic Scintillators," IEEE Trans. Nucl. Sci. **35**, 105-109 (1988).

175) Yin, Wei, Shen and Xie, "A New BGO Crystal with Higher Radiation Hardness," Nucl. Instr. Meth. **A275**, 273-276 (1989).

176) Woody, Levy and Kierstead, "Slow Component Suppression and Radiation Damage in Doped BaF2 Crystals," IEEE Trans. Nucl. Sci. **36**, 536-542 (1989).

177) G. F. Knoll, Radiation Detection and Measurement, John Wiley and Sons, Inc., (1989).

178) Melcher, Schweitzer, Utsu and Akiyama, "Scintillation Properties of GSO," IEEE Trans. Nucl. Sci. **37**, 161-164 (1990).

179) M. Kobayashi and M. Ishii, "Excellent Radiation-Resistivity of Cerium-Doped Gadolinium Silicate Scintillators," Nucl. Instr. Meth. **B61**, 491-496 (1991).

180) M. Kobayashi, et. al., "Cerium Fluoride, A Highly Radiation-Resistive Scintillator," Nucl. Instr. Meth. **A302**, 443-446 (1991).

181) Yanovzky, Chizhov and Skorikov, "BGO Crystals – Radiation Hard Scintillators," Nucl. Instr. Meth. **A309**, 596-597 (1991).

182) Suzuki, Tombrello, Melcher and Schweitzer, "UV and Gamma-Ray Excited Luminescence of Cerium-Doped Rare-Earth Oxyorthosilicates," Nucl. Instr. Meth. **A320**, 263-272 (1992).

183) L. Melcher and J. S. Schweitzer, "Cerium-Doped Lutetium Oxyorthosilicate: A Fast, Efficient New Scintillator," IEEE Trans. Nucl. Sci. **39**, 502-505 (1992).

184) M. Kobayashi and M. Ishii, "Effect of Cerium Doping on the Radiation Hardness of Gadolinium Silicate Gd2SiO5," Nucl. Instr. Meth. B **82**, 85-90 (1993).

185) Ziegler, Rogers, Selivanov and Sinitzin, "Characteristics of the New YAlO3:Ce Compared With BGO and GSO," IEEE Trans. Nucl. Sci. **40**, 194-197 (1993).

186) S. C. Sabharwal, et. al., "Thermoluminescence and Transmission Recovery of Gamma Irradiated Bi4Ge3O12 Single Crystal," Nucl. Instr. Meth. **A329**, 179-182 (1993).

187) M. Ishii, et. al., "Research and Development of Ce-Doped GSO Scintillation Crystals," SPIE **2305**, 68-79 (1994).

188) R.-Y. Zhu, "Crystal gamma-Ray Detectors for High Energy Physics," SPIE **2305**, 80-97 (1994).

189) Yin, Feng and Hu, "Doping Effect and Mechanism of Radiation Damage of Bismuth Germanate (Bi4Ge3O12) Crystals," Ferroelectrics **151**, 287-298 (1994).

190) H. Suzuki, et. al., "The Role of Gadolinium in the Scintillation Processes of Cerium-Doped Gadolinium Oxyorthosilicate," Nucl. Instr. Meth. A **346**, 510-521 (1994).

191) Kobayashi, Ishii, Usuki and Yahagi, "Cadmium Tungstate Scintillators With Excellent Radiation Hardness and Low Background," Nucl. Instr. Meth. A **349**, 407-411 (1994).

192) S. Baccaro, et. al., "Scintillation Properties of YAP:Ce," Nucl. Instr. Meth. A **361**, 209-215 (1995).

193) Kobayashi, Ishii, Harada and Yamaga, "Bismuth Silicate Bi4Si3O12, A Faster Scintillator Than Bismuth Germanate Bi4Ge3O12," Nucl. Instr. Meth. A **372**, 45-50 (1996).

194) M. Moszynski, "Timing Properties of GSO, LSO and Other Ce Doped Scintillators," Nucl. Instr. Meth. A **372**, 51-58 (1996).

195) Fyodorov, et. al., "Progress In PbWO4 Scintillating Crystal," Radiat. Meas. **26**, 107-115(1996).

196) S. K. Sahu, et. al., "Radiation Hardness of Undoped BGO Crystals," Nucl. Instr. Meth. A **388**, 144-148 (1997).

197) Taulbee, Rooney, Mengesha and Valentine, "The Measured Electron Response Nonproportionality of CaF2, BGO, LSO and GSO," IEEE 0-7803-3534-1/97, 326-330 (1997).

198) M. E. Casey, et. al., "Investigation of LSO Crystals for High Spatial Resolution Positron Emission Tomography," IEEE 0-7803-3534-1/97, 1029-1033 (1997).

199) S. Yamamoto, "LSO and GSO: Performance Evaluation for PET," Radioisotopes **46**, 265-271 (1997).

194

200) W. E. van Eijk, "Development of Inorganic Scintillators," Nucl. Instr. Meth. A **392**, 285-290 (1997).

201) Konishi, et. al., "Full Energy Peak Efficiency of GSO(Ce) Detectors for Gamma-Rays," IEEE 0-7803-4258-5/98, 829-832 (1998).

202) H. Ishibashi, et. al., "Scintillation Performance of Large Ce-Doped Gd2SiO5 (GSO) Single Crystal," IEEE 0-7803-4258-5/98, 838-841 (1998).

203) R.Y. Zhu, et. al., "A Study on the Radiation Hardness of Lead Tungstate Crystals," IEEE Trans. Nucl. Sci. **45**, 686-691 (1998).

204) M. Tanaka, et. al., "Applications of Cerium-Doped Gadolinium Silicate Gd2SiO5:Ce Scintillator to Calorimeters in High-Radiation Environment," Nucl. Instr. Meth. A **404**, 283-294 (1998).

205) S. C. Sabharwal and Sangeeta, "Study of Growth Imperfections, optical Absorption, Thermoluminescence and Radiation Hardness of CdWO4 Crystals," J. Crystal Growth **200**, 191-198 (1999).

206) S. Baccaro, "Recent Progress in the Development of Lead Tungstate Crystals," IEEE Trans. Nucl. Sci. **46**, 292-295 (1999).

207) Melcher, Schweitzer, Liberman and Simonetti, "Temperature Dependence of Fluorescence Decay Time and Emission spectrum of Bismuth Germanate," IEEE Trans. Nucl. Sci. **NS-32**, 529- (1985).

CHAPTER 4

208) F R. B. Firestone, *Table of Isotopes CD-ROM*, S. Y. Frank Chu, CD-ROM editor, Eighth Edition, v1.0, (1996).

209) Bogdankevich, Lazareva and Nikolaev, "Inelastic Scattering of Photons by Indium-115 Nuclei," Sov. Phys. JETP **4**, 320-327 (1957).

210) SpIDer Computer code v4.1, Western Kentucky University Nuclear Group, (1997).

211) L. A. Currie, "Limits for Qualitative Detection and Quantitative Determination: Application to Radiochemistry," Anal. Chem. **40**, 586-593 (1968).

212) T. Nakamura, "Monte Carlo Calculation of Efficiencies and Response Functions of NaI(Tl) Crystals for Thick Disk Gamma-Ray Sources and Its Application to Ge(Li) Detectors," Nucl. Inst. Meth. **105**, 77-(1972).

213) T. Nakamura, "Monte Carlo Calculation of Peak Efficiencies and Respose Functions of Coaxial-Type Ge(Li) Detectors for Disk Gamma-Ray Sources," Nucl. Inst. Meth. **131**, 521- (1975).

214) S. Taczanowski, "Correction for the Neutron and Gamma Attenuation Effects In 14 MeV Beutron Activation Analysis," Nucl. Inst. Meth. **144**, 299- (1977).

215) R. B. Galloway, "Corection for Sampl Self-Absorption in Activity Determination by Gamma Spectrometry," Nucl. Inst. Meth. In Phys. Res. **A300**, 367- (1991).

216) R. M. W. Overwater, *The Physics of Big Sample Instrumental Neutron Activation Analysis*, Dissertation, Delft Technological University, Delft, The Netherlands, (1994).

217) I. M. Jureidini, *A Design for a High Energy X-Ray Computed Tomography Sensor for the Study of Solidification Fronts in Aluminum*, S.M. Dissertation, Nuclear Engineering Department, Massachusetts Institute of Technology, Cambridge, MA, (1997).

218) I. M. Jureidini, *Design and Performance of a Compact High-Energy Computed Tomography system for the study of Metal Solidification*, Ph.D. Dissertation, Nuclear Engineering Department, Massachusetts Institute of Technology, Cambridge, MA, (1998).

219) M. M. Hytros, *Development of a High-Energy X-Ray Computed Tomography Sensor for Detecting the Solidification Front Position in Aluminum Casting*, Ph.D. Dissertation, Department of Mechanical Engineering, Massachusetts Institute of Technology, Cambridge, MA, (1999).

220) W. R. Leo, *Techniques for Nuclear and Particle Physics Experiments*, Springer-Verlag, (1992).

221) J. A. Anderson, et. al., "Nuclear Photoactivation Cross Sections for Short-Lived Isomeric States Excited With A 6 MeV Linac," Nucl. Instr. Meth. **B40/41**, 452-454 (1989).

222) Tonchev, Harmon and King, "Application of Low Energy Photon Spectroscopy in Isomer Production of Hf, W, Ir, Pt, Au and Hg using (γ,γ') Reactions," Nucl. Instr. Meth. Phys. Res. A **422**, 510-512 (1999).

223) Tonchev, Harmon and Brey, "Analysis of Ore Samples Employing Photon Activation of the Metastable States of Gold and Silver," Nucl. Instr. Meth. Phys. Res. A **422**, 926-928 (1999).

224) Robinson, Swann and Rasmussen, "Gamma-Ray Widths of the 3.00-MeV Level of Al^{27} and the 3.13-MeV Level of P^{31}," Phys. Rev. **174**, 1320-1323 (1968).

225) V. K. Rasmussen and C. P. Swann, "Gamma-Ray Widths in C^{12}, Li^6, and P^{31}," Phys. Rev. **183**, 918-923 (1969).

226) F. R. Metzger, "Electric Dipole Transitions from the 2.6-MeV Septuplet in Bi^{209}," Phys. Rev. **187**, 1680-1682 (1969).

227) J. Margraf, et. al., "Photoexcitation of low-lying dipole transitions in ^{236}U," Phys. Rev. C. **42**, 771-774 (1990).

228) K. Govaert, et. al., "Polarised Bremsstrahlung Nuclear Resonance Fluorescence Set-Up at the 15 MeV Linac in Ghent," Nucl. Instr. Meth. Phys. Res. A **337**, 265-273 (1994).

229) S. N. Makeev et. al., "Study of Photomultiplier Anode-Current Variation with Pulse Gamma-Neutron Irradiation," translation from Pribory i Tekhnika Eksperimenta (Russian) **6**, 135-137 (1985).

230) S. N. Makeev, et. al., "Variation of Photomultiplier Anode Current for Continuous and Pulsed Gamma Radiation," translation from Pribory i Tekhnika Eksperimenta (Russian) **1**, 160-163 (1986).

231) S. N. Makeev, et. al., "Study of Photomultiplier Anode-Current variation With Pulse Gamma-Neutron Irradiation," translation from Pribory i Tekhnika Eksperimenta (Russian) **6**, 135-137 (1985).

232) J. J. Carroll, "Excitation and De-excitation of Selected Nuclear Isomers Through (gamma,gamma') Reactions," Ph.D. Dissertation, University of Texas, Dallas (1991).

233) C. Hong, "Measurements of Short-Lived Isomers With A Gated Detector," Ph.D. Dissertation, University of Texas Dallas, (1993).

234) A. K. Gupta and N. Nath, "Gain Stability In High-Current Photomultiplies At High Variable Counting Rates," Nucl. Instr. Meth. **53**, 352-354 (1967).

235) C. Weitkamp, et. al., "Count-Rate Dependence of the Gain of RCA 7046 Photomultipliers for Fixed Dynode Potentials," Nucl. Instr. Meth. **61**, 122-124 (1968).

236) M. Yamashita, "Observation of a Hysteresis Effect In Rate-Dependent Photomultiplier Gain Variations," Nucl. Instr. Meth. **142**, 435-437 (1977).

237) D. K. Li, V. G. Epishev and T. D. Radaeva, "The Effect of Ionizing Radiation On A Photomultiplier," translation from Pribory i Tekhnika Eksperimenta (Russian) **2**, 170-172 (1985).

238) A. S. Belousov, et. al., "Stability of Scintillation Spectrometer With NaI(Tl) Crystal and FEU-49 Photomultiplier At high Count Rates," translation from Pribory i Tekhnika Eksperimenta (Russian) **3**, 49-52 (1985).

239) V. N. Evdokimov and M. I. Mutafyan, "Short-Term Instability and Stabilization of Photomultiplier Gain," translation from Pribory i Tekhnika Eksperimenta (Russian) **4**, 134-138 (1986).

240) J. P. Glore, "Equipment for Experiments with Activities Having Half-Lives In the Range From 10μsec to 1 sec," Los Alamos Report LA-2152, (1958).

241) R. R. Fullwood and R. W. Hockenbury, "Neutron Inelastic Scattering Measurements with a Gated Photomultiplier," Nucl. Instr. Meth. **77**, 245-248 (1970).

242) R. R. Fullwood, "A Bistable Symmetrical Photomultiplier Gate Using Integrated Circuits," Nucl. Instr. Meth. **95**, 509-513 (1971).

243) M. Rossetto and D. Mauzerall, "A Simple Nanosecond Gate for Side Window Photomultipliers and Echoes in Such Photomultipliers," Rev. Sci. Instr. **43**, 1244-1246 (1972).

244) M. Yamashita, "Photomultiplier Gate With Gating Times Larger Than A Few Microseconds," Rev. Sci. Instr. **45**, 956-957 (1974).

245) Rosen, Robrish and Jan de Vries, "Design Of A Simple and Inexpensive Analog Gate," Rev. Sci. Instr. **46**, 1115-1116 (1975).

246) J. J. Ramirez and L. W. Kruse, "Gated Scintillator-Photomultiplier Neutron Detector for Time-of-Flight Measurements in the Presence of a Strong X-Ray Background," Rev. Sci. Instr. **47**, 832-835 (1976).

247) H. Sang Lee, et. al., "Gated Photomultiplier Response Characterization for DIAL Measurements," App. Optics **29**, 3303-3315 (1990).

248) M.C. Piton, "An 'On'-Gated Photomultiplier Circuit for the Determination of Phosphorescence Lifetimes," Rev. Sci. Inst. **61**, 3726-3728 (1990).

249) D. J. Creasey, et. al., "Fast Photomultiplier Tube Gating System for Photon Counting Applications," Rev. Sci. Inst. **69**, 4068-4073 (1998).

250) Yoshida, Jovin and Barisas, "A High-Speed Photomultiplier Gating Circuit for Luminescence," Rev. Sci. Inst. **60**, 2924-2928 (1989).

251) T. M. Yoshida, "Measurement of Protein Rotational Diffusion Using Time- and Frequency-Domain Polarized Fluorescence Depeletion," Ph.D. Dissertation, Colorado State University (1989).

252) J. R. Herman, "Development of Laser Optical Instrumentation for Luminescence Measurements in Biological Systems," Ph.D. Dissertation, Colorado State University (1991).

253) J. R. Herman, et. al., "Normally On Photomultiplier Gating Circuit with Reduced Post-Gate Artifacts for Use in Transient Luminescence Measurements," Rev. Sci. Inst. **63**, 5454-5458 (1992).

254) T. R. Londo, "Theoretical and Instrumental Developments in the Measurement of Integral Membrane Protein Dynamics," Ph.D. Dissertation, Colorado State University (1992).

CHAPTER 5

255) US 40 CFR 261.24

256) B. L. Berman, et. al., "Photoneutron Cross Sections for As75, Ag107, and 133Cs," Phys. Rev. **177**, 1745 (1969). Plot from the National Nuclear Data Center, Brookhaven National Laboratory.

257) R. B. Galloway, "Correction for Sample Self-Absrption in Activity Determination by Gamma Spectrometry," Nucl. Instr. Meth. Phys. Res. **A300**, 367-373 (1991).

258) S. Taczanowski, "Correction for the Neutron and Gamma Attenuation Effects in 1 MeV Neutron Activation Analysis," Nucl. Inst. Meth. **144**, 299-309 (1977).

259) T. Nakamura, "Monte Carlo Calculation of Efficiencies and Response Functions of NaI(Tl) Crystals for Thick Disk Gamma-Ray Sources and Its Application to Ge(Li) Detectors," Nucl. Instr. Meth. **105**, 77-89 (1972).

260) T. Nakamura, "Montecarlo Calculation of Peak Efficiencies and Response Functions of Coaxial-Type Ge(Li) Detectors for Disk Gamma-Ray Sources," Nucl. Instr. Meth. **131**, 521-527 (1975).

261) L. A. Currie, "Limits for Qualitative Detection and Quantitative Determination: Application to Radiochemistry," Anal. Chem. **40**, 586-593 (1968).

262) J. I. W. Watterson, "A Theoretical Study of the Sorting of Witwatersrand Gold Ore," Report No. SRCNS 86/03, Schonland Research Centre for Nuclear Science, University of the Witwatersrand, South Africa 1986.

CHAPTER 6

263) Y. N. Bourmistenko, "Gamma-Activation Installation for Fast Determination of Gold and Its Accompanying Elements in Ore Samples," Isotopenpraxis 17, 241-243 (1980).

264) B. N. Rybkin et. al., "Analysis of Geological Samples or Gold and Silver by the Method of Spectral Ratios," trans. from Atomnaya Energiya **66**, 42-44 (1989).

265) I. A. Miransky et. al., "Multielemental Automated INAA System for Gold Ore Samples," J. Radioanal. Nucl. Chem, Articles **168**, 329-336 (1993).

266) T. K. Magagula, "The Production of Nuclear Isomers by the (n,n') Reaction and Its Application to Selective Activation Analysis," M.S. Dissertation, University of the Witwatersrand, Johannesburg, South Africa (1998).

267) Tonchev, Harmon and Brey, "Analysis of Ore Samples Employing Photon Activation of the Metastable States of Gold and Silver," Nucl. Instr. Meth. Phys. Res. A **422**, 926-928 (1999).

APPENDIX

268) L. A. Currie, "Limits for Qualitative Detection and Quantitative Determination: Application to Radiochemistry," Anal. Chem. **40**, 586-593 (1968).

269) P. Kruger, *Principles of Activation Analysis*, Wiley-Interscience, New York, 368-375 (1968).

270)   R. Tallarida, *Pocket Book of Integrals and Mathematical Formulas, 2nd Edition*, CRC Press, 1992.